GEOLOGICAL SURVEY OF NAMIBIA

MINISTRY OF MINES AND ENERGY

AGE DETERMINATIONS IN THE REHOBOTH BASEMENT INLIER, NAMIBIA

by

U. R. F. ZIEGLER and G. F. U. STOESSEL

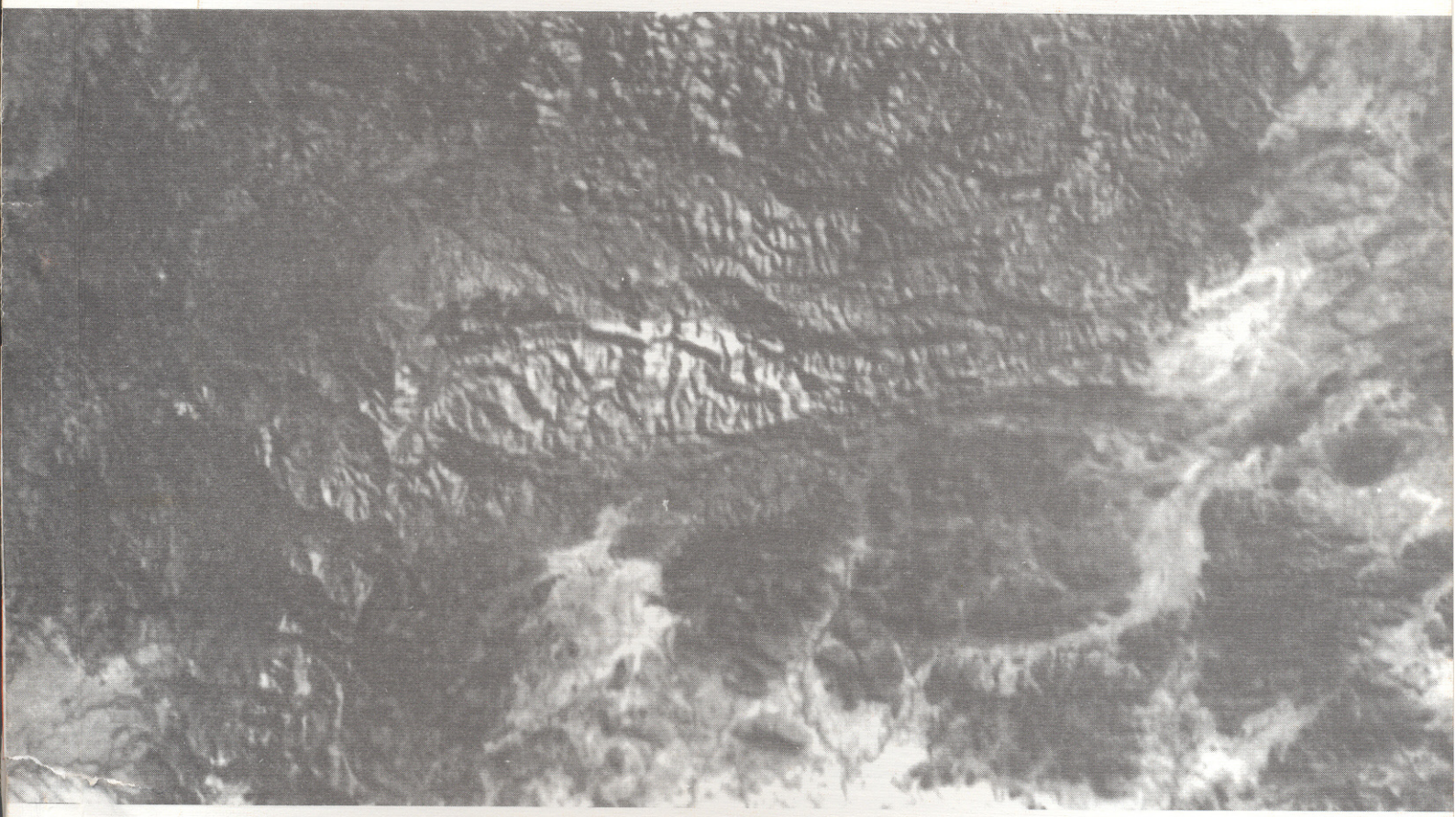

MEMOIR 14

1993

Front cover: Portion of a Landsat Thematic Mapper 5 image which shows the area to the east and north of the Spreetshoogte Pass. Light-coloured rocks of the Mooirivier Complex are bounded to the north by Grauwater metamorphic rocks and to the south by the Gamsberg Granite Suite.

The majority of the area is underlain by rugged rolling topography typical of the dissected interior plateau of Namibia. A portion of the Great Escarpment, which divides the interior plateau from the coastal plain, can be seen in the southwestern (lower left) corner of the image. The Spreetshoogte Pass crosses the Great Escarpment at this point.

The image was processed at the Geological Survey of Namibia using Erdas software on a Sun workstation. The image show portion of band 4 of image 179/76. The Survey is now capable of doing its own full image processing on hardware and software purchased for it by Finnida.

(Imaging by Roger Swart).

GEOLOGICAL SURVEY OF NAMIBIA

MINISTRY OF MINES AND ENERGY

Director: B. G. Hoal

MEMOIR 14

Age determinations in the Rehoboth Basement Inlier, Namibia

by

U. R. F. Ziegler and G. F. U. Stoessel

Editor: Clare Kennedy Galloway

Obtainable from the Geological Survey
P. O. Box 2168, Windhoek, Namibia

	Price
Local (+ GST)	N$20.00
Abroad	N$25.00

ISBN 0 - 86976 - 325 - 5

ABSTRACT

The southern most basement inlier within the Damara Orogen, the Rehoboth Basement Inlier, covers an area of approximately 15000^2 km with its northernmost outcrops situated about 70 km south of Windhoek, the capital of Namibia. The aim of this study is to elucidate the geological history of the inlier, which is composed of a succession of metavolcano-sedimentary acid and basic rock formations which are intruded by granitoid as well as basic magmas. Sm-Nd and U-Pb analyses of granitoids, amphibolites and basic dykes show that the major part of the Rehoboth crust formed during the early Proterozoic between 2.6 and 1.8 Ga as an accretionary belt on the northwest side of the Archaean Kalahari Craton and possibly equivalent to the younger parts of the South African and Zimbabwean Limpopo Province. During the early stages of this crustal evolution the freshly formed crust must also have been readily reworked by various stages of erosional, metamorphic and anatectic processes in order to be present today as a metamorphosed volcano sedimentary sequence, including the lithologies from the Mooirivier Complex at its base to the Billstein Formation at its top. This theory of early reworking of the originally formed crust is supported by the occurrence of granitic pebbles and boulders in various formations of the Rehoboth Sequence. It is worth noting that the majority of the formations from the Mooirivier Complex to the Billstein Formation originally had similar lithological compositions, thus casting doubt on the present stratigraphic classification according to the South African Committee for Stratigraphy (1980) which is, for the most part, based on tectonic and metamorphic considerations. Geochemical and U-Pb studies have shown that the Weener and Piksteel Intrusive Suites intruded the Rehoboth area during the Eburnian orogeny, between about 2.0 Ga and 1.8 Ga, and that these magmas, which all show calc-alkaline characteristics, were probably generated in a collisional tectonic environment. At about 1.4 Ga the Alberta Mafic Complex and related intrusives were emplaced in the northern parts of the Rehoboth Basement Inlier. This was followed between 1.25 and 1.0 Ga by the intrusion of the members of the Gamsberg Granite Suite and related rhyolitic dykes causing strong hydrothermal alteration of the major part of the intruded rock sequence. These magmas could be characterised by the geochemical analyses of this study as being of calc-alkaline composition. The strong hydrothermal alteration of the country rock by the Gamsberg magmatism could be verified by numerous Rb-Sr analyses of samples taken from the intruded rock sequence; the age of the Gamsberg-related rhyolitic dykes was determined by the U-Pb method. The use of the Rb-Sr method and geochemical analyses allowed description of the high-potassium rhyolites of the Nueckopf Formation which formed at about 950 Ma during the final stages of Gamsberg magmatism. About 130 Ma later, at approximately 820 Ma, the whole area of the Rehoboth Basement Inlier was intruded by swarms of basic dykes in a diverging tectonic regime in directions paralleling the Areb shear zone (a major tectonic lineament crosscutting the Rehoboth Basement Inlier in a southwest-northeast direction) as may be deduced from Rb-Sr and geochemical studies on samples from these basic dykes.

Numerous K-Ar age determinations on biotites, white mica and sericite, carried out during this study, have shown that the compressional phase of the Damara orogeny to the north of the Rehoboth Basement Inlier led to metamorphic conditions (300°C) in the northern part of the inlier, capable of resetting the K-Ar systems of biotites and white micas; south of 23° 55'S they were not strong enough to completely reset the K-Ar systems of biotites. The Rehoboth Basement Inlier must therefore have been overridden by nappes of the Damara Orogen, as may be deduced from the previously known Damaran ages of micas from the Namib Naukluft Nappe Complex. After the Damara orogeny, the Rehoboth Inlier was affected by the break-up of Gondwana, which resulted in the opening of the South Atlantic and the reactivation of the Areb shear zone. This is indicated by K-Ar analyses of samples of the Mooirivier Complex and the Elim Formation collected along the Areb shear zone, which show the partial rejuvenation of biotite and white mica separates. These samples currently yield apparent ages of 315 Ma to 427 Ma.

CONTENTS

1. ORGANISATION AND STRATEGY OF THE STUDY 1
1.1 ORGANISATION 1
1.2 OBJECTIVES 1
1.3 ACKNOWLEDGEMENTS 1

2. REGIONAL GEOLOGY 3
2.1 AREA OF INVESTIGATION 4

3. RECONNAISSANCE STUDY ON THE GEOCHEMISTRY OF THE REHOBOTH BASEMENT GRANITOIDS 9
3.1 INTRODUCTION 9
3.2 LITHOLOGY AND FIELD RELATIONS 9
3.2.1 Gamsberg Granite Suite 9
3.2.2 Piksteel Intrusive Suite 9
3.2.3 Weener Intrusive Suite 9
3.3 WHOLE ROCK MAJOR AND TRACE ELEMENT GEOCHEMISTRY 10
3.3.1 Gamsberg Granite Suite 10
3.3.2 Piksteel Intrusive Suite 10
3.3.3 Weener Intrusive Suite 12
3.3.4 Summary 12
3.4 REE GEOCHEMISTRY OF SELECTED GRANITOID SAMPLES 16
3.4.1 Introduction 16
3.4.2 Discussion of the obtained Ree patterns 16
3.4.3 Summary 17

4. MOOIRIVIER COMPLEX 19
4.1 INTRODUCTION 19
4.2 SAMPLE COLLECTION AND DESCRIPTION 19
4.3 DISCUSSION OF THE ANALYTICAL RESULTS 20
4.3.1 Geochemistry 20
4.3.2 K-Ar analyses 21
4.3.3 Rb-Sr analyses 22
4.4 CONCLUSIONS 23

5. NEUHOF FORMATION 25
5.1 INTRODUCTION 25
5.2 SAMPLE COLLECTION AND DESCRIPTION 25
5.3 RESUlTS 26
5.3.1 Geochemistry 26
5.3.2 Rb-Sr analyses 27
5.4 CONCLUSIONS 29

6. ELIM FORMATION 31
6.1 INTRODUCTION 31
6.2 SAMPLE COLLECTION AND DESCRIPTION 31
6.3 RESULTS 33
6.3.1 Geochemistry 33
6.3.2 K-Ar analyses 34
6.3.3 Rb-Sr analyses 36
6.4 CONCLUSIONS 37

7. MARIENHOF AND BILLSTEIN FORMATIONS 39
7.1 INTRODUCTION 39
7.1.1 Marienhof Formation 39
7.1.2 Billstein Formation 40
7.2 SAMPLE COLLECTION AND PREPARATION 40
7.3 DISCUSSION OF THE ANALYTICAL RESULTS 41
7.3.1 Marienhof Formation 41
7.3.2 Billstein Formation 42
7.4 CONCLUSIONS 42

8. PIKSTEEL INTRUSIVE SUITE 43
8.1 INTRODUCTION 43
8.2 SAMPLE COLLECTION AND DESCRIPTION 43
8.3 DISCUSSION OF THE ANALYTICAL RESULTS 45
8.3.1 Some additional geochemical considerations regarding the Piksteel Intrusive Suite 45
8.3.2 K-Ar analyses 46
8.3.3 Rb-Sr analyses 47
8.3.4 U-Pb analyses 53
8.4 CONCLUSIONS 53

9. NUECKOPF FORMATION AND OTHER ACID VOLCANICS 55
9.1 INTRODUCTION 55
9.2 SAMPLE COLLECTION AND DESCRIPTION 55
9.3 DISCUSSION OF THE ANALYTICAL RESULTS 56

9.3.1 Geochemishy 56
9.3.2 Rb-Sr analyses 57
9.3.3 U-Pb analyses 58
9.4 CONCLUSIONS....59

10. BASIC DYKES CROSSCUTTING THE REHOBOTH BASEMENT INLIER....61
10.1 INTRODUCTION 61
10.2 SAMPLE COLLECTION AND DESCRIPTION ..61
10.3 DISCUSSION OF THE ANALYTICAL RESULTS 62
10.3.1 Geochemistry....62
10.3.2 K-Ar results 62
10.3.3 Rb-Sr analyses 63
10.4 CONCLUSIONS....63

11. SM-ND DATING OF THE REHOBOTH BASEMENT INLIER AND ITS IMPLICATIONS FOR THE REGIONAL GEOLOGY....65
11.1 INTRODUCTION 65
11.2 SM-ND ISOTOPE SYSTEMATICS....65
11.3 RB-SR, U-PB AND K-AR ISOTOPE SYSTEMATICS....68
11.4 DISCUSSION 68
11.4.1 The Sm-Nd ages 68
11.4.2 The model ages 69
11.4.3 εNd - εSr studies 70
11.4.4 Regional interpretation of the obtained results 72
11.5 CONCLUSIONS....72

12. SYNTHESIS 73
12.1 GEOCHEMISTRY....73
12.1.1 Granitoids 73
12.1.2 Amphibolites 73
12.1.3 Acid volcanics 74
12.1.4 Basic dykes....74
12.1.5 Metasediments....74
12.2 AGE DETERMINATIONS....74
12.2.1 Sm-Nd dating 74
12.2.2 U-Pb dating 75
12.2.3 Rb-Sr dating 75
12.2.4 K-Ar dating 76
12.3 DISCUSSION OF THE SIGNIFICANCE AND LIMITATIONS OF THE APPLIED ISOTOPIC DATING TECHNIQUES 76
12.4 SHORT SUMMARY OF THE GEOLOGICAL HISTORY OF THE REHOBOTH BASEMENT INLIER .... (BASED ON THE RESULTS OF THIS STUDY) .77

REFERENCES....79

APPENDIX....83
ANALYTICAL TECHNIQUES
1. SAMPLE PREPARATION 83
2. WHOLE-ROCK ANALYSES 83
2.1 K-AR METHOD....83
2.2 RB-SR METHOD....84
2.3 U-PB METHOD 84
2.4 SM-ND METHOD....85

APPENDIX: TABLES....87

1. ORGANISATION AND STRATEGY OF THE STUDY

1.1 ORGANISATION

This study was a University Research Project funded by the Geological Survey of Namibia.

The then director of the Geological Survey of Namibia, Dr R. McG. Miller, guided the field work in Namibia while the whole project was carried out under the supervision of Prof. E. Jaeger of the University of Berne, Switzerland.

Field work and primary sample preparation were carried out during two field seasons in Namibia, between NovembeR1986 and June 1988.

One hundred and four whole-rock samples were collected for age determinations. A total of 98 samples were collected for geochemical analyses in the Weener and Piksteel Intrusive Suites and in the Gamsberg Granite Suite as a base for a reconnaissance survey on the geochemistry of the Rehoboth granitoids. The relatively uncertain lithostratigraphic classification of several outcrops in the Rehoboth area, due to the reconnaissance character of the maps of the Geological Survey on which this study was based, may in some cases have led to a doubtful classification of some of our samples.

Samples containing biotites or white micas suitable for K-Ar determinations were collected from various formations at scattered localities throughout the Rehoboth Basement Inlier in order to show the southwards-diminishing influence of the Damaran orogenesis and to give a better location of the Damaran biotite isograd of Ahrendt *et al.* (1977) crosscutting the inlier. Dating of the latest activities of the Areb shear zone was attempted by the K-Ar analyses of phyllites and mica schists of the Mooirivier Complex and the Elim and Marienhof Formations collected in the vicinity of the shear zone. The dating of contact metamorphic white micas of the Elim Formation collected on the farms Morgenroth and Witkrans should furthermore provide a minimum age for the magmatic activity in this area.

With the exception of the mica schists and phyllites of the Marienhof and Billstein Formations, the Rb and Sr systematics of all the collected samples were studied in order to produce isochron ages, which were expected at least partially to reflect the ages of the formations analysed.

The dating of zircon separates of three plutons of the Piksteel Intrusive Suite should provide intrusion ages for the Piksteel Suite and thus give a minimum age for the Rehoboth Sequence and underlying rocks. Furthermore it was attempted to obtain a minimum age for the Marienhof Formation by the dating of two rhyolitic dykes crosscutting the formation.

The analyses of the Sm-Nd systematics of several whole-rock samples from various formations should provide a maximum age for the formation of the Rehoboth crust and should thus narrow the time span during which the volcano sedimentary sequences and older intrusives of the Rehoboth basement were formed.

The collecting of the samples in Namibia and their preparation in both Windhoek and Berne was shared by the authors. Potassium analyses and the Rb-Sr laboratory work were carried out by U. Ziegler with the kind help of Mr M. Giger and Mrs Hebeisen. The mass spectrometric determination of the Ar, Rb and Sr concentrations, as well as the isotopic composition of Sr, were done by both authors. F. Stoessel was responsible for zircon separation and for the subsequent U-Pb determinations of these separates. U. Ziegler introduced the Sm-Nd technique of dating to the KAW laboratory in Berne with the kind assistance of Dr M. Flisch and O. Krebs. All the laboratory and mass spectrometric work carried out in connection with the Sm-Nd determinations was performed by U. Ziegler, who also created the computer programme for the processing of Sm-Nd data.

1.2 OBJECTIVES

The aim of this study is to elucidate the geological evolution of the Rehoboth Basement Inlier by means of geochemical and isotopic analyses, in order to improve the understanding of the pre-Damaran basement of Namibia. The following crucial questions were of primary interest in order to unravel the unknown parts of the history of the Rehoboth area:

- When did the continental crust of the Rehoboth area start to form and to consolidate ?
- Are there any indications of Archaean rocks in the area?
- Can genetic relationships in the Rehoboth granitoids be observed by means of geochemical investigations?
- Is it possible to date the formation ages of the individual formations, and are the results obtained in agreement with the stratigraphic classification of the analysed formations on the internal maps of the Geological Survey in Windhoek, and are the results of this study consistent with the results of previous workers?
- Are there any datable pre-Damaran tectonothermal events in the Rehoboth Basement Inlier?
- What is the influence of the Damara orogeny, the Karoo period and the final break-up of Gondwana on the Rehoboth Basement Inlier?
- When was the Areb shear zone, crosscutting the Rehoboth inlier, active?

In order to answer these questions it was initially necessary to introduce the Sm-Nd method of dating from scratch at the Laboratory for Isotope Geology in Berne and to write a computer programme for the processing of the expected U-Pb data.

1.3 ACKNOWLEDGEMENTS

This joint-venture project of the University of Berne and the Geological Survey of Namibia would not have been possible without the help of many people.

First of all we wish to thank our supervisor Professor E. Jaeger of the Laboratory for Isotope Geology in Berne for initiating the project and for her ongoing encouragement and critical comment. The logistic and financial support of the Geological Survey of Namibia is gratefully acknowl-

edged as is the help of the previous Director, Dr R. McG. Miller. Dr K. Schalk, Dr R..McG. Miller, Dr B. Hoal, B. Bulley and K. H. Hoffmann are thanked for the introductory field trip to the Rehoboth Basement Inlier, for many hints and helpful discussions and for critically reviewing the annual reports submitted to the Geological Survey.

Dr M. Flisch, O. Krebs and M. Brunner are thanked for their help in installing the Sm-Nd method of dating at our laboratory in Berne and the "Schweizerischer Nationalfonds" for providing funds for the installation. Dr U. Schaltegger is thanked for introducing us to the U-Pb method of dating and for keeping the U-Pb laboratory section going. M. Giger, I. Hebeisen, W. Munardi and H. Oschidari are thanked for their help in the Rb-Sr laboratory. Dr M. Flisch, R. Kraehenbuhl, M. Soom and Dr U. Schaltegger kindly introduced us to the K-Ar method of dating.

Dr Kraehenbuhl of the Institute for Anorganic Chemistry at the University of Berne is thanked for carrying out neutron activation analyses on several granitoid samples, while Dr I. Mercolli, Dr Galetti and D. Vuichard at the University of Fribourg, Switzerland and at the Eidgenoessische Forschungsanstalt Liebenfeld, Berne, Switzerland, are thanked for their help in producing the x-ray fluorescence data for this study.

This project also benefited from discussions with students and staff at the Laboratory for Isotope Geology in Berne, especially A. Buergi, Dr I. Michalski, M. Huegi, D. Baltzer, B. Mueller, U. Haudenschild, U. Kloetzli, F. Bednar, K. Howald and L. Rytz. Dr A. v. Quadt and K. Wenger-Schenk of the Eidgenoessische Technische Hochschule in Zurich provided valuable assistance in the installation of the Sm-Nd technology in Berne.

We would also like to thank Conny Stremming, J. Hintz, Peter, Margit and Sigrid for hosting us during our stays in Windhoek.

Last but not least we wish gratefully to acknowledge our parents, Barbara Stampbach and her parents and Angela Ceresa for their encouragement, patience, interest and support throughout this project.

2. REGIONAL GEOLOGY

The geology of Namibia can be subdivided into five phases of lithogenic activity, according to the Geological Survey of Namibia (1982). The structural framework of the country was defined by at least three major phases of tectonism recognisable in various regions. The older two Eburnian (1/- 2000 Ma) and Kibaran (1400 Ma - 900 Ma) phases of Porada (1979) may, according to Almeida *et al.* (1976), be correlated with the Transamazonian and Uruacuano tectonism in South America. The youngest phase of orogenic activity, the Damara orogeny which belongs to the pan-African event (Martin and Porada, 1977; Fig. 2.1), affected the central and northwestern parts of the country. Remnants of the older orogens of Namibia today only crop out as so-called Basement Inliers within rocks of the Damara Sequence such as the Kamanjab and Rehoboth Basement Inliers and along the escarpments paralleling the Atlantic coast. The interior northern and southern parts of the country are, for the most part covered by rocks coeval with the Damara Sequence and by rocks of the Nama Group, which is considered to have been deposited contemporaneously with parts of the Damara Sequence (SACS, 1980). These formation,s are partly overlain by the

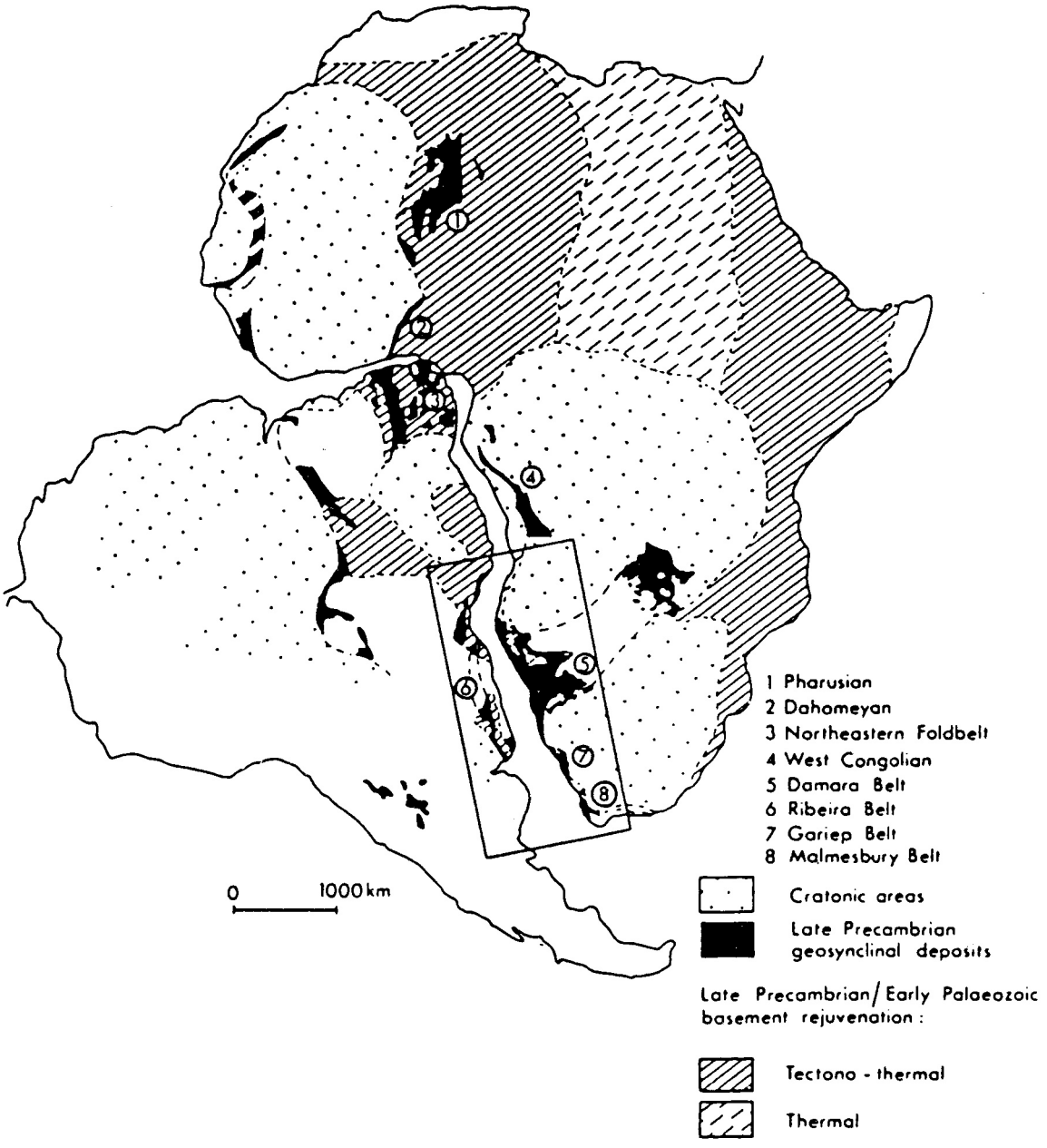

Figure 2.1: Late Precambrian to early Palaeozoic geosynclines and basement rejuvenation in Africa and South America (after Porada, 1979)

Karoo Sequence and by Tertiary sediments of the Kalahari Group. Several post-Karoo intrusive complexes and kimberlites intruded the country between the Cretaceous and the Quaternary. The aeolian and fluviatile sands of the Namib desert were deposited between Tertiary and recent times.

2.1 AREA OF INVESTIGATION

The area of investigation is situated about 80 km south of Windhoek between 23°S and 25°S and between 16°E and 18°E in the central part of Namibia where it forms the southern most inlier of pre-Namibian basement rocks in the Damara Sequence (Fig. 2.2). This Rehoboth Basement Inlier, which was named after the capital of the Rehoboth District, forms an elongate southwest-northeast-trending body with a maximum width of approximately 50 km. Towards the southwest of the area the inlier changes its trend to a more southerly direction, continuing into the Sinclair area as far south as 26°S along the big escarpment separating the Namib desert from the more fertile central parts of the country.

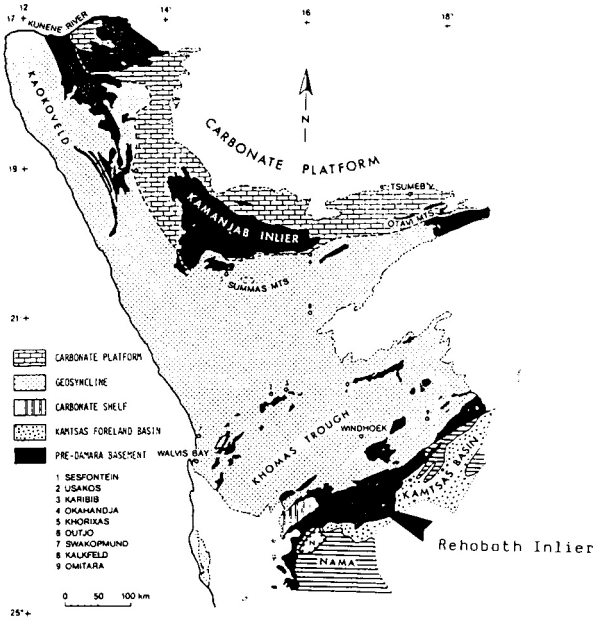

Figure 2.2: Main facies areas of the Damara Orogen (Martin, 1983)

Towards the north, the Rehoboth Basement Inlier is limited by the Southern Marginal Zone of the Damara Orogen while its southern border is indicated by the occurrence of the platform sediments of the Nama Group (Fig. 2.3). The Naukluft Nappe Complex composed of sediments of the Damara Sequence, today rests on Nama sediments with a tectonic contact, indicating a partial override of the Rehoboth Inlier by derivates of the southern zones of the Damara Orogen during orogenesis. The inlier is crosscut by a major shear zone, the Areb mylonite or Areb shear zone (AM on Fig. 2.3), which, according to Schulze-Hulbe (1979), possibly formed during the early Proterozoic and was probably reactivated during the pan-African movements of the south African crust.

The outcrops of basement rocks to the east and south of the Rehoboth Basement Inlier in western Botswana and in the Sinclair area, respectively (Fig. 2.4), are often grouped together with the rocks of the Rehoboth area in the Rehoboth Magmatic Arc (Watters, 1978). This arc, which possibly forms an extension of the Irumide Belt and/or the Eburnian event of the Limpopo Belt, extends for about 1200 km and has a maximum width of about 150 km.

Geological investigations in the area south of Windhoek, including the Rehoboth area, began in 1887 with the observations of Stapff (1887). Between 1891 and 1904 a limited reconnaissance of the area was undertaken by Gurich (1891-92), Stromer von Reichenbach (1896), and Voit and Stollreither (1904). The first detailed survey in the Rehoboth district was done by E. Rimann during the years 1910-1915 (Rimann, 1915). This study was followed by basic geological mapping by De Kock during 1930-31 (De Kock, 1934). Interest in the geology of the Rehoboth area was aroused during the thirties with the discovery of the Rehoboth goldfields which were mined during this period, before exploitation came to a standstill due to low profitability. Not until the early sixties was a mapping project, still in progress, of the Rehoboth area begun by the Geological Survey of Namibia in Windhoek under the supervision of Dr R. McG. Miller and Dr K. Schalk on a scale of 1:50000 and 1:1 000 000. Several internal reports have resulted from this project (Schalk, 1961, 1967, 1970, 1975: Schalk and Haelbich, 1965). Meanwhile, Martin (1965) published a general overview on the Precambrian of South West Africa, De Waal (1966) carried out a detailed study of the Alberta Mafic Complex and Handley (1965) described the lithological succession of the area of the farm Klein Aub.

Somewhat later, the geology of the bordering area between the Rehoboth Inlier and the Damara Orogen was investigated by Haelbich (1970) while the exhalative-sedimentary Zn-Cu mineralisation of the Kobos mine was investigated by Brewitz (1974). Several radiometric age determinations by the U-Pb, K-Ar, ^{40}Ar-^{39}Ar, and Rb-Sr methods have been conducted during the past two decades by various workers (Hugo *et al.*, 1971-72; Ahrendt *et al.,* 1977; Burger *et al.*, 1973, 1973-74, 1975-76a and b. 1977-78, 1980; Mailing, 1978; Seifert, 1986; Reid *et al.*, 1988; this study) in order to establish a stratigraphy for the Rehoboth Basement Inlier.

All these investigations culminated in the present unpublished 1:50 000 and 1:250 000 maps of the Rehoboth area which served as a base for this study.

The lithology of the Rehoboth area can roughly be subdivided into the units according to the 1: 1 000 000 geological map of Namibia (1980 edition) as shown in Figure 2.5.

The Klein Aub Formation regarded as the uppermost formation of the Rehoboth Inlier consists of quartzites, slates, conglomerates and some limestone (Schalk. 1970). It is underlain by the volcano sedimentary Doornpoort and Grauwater Formations comprising felsic basaltic volcanics interlayered with quartzites, conglomerates and slates (Schalk. 1970). The Nueckopf porphyries and ignimbrites

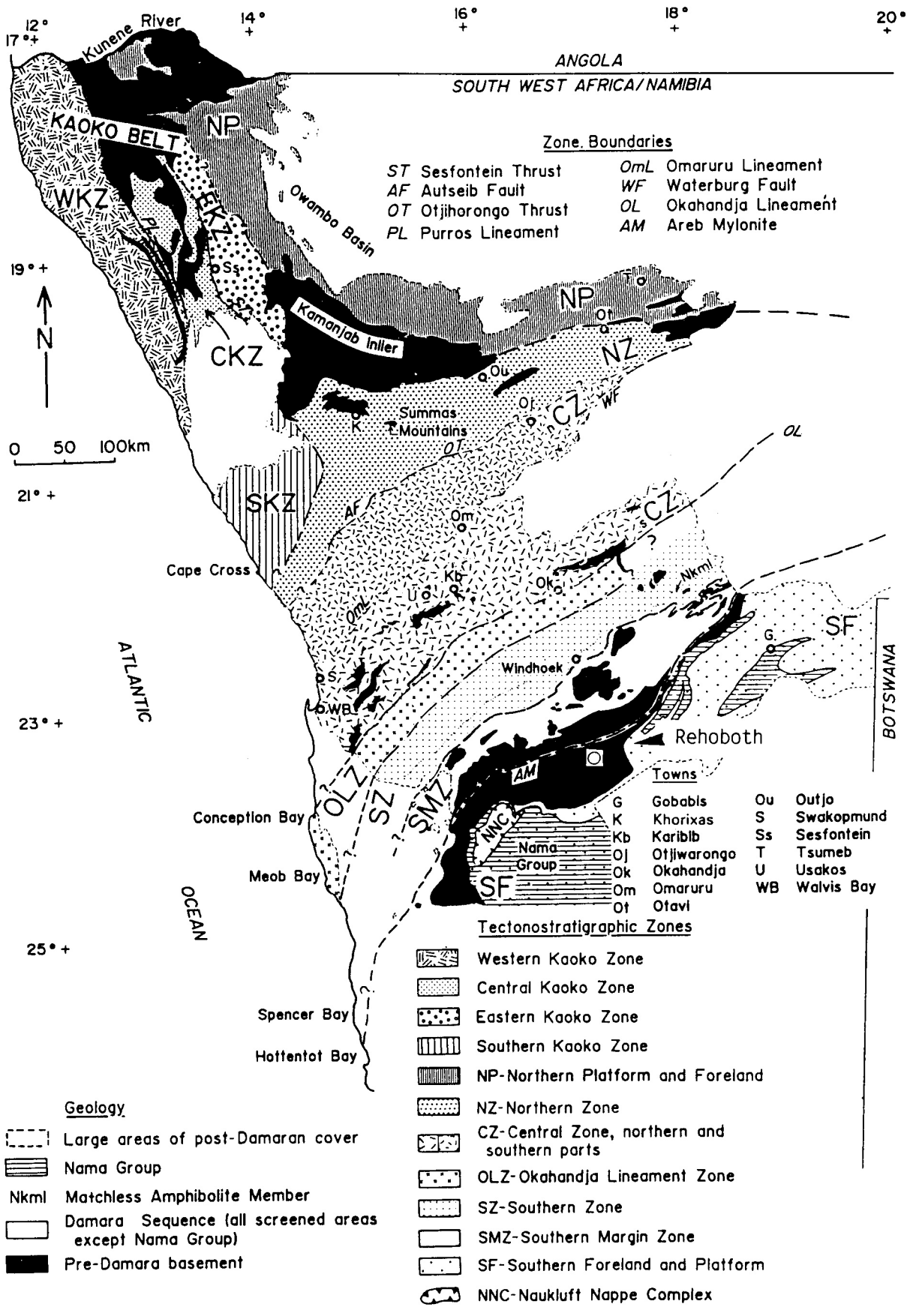

Figure 2.3: Tectonostratigraphic zones of the Damara Orogen (Miller, 1983)

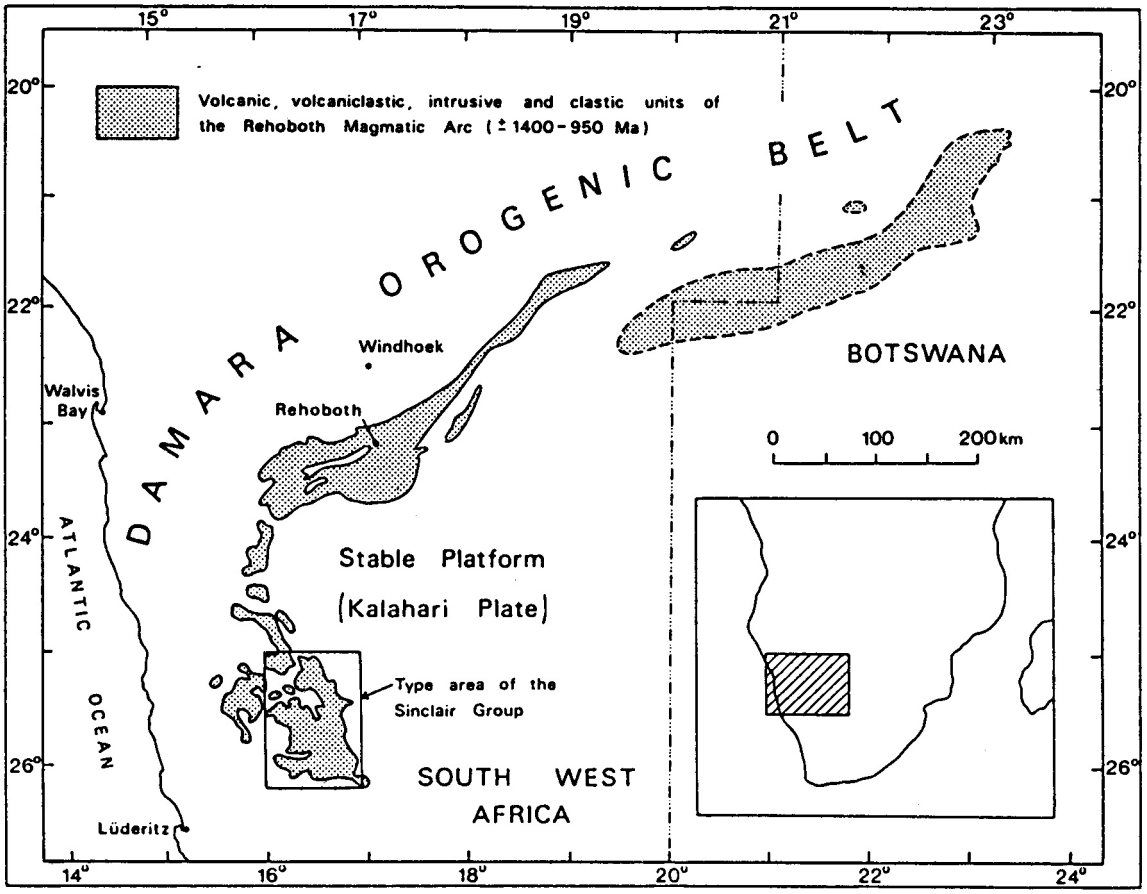

Figure 2.4: The Rehoboth Magmatic Arc in Namibia and western Botswana (after Watters, 1978)

form the lower part of the Grauwater Formation. According to Schalk (1970) all these formations, including the Nueckopf volcanics, are believed to be equivalents of the Sinclair Sequence in the Witvlei-Rehoboth area. The underlying Rehoboth Sequence is divided into the Gaub Valley, Billstein, and Marienhof Formations which largely consist of low- to medium-grade metamorphosed quartzites, mica schists, some phyllites and minor amounts of conglomerates, and of acid to basic volcanics. The base of the Rehoboth Sequence is formed by the low- to medium-grade metamorphosed Elim Formation, composed of quartzites, mica schists, greenschists and minor amounts of amphibolites, calc-silicates and metarhyolites. The oldest parts of the inlier belong to the Neuhof Formation and to the underlying Mooirivier Complex, both of which were metamorphosed under medium- to high-grade conditions. The Mooirivier Complex consists of migmatitic gneisses, amphibolites, quartzites and schists while the Neuhof Formation is composed of metamorphosed acid and basic volcanic rocks, mica schists, green schists, conglomerates and impure marbles.

The Rehoboth Inlier as a whole is intruded by various kinds of acid and basic magmas such as the Weener Quartz Diorite, the Piksteel Intrusive Suite, the Gamsberg Granite Suite and various kinds of acid and basic dykes. Depending on their local position, these intrusives have been partly altered and in various cases even metamorphosed under low-grade metamorphic conditions, due to events such as the intrusion of younger magmas of the same sequence, the Damara orogeny and tectonic activity along the Areb shear zone. The dating of these intrusives by means of radiometric age determinations by Burger *et al.* (1973,1973-74, 1975-76a and b, 1977-78, 1980), Mailing (1978), Seifert (1986), Reid *et al.* (1988) and by us has provided a framework for the cognition of the evolution of the Rehoboth Basement Inlier through the Precambrian and the Palaeozoic. Prior to this study the age of the Weener Intrusives was assumed to be about 1870 Ma (Seifert, 1986), while the age of the Piksteel Intrusive Suite was estimated to range between 1050 and 1750 Ma (Reid *et al.*, 1988; Burger *et al.*, 1975-76). The age of the Alberta Complex was assumed to be about 1440 Ma (Reid *et al.*, 1988), while the age of the Gamsberg Granite Suite was estimated to range between 950 and 1200 Ma (Seifert, 1986; Reid *et al.*, 1988; Burger *et al.*, 1973-74, 1974-75, 1975-76a and b). The age of the basic dykes occurring throughout the Rehoboth area was indicated to be approximately 1030 Ma (Reid *et al.*, 1988).

Figure 2.5 (right): Lithostratigraphy of the Mokolian Era (Legend of the 1:1 000 000 geological map of Namibia, 1980

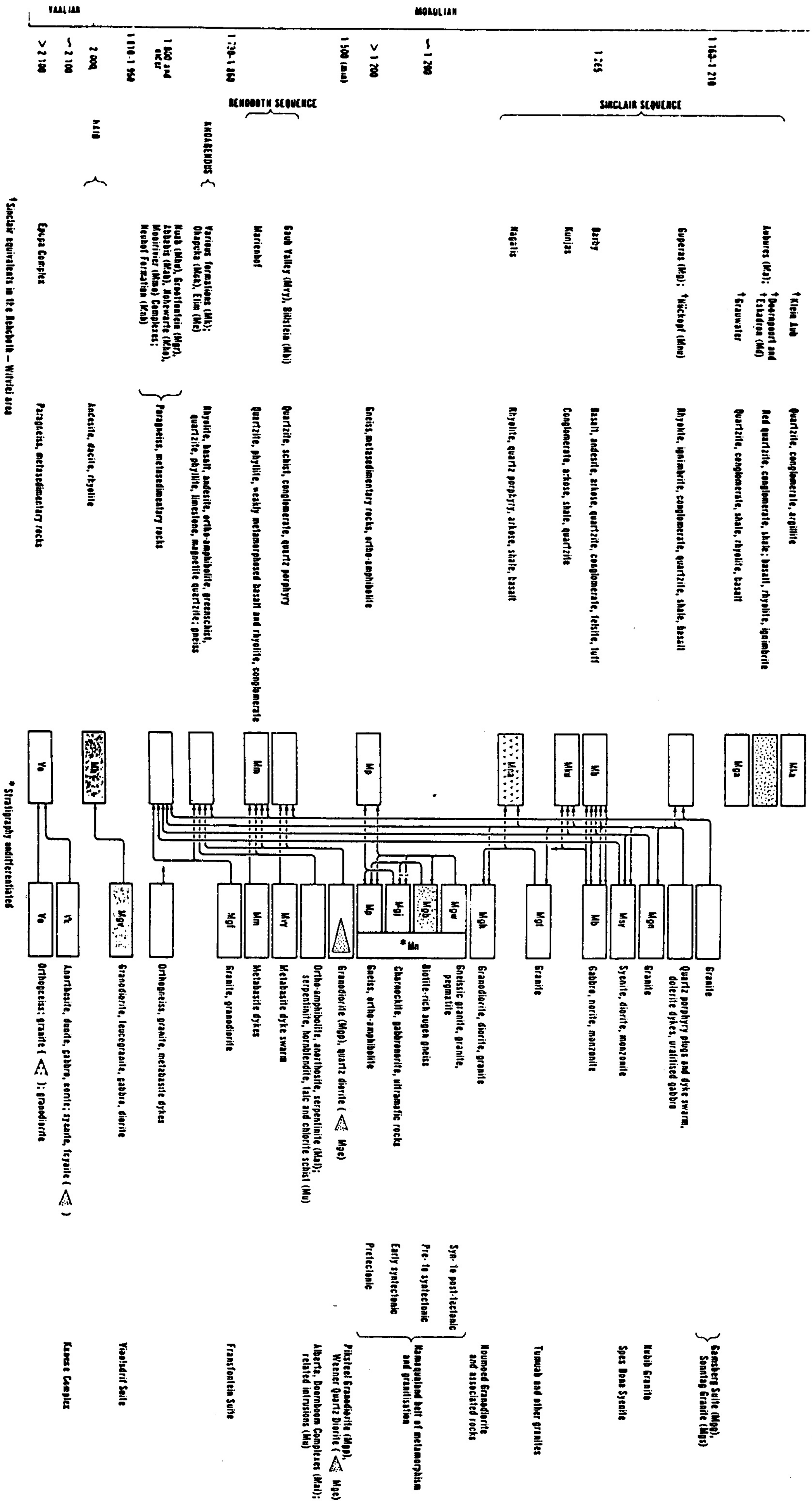
VAALIAN
MOKOLIAN
1 163-1 210
1 265
~ 1 200
> 1 200
1 500 (min)
1 730-1 860
1 800 and older
1 810-1 950
2 000
~ 2 100
> 2 100
SINCLAIR SEQUENCE
REHOBOTH SEQUENCE
KHOABENDUS
HAIB
†Klein Aub
Auborus (Ma): †Doornpoort and †Eskadron (Md)
†Grauwater
Guperas (Mg): †Nückopf (Mnu)
Barby
Kunjas
Nagatis
Gaub Valley (Mvy), Billstein (Mbi)
Marienhof
Various formations (Mk); Okapuka (Mok), Elim (Me)
Nuab (Mhu), Grootfontein (Mgr), Abbabis (Mab), Hohewarte (Mho), Mooirivier (Mmo) Complexes; Neuhof Formation (Mnh)
Epupa Complex
Quartzite, conglomerate, argillite
Red quartzite, conglomerate, shale; basalt, rhyolite, ignimbrite
Quartzite, conglomerate, shale, rhyolite, basalt
Rhyolite, ignimbrite, conglomerate, quartzite, shale, basalt
Basalt, andesite, arkose, quartzite, conglomerate, felsite, tuff
Conglomerate, arkose, shale, quartzite
Rhyolite, quartz porphyry, arkose, shale, basalt
Gneiss, metasedimentary rocks, ortho-amphibolite
Quartzite, schist, conglomerate, quartz porphyry
Quartzite, phyllite, weakly metamorphosed basalt and rhyolite, conglomerate
Rhyolite, basalt, andesite, ortho-amphibolite, greenschist, quartzite, phyllite, limestone, magnetite quartzite; gneiss
Paragneiss, metasedimentary rocks
Andesite, dacite, rhyolite
Paragneiss, metasedimentary rocks
†Sinclair equivalents in the Rehoboth – Witvlei area
Mka
Mga
Mb
Mku
Mna
Mp
Mm
Mhr
Ve
Mgn
Msy
Mgt
Mgh
Mgw
Mgb
Mgj
*Mn
Mvy
Mgf
Mgv
Vk
Granite
Quartz porphyry plugs and dyke swarm, dolerite dykes, uralitised gabbro
Granite
Syenite, diorite, monzonite
Gabbro, norite, monzonite
Granite
Granodiorite, diorite, granite
Gneissic granite, granite, pegmatite
Biotite-rich augen gneiss
Charnockite, gabbronorite, ultramafic rocks
Gneiss, ortho-amphibolite
Granodiorite (Mgp), quartz diorite (Mge)
Ortho-amphibolite, anorthosite, serpentinite (Mal); serpentinite, hornblendite, talc and chlorite schist (Mu)
Metabasite dyke swarm
Metabasite dykes
Granite, granodiorite
Orthogneiss, granite, metabasite dykes
Granodiorite, leucogranite, gabbro, diorite
Anorthosite, dunite, gabbro, norite; syenite, fayalite ( )
Orthogneiss; granite ( ); granodiorite
* Stratigraphy undifferentiated
Syn- to post-tectonic
Pre- to syntectonic
Early syntectonic
Pretectonic
Gamsberg Suite (Mgg), Sonntag Granite (Mgs)
Kubib Granite
Spes Bona Syenite
Tumuab and other granites
Noumoed Granodiorite and associated rocks
Namaqualand belt of metamorphism and granitisation
Piksteel Granodiorite (Mgp), Weener Quartz Diorite (Mge)
Alberta, Doornboom Complexes (Mal); related intrusions (Mu)
Fransfontein Suite
Vioolsdrif Suite
Kunene Complex

3. RECONNAISSANCE STUDY ON THE GEOCHEMISTRY OF THE REHOBOTH BASEMENT GRANITOIDS

3.1 INTRODUCTION

The large bodies of intrusive granitoids underlying the Rehoboth area of Namibia were first investigated by De Kock (1934). He described these granitoids as granites, diorites, quartz diorites and quartz porphyries which were derived from a common magma source. De Waal (1966) distinguished between the Nauchas Granite Suite, comprised of the Gamsberg, Piksteel, Koepel and Korabis granites, a green granodiorite, and the Weener Quartz Diorite. SACS (1980) renamed De Waal's (1966) Nauchas Granite Suite the "Gamsberg Granite Suite", but excluded the Piksteel Granodiorite which was believed to belong to an earlier magmatic event.

The aim of this geochemical reconnaissance study on the Rehoboth Basement granitoids is to provide a general fundamental knowledge of their geochemical relationships and to investigate the possibility of a further subdivision by means of geochemical properties. In order to cover the whole area of the Rehoboth Inlier we collected a total of at least four geochemistry samples in the 25 largest granitoid plutons occurring in the approximately 15 000 km^2 Rehoboth area. It is clear that this part of the study can only provide a very basic impression of the complex genetic relationships of the Rehoboth granitoids and that great care must be taken not to over interpret the results obtained. Some more precise information was gained on three plutons of the Piksteel Intrusive Suite which were included in the isotope studies. In Chapter 8 the results of these analyses are discussed and compared with the results of this chapter.

3.2 LITHOLOGY AND FIELD RELATIONS

3.2.1 Gamsberg Granite Suite

The Gamsberg Granite Suite is predominantly made up of large plutons which have intruded both metavolcano-sedimentary formations, namely the Mooirivier, Neuhof, Elim, Marienhof, Gaub Valley, Nueckopf and Grauwater Formations, and older granitoids, such as the Piksteel and the Weener Intrusive Suites. Smaller plutons of the Gamsberg Granite Suite are irregularly distributed throughout the Rehoboth area.

U-Pb and Rb-Sr age determinations of the Gamsberg Granite Suite yielded a range of ages between 1079 Ma and 1222 Ma (Reid *et al.*, 1988; Seifert, 1986 and 1986a; Burger *et al.*, 1973, 1973-74, 1975-76), while Nueckopf volcanics yielded ages between 1080 Ma and 1232 Ma (Burger *et al.*, 1973, 1973-74, 1975-76) which are consistent with the results of this study (see Chapter 8).

Granites of the Gamsberg Granite Suite are typically greyish to reddish in colour, mostly medium- to coarse-grained and occasionally porphyritic. These granites further exhibit moderate alteration and saussuritisation, sometimes with significant growth of muscovite and epidote. In the northern parts of the area, towards the southern margin of the Damara Orogen, the granites may develop a strong foliation together with widespread albitisation of plagioclase and recrystallisation of quartz.

3.2.2 Piksteel Intrusive Suite

In this memoir the term "Piksteel Intrusive Suite", is preferred to the term "Piksteel Granodiorite" which was introduced by SACS (1980), since this unit comprises not only granodiorites but also extensive granites and tonalites. Rocks of the Piksteel Intrusive Suite, first described by De Waal (1966), occur throughout the Rehoboth basement area and have intruded the Weener Intrusive Suite as well as the Mooirivier, Neuhof, Elim, Marienhof and Gaub Valley Formations. These granitoids have in turn been intruded by plutons of the Gamsberg Granite Suite. U-Pb age determinations range between 986 Ma and 1784 Ma (Burger *et al.*, 1973-74, 1975-76; Burger and Walraven, 1977-78; this study), while Rb-Sr isochrons for members of the Piksteel Intrusive Suite yielded ages between 1057 Ma and 1725 Ma (Mailing, 1978; Reid *et al.*, 1988; Seifert, 1986; this study).

Granitoids of the Piksteel Intrusive Suite are mostly greyish to greenish in colour, fine- to medium-grained and often porphyritic. They show wide compositional variation from granite through granodiorite to tonalite. In contrast to the Gamsberg Granite Suite these granitoids exhibit widespread and pervasive saussuritisation. A strong foliation, sometimes shear-related, is developed in the northern and eastern parts of the Rehoboth basement.

3.2.3 Weener Intrusive Suite

Tonalites, quartz diorites, diorites and granodiorites of the "Weener Intrusive Suite", previously termed the "Weener Quartz Diorite" (SACS, 1980), were first described by De Waal (1966). The granitoids of the Weener Intrusive Suite are confined to the western part of the Rehoboth area where they have intruded the Mooirivier, Elim and Gaub Valley Formations and have in turn been intruded by rocks of the Piksteel Intrusive Suite. Rb-Sr age determinations of the Weener Intrusive Suite by Reid *et al.* (1988) and Seifert (1986) yielded reference ages between 1206 Ma and 1871 Ma, respectively. The fine- to medium-grained rocks of the Weener Intrusive Suite are generally greyish to brownish in colour. Besides plagioclase, quartz, biotite and minor amounts of potassium feldspar, the occurrence of bluish amphiboles is distinctive. Accessory minerals include muscovite, sphene, opaque minerals, epidote, clinozoisite, garnet, apatite, chloritoid and chlorite (after biotite). As in the Gamsberg Granite Suite and Piksteel Intrusive Suite, the granitoids of the Weener Intrusive Suite are locally strongly sheared and folded.

3.3 WHOLE ROCK MAJOR AND TRACE ELEMENT GEOCHEMISTRY

3.3.1 Gamsberg Granite Suite

The relatively linear patterns obtained in the Harker variation diagrams (Fig. 3.1) probably reflect original magmatic processes and suggest that the effect of post-cooling alteration was minimal. Data for 55 samples were plotted on the R1 versus R2 diagram of De La Roche *et al.* (1980) in order to chemically classify members of this suite (Fig. 3.2). The vast majority of the data points fall within the "granite" field with only a slight scatter of data points in the "alkaline granite" and "granodiorite" fields. According to Shand (1927) and Chappell and White (1974), the degree of alumina saturation allows a first-order classification of granitoids. Accordingly, the data were plotted on a wt% Al_2O_3-CaO-(Na_2O+K_2O) ternary diagram (Fig. 3.3), which illustrates that all samples have Al_2O_3 greater than (Na_2O+K_2O+CaO) and can, therefore, be classified as peraluminous. The generally high degree of alumina saturation for most of the Gamsberg granitoids is further illustrated in the mol.% Al_2O_3 versus mol.% (CaO+Na_2O+K_2O) diagram (Fig. 3.4) where the ratio A/CNK exceeds unity. However, the degree of alumina saturation is insufficient to classify these granitoids as S-type granites according to Chappell and White (1974) since the A/CNK ratio is generally less than 1.1. On an AFM diagram of Kuno (1968) the data points of the Gamsberg Granite Suite clearly define a calc-alkaline trend (Fig. 3.16). In the tectonic discriminant diagram of Pearce *et al.* (1984), whose limitations, according to Wilcox (1979), have to be borne in mind, the relatively low Rb, Nb and Y contents of these granitoids result in the majority being classified as "Volcanic Arc Granites" (Fig. 3.5). However, since high alumina contents and low Nb and Y values are thought to be typical of crustal melt granitoids (Pearce *et al.*, 1984; McDermott, 1986), it can be proposed that the peraluminous Gamsberg Granite Suite represents I-type upper crustal melts. This proposal broadly coincides with the high younger parts of the $^{87}Sr/^{86}Sr$ initial value of 0.708 which was reported by Reid *et al.* (1987). However, while the low $^{87}Sr/^{86}Sr$ initial ratios of between 0.700 and 0.702 reported by Seifert (1986 and 1986a) confirm I-type

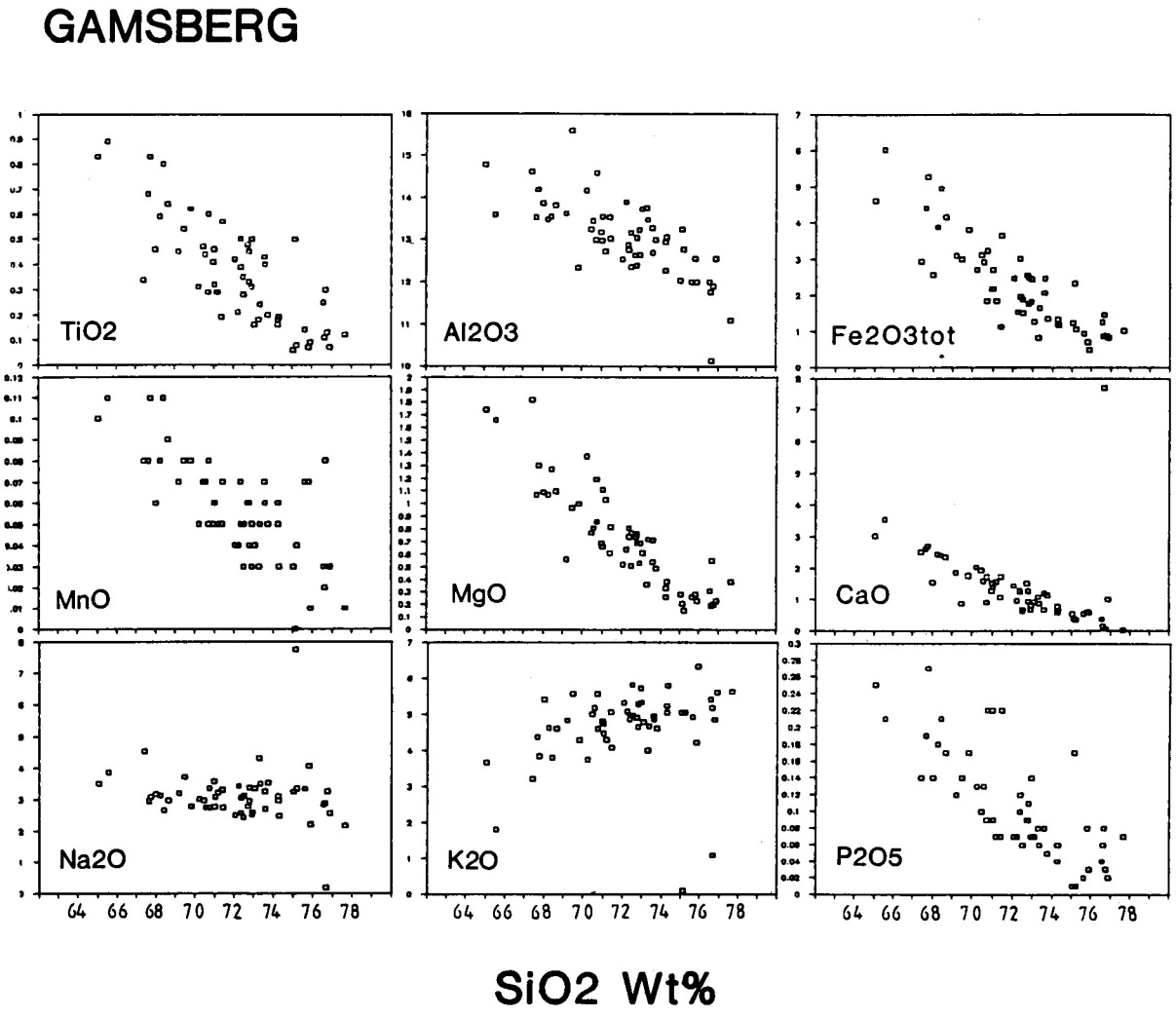

Figure 3.1: Harker diagrams for the Gamsberg Granite Suite

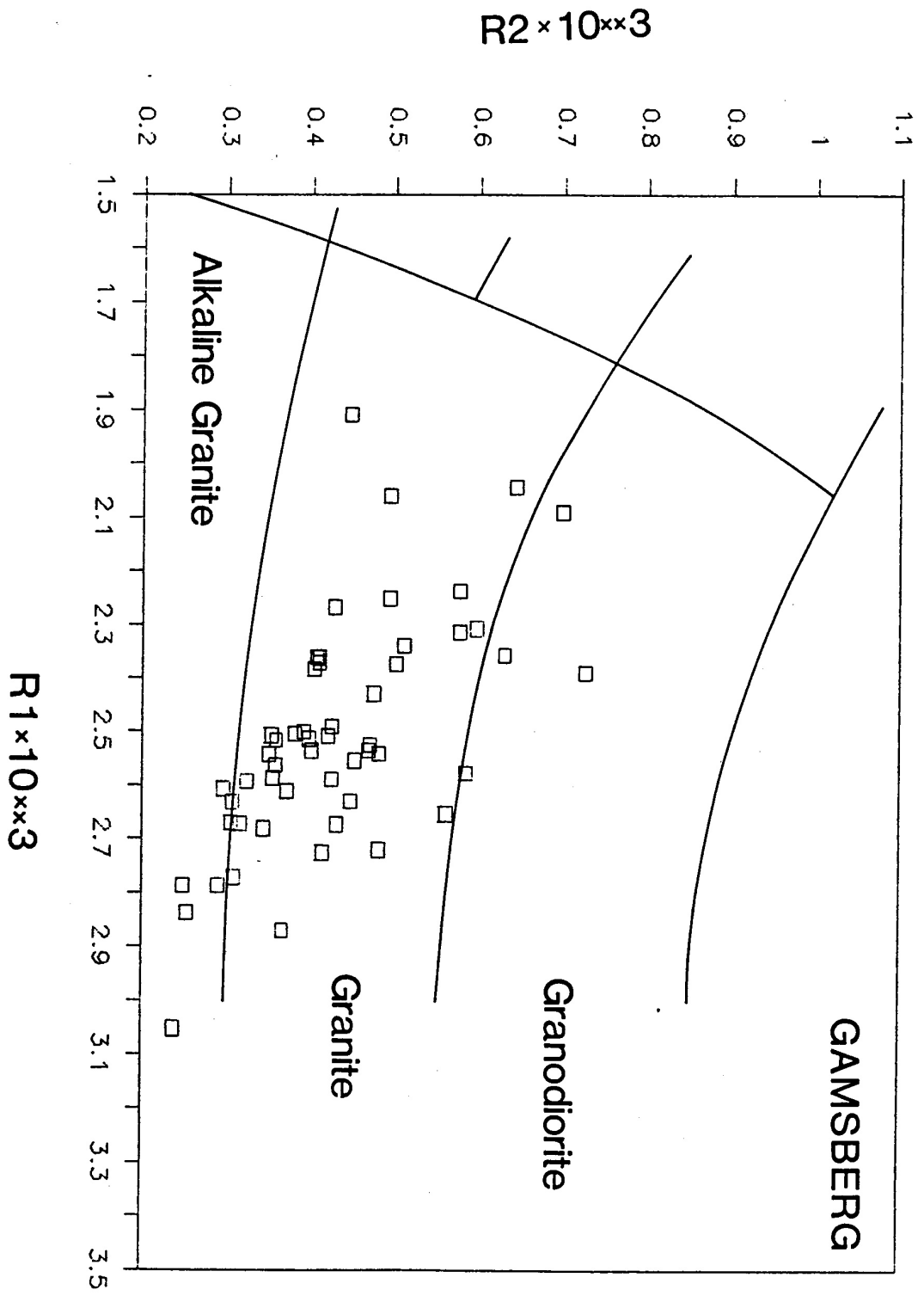

Figure 3.2: Classification diagram of De La Roche *et al.* (1980) for the Gamsberg Granite Suite (R1 = 6Ca + 2Mg + Al; R2 = 4Si - 11(Na + K) - 2(Fe + Ti))

magmatism for the Gamsberg Granite Suite, they do not support an upper crustal source.

3.3.2 Piksteel Intrusive Suite

Linear data arrays for 36 Piksteel samples on Harker diagrams (Fig. 3.6) probably reflect magmatic processes. However, the non-linear scatter of data points in plots of Na_2O and K_2O versus SiO_2 are most probably the result of post-intrusive alteration (saussuritisation) processes. The diagram of De La Roche *et al.* (1980; Fig. 3.7), although being sensitive to the mobility of alkalis, nevertheless illustrates that the Piksteel Intrusive Suite is made up largely of granodiorite with lesser plutons of granite, alkali granite, di-

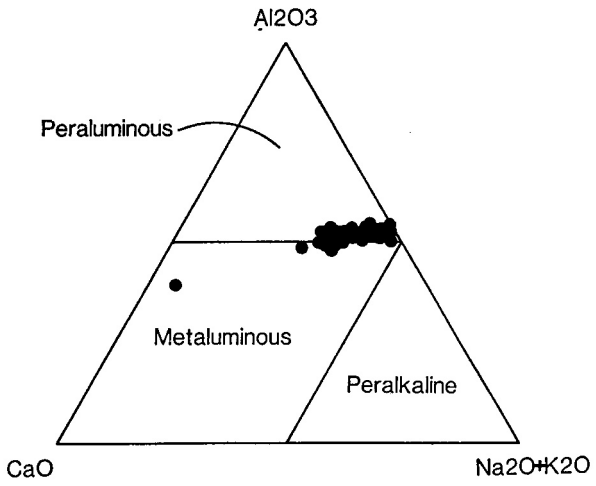

Figure 3.3: Wt% Al_2O_3-CaO-(Na_2O+K_2O) ternary diagram afetr Shand (1927 and 1951) for the Gamsberg Suite

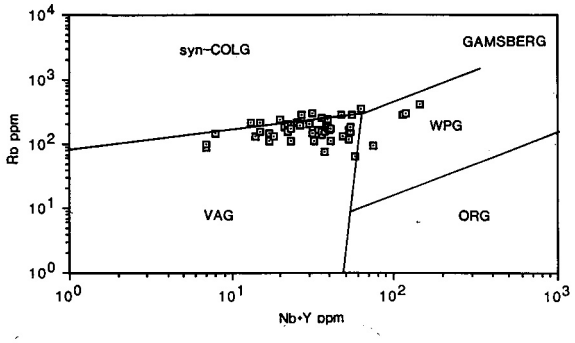

Figure 3.5: Rb versus Nb+Y diagram after Pearce *et al* (1984) for the Gamsberg Granite Suite (VAG = Volcanic Arc Granites; syn-COLG = syn-Collision Granites; WPG = Within Plate Granites; ORG = Ocean Ridge Granites

orite, quartz monzonite and tonalite. All of these granitoids plot within the peraluminous field on a wt% Al_2O_3-CaO-(Na_2O+K_2O) diagram (Fig. 3.8). In the mol.% Al_2O_3 versus mol.% (Na_2O+K_2O+CaO) diagram (Fig. 3.9) the wide range of A/CNK values from less than 1.0 to greater than 1.4 contrasts markedly with the Gamsberg data. The strong alumina oversaturation (A/CNK > 1.1) of many of the Piksteel samples suggests an S-type origin, while the few samples which plot below the A/CNK = 1.1 line are probably of I-type origin. Again, the Piksteel samples which define a calc-alkaline trend in the AFM diagram of Kuno (1968) (Fig. 3.16) are classified as "Volcanic Arc Granite" according to Figure 3.10. Here the low contents of Rb, Nb and Y and the peraluminous nature are also indicative of an upper crustal origin. A crustal origin is supported by the high initial $^{87}Sr/^{86}Sr$ ratios for Piksteel intrusives obtained by Reid *et al.* (1987) which range between 0.707 and 0.709.

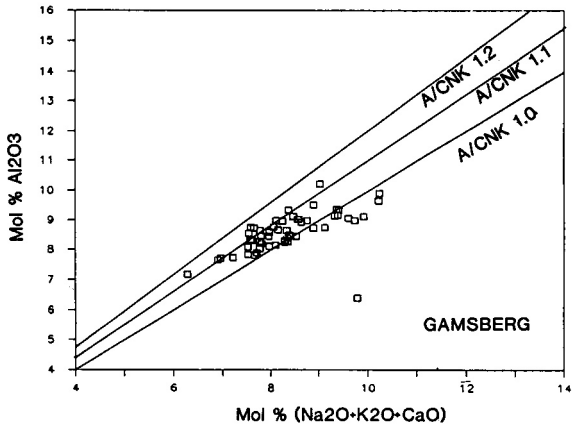

Figure 3.4: Mol.% Al_2O_3 versus mol.% (CaO + Na_2O + K_2O) diagram for the Gamsberg Granite Suite showing A/CNK alumina saturation values after Chappell and White (1974)

At this stage of the study the geochemical data are insufficient to allow an overall genetic interpretation. However, detailed work on single intrusions and the application of isotope geochemistry has permitted a better understanding of the Piksteel lntrusive Suite as shown in Chapters 8, 11 and 12.

3.3.3 Weener Intrusive Suite

AltogetheR12 samples were collected from the three largest bodies of the Weener Intrusive Suite. Despite the fact that data plot on similar differentiation trends in Harker diagrams (Fig. 3.11), the data points can be grouped together on a regional basis. The Weener Intrusive Suite is made up of granite, granodiorite, tonalite, diorite and gabbro as indicated by the diagram of De La Roche *et al.* (1980) (Fig. 3.12). As for the Gamsberg Granite Suite and Piksteel Intrusive Suite, all the Weener samples are peraluminous according to a wt% Al_2O_3-CaO-(Na_2O+K_2O) plot (Fig. 3.13). However, A/CNK ratios of the Weener Intrusive Suite are notably higher than those of the Gamsberg Granite Suite and the major part of the Piksteel Intrusive Suite, although being within the range of the Piksteel Intrusive Suite (Fig. 3.14). A/CNK ratios above 1.1 indicate an S-type origin for the Weener rocks according to the criteria of Chappell and White (1974). Such an origin is supported by the low Rb, Nb and Y contents which classify these granitoids as "Volcanic Arc Granites" (Fig. 3.15) according to Pearce *et al.* (1984), but is in contradiction to the relatively low initial $^{87}Sr/^{86}Sr$ values of 0.700 - 0.705 reported for the Weener Intrusive Suite by Seifert (1986a and 1986b) and Reid *et al.* (1987).

3.3.4 Summary

All the analysed samples of granitoids from the Rehoboth basement area are peraluminous according to the criteria of Shand (1927) and Chappell and White (1974). The Gamsberg Granite Suite, Piksteel Intrusive Suite and Weener Intrusive Suite are calc-alkaline in character according to the AFM diagram of Kuno (1968). A/CNK ratios

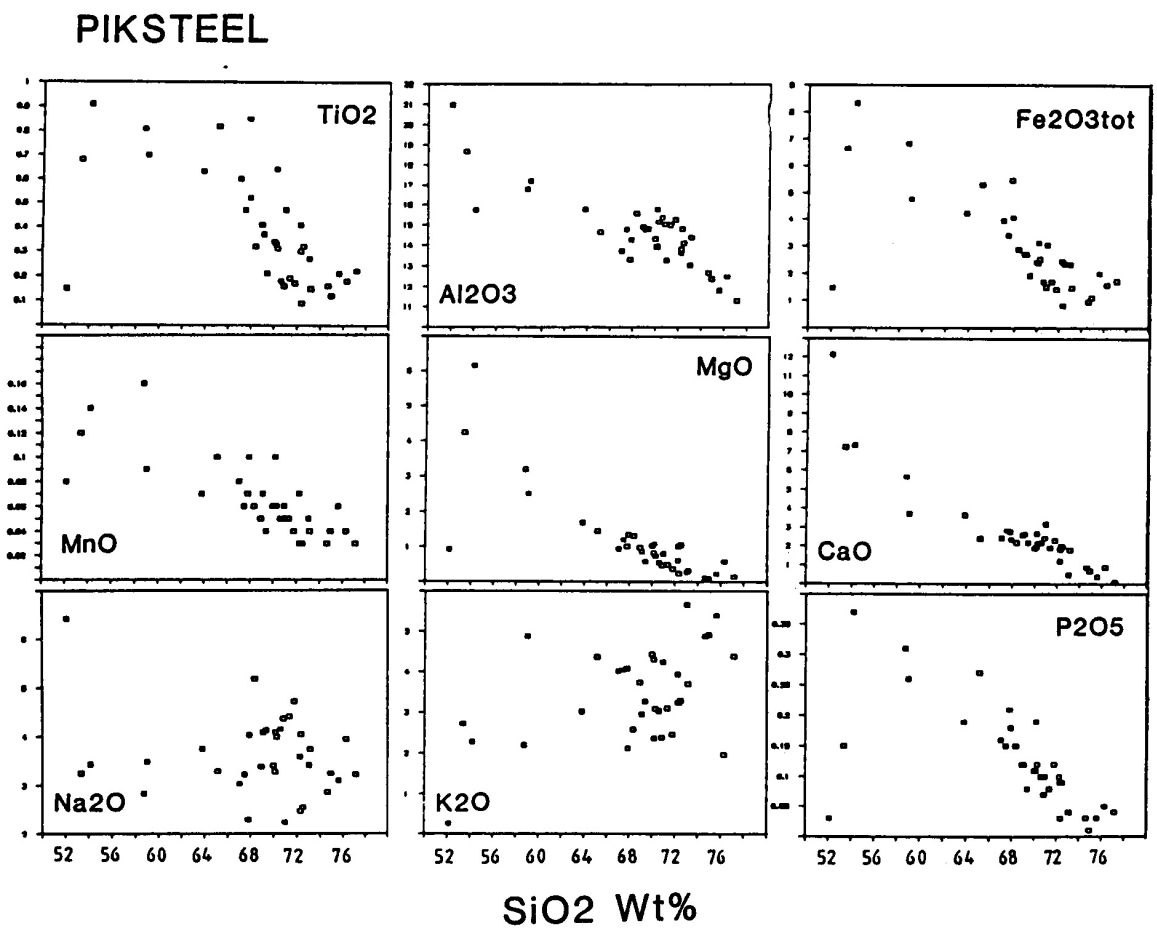

Figure 3.6: Harker diagrams for the Piksteel Intrusive Suite

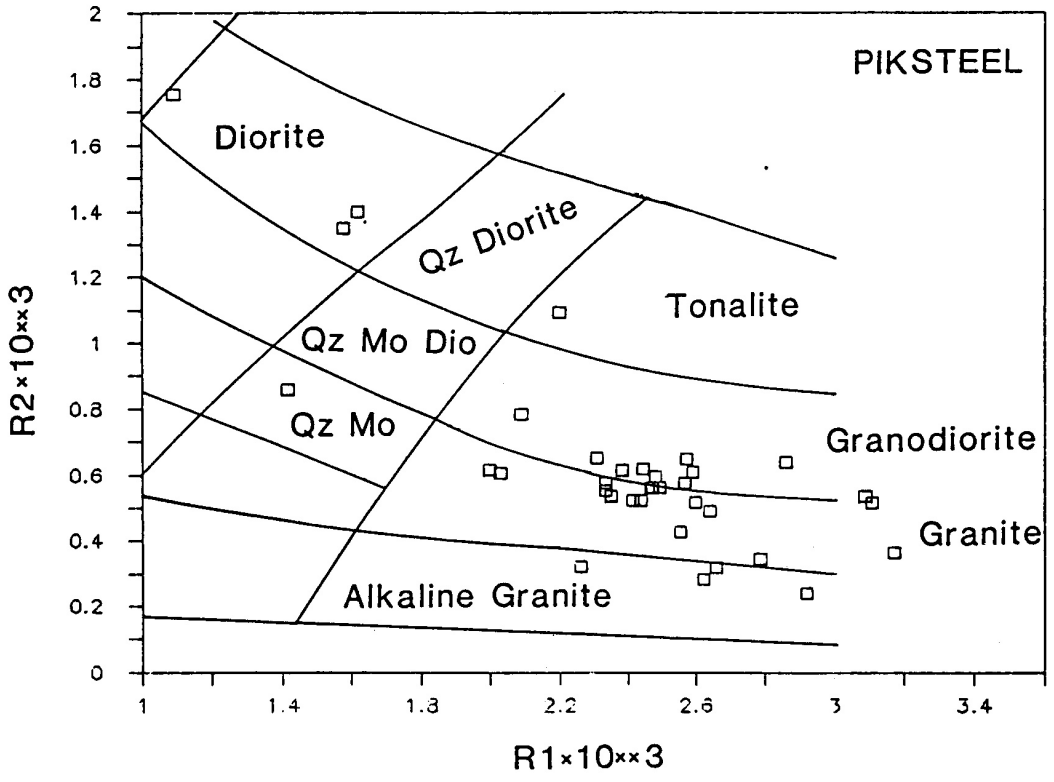

Figure 3.7: Classification diagram of De La Roche *et al.* (1980) for the Piksteel Intrusive Suite (R1 = 6Ca+2Mg+Al: R2 = 4Si-11(Na+K)-2(Fe+Ti))

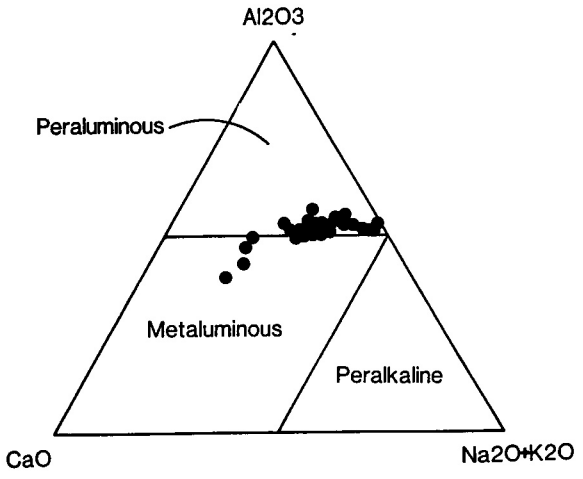

Figure 3.8: Wt% Al_2O_3-CaO-(Na_2O+K_2O)) ternary diagram after Shand (1927 and 1951) for the Piksteel Suite

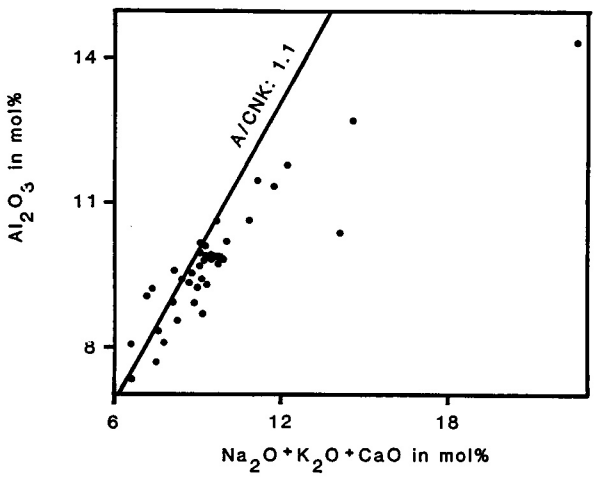

Figure 3.9: Mol.% Al_2O_3 versus mol.% (Na_2O+K_2O+CaO) diagram for Piksteel granitoids showing A/CNK alumina saturation values after Chappell and White (1974)

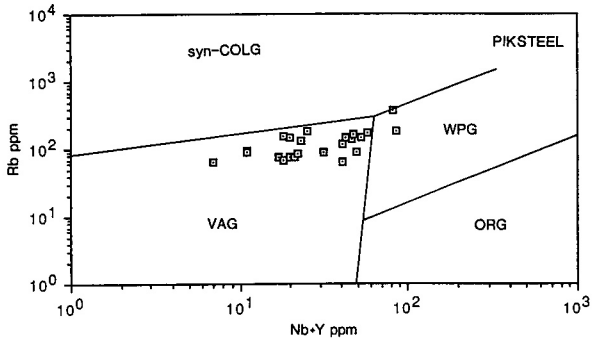

Figure 3.10 (left): Rb versus Nb+Y diagram after Pearce *et al.* (1984) for the Piksteel Intrusive Suite (VAG = Volcanic Arc Granites; syn-COLG = syn-Collision Granites; WPG = Within Plate Granites; ORG = Ocean Ridge Granites)

Figure 3.11 (below): Harker diagrams for the Weener Intrusive Suite (1,2,3 = different plutons of the Weener Intrusive Suite)

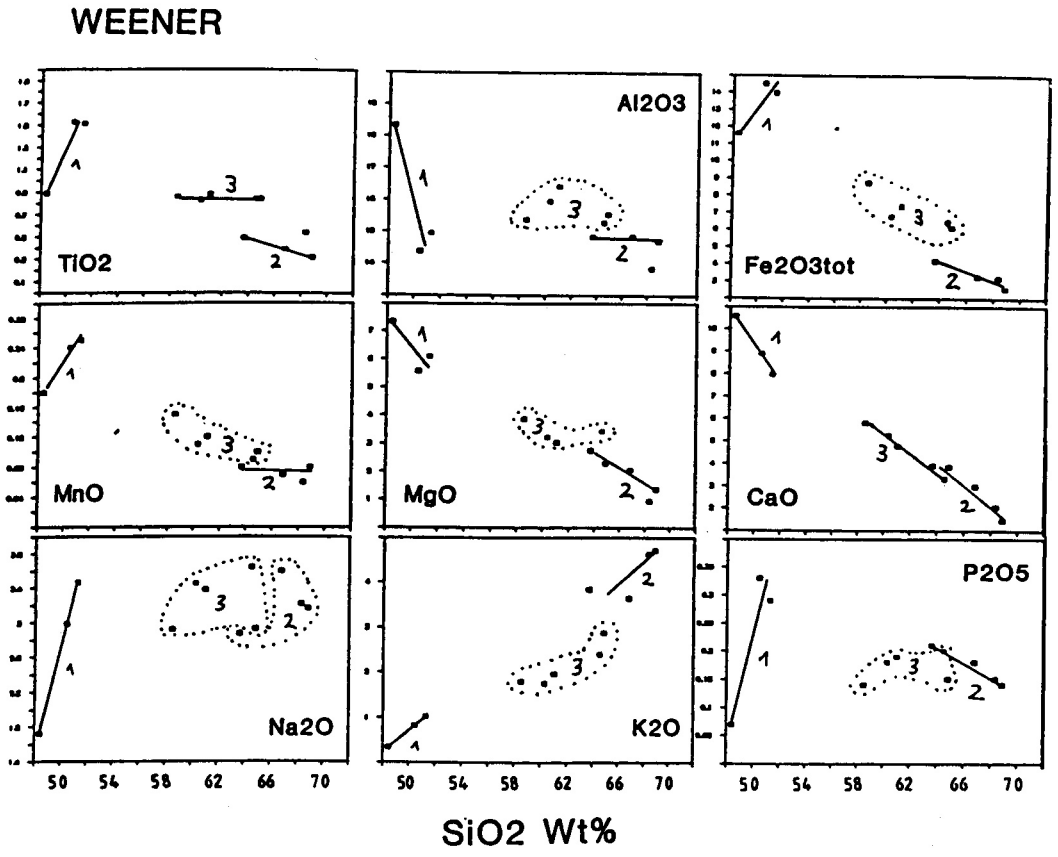

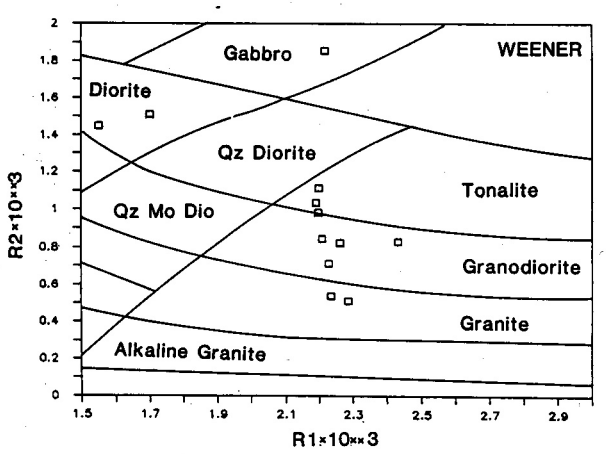

Figure 3.12: Classification diagram of De La Roche *et al.* (1980) for the Weener Intrusive Suite (R1 = 6Ca+2Mg+Al; R2 = 4Si-11(Na+K)-2(Fe+Ti))

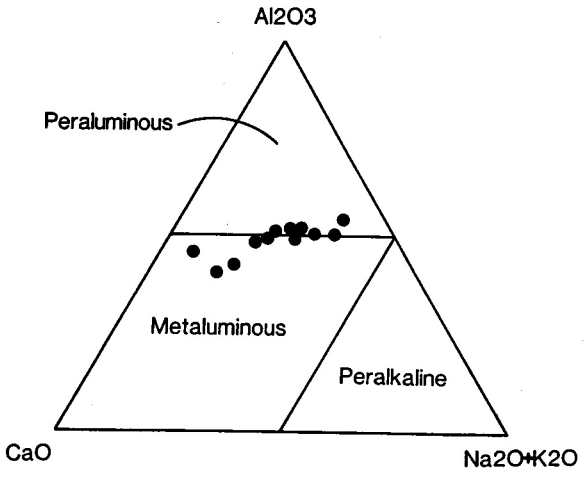

Figure 3.13: Wt% Al_2O_3-CaO-(Na_2O_3+K_2O) ternary diagram after Shand (1927 and 1951) for the Weener Intrusive Suite

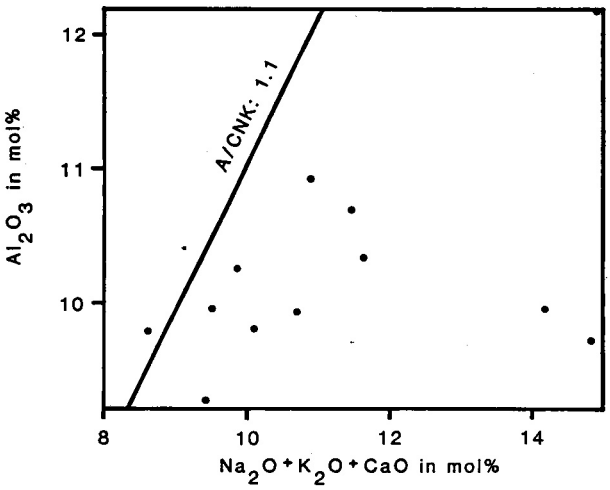

Figure 3.14: Mol.% Al_2O_3 versus mol.% (Na_2O+K_2O+CaO) diagram for the Weener Intrusive Suite showing A/CNK saturation values after Chappell and White (1974)

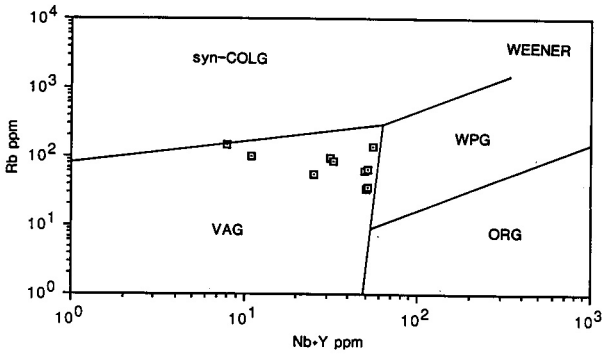

Figure 3.15: Rb versus Nb+Y diagram after Pearce *et al.* (1984) for the Weener Intrusive Suite (VAG = Volcanic Arc Granites; syn-COLG = syn-Collision Granites; WPG = Within Plate Granites; ORG = Ocean Ridge Granites)

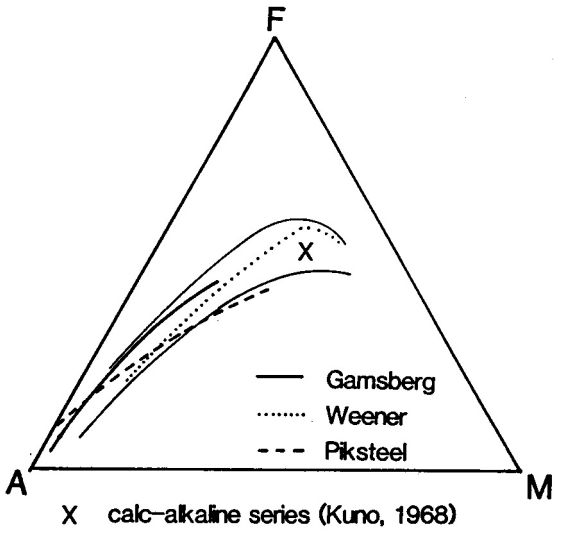

Figure 3.16 (left): Trends for all the analysed Rehoboth granitoids on an AFM diagram after Kuno (1968)

indicate an S-type origin for the Weener granitoids, an S- or I-type origin for the Piksteel granitoids and predominantly I-type origins for the Gamsberg granitoids. These results only partly coincide with Sr isotopic data of Reid *et al.* (1988) and Seifert (1986 and 1986a) and this study, which to a greater extent indicate I-type origins for the majority of the Rehoboth granitoids. However, the high alumina saturation of most of the analysed samples suggests that the vast majority of the granitoids in the Rehoboth Basement Inlier are derived from upper crustal melts which thus must have had low initial $^{87}Sr/^{86}Sr$ ratios and a low Rb-Sr fractionation factor. They therefore probably represent the result of a reworking of material of a primitive crust with the same Rb-Sr characteristics.

3.4 REE GEOCHEMISTRY OF SELECTED GRANITOID SAMPLES

3.4.1 Introduction

By the analyses of the Rare Earth Element (REE) distribution patterns of a total of 12 whole-rock samples from five plutons of the Piksteel Intrusive Suite and one pluton of the Gamsberg Granite Suite, all selected for neutron activation analysis based on geochemical and logistic criteria (a maximum of 12 analyses was possible in the given time range), more information on the geochemical properties and the genesis of the Piksteel and Gamsberg intrusives was sought. Pairs samples, in which one sample always showed a significantly higher SiO_2 content than the other, were selected from the Piksteel, Karikomasis/Groendraai, Borodino, Kabiras and Opetjie plutons of the Piksteel Intrusive Suite and from the Gamsberg pluton of the Gamsberg Granite Suite. The exact coordinates of the sample localities are listed in Table 4 (see appendix).

3.4.2 Discussion of the obtained Ree patterns

The results obtained for the 12 analysed samples are listed in Table 4 (see Appendix). In addition the chondrite-normalised La/Yb, La/Sm, Eu/Eu* and Tb/Yb ratios are tabled in order to give a numerical characterisation of the obtained REE patterns. Figure 3.17 is a graphical display of the results in Masuda-Coryell diagrams in chondrite-normalised patterns. The values used for chondrite normalisation are those of the Leedey chondrite of Masuda (1973) divided by 1.20, according to Taylor *et al.* (1977).

With the exception of the samples P11 and P17, whose total amounts of analysed REEs are 361 ppm and 32 ppm respectively, the sum of the analysed REEs is moderate and quite constant with a range of 99 to 210 ppm. If the highly anomalous REE pattern of P17 is not the result of strong hydrothermal alteration processes, a possibility which cannot be discounted, it is probably the result of analytical error (see Fig. 3.17). An interpolation of the total amount of the REEs in the analysed samples based on the known concentrations of seven REEs and their distribution patterns shows that the total REE concentration of the analysed samples is within the commonly observed range in granitoid rocks according to Cullers *et al.* (1984) and Wedepohl (1969). With the exception of the Kabiras and Gamsberg plutons the REE contents increase with increasing SiO_2 contents. The obtained REE patterns (Fig. 3.17) are quite flat and show a decrease from light REEs (LREE) to heavy REEs (HREE). This pronounced flatness of the patterns, which is quite common for granitic rocks (Cullers *et al.*, 1984), is also shown by the relatively low La/Yb ratios which range between 0.95 and 16.08. This is also reflected by the chondrite-normalised La/Sm and Tb/Yb ratios which vary between 7.5 and 2.4 and 2.4 and 0.2 respectively. In general there is nonetheless a strong decrease in the LREE

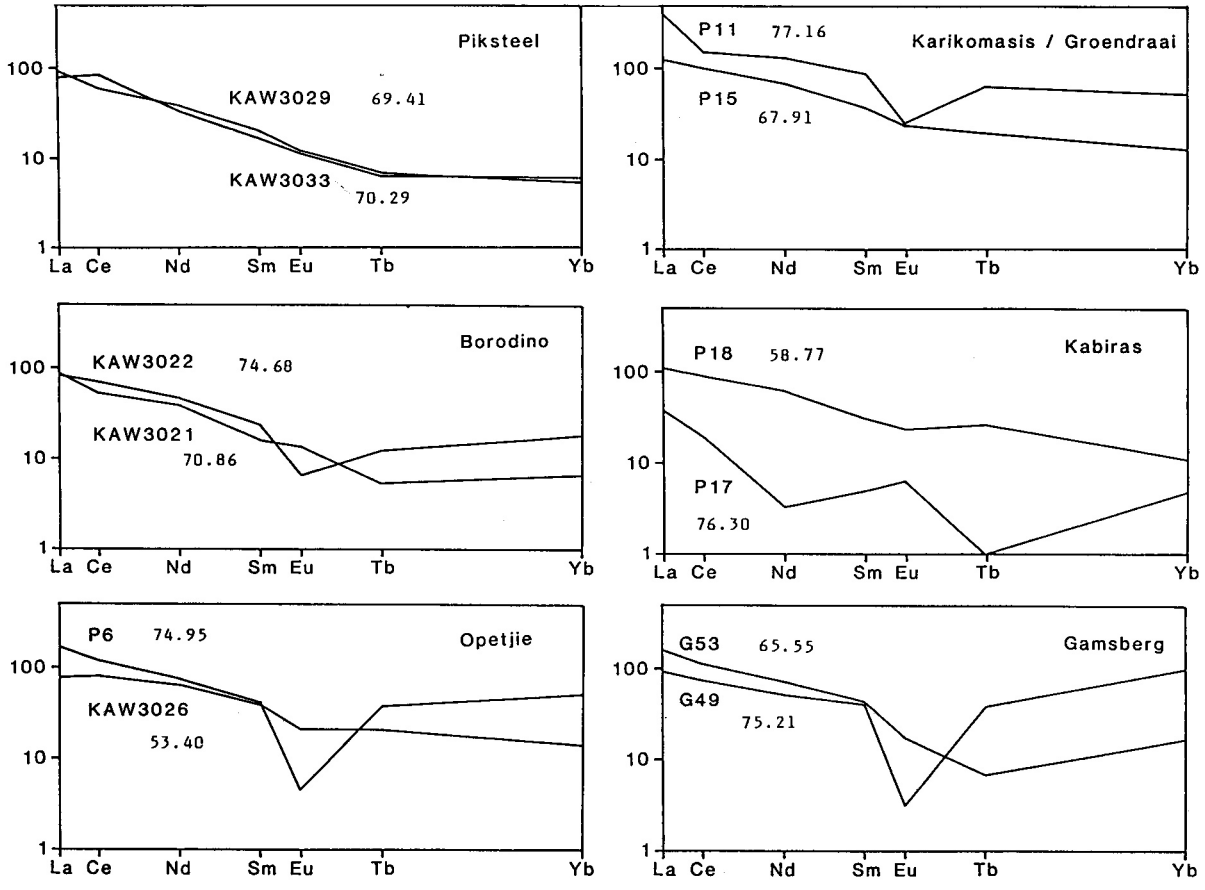

Figure 3.17: Chondrite-normalised REE patterns of 12 selected Rehoboth granitoids. Numbers in the diagrams denote SiO_2 contents of the respective samples in wt% (see text for discussion)

section of the patterns while the slope of the HREE section of the patterns is rather flat and in the case of six samples even shows an increase, giving these patterns a slightly concave-up appearance. According to Cullers *et al.* (1984), an increase of the HREE section is a feature which is sometimes observed in granitic rocks and which, according to McCarthy *et al.* (1978), may be attributed to the crystallisation of minor minerals from the primary melt-controlled REE distributions, resulting in concave-up REE patterns in the residual magmas. Therefore the observed concave-up patterns may not readily be attributed to anomalous source-rock composition or to hydrothermal alteration. Sample KAW3021 which does not show a detectable Eu anomaly (Eu/Eu* = 1.09), and sample P17 with a positive Eu anomaly of Eu/Eu* = 1.76, are in contrast with the remainder of the samples showing negative Eu anomalies with Eu/Eu* ratios ranging between 0.85 and 0.08.

Possible fractionation of the REEs during magmatic evolution could not be studied for the Piksteel pluton as the SiO_2 contents of the two samples from the Piksteel pluton were too close. The more acid samples from the Borodino. Opetjie and Karikomasis/Groendraai plutons of the Piksteel Intrusive Suite show higher REE contents than the more basic ones, indicating an enrichment of REEs during magmatic evolution. The enrichment of the LREEs in the more basic sample of the two Gamsberg samples, in comparison with the more acid sample, is in sharp contrast with the behaviour of the samples from the Piksteel Intrusive Suite.

3.4.3 Summary

Although moderate hydrothermal post-formation alteration of the analysed samples (which in fact was not capable of significantly disturbing the Sm-Nd age pattern of the Rehoboth Basement Inlier) should be taken into consideration, it is nonetheless possible to discuss some REE systematics of the analysed plutons. The REE patterns of all the samples are relatively flat. A general increase of the REE contents with increasing SiO_2 contents must be assumed for the members of the Piksteel Intrusive Suite but not for the Gamsberg pluton. In the case of the Borodino. Opetjie and Karikomasis/Groendraai plutons the increasing REE contents are also accompanied by Eu anomalies. These two features possibly reflect primary magmatic evolution processes with liquid-feldspar interactions, e.g. fractional crystallisation.

The increase of HREEs in some of the plutons of the Piksteel Intrusive Suite and in the Gamsberg pluton of the Gamsberg Granite Suite may be explained in four different ways:

- The increase of HREEs in a residual magma was produced by the crystallisation of minor minerals from this magma. This hypothesis is partially supported by the occurrence of Eu anomalies (which are probably related to fractional crystallisation) in many of the samples with concave-up HREE patterns;
- the source material available for the genesis of the present granitoids had abnormally low LREE/HREE ratios; or
- there was little or no fractional crystallisation of minerals with high crystal-melt distribution coefficients for HREEs such as hornblende, garnet, allanite; or
- as the least possible solution to the problem (according to the aforementioned consistency of Sm-Nd data in the Rehoboth area) the LREE were favourably mobilised or the HREEs were preferentially precipitated by circulating metasomatic hydrothermal fluids during post-formation alteration processes.

As it is not known to what extent the original REE distribution patterns of some of the analysed samples (e.g. P 17) have been disturbed by post - formation hydrothermal fluid reactions whose occurrence has been shown (e.g. Chapter 8), we considered that geochemical modelling by computer would not be practical. Nonetheless it can be said that the general appearance of the majority of the observed REE patterns probably reflects primary magmatic processes leading to the formation of the analysed plutons of the Rehoboth Basement Inlier. REE patterns of the majority of the analysed granitoids seem to have been well preserved throughout the Mokolian until more recent geological evolution of the Rehoboth Basement Inlier. This is particularly helpful in the interpretation of Sm-Nd data of the area (see Chapter II) as these are generally reliable. Furthermore it is of interest to see that the REEs were relatively stable in comparison with the Rb-Sr, U-Pb and K-Ar systems of the analysed samples which have all been severely disturbed by post-formation alteration processes (see Chapter 8),

4. MOOIRIVIER COMPLEX

4.1 INTRODUCTION

The migmatites and associated rocks of the Mooirivier Complex were assigned to various other Formations prior to SACS (1980).

De Kock (1934) was the first to find several outcrops of migmatites which he mapped as part of the "Mixed Rocks" on his map of the western Rehoboth area. In 1966 De Waal interpreted Piksteel granodiorites, streaked granodiorites and migmatitic gneisses of the Nauchas area, which he partly mapped as "Piksteel granodiorite and associated migmatite", as being the products of granodioritisation of Marienhof sedimentary rocks. Mailing (1978) included all the migmatites and migmatitic gneisses occurring between the farms Ubib 396 and Piksteel 209 in his "Swartfontein Formation" which he found to be intruded by Weener tonalite and Gamsberg granite.

In 1980, SACS introduced a new stratigraphic classification of the area by subdividing the "Archaean Complex" of the Geological Map of 1963 into several successions of which the oldest Formation is the Mooirivier Complex. It contains the migmatitic gneisses, amphibolites and remnants of quartzite and schist occurring in the Rehoboth district and in the southwestern part of the Windhoek District, as well as outcrops of the same lithologies in the area of the farms MooirivieR160 and Neuhof 100 in the northern part of the Maltahöhe district. The Kumbis Formation of the southwestern Maltahöhe district introduced by Watters (1974) was also included in the Mooirivier Complex by SACS (1980) because of its similarity of rock types and their similar stratigraphic position.

Generally the rocks of the Mooirivier Complex occur as large xenoliths in granodiorite and granite but also as continuous outcrops of considerable extent (Schalk and Germs, 1975). These larger outcrops of the Mooirivier Complex are always intruded by granites, granodiorites and various basic rocks. The Mooirivier Complex is unconformably overlain by the Neuhof Formation in the area of the farms MooirivieR160 and Neuhof 100. Gneisses of the Mooirivier Complex tectonically border the Elim Formation in the area of the farm Alberta 175. According to Schalk (pers. comm., 1987) they have possibly been upthrust onto this stratigraphically younger formation from the south. In the same area the Gaub Valley Formation tectonically overlies the Mooirivier Complex, according to Schulze-Hulbe (1975).

A minimum age of 1730 Ma is estimated for the Mooirivier Complex by Schalk (pers. comm., 1987) based on whole-rock Rb-Sr determinations of the intrusive Naub diorite by Mailing (1978) and Reid *et al.* (1988). A K-Ar age for a muscovite from a "pegmatite in pegmatitic (migmatitic?) gneisses just south of the Naukluft mountains" yielded an age of 1158 ± 35 Ma (Ahrendt *et al.*, 1977) and is therefore indicative of the long time span during which the Mooirivier Complex was intruded by various magmatic rocks.

The densely granite-injected southern part of the Mooirivier Complex consists mainly of partly migmatised banded gneisses, amphibolites, amphibole schists, sericite quartzites, garnetiferous mica schists, mica-rich granite gneisses and strongly altered basic dykes. Fold structures trending in north-northwesterly and northeasterly directions are often observed within less altered metasedimentary rocks (Schalk, pers. comm., 1987).

In its northern part, in the area of the Spreetshoogte Pass, the Mooirivier Complex is mainly represented by an often well-banded succession of quartzite, porphyroblastic plagioclase-biotite schist, partly strongly foliated amphibolite and chlorite schist. It is penetrated by granitic rocks assigned to the Piksteel and Gamsberg Intrusive Suites (Schalk, pers. comm., 1987) which are often strongly sheared. In this area the fold axes of the Mooirivier rocks trend in a northeasterly direction.

4.2 SAMPLE COLLECTION AND DESCRIPTION

Five 30 kg samples (KAW3060-KAW3064) of partly garnetiferous biotite schists were collected in the vicinity of the Spreetshoogte Pass (Fig. 4.1). The modal composition of the foliated and partly banded samples is 20-35% saussuritised plagioclase, 5-20% partly chloritised biotite, 20-45% quartz, 0-7% actinolitic hornblende, 0-35% poikiloblastic garnet, 4-10% epidote minerals and accessory potassic feldspar, tourmaline, calcite, sericite and magnetite/hematite.

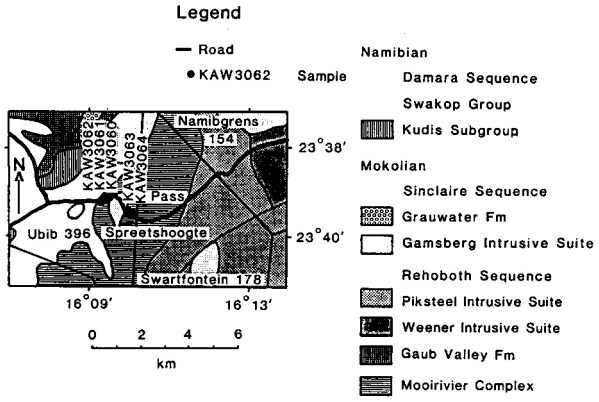

Figure 4.1: Sample map of the northern part of the Mooirivier Complex

Four amphibolitic and two granitic samples of 30 kg each (KAW3082- KAW3087) were collected on the farm MooirivieR160 (Fig. 4.2). The amphibolites consist by volume of 50-60% brown, slightly chloritised amphiboles, 20-35% strongly saussuritised plagioclase, 0-15% quartz, 0-10% ,opaque minerals and accessory epidote minerals, chlorite, sphene, apatite and sericite. They partly occur as massive rocks but mostly they show a strong foliation on a sub-millimetre scale with intense small-scale folding. Brown amphiboles of different generations were observed in sample KAW3085.

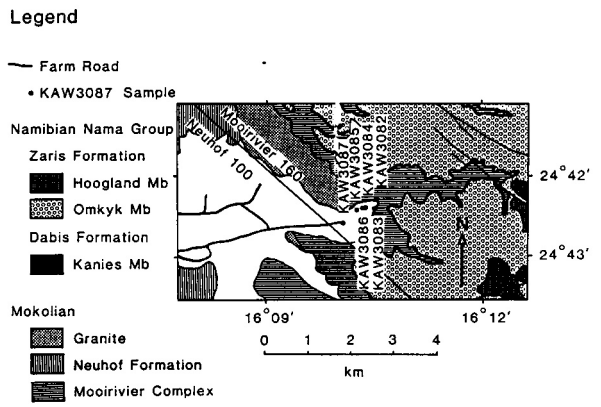

Figure 4.2: Sample map of the southern part of the Mooirivier Complex

In spite of moderate alteration of the two granitic samples and shearing of one of them (KAW3087), magmatic textures have partly been preserved. Zoned relictic clinopyroxene is found as an accessory mineral in sample KAW3086.

4.3 DISCUSSION OF THE ANALYTICAL RESULTS

4.3.1 Geochemistry

The results obtained for all the analysed specimens are listed in Table 5 (see Appendix).

As the number of analyses is not sufficient to make statistically relevant statements on the basis of the commonly used tectonic discriminant diagrams, the results obtained are presented in the form of a spider diagram (Fig. 4.3), It shows the normalised element concentration patterns of the five whole-rock samples from the Spreetshoogte Pass area and the two granitic and four amphibolitic samples from the farm MooirivieR160, plotted in order of decreasing continental abundances (from Taylor and McLennan, 1985 and Hoffmann, 1988), in comparison with average continental crust. The concentrations are normalised by dividing each by the respective concentration in the primitive mantle. The data for the primitive mantle are taken from Jochum *et al.* (1988).

The resulting abundance patterns for the acid rocks are quite similar to that of continental crust of average composition after Taylor and McLennan, which is represented by a solid line in Figure 4.3. A slight enrichment of highly incompatible elements such as Rb, Ba, K, La, Ce, Nd and Zr can be observed in our samples in comparison with average crust. A depletion of compatible elements such as Al, Ca, Sc, Fe, Mg and Ni is also notable. This trend of an enrichment of incompatible elements and a depletion of compatible elements in comparison to average continental crust is contradicted only by a degree of Sr depletion. Nevertheless it can be noted that the degree of element fractionation of the analysed specimens is higher than that of average continental crust as would be expected for rocks of a probable sedimentary origin.

According to Froehlich (1960), amphibolites with Cr-contents greater than 150 ppm are of orthogenic origin while samples with Cr-contents less than 20 ppm are paragenic. Therefore three of the analysed amphibolites from the farm MooirivieR160 should be regarded as orthogenic while the origin of one sample (KAW3082), yielding a Cr-content of 49 ppm, remains uncertain.

In Figure 4.3 the analysed amphibolites more or less follow the trend of average continental crust although they are comparatively enriched in La, Ce, Nd, Zr. Y and TiO_2.

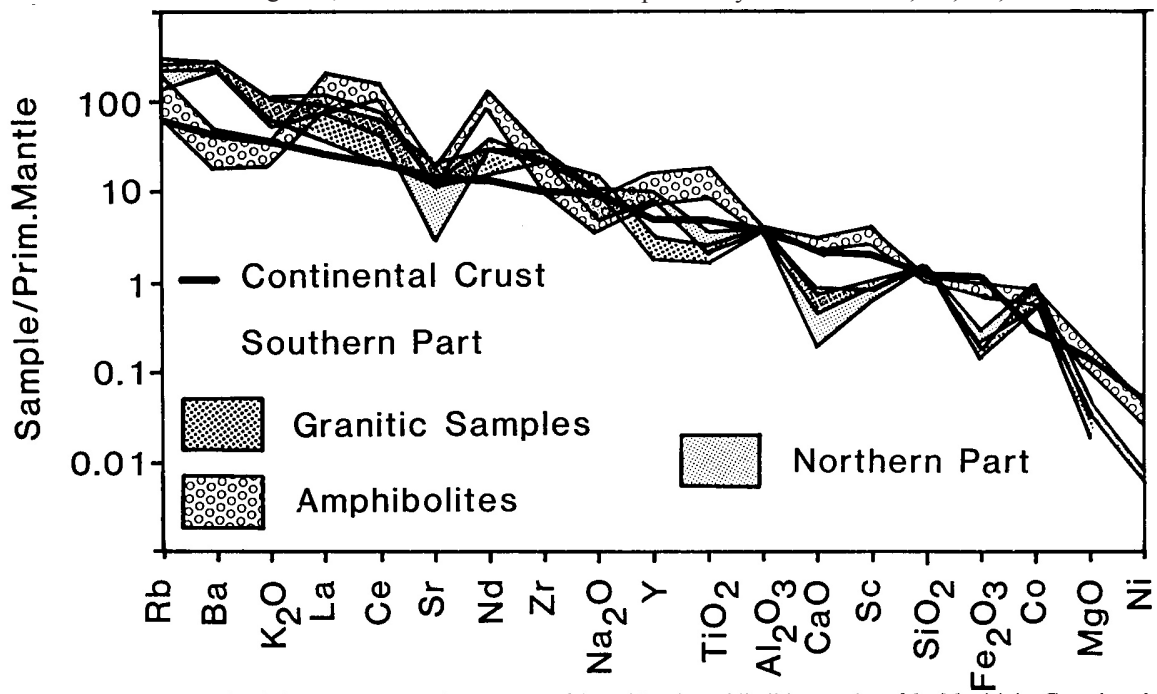

Figure 4.3: Mantle-normalised element concentration patterns of the acid and amphibolitic samples of the Mooirivier Complex plotted in the order of increasing compatibility (see text for explanation)

4.3.2 K-Ar analyses

The results of the analyses are listed in Table 6 (see Appendix). The individual ages of the biotite separates of the five samples from the Spreetshoogte pass range between 330.3 ± 5.0 Ma and 545.1 ± 5.5 Ma with a percentage of radiogenic ^{40}Ar from 91.14% to 99.32%. The samples collected closer to the road pass show higher ages (537.1 Ma and 545.1 Ma) than those collected further towards the west, whose apparent K-Ar age ranges between 330.3 Ma and 427.1 Ma. Age and percentage of radiogenic ^{40}Ar are positively correlated, as the content of radiogenic ^{40}Ar diminishes parallel to the apparent individual age of a sample in a westerly direction from the Spreetshoogte pass. This trend is indicative of a loss of ^{40}Ar from the minerals and/or a post-formation contamination of the samples with atmospheric argon. An indication for simultaneous loss of potassium is given by a comparison of the K content of the analysed biotites, ranging between 20.86*(10^{-8}) mol K/g and 23.37*(10^{-8}) mol K/g, with the K content of average biotites, which lies between 26*(10^{-8}) mol K/g and 30* (10^{-8}) mol K/g.

The previously suspected contamination of the argon in the biotites with atmospheric argon is disclosed by the $1/^{36}Ar$ versus $^{40}Ar/^{36}Ar$ diagram, where all the data plot on a well-correlated regression line (Fig. 4.4) whose very high correlation coefficient of 0.9998 leaves no doubt about the line being a mixture line. However, the very low intercept of this line at $^{40}Ar/^{36}Ar = -3249$ shows that it not only represents an admixture of atmospheric argon but also indicates that a combination of various processes must have affected the analysed biotites.

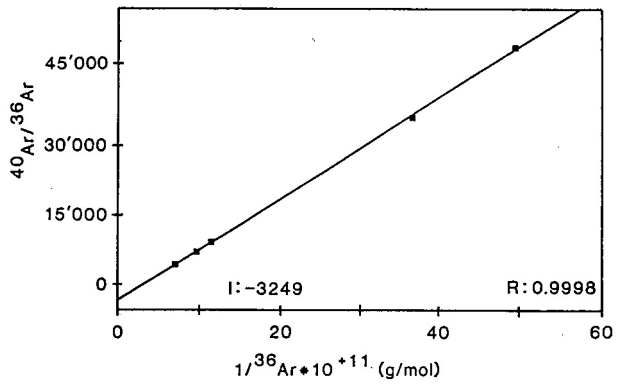

Figure 4.4: $1/^{36}Ar$ versus $^{40}Ar/^{36}Ar$ diagram for the analysed biotites of the Mooirivier Complex from the Spreetshoogte Pass area. The calculated regression line has a slope of 9.2795*(10^{-9}) and a correlation coefficient R of 0.9998

In the Harper diagram (1970) the $^{40}Ar_{rad}$ contents of the samples were plotted versus their ^{40}K contents (Fig. 4.5). A regression line, showing a correlation of 0.949 and a slope corresponding to an age of 1718 Ma, was then calculated through the data points. This line intercepts the y-axis at

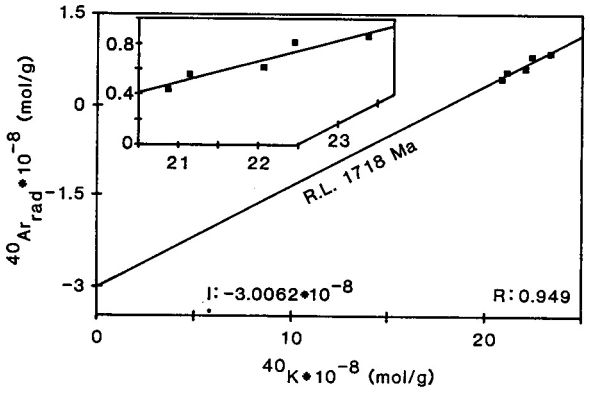

Figure 4.5: ^{40}K versus $^{40}Ar_{rad}$ diagram after Harper (1970) for the analysed biotites of the Mooirivier Complex from the Spreetshoogte Pass area. The calculated reference line representing an age of 1718 Ma has an intercept I of -3.0062*(10^{-8}) and a correlation coefficient R of 0.949. Although it looks promising, this line probably has no geological significance (see text for explanation)

-3.0062*(10^{-8}) mol$^{40}Ar_{rad}$/g thus making the presumed severe loss of $^{40}Ar_{rad}$ evident. According to Harper (1970), the intercept of such a well-correlated regression line directly quantifies the loss of $^{40}Ar_{rad}$ from the analysed samples in mol$^{40}Ar_{rad}$/g * (10^{-8}). After a correction allowing for this apparent loss of $^{40}Ar_{rad}$ the individual ages of the samples would range between 1701.0 Ma and 1740.7 Ma and would therefore coincide with the age of the calculated reference line. Although such K-Ar ages ranging between 1701 Ma and 1740 Ma could represent a reasonable formation age for the Mooirivier Complex, they probably ought to be interpreted as geologically meaningless, because the analysed biotites not only suffered from a severe loss of ^{40}Ar which would have had to be proportional in all samples, but also from a certain loss of potassium which is discussed above. Unless the observed loss of potassium was propor-

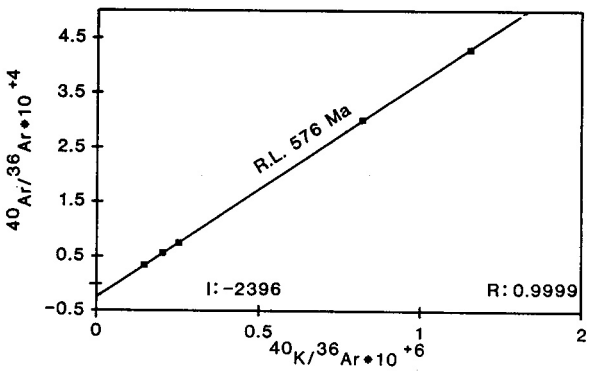

Figure 4.6: $^{40}K/^{36}Ar$ versus $^{40}Ar/^{36}Ar$ diagram for the analysed biotites of the Mooirivier Complex from the Spreetshoogte-Pass area. The calculated reference line of 576 Ma is probably without geological significance as is shown in the text

tional to the loss of $^{40}Ar_{rad}$ it must have caused a change of the slope of the reference line in the Harper diagram. Such an uncontrolled change of slope in turn would result in erroneous readings for the loss of $^{40}Ar_{rad}$ on the y-axis and in erroneous "corrected" individual ages. To give a geologically relevant age, i.e. to still plot on a well-correlated and meaningful reference line, the analysed biotites should therefore have suffered from a proportional loss of argon and potassium. Although the loss of argon and potassium parallels the decrease of the apparent ages of the individual samples, such a proportionality seems to be rather unlikely when considering that the analysed samples were collected over a distance of almost 2 km.

In addition, the $^{40}K/^{36}Ar$ versus $^{40}Ar/^{36}Ar$ isochron diagram (Fig. 4.6) with its highly correlated reference line (R = 0.99996) might suggest a geologically meaningful age of 576 Ma which could easily be explained by a metamorphic event in connection with the Damara orogeny. But, analogous to the results of the Harper diagram, where the resulting reference line of 1718 is geologically meaningless, the apparent isochron age of 576 Ma in Figure 4.6 also proves to be meaningless under careful examination. It has no geological significance as the resulting "isochron" must have formed due to the combination of the partial loss of potassium and argon from the analysed biotites, as was shown in the discussion of the Harper diagram (Fig. 4.5), and due to the addition of atmospheric argon which is indicated by the $^{40}Ar/^{36}Ar$ versus $1/^{36}Ar$ diagram (Fig. 4.4). These processes rotated and tilted the original isochron in a way that the resulting "isochron" of 576 Ma now intercepts the y-axis at an unreal $^{40}Ar/^{36}Ar$ value of -2396.

In summary it can be said that the $^{40}K/^{36}Ar$ versus $^{40}Ar/^{36}Ar$ and ^{40}K versus $^{40}Ar_{rad}$ isochron diagrams did not yield geologically significant results although their respective reference lines looked reasonable at first glance. The only reliable statements on the K-Ar age of the biotites from the northern part of the Mooirivier Complex are provided by the individual ages of the biotites, which clearly show that the northern part of the Complex has been affected by post-Damaran processes. The K-Ar system of the analysed biotites was probably initiated during the Damara orogeny, as is indicated by the age of 545 Ma of biotites from the easternmost sample which have shown the least contamination by atmospheric argon and which yielded the highest K content. The individual biotite ages decrease in a westward direction to about 330 Ma, indicating that the processes disturbing the K-Ar system took place at least until 330 Ma ago and might therefore reflect thermo/tectonic processes during the Karoo period, such as the opening of the South Atlantic.

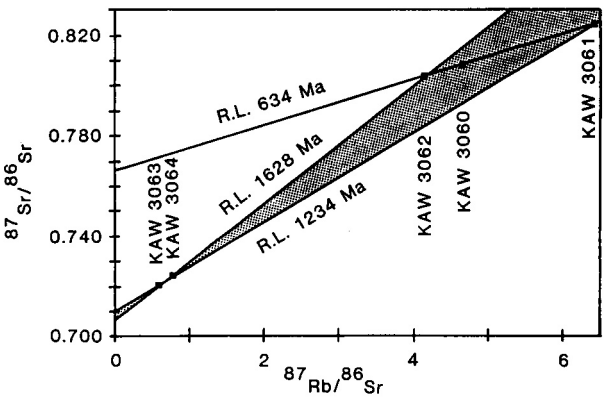

Figure 4.7: $^{87}Rb/^{86}Sr$ versus $^{87}Sr/^{86}Sr$ isochron diagram for the analysed whole-rock samples of the Mooirivier Complex from the Spreetshoogte Pass area. See text for explanation

4.3.3 Rb-Sr analyses

A tabular listing of the analytical results obtained for the whole-rock Rb-Sr analyses is given in Table 7 (see Appendix). As is to be expected based upon the results of the K-Ar analyses, a plot of the $^{87}Sr/^{86}Sr$ ratios of the samples versus their $^{87}Sr/^{86}Sr$ ratios (Fig. 4.7) mainly reflects the disturbances of the Rb-S system which must have affected the Mooirivier Complex after its formation. The data do not plot on a well-defined isochron but scatter within a fan of reference lines calculated after York (1969), with no correlation of errors and equal weighing of samples, which has an upper limit of 1 628 ± 3 Ma and a lower limit of 1 234 ± 9 Ma. The resulting intercepts with the y-axis range between initial $^{87}Sr/^{86}Sr$ values of 0.7070 ± 0.0001 and 0.71 09 ± 0.0009.

An interesting feature is a reference line of 634.2 ± 12.1 Ma and an intercept of 0.7663 ± 0.0009 which can be calculated through the points representing the samples collected further away from the Spreetshoogte Pass (KAW3060-KAW3062). This "small scale isochron" gives some evidence that homogenising processes affecting the Rb-Sr system of the samples also postdate the lower limit of the fan of reference lines of 1234 Ma and thus most probably took place contemporaneously with the processes disturbing the K-Ar system of the biotites from the same samples. Accordingly it can be said that these processes were not capable of completely resetting the Rb-Sr isotopic system of the analysed whole-rock samples although the K-Ar sys-

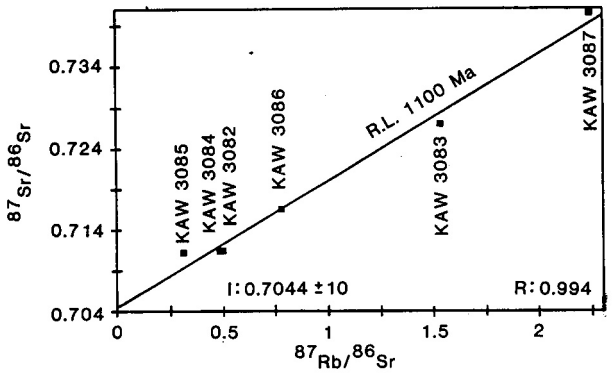

Figure 4.8: $^{87}Rb/^{86}Sr$ versus $^{87}Sr/^{86}Sr$ isochron diagram for the analysed granitoids and amphibolites from Mooirivier 160. See text for explanation

tem of the biotites from the samples has completely been reset.

In Figure 4.8 the whole-rock analyses of the four amphibolite samples and the two granitic samples collected on the farm MooirivieR160 plot on a reference line, calculated after York (1969), with no correlation and equal weighing of samples, of 1 100 ± 58 Ma with an intercept at $^{87}Sr/^{86}Sr$ = 0.7044 ± 0.001 and a correlation coefficient R of 0.994. If the amphibolites and granitic rocks are calculated separately they yield a reference age of 983 Ma and 1141 Ma repetitively, with intercepts of 0.7053 and 0.7040. It should be assumed that all these calculated ages reflect the age of intrusion of the surrounding masses of Mokolian granites as the analysed samples mostly show a strong foliation while the intrusive granites are practically undeformed.

4.4 CONCLUSIONS

This chapter shows that dating of the Mooirivier Complex by the K-Ar and Rb-Sr methods is most difficult as both isotopic systems have been strongly disturbed by post-formation processes. The argon system of the analysed biotites suffered from a severe loss of argon and potassium and an addition of atmospheric argon while the Rb-Sr system was disturbed in an undetectable manner. Nevertheless it is possible to make a few statements on the history of the Mooirivier Complex:

- The K-Ar system of the biotite separates from samples which were collected in the northern part of the Mooirivier Complex in the area of the Spreetshoogte Pass was most probably completely reset during the Damara orogeny as is indicated by the age of 545.1 ± 5.5 Ma obtained for the biotite separate with the smallest percentage of atmospheric argon and the highest K -content.
- A combined effect, including a partial loss of argon and potassium and the admixture of atmospheric argon until at least 330 Ma ago, is indicated by the individual ages of some of the biotite separates. This date clearly postdates the Damara orogeny which ended about 450 Ma ago and might thus reflect a partial attenuation of the analysed biotites in connection with post-Ordovician tectonic events such as the opening of the South Atlantic during the Karoo period along the western margin of Namibia.
- The formation and attenuation of the K-Ar systems has been accompanied by disturbances of the whole-rock Rb-Sr systems.
- The whole-rock Rb-Sr data obtained for the granitic samples and for the orthogenic amphibolites from the farm MooirivieR160 in the southern part of the Mooirivier Complex plot on a reference line of 1100 ± 58 Ma. As indicated by structural data, K-Ar dating of the northern part of the Mooirivier Formation and the age of the acid intrusive rocks of the region, these ages are too low to represent the formation age of the Mooirivier Complex. They might reflect a homogenisation phase of the Rb-Sr systems in the analysed specimens which occurred due to the intrusion of the Mokolian granites in the area of MooirivieR160.

A higher degree of disturbance of the investigated Rb-Sr isotopic systems has been observed in the northern part of the Mooirivier Complex in comparison with the southern part. This probably reflects the decreasing influence of the Damara orogeny on the Rehoboth Basement Inlier towards the south.

5. NEUHOF FORMATION

5.1 INTRODUCTION

The outcrops of the Neuhof Formation in the Rehoboth area have been included into the pre-Damara "Mixed Rocks" and "Marienhof Series" and the "Pebbly grits, sandstones and quartzites" of the Nama System on de Kock's (1934) map of the Western Rehoboth area. Later they were considered as part of the "Archaean Complex" and "Granite and Gneiss" on the Geological Map of South West Africa (1963) before they were grouped in the Kamasis Formation by Schalk (1973). SACS (1980) united the rocks of the Kamasis Formation of the Rehoboth area with metamorphic rocks occurring in the western Maltahöhe District along the escarpment which can be traced beyond Helmeringhausen in the south (Schalk, pers. comm., 1987), because of their strong resemblance with them. Some of the southern most representatives of today's Neuhof Formation have been described by Watters (1974) as "Nubib and Barby metarocks of the Nama shear belt" of Sinclair age. This classification is doubted by K. Schalk of the Geological Survey in Windhoek (pers. comm., 1987).

The Neuhof Formation consists of a succession of metamorphosed acid and basic volcanic rocks and metasediments which, as a whole, are intruded by various younger granitoid magmas. The metasediments are composed of interbedded very fine- to coarse-grained quartzites, polimict conglomerates, mica schists, chlorite schists, biotite-amphibole schists and calcitic to dolomitic, partly diopside-bearing limestones. A major part of the succession is made up of fine-grained, partly porphyric acid volcanic rocks (Schalk, pers. comm., 1987), some of which have preserved their primary textures. Fine-grained basic lavas or tuffs consisting of uralitised pyroxene, plagioclase, chlorite and opaque phases which in some cases show amygdales, are intercalated with the aforementioned sedimentary and acid volcanic rocks. The basic lavas have mostly been altered to partly strongly foliated amphibolites.

The Neuhof Formation overlies the Mooirivier Complex unconformably but seems to be closely associated with this probably oldest Formation of the Rehoboth Basement Inlier. The Neuhof Formation, similar in lithology to the Elim Formation, is considered to be older than the Elim Formation because of the locally higher degree of metamorphism (SACS, 1980) of the Neuhof Formation. This argument seems to be rather weak to form the basis for the stratigraphy of an entire area, as in many regions of the world a higher degree of metamorphism does not necessarily mean a higher age of the formation in question. No contacts between the Neuhof and the Elim Formations are known from the Rehoboth Basement Inlier. To the southwest of Rehoboth the rocks of the Neuhof Formation are unconformably overlain by the Marienhof Formation and in the area of the Nubib mountains they are overlain by the Barby Formation and tectonically bordered by unmetamorphosed rocks of the Sinclair Sequence. Granites mapped as members of the Piksteel Intrusive Suite by the Geological Survey in Windhoek intrude the Neuhof Formation in the area southwest of Rehoboth and along the escarpment in the western Maltahöhe district.

The Piksteel Intrusive Suite shows Rb-Sr isochron ages ranging between 1057 Ma and 1725 Ma (Reid *et al.*, 1988; this study) in the western Rehoboth area, while Burger and Coertze (1973-74, 1975-76) and Burger and Walraven (1977-78) give U-Pb ($^{207}Pb/^{206}Pb$) ages ranging between 986 Ma and 1784 Ma for members of the Piksteel Intrusive Suite. Discordia U-Pb ages of this study for several plutons of the Piksteel Intrusive Suite are also within this range of ages (see Chapter 8). The age of the Gamsberg Granite Suite was determined by the U-Pb and Rb-Sr methods to be between 1079 Ma and 1222 Ma (Reid *et al.*, 1988; Seifert, 1986; Burger *et al.*, 1973-74). The Nubib granite which intrudes the Neuhof Formation in the western Maltahöhe district has yielded a Rb-Sr errochron age of 1104 Ma (Mailing, in prep.) and U-Pb ($^{207}Pb/^{206}Pb$) ages of 1350 ± 40 Ma and 1360 ± 50 Ma (Rooikam granite) (Burger and Coertze, 1973 and 1973-74), respectively.

The Barby Formation, which overlies the Neuhof Formation in the Maltahöhe district, has yielded Rb-Sr ages of 1200 Ma, 1263 Ma and 1265 Ma (Watters, 1974; Mailing, in prep., Kroener, 1975). U-Pb dating of a quartz porphyry of the Barby Formation yielded a $^{207}Pb/^{206}Pb$ age of 1656 ± 40 Ma (Burger and Walraven, 1977-78).

U-Pb age determinations ($^{207}Pb/^{206}Pb$) of metamorphosed acid lavas from the Neuhof Formation itself range between 594 ± 10 Ma and 1784 ± 45 Ma (Burger and Coertze, 1975-76 and Burger and Walraven, 1980).

5.2 SAMPLE COLLECTION AND DESCRIPTION

Five whole-rock samples of Neuhof amphibolites weighing 30 kg each were collected southwest of Rehoboth on the farms Koichas 372 and Swartskaap 332 (Fig. 5.1). Two whole-rock samples of Neuhof amphibolites and four samples of granitoid Neuhof rocks were collected on the farm Neuhof 100 (Fig. 5.2).

The analysed amphibolites from Koichas, Swartskaap and Neuhof are fine-grained massive rocks which contain clefts filled with epidote minerals. They are composed of 40-70% greenish to bluish-green, partly altered amphiboles which are embedded in a mostly strongly suassuritised plagioclase matrix. Apatite, sphene, biotite, garnet and opaque minerals occur as accessories. Abundant secondary minerals are epidote minerals, chlorite, sericite, calcite and quartz.

The analysed granitoids from Neuhof are fine- to medium-grained massive rocks which are penetrated by a multitude of small shear zones and calcite ± epidote-filled clefts. Local kakiritisation phenomena are quite abundant throughout the analysed samples. Original magmatic textures, however, have been partly preserved. According to X-ray diffraction data the analysed granitoids are composed of 10-33% quartz, 15-35% plagioclase and 30-55% potassium feldspar. None of the analysed samples showed more than I % by volume partly chloritised biotite. Acces-

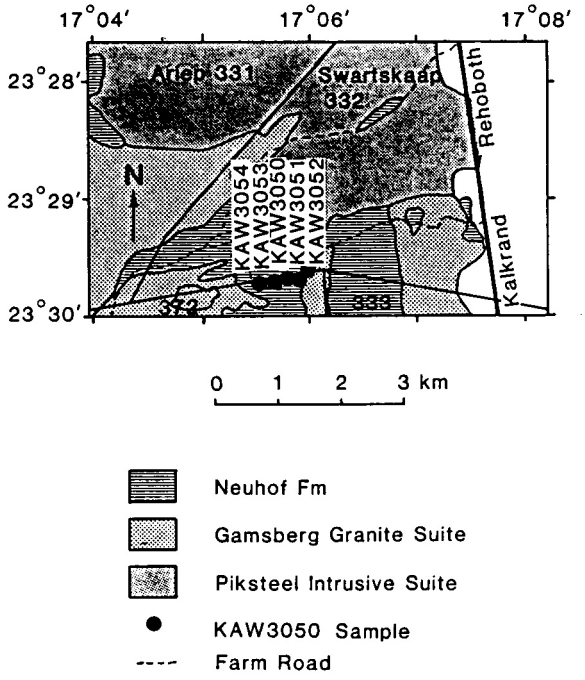

Figure 5.1: Map of the Neuhof sample localities in the area southwest of Rehoboth

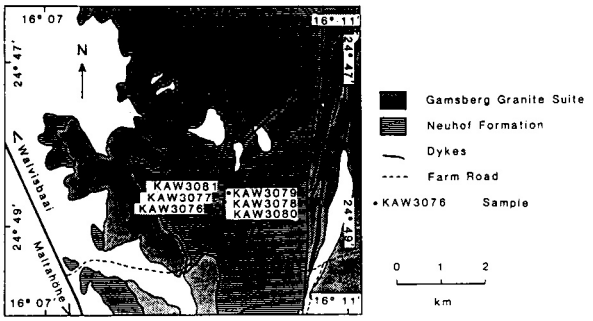

Figure 5.2: Sample localities on the farm Neuhof 100

sories are opaque minerals, sphene and zircon. The analysed Neuhof granitoids are similar in appearance to those rocks which are considered by K. Schalk of the Geological Survey in Windhoek (pers. comm., 1987) to be subvolcanic granitic intrusions corresponding in composition to the acid lavas of the Neuhof Formation.

5.3 RESULTS

5.3.1 Geochemistry

The analytical results are listed in Table 8 (see Appendix). With the exception of KAW3054 all the analysed Neuhof amphibolites are of orthogenic origin according to the criteria of Froehlich (1960) (Fig. 5.3). In this diagram it is evident that six out of seven analysed specimens plot on an imaginary well-correlated line which thus might indicate magmatic differentiation processes.

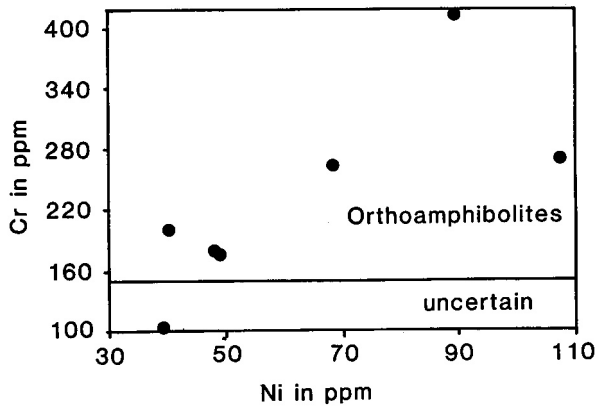

Figure 5.3: Ni versus Cr diagram for the analysed Neuhof amphibolites. Amphibolites with Cr contents > 150 ppm are likely to be of orthogenic origin (Froehlich, 1960)

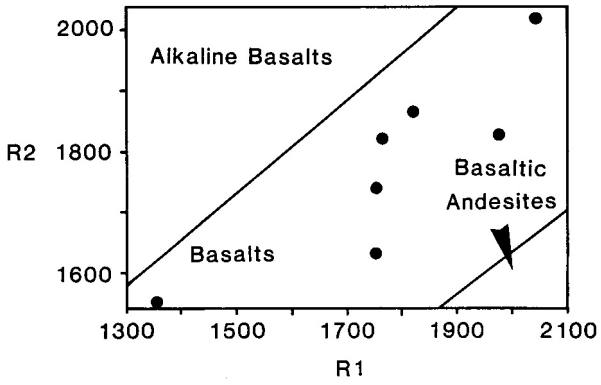

Figure 5.4: R1 versus R2 classification diagram of De La Roche *et al.* (1980) modified by Streckeisen (1981) for the analysed Neuhof amphibolites (R1 = 6Ca+2Mg+Al; R2 = 4Si-(11Na+K)-2(Fe+Ti))

The analysed amphibolites plot entirely in the basalt field of the R1 versus R2 diagram of De La Roche *et al.* (1980) modified after Streckeisen (1981) (Fig. 5.4). With the exception of KAW3081 all the amphibolites are of tholeiitic chemistry according to the Zr/P_2O_5 versus TiO_2 diagram of Winchester (1976) (Fig. 5.5). Bearing in mind the limitations of tectonic discriminant diagrams as discussed by Wilcox (1979), who states that only glassy or very fine-grained samples should be analysed in order to permit a determination of the liquid line of descent of a magma, the data obtained were plotted onto the tectonic discriminant ternary Ti/100-Zr-3*Y diagram of Pearce and Cann (1973) (Fig. 5.6). The samples plot in the fields for Mid Ocean Ridge Basalts and for Calc-Alkaline Basalts (Fig. 5.6). One sample plots on the boundary between the fields for Within Plate Basalts and Calc-Alkaline Basalts.

It has thus to be assumed that the analysed amphibolites represent predominantly tholeiitic magmatism. The scatter of data points in the tectonic discriminant diagram does not allow attribution of a specific tectonic setting to the formation of the analysed amphibolites and thus leaves doubts about the significance of such tectonic discriminant diagrams for metamorphic rocks.

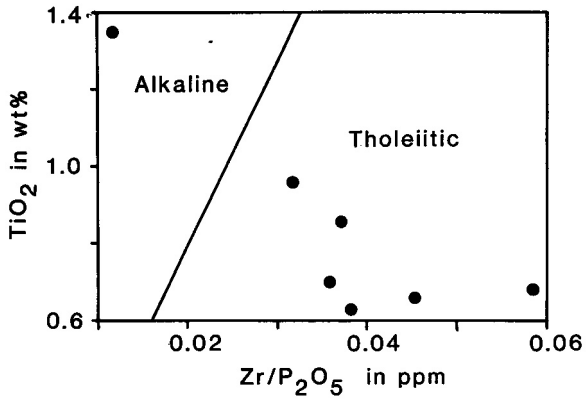

Figure 5.5: Zr/P_2O_5 versus TiO_2 diagram of Winchester (1976) for the analysed Neuhof amphibolites

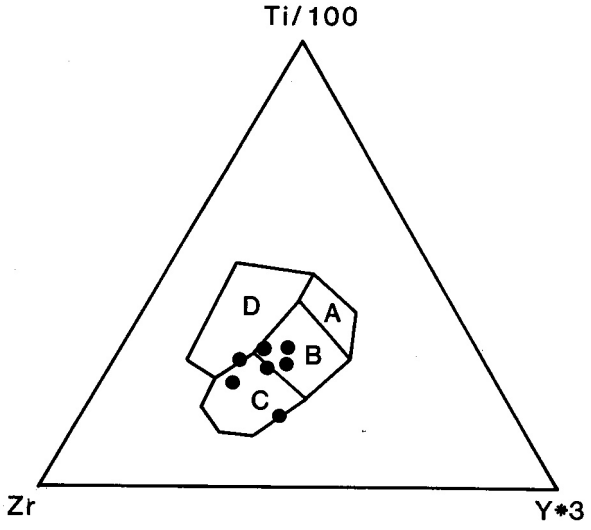

Figure 5.6: Ti/100-Zr-3*Y ternary diagram of Pearce and Cann (1973) for the analysed Neuhof amphibolites (A = Island Arc Tholeiites; B = Mid Ocean Ridge Basalts; C = Calc-Alkaline Basalts; D = Within Plate Basalts)

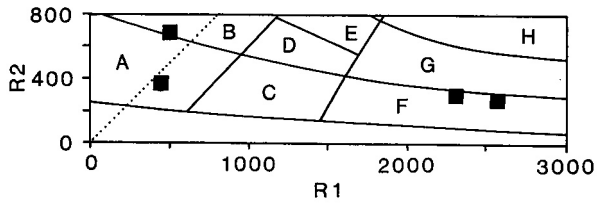

Figure 5.7: R1 versus R2 classification diagram of De La Roche *et al.* (1980) modified by Streckeisen (1981) for the analysed Neuhof granitoids (R1 = 4Si-11(Na+K)-2(Fe+Ti); R2 = 6Ca+2Mg+Al)
(A = alkaline syenites; B = syenites; C = quartz alkaline syenites; D = quartz syenites; E = quartz monzonite; F = alkaline granite; G = granite; H = granodiorite)

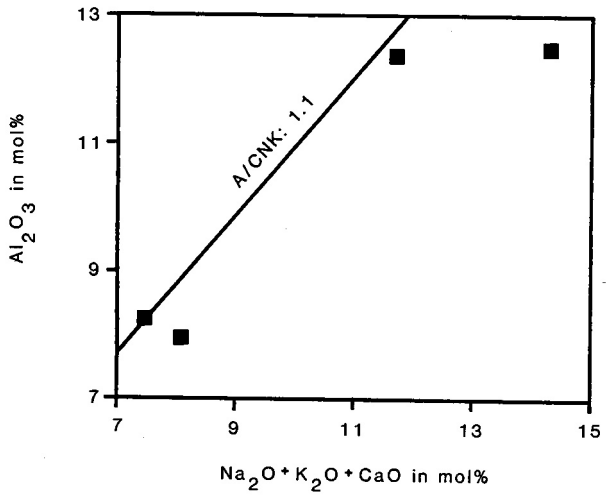

Figure 5.8: Mol.% (Na_2O+K_2O+CaO) versus mol.% Al_2O_3 diagram for the analysed Neuhof granitoids

Two of the four analysed Neuhof granitoids plot in the field for alkalic granites in the R1 versus R2 diagram of De La Roche (1980) modified by Streckeisen (1981) (Fig. 5.7), while one of the samples plots into the syenite field and another plots into the field for alkalic syenites. This scatter of the data points certainly has its cause in primary compositional differences of the analysed granitoids as can be deduced from their highly variable contents of, on such a scale, relatively immobile elements such as SiO_2 and Al_2O_3 (see Table 8; Appendix). Strong variations of the degree of differentiation as observed in the four analysed granitoids are usually also accompanied by variations of the alkali contents. Such possible primary variations of the alkali contents are also present in the analysed samples (Table 8; Appendix) and are thus responsible for the observed spread of the data points along the RI axis. According to the index of Shand (1951) all the analysed granitoids are of peraluminous nature. Whether the analysed granitoids are of a sedimentary or igneous origin is not clarified by the mol.% (Na_2O+K_2O+CaO) versus mol.% Al_2O_3 diagram (Fig. 5.8), where two of the four specimens plot beyond a line representing an A/CNK ratio of 1.1, and two samples plot below this line, which separates S-type magmas from I-type magmas according to Chappell and White (1974). In the Nb+Y versus Rb diagram of Pearce *et al.* (1984) (Fig. 5.9) three data points plot in the field for Within Plate Granites and one point plots into the Volcanic Arc Granite field.

5.3.2 Rb-Sr analyses

The results of the Rb-Sr analyses are listed in Table 9 (see Appendix).

The analytical results of the amphibolites from Koichas and Swartskaap do not form an isochron in the $^{87}Rb/^{86}Sr$

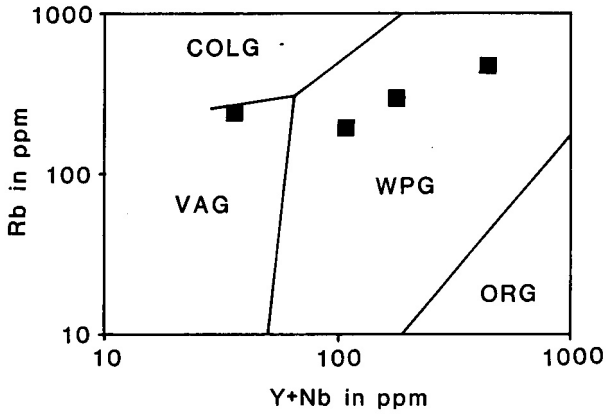

Figure 5.9: Nb+Y versus Rb diagram of pearce (1984) for the analysed Neuhof granitoids (COLG = Collision Granites; VAG = Volcanic Arc Granites; WPG = Within Plate Granites, ORG = Ocean Ridge Granites)

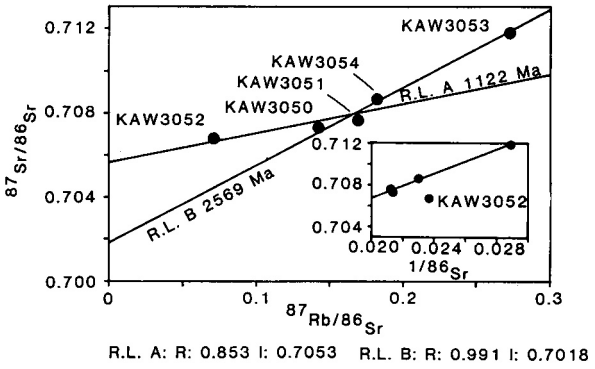

Figure 5.10: $^{87}Rb/^{86}Sr$ versus $^{87}Sr/^{86}Sr$ diagram for the analysed Neuhof amphibolites from the area to the southwest of Rehoboth (inset = $1/^{86}Sr$ versus $^{87}Sr/^{86}Sr$ diagram for the same samples)

versus $^{87}Sr/^{86}Sr$ diagram (Fig. 5.10). It is nonetheless possible to fit two reference lines through the scattered data which, as a matter of fact, both represent not very reliable two-point regression lines depending on KAW3052 in the case of reference line A and on KAW3053 in the case of reference line B. Reference line A, which connects the samples KAW3050, KAW3051, KAW3052 and KAW3054 yields an age of 1122 Ma ± 428 Ma with a low correlation coefficient R of 0.853 and an intercept I at $^{87}Sr/^{86}Sr$ = 0.7053 ± (1.0009. Reference line B, which connects the samples KAW3050, KAW3051 and KAW3054 yields an age of 2569 Ma ± 244 Ma with a good correlation coefficient R of 0.991 and an intercept I at $^{87}Sr/^{86}Sr$ = 0.7018 ± 0.0007. A plot of the $1/^{86}Sr$ ratios of the samples versus their $^{87}Sr/^{86}Sr$ ratios (see inset in Fig. 5.10) shows a good correlation of the data points of four out of five samples (KAW3050-51 and KAW3053-54), thus indicating that Sr mixing processes, such as the admixture of common Sr from a source outside the analysed parts of the Neuhof Formation, may have occurred in the northern outcrop area of the Neuhof Formation if the linear grouping of the data points is not due to primary magmatic effects, such as the fractional crystallisation of feldspar, a question which could not be resolved on the basis of the present sample material. A possible admixture of common Sr might have occurred in relation with the intrusion of Gamsberg-type granites in the area, and might also be responsible for the formation of reference line A with its age of 1122 Ma. As a Rb-Sr age of 2569 Ma is quite unlikely for rocks of the Neuhof Formation based on Sm-Nd data on the Rehoboth Inlier (see Chapter II), the steep slope of reference line B and its corresponding age of 2569 Ma probably has to be attributed to mixing processes and thus should be regarded as geologically meaningless. It must be stated, however, that the intercepts of both reference lines give reasonable values of $^{87}Sr/^{86}Sr$ = 0.7053 and 0.7018, respectively, which also could be found in common basic magmas. This indicates that the whole-rock $^{87}Sr/^{86}Sr$ ratios were not significantly changed during the observed homogenisation processes, which in turn confirms the orthogenic origin of the analysed amphibolites.

A different pattern is shown by the analytical results of the amphibolitic and granitoid samples from the farm Neuhof 100. With the exception of KAW3078 all the data points plot on a highly correlated (R = 0.99991) isochron yielding an age of 1167 Ma ± 9 Ma with an intercept I at $^{87}Sr/^{86}Sr$ = 0.704 ± 0.003 in the $^{87}Rb/^{86}Sr$ versus $^{87}Sr/^{86}Sr$ diagram (Fig. 5.11). This indicates a complete homogenisation of the Sr systems of the analysed amphibolites and granitoids at the obtained age of 1167 Ma. This homogenisation phase probably should be attributed to the intrusion of Gamsberg-type magmas into the Neuhof Formation. A homogenisation and/or a mixing of the Sr systems of the analysed samples may also be assumed based on the $1/^{86}Sr$ versus $^{87}Sr/^{86}Sr$ diagram (see inset of Fig. 5.11) if the formation of a linear array by the granitoid samples in this diagram is not due to primary fractional crystallisation, a possibility which could not be ruled out given the present sample material.Also

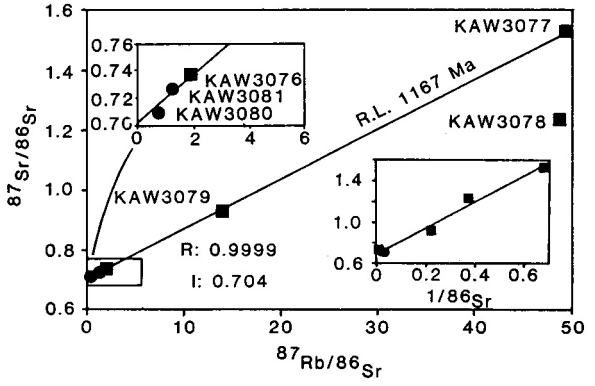

Figure 5.11: $^{87}Rb/^{86}Sr$ versus $^{87}Sr/^{86}Sr$ diagram for the analysed amphibolitic and granitoid specimens from Neuhof 100 (inset = $1/^{86}Sr$ versus $^{87}Sr/^{86}Sr$ diagram for the same samples). The granitoid samples are represented by filled squares while the amphibolites are represented by filled circles

of note here is that the obtained intercept in the isochron diagram at $^{87}Sr/^{86}Sr = 0.704$ represents a low value which would more likely be expected in a primary magmatic system than in a system which suffered from the admixture of Sr from common sources. It should thus be assumed that the changes of the whole-rock $^{87}Sr/^{86}Sr$ ratios by admixing processes were of relatively small magnitude. Thus the quite low initial $^{87}Sr/^{86}Sr$ ratio clearly points at I-type origins for the analysed granitoids. This in turn would mean that major-element based geochemical classification of the analysed granitoids of Chapter 5.3.1, (which, for instance indicates S-type origins for half of the analysed granitoids), is doubtful due to the mobility of various elements (alkalis) during post-formation alteration processes.

5.4 CONCLUSIONS

This chapter shows that most of the analysed amphibolites of the Neuhof Formation are of orthogenic origin and that their protoliths are best described as mostly tholeiitic basalts, which, according to the classification scheme of Pearce and Cann (1973), possibly formed in a mid ocean ridge or volcanic arc tectonic setting. Although the mobility of various elements during the alteration has obscured the origins of the analysed granitoids, it may be postulated according to their low $^{87}Sr/^{86}Sr$ initial ratios that they represent I-type magmatism, which, according to the classification of Pearce and Cann (1984), should have taken place in within plate- and volcanic arc tectonic settings. Both attempts to classify the analysed specimens by the methods of Pearce *et al.* (1973, 1984) thus yielded confusing results and point at the limitations of these classification schemes due both to post-formation alteration and to primary effects as discussed by Wilcox (1979).

The Rb-Sr whole-rock analyses have shown that all the analysed Rb-Sr systems have been disturbed by post-genetic homogenising processes. The observed small changes of the initial $^{87}Sr/^{86}Sr$ ratios of the analysed specimens during homogenisation show that the analysed whole-rock systems were not affected by the admixture of large amounts of highly radiogenic Sr from distant sources, but that their Sr systems were homogenised "locally". The homogenisation processes can be assumed to have taken place in relation with the intrusion of granitic (Gamsberg-type) magmas, such as the Nubib granite, into the Neuhof Formation between 1100 and 1200 Ma. They at least resulted in a complete homogenisation of the Sr systems of the analysed amphibolitic and granitoid samples from Neuhof 100.

The present study therefore cannot give evidence on the formation age of the Neuhof Formation. It can, however, be deduced from the present data that the results of other workers in the area should be interpreted carefully before a formation age can be assigned to the Neuhof Formation based on radiometric age determinations, considering that post-formation processes were able to completely reset the Sr systems of parts of the Formation. The influence of these homogenisation processes on other isotopic systems is best shown by the high variance of the discordant U-Pb ages obtained for the Neuhof acid lavas by Burger and Coertze (1975-76) and Burger and Walraven (1980) which range between 594 Ma and 1784 Ma.

6. ELIM FORMATION

6.1 INTRODUCTION

Rocks of the Elim Formation were first described by De Kock (1934) who included them with the "Mixed Rocks" on his map of the Western Rehoboth area. Later De Waal (1966) included them with the "Banded Granulite, Quartzite and Schist" section of his Marienhof Formation before they were separated from this formation by Schalk (1967) in order to form the present Elim Formation. Brewitz (1974) gave a detailed description of the occurrences of the Elim Formation in the vicinity of the former Kobos mine. He subdivided the formation into an Elim1, Elim2 and Elim3 (Gaub Valley Schists) Formation. This subdivision was not maintained by SACS (1980) who followed Schalk's (1967) proposals on the extent of the present Elim Formation.

The base of the formation is nowhere exposed. The contacts towards the overlying Marienhof Formation are always tectonically disturbed. The Elim Formation was deformed and metamorphosed under amphibolite facies conditions (Brewitz, 1974) before it was intruded by the Alberta Complex, members of the Weener and Piksteel Intrusive Suites, members of the Gamsberg Granite Suite and various basic and acid dykes. On the farms Naub 274 and Biesiespoort 275 it is also intruded by the Naub diorite which yielded a Rb-Sr isochron age of 1725: ± 74 Ma (Reid *et al.*, 1988). Based on this minimum age and on lithologic descriptions the Elim Formation is regarded by geologists of the Geological Survey (Windhoek) as a probable correlate of the Khoabendus Group of the Kamanjab Inlier (SACS, 1980). According to De Waal (1966) and Brewitz (1974) the Elim Formation underwent three different metamorphic phases. A first regional metamorphism under almandine-amphibolite facies conditions paralleled the tectogenesis of the Nauchas granites, while the second regional metamorphism under greenschist facies conditions was related to the Damara orogeny whose convergent phase took place between 650 Ma and 420 Ma, according to Miller (1983). A late post-Damaran tectonic deformation and hydrothermal alteration of the formation was regarded by these authors as a third major phase in the area. This subdivision of the metamorphic history of the area is untenable in the light of more recent radiometric age determinations. Reid *et al.* (1988) have shown that the Naub diorite with a Rb-Sr isochron age of 1725 ± 74 Ma and the Alberta Complex with a Rb-Sr isochron age of 1440 ± 25 Ma intrude an already deformed and metamorphosed Elim Formation. Although the significance of the Naub isochron is to some extent doubted by these authors (see below), it can be said that the first regional metamorphism cannot be correlated with the intrusion of the Nauchas granites, which, as a part of the Gamsberg Granite Suite, did not intrude until much later at 1079 ± 25 Ma. In the northern part of the Rehoboth Basement Inlier the Damara orogeny certainly played an important role in the metamorphic history of the Elim Formation as shown by K-Ar determinations of various authors (Clifford, 1967; Weber *et al.*, 1983; this study) which have proved that in this area the K-Ar systems of biotites and white micas were completely reset in relation to the Damara orogeny.

The formation consists of a more than 3000-m-thick succession of low- to medium-grade metamorphic rocks which is nowhere continuously exposed.

The major part of the formation is made up of quartzitic rocks. They range in composition from sericitic quartzites to magnetite-rich quartzites which partly grade into itabirites. Primary sedimentary structures have been preserved in all the quartzite varieties in spite of local polyphase metamorphism. Albite, microcline, amphiboles and epidote are abundant accessory minerals within most of the quartzites.

Amphibolites of a wide range of compositional and textural varieties form the major portion of the remaining part of the Elim Formation. Layers of massive fine- to coarse-grained amphibolites are as abundant as schistous and banded varieties partly interlayered with limestone bands. The composition of the amphibolites ranges from chlorite-epidote amphibolites and schists to garnet-bearing amphibolites. The amphibolites partly grade into chlorite-epidote greenschists. The Cu-Zn-Au mineralisation in the Kobos area is associated with the amphibolites and greenschists of the Elim Formation (Brewitz, 1974).

To the west of Rehoboth, calcareous rocks are prominent features at several levels of the Elim Formation. They range in composition from limestone to dolomite and ankerite and contain abundant nodular chert inclusions. Accessory plagioclase, (tremolitic) amphiboles, biotite and white micas are present in most of the Elim marbles. The occurrence of pyroxene- and garnet-bearing wollastonite fels, and diopside-bearing carbonates was described by De Waal (1966) for areas which are today included in the Elim Formation.

Phyllitic to quartzitic partly garnet-bearing mica schists of sedimentary and partly of possible volcanic origin are often intercalated within the mostly quartzitic and amphibolitic succession.

6.2 SAMPLE COLLECTION AND DESCRIPTION

The sample localities of most of the samples collected are shown on Figure 6.1 while the coordinates of all the sample localities are listed in Table 10 (see Appendix). Nineteen whole-rock samples each weighing 30-50 kg of amphibolites and greenschists were collected in various outcrops of the Elim Formation throughout the Rehoboth Basement Inlier (KAW3003-KAW3006, KAW3008-KAW3012, KAW3045-KAW3049 and KAW3068-KAW3072). Whole-rock samples of three mica schists (KAW3014-KAW3016) were collected on the farm Morgenroth 17 in the contact aureole of the intrusion of a member of the Piksteel Intrusive Suite (Geol. Survey of Namibia, unpubl. 1:250 000 map 2316 Rehoboth) while two other samples were collected on the farms Kabiras 343 (KAW3013) and Witkrans 342 (KAW3017). Five other whole-rock samples of mica schists were collected on Areb 76 (KAW3066, KAW3067, KAW3073-KAW3075) close to the Areb shear zone. One

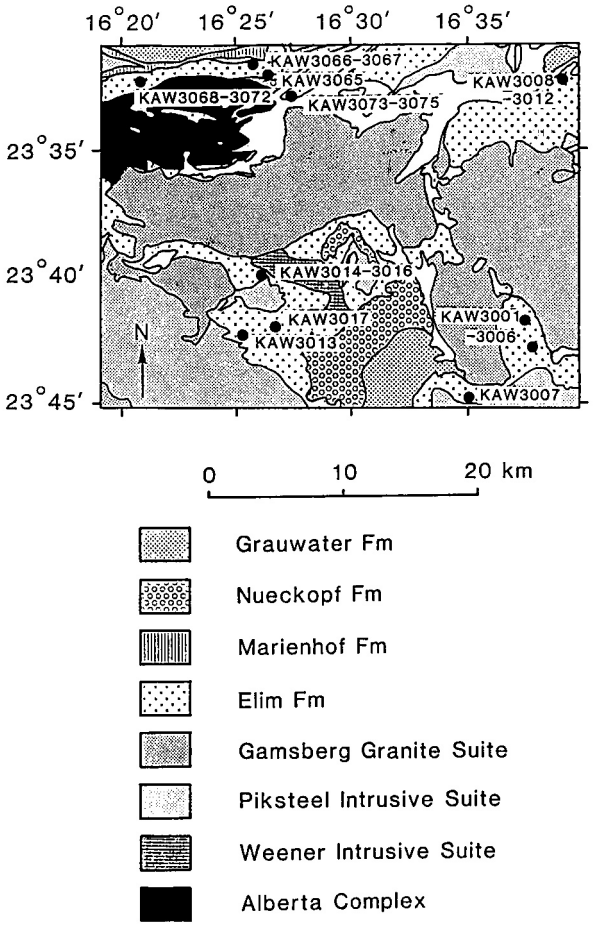

Figure 6.1: Sample localities of the analysed Elim specimens. (KAW3045 - KAW3049 are outside the range of the sketch map; see Table 10 (Appendix) for precise coordinates of the analysed specimens)

whole-rock sample of an itabirite (KAW3002) and a biotite-sericite schist (KAW3001) come from the farm Samkubis 516. Finally. two whole-rock samples of Elim marbles were collected on Grauwater 341 (KAW3007) and on Areb 76 (KAW3065).

The massive and mostly fine-grained amphibolites from Samkubis 516 (KAW3003- KAW3006) are composed of 50-60% actinolitic hornblende, 35-40% mostly strongly saussuritised plagioclase, up to 15% quartz and accessory apatite, opaque minerals, sphene, epidote minerals, chlorite and calcite. All the samples are strongly folded and show a foliation on a sub-millimetre scale. According to their appearance in thin section they might very well be of orthogenic origin. KAW3008-KAW3012 which come from the farm Kobos 321 are massive fine- to medium-grained amphibolites with the exception of KAW3008, which represents a typical Elim greenschist. Original small-scale folding and a narrow foliation have been partly preserved in the otherwise mostly massive samples whose ortho- or paragenic origin cannot be detected by thin section investigation alone. The amphibolites consist of 50-60% partly chloritised actinolitic hornblendes, which are embedded in a mostly very fine-grained matrix consisting of epidote minerals, sphene, albite, sericite, quartz and calcite, while the greenschist is composed of 47% actinolitic hornblende, 30% albite, 15% quartz, 3% epidote minerals, 5% chlorite and white mica and accessory sphene and opaque minerals.

With the exceptions of KAW3045 which represents a massive, fine-grained and strongly altered amphibolite and KAW3047 representing a biotite schist. the samples from Naub 274 (KAW3045-KAW3049) may be described as greenschists which partly grade into hornblende garbenschiefer. These fine- to medium-grained, strongly foliated and partly altered schists are composed of 40-75% acti-oolitic amphibole, 5-20% plagioclase, 5-25% chlorite, 7-20% epidote minerals, 3-10% quartz and up to 3% opaque minerals and accessory sphene. The Naub samples either originate in tuffaceous volcanic layers or in entirely sedimentary deposits.

Five samples of fine-grained, massive amphibolites (KAW3068-3072) were collected near the Areb shear zone on the farm Alberta 175. They derive from a part of the Elim sequence which is interlayered on a decimetre scale with calcareous layers and might be of orthogenic (tuffaceous ?) as well as of paragenic origin. A narrow foliation and small-scale folds can be recognised in thin section. The amphibolites are composed of 45-80% bluish-green to brownish amphiboles which have been partly chloritised, 4-25% partly altered plagioclase, 7-18% epidote minerals, up to 15% quartz, up to 3% sphene and accessory opaque minerals, apatite, biotite and calcite.

The strongly foliated and folded, fine-grained mica schists from the farm Morgenroth 17 (KAW3014-KAW3016) consist of 25-50% quartz, 10-25% feldspar (albite), 25-45% muscovite, 3% chloritised biotite, 2% opaque minerals and accessory garnet and epidote minerals. The muscovite in these samples certainly grew after the major deformation phase which affected the rock. The mica schists from the farms Kabiras 343 (KAW3013) and Witkrans 342 (KAW3017) are similar in compostion. except for their lack of garnet. Sample KAW3017 is crosscut by several aplitic veinlets indicating that the major part of this outcrop of the Elim Formation was affected by the intrusion of granitic material.

The two mica schists from Areb 76 (KAW3066 and KAW3067) which were collected close to the Areb shear zone, represent strongly sheared and partly mylonitised, fine-to very fine-grained metagreywackes, showing a high grade of alteration of their mineral content including the formation of sericite. The other three mica schists from Areb 76 (KAW3073-KAW3075) have been much less affected by the tectonic activity along the Areb shear zone. These fine-grained and tightly folded mica schists show a narrow foliation and are composed of 30-60% quartz, 3-10% albite, 12-30% muscovite/sericite, 3-30% chlorite, 4-5% epidote minerals and accessory opaque minerals, sphene and opaque minerals.

The fine-grained and narrowly foliated and folded itabirite from the farm Samkubis 516 (KAW3002) is composed of 32% opaque minerals (mostly magnetite/hematite), 20% actinolitic hornblende. 45% quartz, 3% epidote minerals and accessory apatite, chlorite and sericite, while sample KAW3001 from the same farm represents a typical biotite-sericite schist of the Elim formation.

X-ray diffractometer analyses have shown that the medium grained, massive marble from the farm Grauwater 341 (KAW3007) is composed of 72% dolomite and 23% calcite while the fine-grained and strongly tectonised marble from Areb 76 (KAW3065) is entirely dolomitic. Both marbles contain small amounts of white micas, chlorite, quartz and opaque minerals.

6.3 RESULTS

6.3.1 Geochemistry

All the results of the geochemical analyses are listed in Table 10 (see Appendix). The corresponding Niggli values are listed in Table 10A (see Appendix). Bearing in mind the problems of the graphic analyses of geochemical diagrams as discussed by Wilcox (1979), we nonetheless attempted to obtain information on the origin of the analysed samples using the various discriminant diagrams.

The Niggli mg values of all the analysed samples of the Elim Formation were plotted versus the c values in the c-mg diagram of Leake (1964) (Fig. 6.2). The analysed mica schists plot for the most part in and around the field for pelites, while the analysed carbonates plot towards the upper right (dolomite) corner of the diagram. The amphibolitic samples plot between the areas typical for pelites and carbonates but they do not lie on the general igneous trend which is represented in the diagram by an arrow.

More information on the origin of the analysed samples is given by the c-100*mg-(al-alk) ternary diagram of Leake (1964) (Fig. 6.3), where all but one (KAW3046) of the analysed amphibolitic samples plot on the general magmatic trend, while the analysed mica schists and marbles plot either along sedimentary trends or in areas typical of pelites and dolomites.

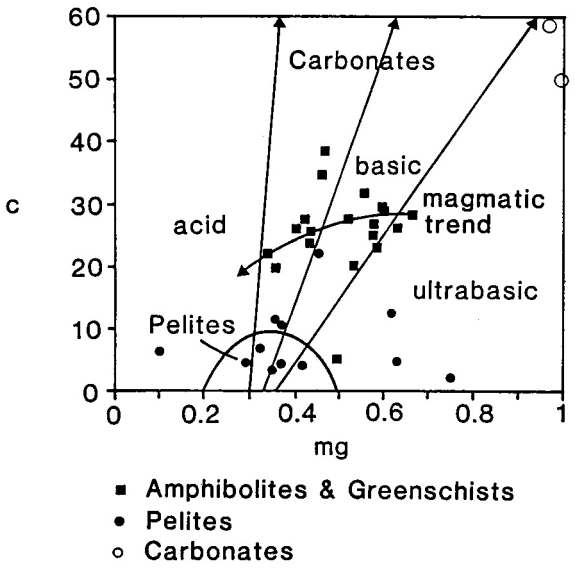

Figure 6.2: Niggli mg versus c diagram for all the analysed samples of the Elim Formation

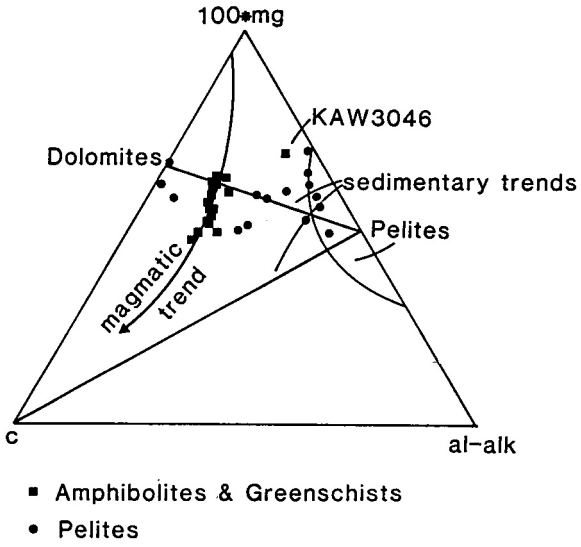

Figure 6.3: C-100*mg-(al-alk) ternary diagram of Leake (1964) for all the analysed samples of the Elim Formation

According to Figures 6.2 and 6.3 a magmatic origin must be assumed for most of the amphibolitic samples. Their Ni contents were plotted against their Cr contents in order to confirm this assumption (Fig. 6.4). A comparison of the classification criteria of various workers shows that the inconsiderate use of this diagram may lead to incorrect interpretations as none of the amphibolitic samples plots into the field for ortho-amphibolites of Walker *et al.* (1960) (Cr> 250 ppm; Ni > 200 ppm), while all the data points are of orthogenic origin according to the criteria of Kukley *et al.* (1975) (Cr/Ni > 1). Three quarters of the samples are of orthogenic origin according to Froehlich (1960), who states that amphibolites having Cr > 150 ppm are of orthogenic origin while amphibolites with Cr < 20 ppm are of paragenic origin. Nonetheless, it is of interest that sample KAW3046, which plots far off the general igneous trend in Figure1, would also have to be considered to be of igneous origin according to the criteria of Froehlich (1 960) and Kukley *et al.* (1975) in Figure 6.4.

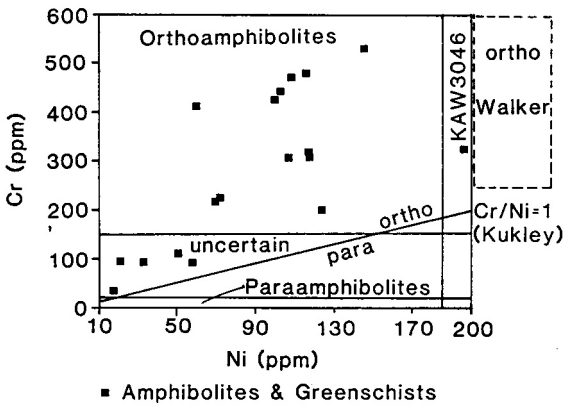

Figure 6.4 (right): Ni versus Cr diagram for the analysed Elim amphibolites. The different field limitations are according to Walker (1960), Froehlich (1960) and Kukley (1975)

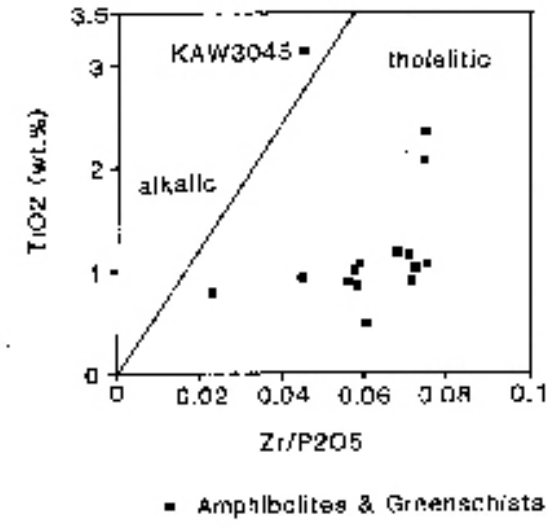

Figure 6.5: Zr/P_2O_5 versus TiO_2 diagram of Winchester (1976) for the analysed Elim amphibolites

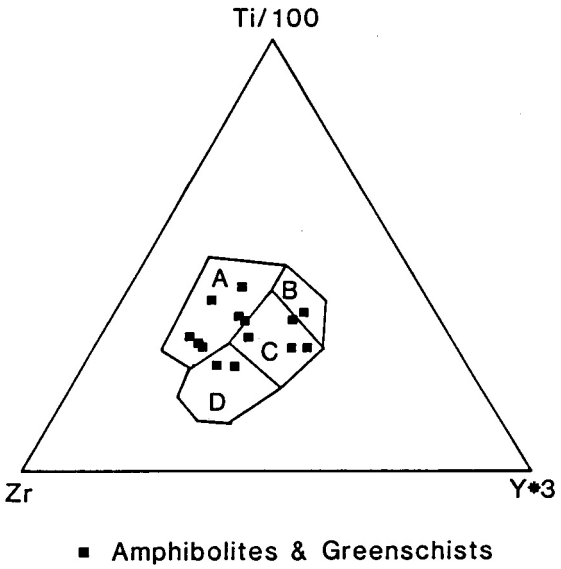

Figure 6.6: Zr-Ti/100-Y*3 ternaty diagram of Pearce and Cann (1973) for the analysed Elim amphibolites. (A = Within Plate Basalts; B = Island Arc Tholeiites; C = Mid Ocean Ridge Basalts; D = Calc-Alkaline Basalts)

In spite of all the problems encountered in elucidating the origin of the analysed amphibolites, we believe that the major part of the Elim amphibolites is probably of partly tuffaceous orthogenic origin. As most major elements may be mobilised by metamorphic processes, only the relatively stable elements TiO_2, P_2O_5, Zr, Y and Nb were used to investigate the plate tectonic situation from which the analysed samples derived.

The data were plotted in the Zr/P_2O_5 versus TiO_2 diagram of Winchester (1976) where all but one (KAW3045) of the samples plot in the field for tholeiitic rocks (Fig. 6.5). Three data points representing amphibolites from Kobos (KAW3010-KAW3012) could not be plotted as their Zr content is below the XRF detection limit. However, examining the TiO_2 contents of these samples which are below 0.3% by weight it should be assumed that these three samples are also of tholeiitic nature.

The very low Nb contents of the analysed samples (with one exception, KAW3045, yielding 19 ppm Nb) all fall below the detection limit of II ppm and thus also point to a tholeiitic origin of the amphibolites.

We then tried to plot all the amphibolites into the tectonic discriminant Zr-Ti/100-Y*3 ternary diagram of Pearce and Cann (1973) (Fig. 6.6). With the exceptions of the three Kobos amphibolites which are poor in zircon, and a Naub schist (KAW3048) whose Y content is below the detection limit, the data points scatter into all the different areas assigned to various typical plate tectonic settings by Pearce and Cann (1973). Therefore it is not possible to assume a specific plate tectonic setting for the basic Elim rocks based upon this classification diagram. The observed scatter of data points can be interpreted in several ways:

- The Elim Formation is formed of rocks which derived from different plate tectonic settings and therefore cannot be interpreted by a simplistic model.
- It is composed of rocks whose original geochemical patterns (including trace elements) have been strongly altered by metamorphic processes.
- The classification systems of Pearce and Cann (1973) are not suitable for the type of rocks analysed as might be suspected according to the considerations of Wilcox (1979), who states that the liquid line of descent of any kind of magma can only be reconstructed from material which is glassy or sufficiently fine-grained to ensure that the analysed material is representative of its parent liquid. Even if metamorphism did not affect the trace element composition of the analysed specimens these constraints have possibly not been fulfilled in the magmatic parent material of the analysed metamorphic rocks, thus preventing a tectonic classification according to the model of Pearce and Cann (1973).

6.3.2 K-Ar analyses

The results of all the K-Ar analyses are listed in Table II (see Appendix).

The analysed white micas from a contact aureole around a small granitic intrusion assigned to the Piksteel Intrusive Suite on Morgenroth, yielded individual K-Ar ages ranging between 1062.3 ± 10.6 Ma and 1142.3 ± 11.4 Ma. The youngest age was obtained for the sample which was collected closest to the next surface outcrop of the intrusion, while the oldest age was obtained for a sample which was collected 250 metres away from the contact. The white micas from a sample which is crosscut by some aplitic veinlets and which was collected in the centre of the area covered by the Elim Formation on the farm Witkrans 342, yielded an age of 1229.5 ± 12.3 Ma. The content of radiogenic ^{40}Ar generally exceeds 99.6%. A major admixture of non-radiogenic argon to the argon of the samples can be ruled out when considering that the content of ^{36}Ar is generally below $0.36 * 10^{-12}$ mol/g for these samples. It can thus be assumed that the intruding granitic magmas in the area were the source of energy leading to the formation of

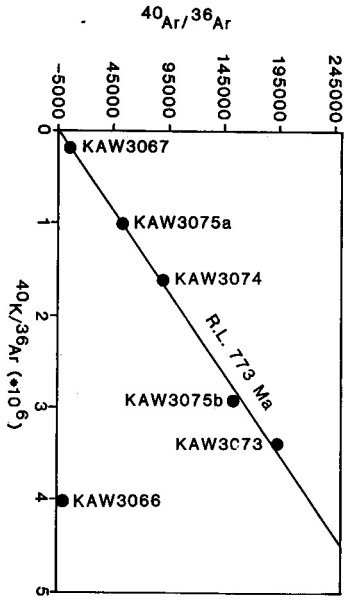

Figure 6.7: $1/^{36}Ar$ versus $^{40}Ar/^{36}Ar$ diagram for the analysed white micas and biotites of the Elim Formation from the farm Areb (see text for discussion)

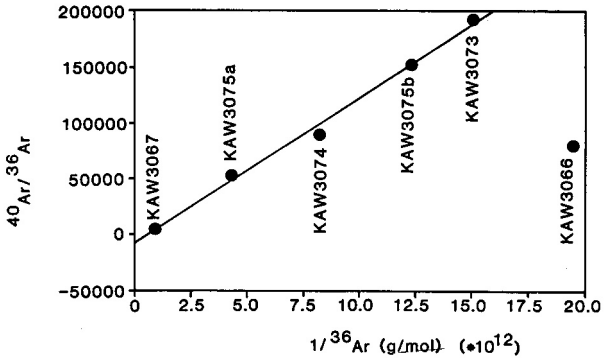

Figure 6.8: $^{40}K/^{36}Ar$ versus $^{40}Ar/^{36}Ar$ diagram for the analysed white micas and biotites of the Elim Formation from the farm Areb (see text for discussion)

the analysed white micas from Morgenroth and possibly also for the formation of the analysed white micas from Witkrans. The effect of decreasing ages towards the intrusion in question may be assigned to the cooling history of the granite body whose radius of energy (and hydrothermal circulation), capable of keeping the K-Ar systems of white micas open, must have been continuously diminishing with time. Thus it should optimistically be assumed that the individual ages obtained of the analysed white micas of the Morgenroth-Witkrans area only indicate a minimum age for reaching the blocking temperature of the analysed minerals due to the decreasing heat-producing energy of an intrusive body, and are not due to a gain of radiogenic argon.

The individual ages of the five white mica samples and the single biotite separate from the vicinity of the Areb shear zone on the farm Areb range between 314.7 ± 3.3 Ma and 781.7 ± 7.8 Ma. All the analysed white micas yielded a radiogenic argon content exceeding 99.45% while the $^{40}Ar_{rad}$ content in the analysed biotite separate (KAW3067), whose K-content of 20.6* 10^{-8} mol/g indicates some alteration (chloritisation ?), is only 94.38%. With the exception of the biotite sample KAW3067 which showed a higher ^{36}Ar content of $1.07*10^{-12}$ mol/g (due possibly to the aforementioned chloritisation processes), all the analysed Areb mica separates showed ^{36}Ar contents below $0.25 * 10^{-12}$ mol/g thus indicating that no significant admixture of non-radiogenic argon occurred. It is of interest that the youngest ages of 314.7 Ma and 396.5 Ma were measured on samples collected close to the Areb shear zone while all the samples collected a few hundred metres away from the shear zone (KAW3073-KAW3075) range between 727.9 Ma and 730.4 Ma. This age distribution clearly shows that the analysed K-Ar systems of the samples collected close to the Areb shear zone (KAW3066 and KAW3067) have formed or have been opened and rejuvenated even after the Damara orogeny by tectonic processes along the Areb shear zone, while the K-Ar systems of the more distant samples were indeed affected (rejuvenated) but not completely reset by the Damara orogeny and/or later processes. This statement is also supported by the observation that the white mica fraction of KAW3066, which was collected close to the shear zone, consists entirely of sericitic micas while the mica fraction of the samples KAW3073-KAW3075 is composed of coexisting white micas and younger (sericitic) aggregates.

The result of the graphic analysis of the K-Ar data of the Areb samples shows that with the exception of KAW3066 the analysed Areb samples define a linear array with a high correlation coefficient R of 0.996 and an intercept I of $^{40}Ar/^{36}Ar = -7376$ in the $1/^{36}Ar$ versus $^{40}Ar/^{36}Ar$ diagram (Fig. 6.7). If the biotite separate KAW3067 is disregarded, the regression line has a correlation coefficient of 0.995 and an intercept 1 of $^{40}Ar/^{36}Ar = -7875$. The high correlation of both regression lines indicates that mixing phenomena might have affected the argon systems of the analysed samples, which is not surprising when considering the coexistence of different generations of white micas and the fact that the Areb shear zone must have been active during the Damara orogeny (see e.g. Chapter 7). As in the $^{40}K/^{36}Ar$ versus $^{40}Ar/^{36}Ar$ diagram (Fig. 6.8), the Areb data points form a linear array similar to that obtained for the $1/^{36}Ar$ versus $^{40}Ar/^{36}Ar$ diagram with a similar intercept I of $^{40}Ar/^{36}Ar = -3640$ and a correlation coefficient R of 0.997 (-2847 and 0.995, respectively, if KAW3067 is disregarded) it may be assumed that the K contents of the samples were not significantly affected by the suspected mixing processes. Furthermore the highly negative intercepts of the regression lines in both diagrams point to a possible loss of argon. As a significant admixture of atmospheric argon can be excluded, except fur KAW3067, due to the low contents of ^{36}Ar of the samples and because of the relative stability of K in the samples, it should be taken into consideration that the processes affecting the K-Ar system of the samples are restricted to loss of $^{40}Ar_{rad}$ and/or total argon and to a gain of $^{40}Ar_{rad}$. It should therefore be assumed that the samples in question were affected by exchange processes

in such a way that the analysed minerals were percolated by fluids which led to a loss of $^{40}Ar_{rad}$ and to the addition of minor amounts of argon of atmospheric composition. This fluid percolation may also have led to the partial chloritisation of the biotites of KAW3067 which was accompanied by the admixture of larger amounts of atmospheric argon with these biotites, which in turn caused the data point of KAW3067 to plot close to the origin in the lower left corner of Figure 2.4. The scatter of data points along the y-axis in the Harper diagram (Fig. 6.9) strongly supports this suggestion but it also shows that not all of the samples were affected by similar and proportional exchange processes of ^{40}Ar. Summarising the results obtained for the Areb samples, it can be said that if no gain of $^{40}Ar_{rad}$ occurred then the individual ages of the samples represent minimum ages for the closure of the analysed K-Ar systems.

The single individual age of 874.4 ± 8.7 Ma obtained for a biotite separate from a biotite schist on the farm Naub (KAW3047), with radiogenic argon content of 99.56% corresponding to $0.21 * 10^{-12}$ mol/g ^{36}Ar, shows that this area was also affected by post-Mokolian rejuvenation processes. These processes, which probably also led to a partial chloritisation of the analysed biotites as indicated by their slightly lowered K content of $21.5 * 10^{-8}$ mol/gK, should probably be connected with Damara-induced metamorphism, which in this area was obviously not strong enough to reset the K-Ar system of the analysed biotite separate.

6.3.3 Rb-Sr analyses

The results of all the whole-rock Rb-Sr analyses are listed in Table 12 (see Appendix).

In Figure 6.10 the $^{87}Rb/^{86}Sr$ ratios of all the whole-rock samples from Samkubis were plotted against their $^{87}Sr/^{86}Sr$ ratios. A reference line calculated through all the amphibolitic samples (KAW3003-KAW3006) (R.L.I) yields an age of 948 ± 197 Ma with an intercept I of $^{87}Sr/^{86}Sr$ at 0.704 ± 0.001 and a low correlation coefficient R of 0.956. The data point of an analysed biotite schist (KAW3001) plots far off this reference line while the analysis of an itabirite (KAW3002) plots in the vicinity of the line. A regression line drawn through three of the data points representing amphibolitic samples (KAW3003, KAW3005 and KAW3006) (R.L.2) yields an age of 396.2 ± 10.6 Ma. Its correlation coefficient R2 is 0.9996 and the intercept 12 is at $^{87}Sr/^{86}Sr$ = 0.70604 ± 0.00004. The point representing the itabirite sample (KAW3002) plots surprisingly well on this second reference line. As neither reference line gives the age of a major tectonic phase of the area it must be assumed that they represent fluid reactions which affected the analysed specimens. The older reference line, with an age of 948 Ma, might have formed during homogenisation processes during the intrusion of magmas related to the Gamsberg Granite Suite, and has probably been rejuvenated by post-intrusive alteration processes. The age of the younger reference line of 396 Ma is even below the biotite cooling ages of the Damara Orogen itself, for which an age of 420 Ma is given by Miller (1983). Provided that the younger reference line has a geological meaning, this would indicate that the samples which plot on reference line 2 have been affected by post-Damaran alteration processes.

The Rb-Sr results obtained for the amphibolites from Kobos are presented in Figure 6.11. The scattering of data points is most striking and is best explained either by post-genetic exchange processes affecting the analysed samples, or possibly by primary compositional differences between the analysed specimens, which to a certain degree is Indicated by the results of whole geochemistry (see Table 10, see Appendix)). A reference line calculated through all the data points yields an age of 1174 Ma ± 214 Ma with a relatively low correlation coefficient R of 0.949 and an intercept I at $^{87}Sr/^{86}Sr$ = 0.7034 ± 0.0008. A small-scale isochron representing an age of 685 Ma ± 7 Ma may be calculated through the data points representing the samples KAW3010-KAW3012 which have been collected within a distance of a few hundred metres. Its correlation coefficient is 0.9999 and its intercept is at $^{87}Sr/^{86}Sr$ = 0.70575 ± 0.00003. The age of 1174 Ma of the reference line representing the total population might again indicate a homogenisation phase triggered by the intrusion of members of the Gamsberg Granite Suite. The age of the small-scale reference line of 685 Ma indicates that the Kobos area was affected by post-Mokolian alteration processes probably related to the Damara orogeny, and thus accounts for the scatter of data points on an overall scale.

The $^{87}Rb/^{86}Sr$ and $^{87}Sr/^{86}Sr$ ratios obtained for the analysed Elim Naub schists are presented in Figure 6.12 where they have been plotted together with Rb-Sr data for the Naub diorite which were taken from literature (Reid *et al.*, 1988). The Elim schists do not plot on a well-defined reference line. Surprisingly they plot quite well on a reference line representing an age of 1788 ± 50 Ma with an intercept I of $^{87}Sr/^{86}Sr$ = 0.7034 ± 0.0003 which was calculated through the data points of the Naub diorite and the Elim schists. This result raises the suspicion that the reference line obtained might be a mixing line. Such a suspicion is disproved by the 1/Sr versus $^{87}Sr/^{86}Sr$ diagram (Fig. 6.12) where four of the Naub diorites plus the Elim biotite schist and the remaining four Elim schists define two highly correlated (R = 0.995 and 0.722 respectively) mixing lines. The occurrence of two lines showing two completely different trends on one hand denies the possibility of an overall two-component mixture but on the other hand confirms that the investigated rocks from the Naub area were affected by various mixing processes. This in turn raises doubts about the reliability of the Naub diorite isochron of Reid *et al.* (1988) which was supposed to give a minimum age for the Elim Formation and the Mooirivier Complex. Nonetheless it is possible that the obtained reference line of 1788 Ma dates a homogenisation phase of the intrusive Naub diorite with the surrounding wall rocks of the Elim Formation and thus still could provide a minimum age for the formation of the Elim Formation.

With the exception of KAW3068, the data points of the analysed amphibolites from Alberta plot within a fan of reference lines representing an age range of 548 Ma to 859 Ma, with intercepts of between $^{87}Sr/^{86}Sr$ = 0.70635 and 0.70629, respectively in the $^{87}Rb/^{86}Sr$ versus $^{87}Sr/^{86}Sr$-diagram (Fig.

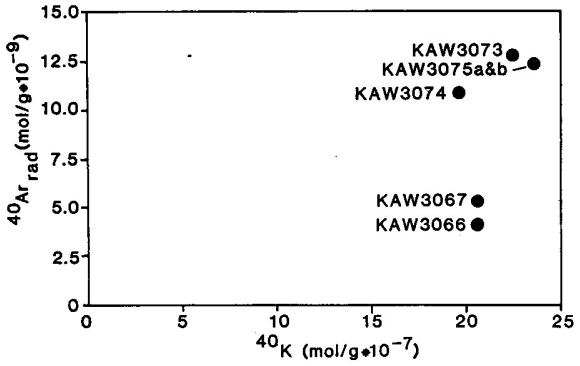

Figure 6.9: Harper (1970) ^{40}K versus $^{40}Ar_{rad}$ diagram for the analysed white micas and biotites of the Elim Formation from the farm Areb

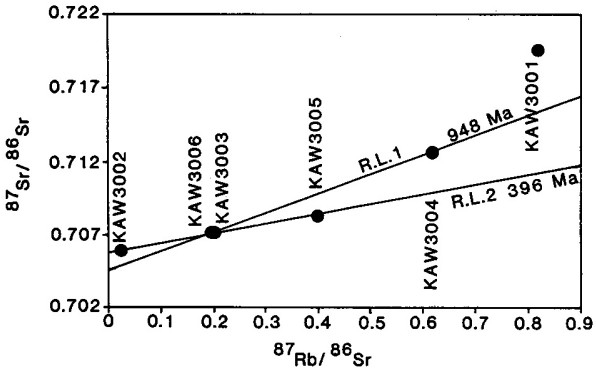

Figure 6.10: $^{87}Rb/^{86}Sr$ versus $^{87}Sr/^{86}Sr$ isochron diagram for the analysed Elim amphibolites from the farm Samkubis

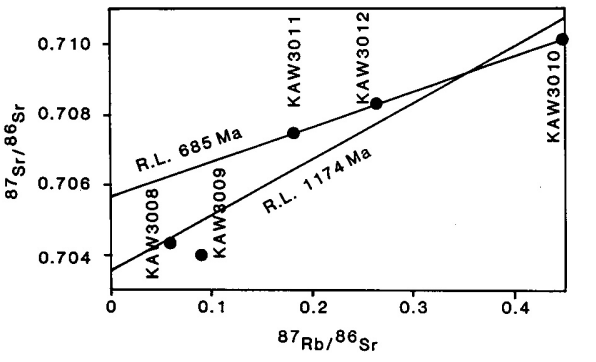

Figure 6.11: $^{87}Rb/^{86}Sr$ versus $^{87}Sr/^{86}Sr$ isochron diagram for the analysed Elim amphibolites from the farm Kobos

6.13). The 1/Sr versus $^{87}Sr/^{86}Sr$ diagram (see inset in Figure 6.13) shows that mixing processes might be the reason for the relatively young ages obtained for the fan of reference lines in the $^{87}Rb/^{86}Sr$ versus $^{87}Sr/^{86}Sr$ diagram because of the relatively high correlation of 0.919 of a regression line calculated through the data points. As the reference age obtained of the Alberta amphibolites does not date a major geological event of the area it is a valid assumption that the obtained range of ages of 548 Ma to 859 Ma is the result of incomplete rejuvenation processes related to the Damara orogeny and/or to later tectonic processes along the Areb shear zone.

The analysed marbles from Grauwater and Areb yielded present-day $^{87}Sr/^{86}Sr$-ratios of 0.70729 and 0.71436 respectively. The initial $^{87}Sr/^{86}Sr$ ratios were then calculated for an assumed maximum age of 1800 Ma by correcting the present $^{87}Sr/^{86}Sr$ ratios for the respective Rb contents of the samples. After this correction, the initial whole-rock $^{87}Sr/^{86}Sr$ ratios of the Grauwater and Areb marbles are 0.70698 and 0.7108, respectively. As, according to Faure (1986), the $^{87}Sr/^{86}Sr$ ratio of sea water was always below 0.707 before 1000 Ma, it is apparent that the $^{87}Sr/^{86}Sr$ ratios of the analysed marbles obtained represent mixing processes of primary carbonate material with later metamorphic fluids. The composition of these fluids is not known but their $^{87}Sr/^{86}Sr$ was certainly above 0.710 in the case of the Areb marble and above 0.707 in the case of the Grauwater marble.

6.4 CONCLUSIONS

Because the respective isotope systems have been affected by a multitude of post-genetic alteration processes, K-Ar and Rb-Sr age determinations could not reveal the age of formation of the analysed whole-rock samples and mineral separates. Nevertheless it is possible to give possible minimum ages, ranging between 1062.3 ± 10.6 Ma and 1229.5 ± 12.3 Ma, for the intrusion and cooling of granitic magmas into the Elim Formation by the K-Ar results obtained for white micas from the area of the farm Morgenroth 17, which were affected by contact metamorphism but whose K-Ar isotopic system has not been reset by the later Damara orogeny. The K-Ar analyses of separates of sericites, white micas and biotites of mica schists from the farm Areb 76 have shown that the Areb shear zone was probably active as late as 315 Ma. This is in agreement with K-Ar results obtained for biotites of the Mooirivier Formation which have shown that their K-Ar systems were rejuvenated by post-Damaran tectonic activities which lasted at least until 330 Ma and which possibly are related to the opening of the South Atlantic (see Chapter 4). The cooling paths for Damaran-related metamorphism in the Central to Southern Marginal Zones of the Damara Orogen as proposed by Miller (1983), show that this area at present erosion levels had increased temperature levels until Karoo peneplanation started about 280 Ma before today. Although Miller's (1983) proposed temperature level of 150°C-250°C for this time span, for the Southern Marginal Zone neighbouring the Rehoboth Basement Inlier in the north, was below the K-Ar blocking temperature of biotites and muscovites of 300°C ± 50°C and 350°C ± 50°C, respectively, it might have facilitated the partial opening of K-Ar isotopic systems in tectonically active regions; the partial opening of K-Ar systems along the Areb shear zone (possibly during the opening of the South Atlantic) would be such an example. Based on the K-Ar analyses of the Areb mica schists

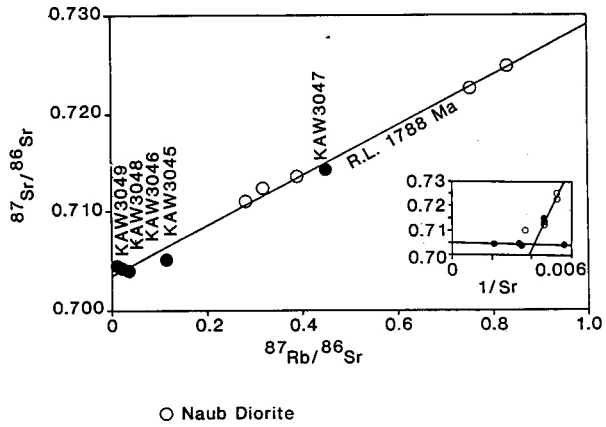

Figure 6.12: $^{87}Rb/^{86}Sr$ versus $^{87}Sr/^{86}Sr$ isochron diagram for the analysed Elim schists from the farm Naub. (Inset = 1/Sr versus $^{87}Sr/^{86}Sr$ diagram for the same samples). Open circles represent ths data of Reid *et al.* (1988) for the Naub diorite

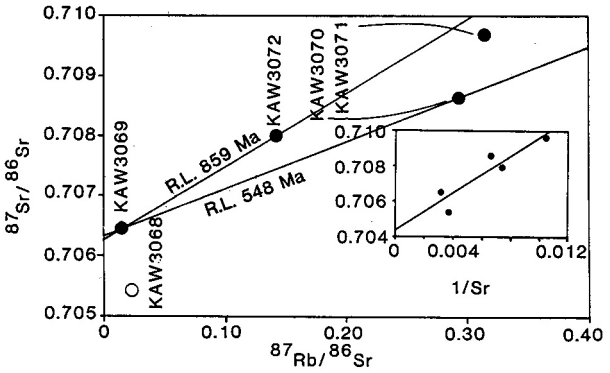

Figure 6.13: $^{87}Rb/^{86}Sr$ versus $^{87}Sr/^{86}Sr$ isochron diagram for the analysed Elim amphibolites from the farm Alberta. (Inset = 1/Sr versus $^{87}Sr/^{86}Sr$ diagram for the same samples)

it can furthermore be said that the K-Ar systems of mica separates from samples which were collected a few hundred metres away from the Areb shear zone, although being rejuvenated to apparent ages between 730 Ma and 782 Ma, have neither completely been reset by the Damara orogeny nor by later tectonic processes. This is equally valid for the K-Ar analysis of a biotite separate from a biotite schist from the farm Naub 274, which yielded an age of 874 Ma. In order to give more evidence on the evolution path of the K-Ar systems analysed, further work will have to answer the questions concerning the availability of excess argon during the formation of other mineral phases, such as quartz.

The results of the Rb-Sr analyses of 23 whole-rock samples have shown that the formation age of the Elim Formation is not datable by the Rb-Sr method. This is due to the multitude of metamorphic and tectonic processes which affected and partly opened the Rb-Sr isotopic systems of the Formation after its deposition. Nonetheless it can be stated that the Elim Formation as a whole was affected by homogenisation processes in relation to the intrusion of members of the Gamsberg Granite Suite, and by post-Mokolian alteration processes. Some of these processes, in part or wholly, have probably been strong enough to completely reset the Rb-Sr systems of some of the analysed outcrops, indicated for example by the Alberta amphibolites, but none of these processes has been preserved in an unaffected way. A comparison of our data of the Elim Formation with data of the Naub diorite (Reid *et al.*, 1988) shows that the Rb-Sr age of this intrusion, which is supposed to give a minimum age for the formation of the Elim Formation (SACS, 1980), is doubtful as well, as four of the Naub samples seem to form a mixing line in the l/Sr versus $^{87}Sr/^{86}Sr$ diagram.

The intercepts of all the discussed reference lines range between $^{87}Sr/^{86}Sr = 0.7034$ and 0.7064. This indicates that the observed homogenisation and mixing processes may not have changed the original initial $^{87}Sr/^{86}Sr$ ratios of the analysed Rb-Sr systems by large orders of magnitude. This, in turn, indicates that the participating Sr systems had $^{87}Sr/^{86}Sr$ ratios similar to those of the educts, or that in the case of a highly radiogenic participant the admixed amount of such a component was low.

7. MARIENHOF AND BILLSTEIN FORMATIONS

7.1 INTRODUCTION

7.1.1 Marienhof Formation

The name "Marienhof Series" was first introduced by De Kock (1934) for an assemblage- of metamorphic, sedimentary and volcanic rocks which underlie the area to the west of Rehoboth (Fig. 7.1). According to SACS (1980), the Marienhof Formation is the lowermost unit of the Rehoboth Sequence which comprises the Marienhof, Billstein and Gaub Valley Formations. The Marienhof Formation is separated from the older Neuhof Formation by a sedimen¬tary unconfoollity (Schalk, 1987, pers. comm.) and is in tum unconformably overlain by the Nueckopf and Billstein Formations. Intrusion by the Piksteel Intrusive Suite and the Gamsberg Granite Suite provides a minimum age for this formation of about 1064 Ma (Seifert, 1986; Mailing, 1978; Schalk, 1987, pers.comm.).

Outcrops of the present Marienhof Formation occur to the west of Rehoboth between the farms Marienhof 577, Aroams 315 and the town of Rehoboth. To the southwest of Rehoboth, a narrow strip of the Marienhof Formation crops out as far as the farm Auchas East 522. A large xenolith of the Marienhof Formation occurs within the Piksteel Intrusive Suite on the farm Omdraai 210. Between the towns of Rehoboth and Dordabis, rocks assigned to the Marienhof Formation occur as a chain of inselbergs and as strongly weathered schists below the Nueckopf Formation.

The Marienhof Formation with its estimated thickness of up to 2000 m (SACS, 1980) consists of a series of white and grey quartzites, sericite-quartzites, quartzitic conglomerates, phyllites and some minor amounts of acid and basic volcanic rocks which have been metamorphosed under regional greenschist facies conditions.

The very fine- to coarse-grained quartzitic rocks may preserve original sedimentary structures and are predomi¬nantly composed of quartzitic rock fragments in a very fine-grained quartzitic matrix. These rocks consist of 95¬99% recrystallised quartz, 0-3% albite, 1-3% white mica and accessory magnetite, epidote, biotite and chlorite. The metamorphic growth of white mica and biotite is parallel to the penetrative schistosity which also parallels the original bedding. The conglomerates consist mostly of quartzitic components embedded in a fine-grained quartz matrix. Granitic, acid volcanic, amphibolitic and phyllitic compo¬nents may be present. Greyish phyllites, up to several hundred metres thick, are closely associated with the quart¬zitic rocks and represent the pelitic portion of the Marienhof Formation. In contrast to the quartzites, these phyllites are often strongly altered due to weathering and therefore often form topographic depressions. They are very fine-grained and are composed of 45-60% sericitic white mica, 25-40% quartz, 2-9% albite, 1-2% chlorite, 2-7% magnetite-he¬matite and accessory epidote. Chloritoid is a rare consti¬tuent. Thin-section investigations by the authors have shown that deformation of the phyllites is complex and comprises at least three phases.

Layers of porphyritic rhyolite with a thickness of up to several tens of metres are interbedded with the Marienhof sedimentary sequence. Perthitic potassium feldspars are embedded in a fine- to very fine-grained matrix consisting of quartz, albite, biotite, chlorite, muscovite, magnetite and scattered accessory epidote and zircon.

Basic magmatic rocks, now present as highly altered amphibolites, have also been found within the sedimentary sequence. They are composed of amphiboles (in the process of alteration to chlorite and epidote), strongly saussuritised plagioclase, sphene and magnetite.

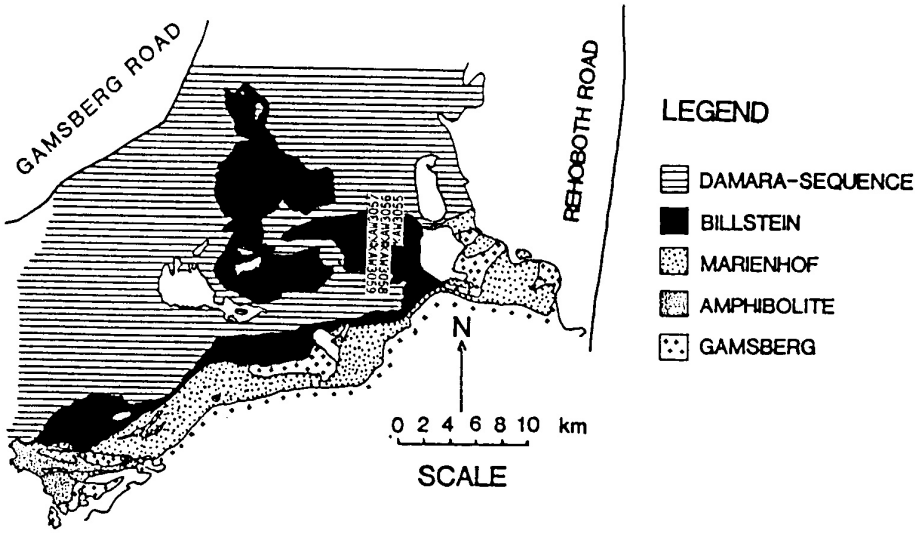

Figure 7.1: Geological sketch map of the Marienhof Formation showing sample localities

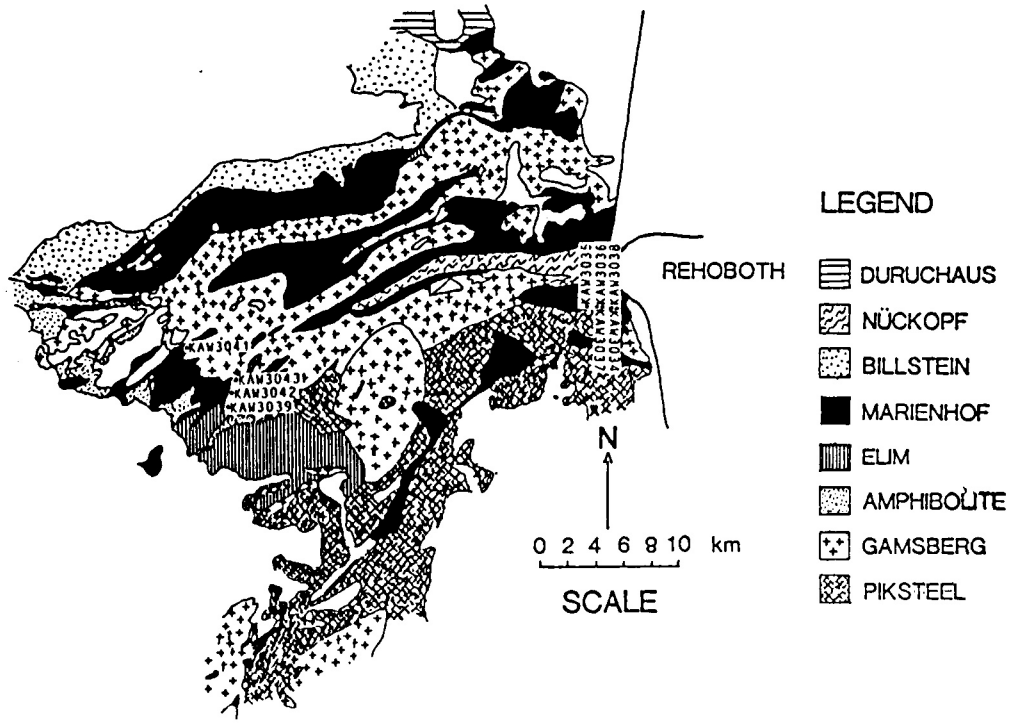

Figure 7.2: Geological sketch map of the Billstein Formation showing sample localities

7.1.2 Billstein Formation

The Billstein Formation, which was established by a working group of SACS (1980), forms the middle section of the aforementioned Rehoboth Sequence.

The Billstein Formation only occurs north of an imaginary line drawn between the farms Aroams 315 in the west and Opdam 284 in the northeast of the northern part of the Rehoboth Basement Inlier (Fig. 7.2). The strata have been intensely thrust-faulted and strongly folded to form several nappe structures. This formation may attain a thickness of 1500 m (SACS, 1980) and either overlies the Marienhof Formation unconformably or rests with a tectonic contact on younger rocks of Namibian age. Rocks of the Damara Sequence of Namibian age unconformably overlie the Billstein Formation.

The Billstein Formation consists of a series of quartzitic conglomerates comprising quartzitic, granitic and basic rock fragments, gritty quartzites, sericitic quartzites, partly garnet-bearing mica schists and sericitic phyllites which are often also garnet-bearing. The phyllites may contain staurolite (Schalk and Hoffmann, 1987, pers. comm.) in addition. Numerous layers of basic rocks and some of quartz porphyry are included in the sedimentary sequence. Since most of the magmatic rocks within the Billstein Formation have been altered to amphibole schists ± biotite, amphibolites and mica schists with a schistosity parallel to the bedding of the surrounding sediments, it is not yet clear whether these magmatic rocks represent syn-sedimentary lavas or post-depositional sills. On the farm Kwakwas 251, the Billstein succession has been intruded by reddish, fine-grained granite of the Gamsberg Granite Suite (Schalk, 1987, pers.comm.), thus indicating that its original deposition is of pre-late Sinclair age. According to our field and petrographic observations, the Billstein Formation underwent at least three major phases of deformation.

7.2 SAMPLE COLLECTION AND PREPARATION

Metamorphic conditions have never reached Rb-Sr blocking temperatures for white micas in the Marienhof and Billstein Formations, as shown by the mineral parageneses of these formations, and the country rock is mostly strongly altered. Accordingly, the use of the K-Ar method was favoured in order to date the last metamorphic event in the northern part of the Rehoboth Basement Inlier. Large samples (30-50 kg each) of three Marienhof quartzites, five Marienhof phyllites and a single rhyolite crosscutting the Marienhof Formation on the farm Marienhof were collected in the vicinity of the Areb shear zone, whose main branches partly cut across the sampled outcrops (Fig. 7.1). In addition, four samples of garnet-bearing Billstein mica schists and one sample of a sericitic Billstein quartzite with masses of about 50 kg each were collected on the farm Kwakwas 251 (Fig. 7.1).

The samples were crushed and the white micas were subsequently separated from the Marienhof quartzites and Billstein quartzites and mica schists by the use of sieves, a dry shaking table and magnetic separators. Biotite was separated in the same way from Marienhof rhyolite. As the grain size of the Marienhof phyllites ($< 100\ \mu$) was much too small to use standard separation techniques for micas, an enrichment of the sericitic white micas was attained by the multiple use of Atterberg cylinders. The resulting separates of different degrees of purity (as shown by their K content) were analysed separately in order to compare these results with the

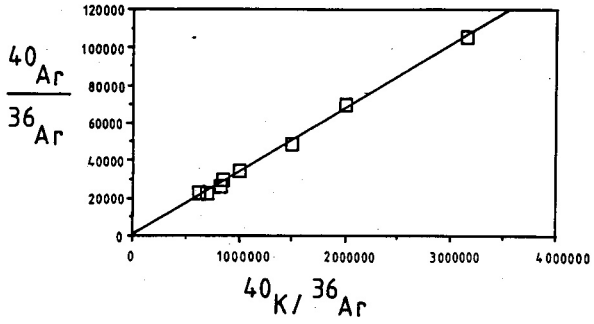

Figure 7.3: $^{40}Ar/^{36}Ar$ versus $^{40}K/^{36}Ar$ diagram for the 2-30 µ and 30-80 µ fractions of the Marienhof phyllites

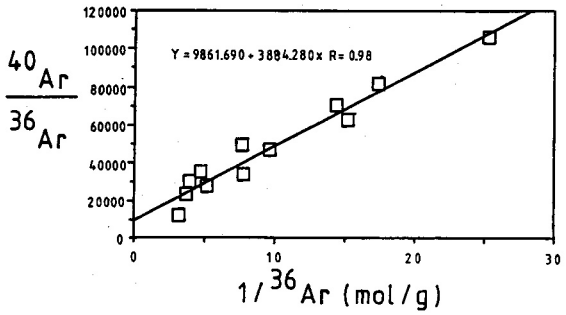

Figure 7.5: $^{40}Ar/^{36}Ar$ versus $1/^{36}Ar$ diagram for all the Marienhof phyllite analyses

results obtained for the very finely ground whole-rock aliquots of the samples.

7.3 DISCUSSION OF THE ANALYTICAL RESULTS

7.3.1 Marienhof Formation

The individual ages obtained for the 2-30 µ and 30-80 µ fractions of the analysed phyllites range between 496.5 ± 5.0 Ma and 523.8 ± 7.2 Ma (Table 13, see Appendix). A reference line calculated on the basis of the $^{40}Ar/^{36}Ar$ and $^{40}K/^{36}Ar$ ratios shows a correlation coefficient of 0.9991, an intercept at $^{40}Ar/^{36}Ar = 959.8$ and yields an age of 500.6 ± 5.0 Ma (Fig. 7.3). However, a reference line in the $^{40}Ar_{rad}$mol/g versus ^{40}Kmol/g diagram after Harper (1970) gives an older age of 530.9: ± 5.3 Ma with a correlation coefficient of 0.991 (Fig. 7.4). The intercept of the reference line in Figure 7.4 is slightly negative: $0.0297*10^{-8}$mol^{40}Ar rad/g. The intercepts of the reference lines in the $^{40}Ar/^{36}Ar$ versus $^{40}K/^{36}Ar$ and $^{40}Ar_{rad}$mol/g versus ^{40}Kmol/g diagrams, which are slightly different from their theoretical values of 295.5 and 0 respectively, might be indicative of slight argon diffusion within the Marienhof phyllites.

Since it was impossible to produce very pure mica separates due to the very small grain size of the phyllites, a whole-rock aliquot of each phyllite was analysed in order to determine the effects of impurity on the ages obtained for the mineral separates. Ages determined for these whole-rock aliquots range between 489.6 : ± 5.0 Ma and 504.6 : ± 5.0 Ma and correspond surprisingly well with the data from the mineral separates. This indicates that grinding did not cause a significant loss of argon in the whole-rock aliquots of the Marienhof phyllite samples. In the $^{40}Ar/^{36}Ar$ versus $1/^{36}Ar$ diagram (Fig. 7.5) which contains all the data obtained, the intercept of a linear regression line drawn through the scattered data points is at $^{40}Ar/^{36}Ar = 9861$. This intercept, together with the high percentage of radiogenic ^{40}Ar (see Table 13 in Appendix), allows one to exclude the possibility that the reference line in the $^{40}Ar/^{36}Ar$ versus $^{40}K/^{36}Ar$ diagram represents an air mixture line. Figure 7.6 shows the calculated reference line of 495.3 : ± 5.0 Ma for all the phyllite fractions in the $^{40}Ar/^{36}Ar$ versus $^{40}K/^{36}Ar$ diagram. The correlation coefficient of the plotted data is 0.999 and the intercept of the calculated reference line is at $^{40}Ar/^{36}Ar = 1065.7$. The Harper $^{40}Ar_{rad}$mol/g versus ^{40}Kmol/g diagram (Fig. 7.7) for all the analysed phyllite fractions shows a slightly older age for the reference line of 532.8 ± 5.3 Ma with a correlation coefficient of 0.995 and an intercept at $^{40}Ar_{rad}$mol/g = $-0335*10^{-8}$ which may suggest a diffusive loss of argon. Individual sample ages which have been recalculated to allow for this possible argon loss vary between 519.9 Ma and 547.6 Ma (Table 13, see Appendix).

The individual ages for white micas from quartzites are in agreement with the results obtained for the phyllites and range from 506.4 ± 5.1 Ma to 528.6 ± 5.5 Ma (Table 13, see Appendix). In addition to the results obtained for miner-

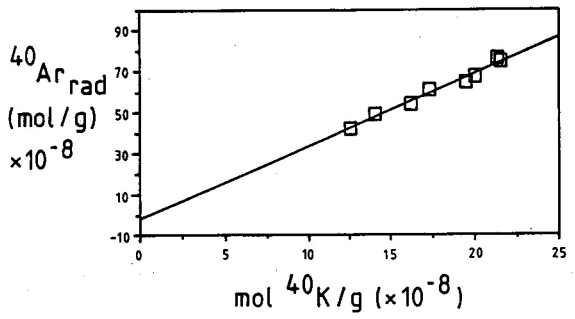

Figure 7.4: $^{40}Ar_{rad}$mol/g($*10^{-8}$) versus ^{40}Kmol/g($*10^{-8}$) diagram for the 2-30 µ and 30-80 µ fractions of the Marienhof

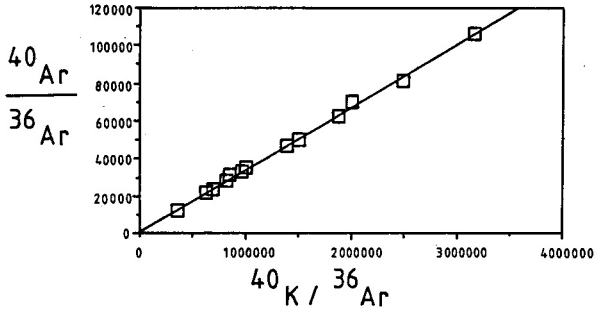

Figure 7.6: $^{40}Ar/^{36}Ar$ versus $^{40}K/^{36}Ar$ diagram for all the Marienhof phyllite analyses

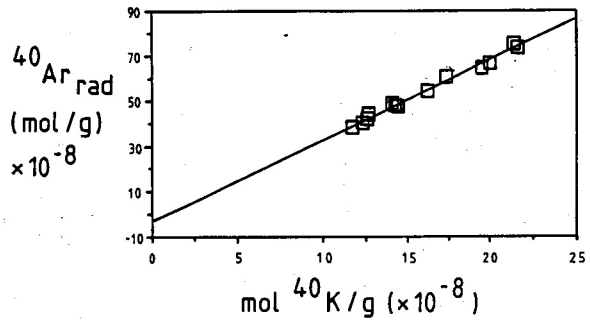

Figure 7.7: $^{40}Ar_{rad}$mol/g(*10^{-8}) versus ^{40}Kmol/g(*10^{-8}) diagram for all the Marienhof phyllite analyses

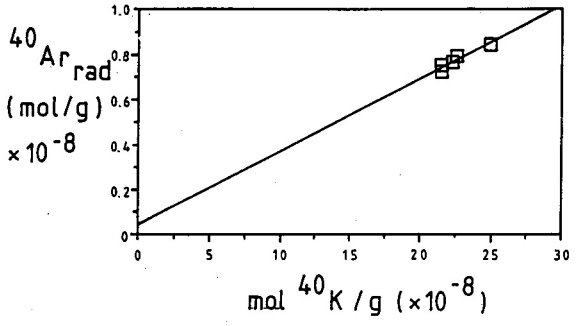

Figure 7.9: $^{40}Ar_{rad}$mol/g(*10^{-8}) versus ^{40}Kmol/g(*10^{-8}) diagram for white micas of the Billstein Formation

als separated from metamorphosed sedimentary rocks, the analysis of biotites from a Marienhof rhyolite yielded an age of 516.6 ± 5.2 Ma (Table 13, see Appendix).

7.3.2 Billstein Formation

The individual white mica K-Ar ages obtained for the Billstein Formation range from 504.8 ± 5.2 Ma to 519.0 ± 5.5 Ma (Table 14, see Appendix). The calculated reference lines in diagrams of $^{40}Ar/^{36}Ar$ versus $^{40}K/^{36}Ar$ (Fig. 7.8) and $^{40}Ar_{rad}$mol/g versus mol^{40}K/g (Fig. 7.9), yielding ages of 512.9 ± 5.1 Ma and approximately 481.3 ± 4.8 Ma, respectively, reveal neither significant argon loss nor significant argon inheritance for the measured white mica separates. The intercept of the reference line in the $^{40}Ar/^{36}Ar$ versus $^{40}K/^{36}Ar$ diagram (Fig. 7.8) of $^{40}Ar/^{36}Ar = 282$ is slightly low when compared to the $^{40}Ar/^{36}Ar$ ratio of 295.5 of the atmosphere, which still lies within the analytical error of the measured value, due to the very small amount of ^{36}Ar found in samples with less than 1 % of air-argon contamination. The slightly positive intercept of the $^{40}Ar_{rad}$mol/g versus mol^{40}K/g reference line at approximately $^{40}Ar_{rad}$mol/g = 0.05*10^{-8} is also not indicative of significant inherited argon (Fig. 7.9), as slope and intercept of the reference line could not be determined with sufficient accuracy due to the small spread in the ^{40}K concentrations of the individual samples.

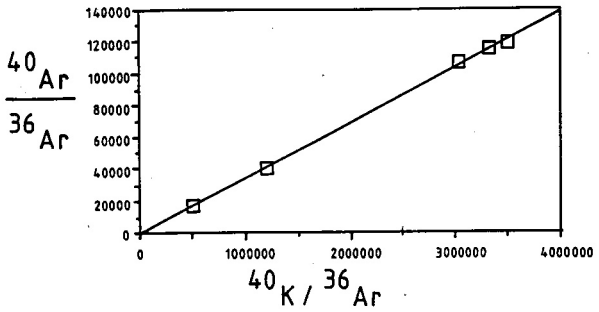

Figure 7.8: $^{40}Ar/^{36}Ar$ versus $^{40}K/^{36}Ar$ diagram for white micas of the Billstein Formation

7.4 CONCLUSIONS

The coherent age pattern shown by individual minerals and whole-rock samples (489-532 Ma) from the Marienhof Formation suggests that lower greenschist facies conditions (i.e. 300°C ± 50°C) were reached in the area between the farm Marienhof 577 and the town of Rehoboth during the Damara orogeny. The $^{40}Ar_{rad}/^{40}K$ reference line age of 532.8 ± 5.3 Ma of the Marienhof phyllites and individual mineral ages of 516.6 ± 5.3 Ma for a biotite separated from a Marienhof rhyolite, and 506.6 - 528.6;1: 5.5 Ma for white micas from Marienhof quartzites, are in agreement with the conclusions drawn by Clifford (1967) and Weber *et al.* (1983) that folding and metamorphism reached the southern margin of the Damara Orogen about 530 Ma ago. The on-average somewhat younger individual ages of 489.6 - 523.8 ± 7.2 Ma determined for the different size fractions from the Marienhof phyllites may perhaps be explained by minor loss of argon at temperatures below the blocking temperatures consequent to later tectonic movements along the Areb shear zone. This assumption is supported by a recalculation of the ages of these samples allowing for this loss of radiogenic ^{40}Ar, after which their individual ages range between 518.8 and 547.6 ± 7.3 Ma and therefore are also in agreement with the aforementioned conclusions.

The mineral ages of 504.8 - 519.0 ± 5.5 Ma obtained for the analysed white micas of the Billstein Formation fall within the age range obtained for the Marienhof samples, thus suggesting that the Billstein Formation underwent a similar metamorphic overprint during the Damara orogeny.

8. PIKSTEEL INTRUSIVE SUITE

8.1 INTRODUCTION

The aim of this part of the study is to provide more information on the age of emplacement and the geological history of the Piksteel Intrusive Suite, in order to obtain minimum ages for the formation of the metamorphic rocks of the Rehoboth Sequence and the older formations of the Rehoboth Basement Inlier which are intruded by members of the Piksteel Intrusive Suite.

The granites of the Piksteel Intrusive Suite were first described and established as a stratigraphic unit by De Waal (1966) who separated the "Piksteel granodiorite" from De Kock's (1934) granite formation and included it into his Nauchas Granite Suite. Schalk (1967) found the Piksteel Granodiorite to be emplaced during a tectogenetic cycle earlier than the younger part of De Waal's (1966) Nauchas Granite Suite, and consequently introduced the Piksteel granodiorite as an independent stratigraphic unit while he placed the younger granitoid intrusives into the Gamsberg Granite Suite. Radiometric age determinations by various earlier workers could not provide final solutions to the problem of the age relationships amongst the various granitic intrusions of the Rehoboth Basement Inlier. U-Pb dating of single-zircon fractions of individual samples by Burger and Coertze (1973-74, 1975-76) and Burger and Walraven (1977-78) yielded minimum ages ranging between 986 Ma ± 20 Ma and 1784 Ma ± 45 Ma for granites mapped as members of the Piksteel granodiorite on the 1:1 000 000 map of Namibia (1980), while members of the Gamsberg Granite Suite were dated by the same authors as having formed between 1110 Ma ± 30 Ma and 1178 Ma ± 20 Ma. Whole rock Rb-Sr dating by Reid *et al.* (1988) and Seifert (1986) yielded isochron ages ranging between 1170 Ma ± 29 Ma and 1725 Ma ± 74 Ma for members of the Piksteel granodiorite, while the isochron ages of the Gamsberg Granites range between 1079 Ma ± 25 Ma and 1222 Ma ± 43 Ma. K-Ar and $^{40}Ar/^{39}Ar$ dating by Seifert (1986) and Burger and Coertze (1975-76), respectively yielded ages ranging between 384 Ma ± 4 Ma and 875 Ma ± 5 Ma, thus clearly indicating rejuvenation processes of the K-Ar systems of the analysed samples. Only the Biesiepoort granite of the Gamsberg Suite yielded older ages of 1246 Ma ± 39 Ma (Burger and Coertze, 1973) and 1529 Ma ± 5 Ma (Burger *et al.*, 1975-76), which were interpreted as either representing a primary age of crystallisation or a total overprint.

SACS (1980) drew a number of conclusions from this age scheme provided by several previous workers. It was assumed that the Piksteel Intrusives were emplaced between 1600 Ma and 1800 Ma. As they are found to intrude the Rehoboth Sequence, it was suggested that the Rehoboth Sequence must be older than 1784 Ma ± 45 Ma. It was furthermore concluded that the members of the Gamsberg Granite Suite intruded only much later, between 1079 Ma and 1246 Ma.

The geochemical investigations on the Rehoboth granitoids which are part of this study (see Chapter 3) could not provide a tool to separate intrusives of the Piksteel Intrusive Suite from members of the Gamsberg Granite Suite by geochemical methods. According to these investigations all the large bodies of granitoids of the Rehoboth Basement Inlier derive from peraluminous, calc-alkaline melts. The initial $^{87}Sr/^{86}Sr$ ratios, which range between 0.700 and 0.702 for the Gamsberg Granite Suite according to Seifert (1986), suggest an origin of these granitoids in the lowermost crust, while the results of Reid *et al.* (1988), which indicate initial $^{87}Sr/^{86}Sr$ ratios of 0.707 to 0.713 (with one exception of 0.704) tend to indicate upper-crustal origins for these granitoids. The only currently available Sr data on the Piksteel Intrusive Suite indicate initial $^{87}Sr/^{86}Sr$ ratios of 0.704 to 0.710 (Reid *et al.*, 1988). An interpretation of the genetic origins of these granitoids on the basis of Sr studies is therefore not feasible.

8.2 SAMPLE COLLECTION AND DESCRIPTION

A total of 21 whole-rock samples weighing 30-100 kg each were collected from three of the largest plutons assigned to the Piksteel Intrusive Suite on the 1:1 000 000 geological map of Namibia (1980). A schematic location of the samples is shown in Figure 8.1 while the exact coordinates of the sample localities are listed in Table 15 (see Appendix). As most of the analysed samples show signs of alteration of their primary mineral content (e.g. saussuritisation of plagioclase), all the specimens have been classified according to the geochemical classification scheme of De La Roche *et al.* (1980) modified after Streckeisen (1981). (See Chapter 8.3.1).

The samples KAW3018-3023 and KAW3171 come from the farm Borodino 179. KAW3024-3028 and KAW3163 were collected on Opetjie 357. Eight samples (KAW3029-3033, KAW3174-3176) were collected on the farm Piksteel 209, the type locality of the Piksteel Intrusive Suite.

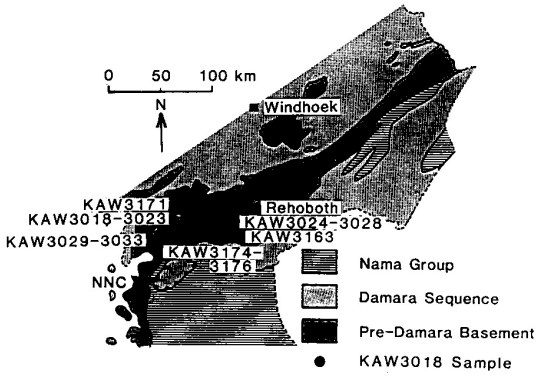

Figure 8.1: Schematic map of sample localitites (NNC = Naukluft Nappe Complex; KAW3018-KAW3023 and KAW3171 = Borodino pluton; KAW3024-KAW3028 and KAW3162 = Opetjie pluton; KAW3029-KAW3033 and KAW3174-KAW3176 = Piksteel pluton)

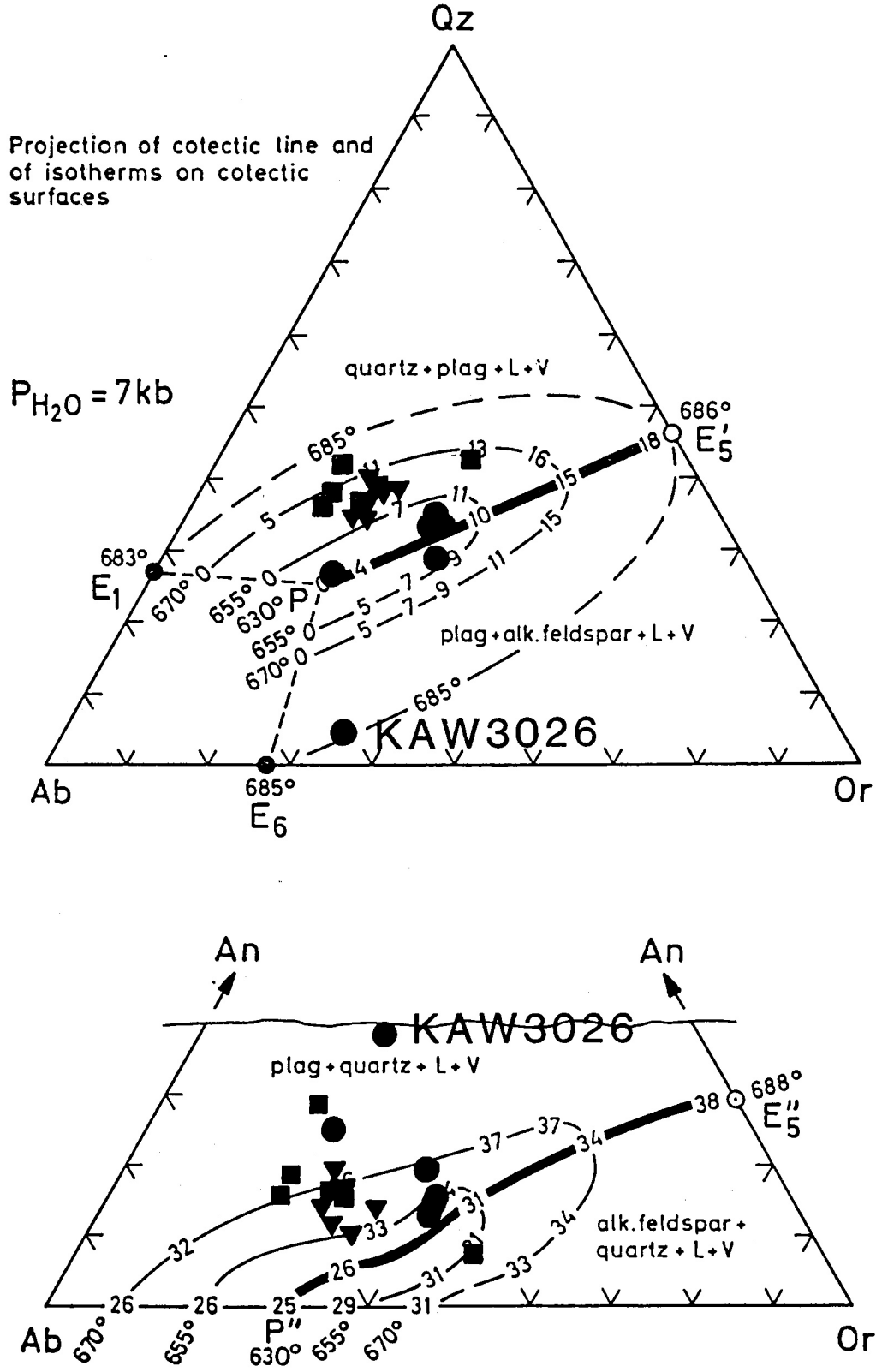

Projection of the isobaric cotectic line P-E_5 and of isotherms on the three cotectic surfaces of the system Qz-Ab-Or-An-H_2O. Data valid for 7 kb water pressure.

Figure 8.2: Ternary Qz-Ab-Or and An-Ab-Or diagrams for the analysed granitoids of the Piksteel Intrusive Suite for an assumed pH_2O of 7 kb. (Squares = Borodino pluton; circles = Opetjie pluton; triangles = Piksteel pluton). See text for explanation

The samples from Borodino are fine- to medium-grained, partly porphyritic granites (KAW3018-3023) and granodiorites (KAW3171). The fine-grained plagioclase is mostly strongly saussuritised. The K-feldspar is often perthitic and shows the typical cross-hatched patterns of microcline. Quartz is mostly found completely recrystallised and shows undulatory extinction. It often forms kakiritic to mylonitic textures in which the other minerals are embedded. Biotite, which has been partly chloritised, only comprises 0.5-3% by volume of the mineral content of the analysed specimens. Accessory minerals are zircon, apatite and opaque minerals. Epidote minerals, sericite, chlorite and small amounts of Fe-hydroxides are the products of alteration processes, such as the saussuritisation of plagioclase and the partial chloritisation of biotite.

The samples from Opetjie are fine-to medium-grained granites (KAW3024, KAW3025, KAW3027), granodiorites (KAW3028, KAW3163) and diorites (KAW3026). The Opetjie granites are composed of strongly saussuritised plagioclase, partly perthitic and cross-hatched K-felspar, undulous quartz and up to 4% of partly chloritised biotite. The high sphene content of up to I % by volume is most striking. Accessory primary and secondary minerals are chlorite, zircon, apatite, epidote minerals, leucoxene and opaque minerals. The mineralogical composition of the analysed granodiorites is similar to that of the granites except for the occurrence of amphiboles which have partly been altered to aggregates of biotite, chlorite and epidote minerals. The slightly foliated diorite specimen has a content of partly altered amphiboles of about 20% by volume while biotite only occurs as an accessory mineral.

Seven of the fine- to medium-grained samples from the type-locality on the farm Piksteel 209 are of granitic composition (KAW3029. KAW3031-3033, KAW3174-3176) while one sample (KAW3030) represents a granodiorite. Plagioclase is mostly strongly saussuritised and the 1-3% of biotite are often partly chloritised. Cross-hatched and perthitic K-feldspars are frequent. Accessory primary and secondary minerals are zircon, apatite, sericite, epidote minerals, sphene and opaque minerals.

8.3 DISCUSSION OF THE ANALYTICAL RESULTS

8.3.1 Some additional geochemical considerations regarding the Piksteel Intrusive Suite

As the basic geochemical properties of the peraluminous Piksteel granitoids have already been outlined in Chapter 3 only a few additional aspects of the geochemistry are discussed in this chapter. The major- and trace-element analyses of the Piksteel whole-rock samples, including some additional analyses, are listed in Table 15 (see Appendix). The values of the CIPW-normative mineral calculations are listed in Table 15A (see Appendix).

All the whole-rock samples of the Piksteel Intrusive Suite dealt with in this study are peraluminous, calc-alkaline granitoids (see Chapter 3) and, with the exception of KAW3026 which is a diorite, have normative corundum between 0.32 and 2.38% according to the CIPW-normative calculations (Table 15A, see Appendix). The $Al_2O_3/CaO+Na_2O+K_2O$ (molecular percentage) ratios of the samples, again with the exception of KAW3026 whose A/CNK ratio is 0.87, range between 0.99 and 1.17 and thus plot closely around the value of 1.1 which separates I-type granites from S-type granites, according to Chappell and White (1974). A classification of the analysed samples as derivates of either S-type or I-type melts is not possible as major-element geochemical properties similar to those observed may be found in both kinds of magmas.

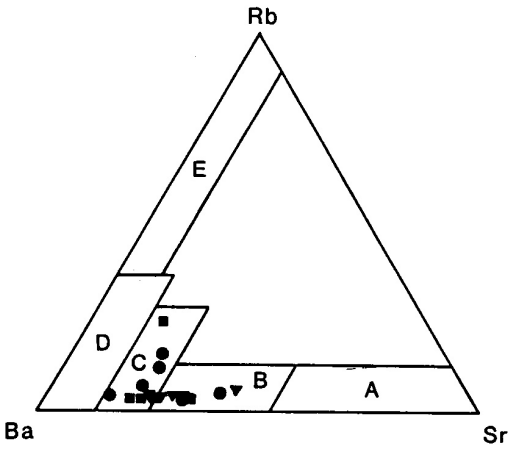

Figure 8.3: Ternary Rb-Ba-Sr diagram of El Bouseily *et al.* (1975) for the analysed granitoids. (Same symbols as in Figure 8.2: Field A = diorites; B = quartz diorites and granodiorites; C = anomalous granites; D = normal granites; E = highly differentiated granites)

Slightly more information on the genesis of the analysed samples may be deduced from ternary Qz-Ab-Or and An-Ab-Or representations of the normative mineral contents according to Winkler (1979), at pH_2O = 7 kb showing the cotectic line and the isotherms on the cotectic planes (Fig. 8.2). With the exception of the dioritic KAW3026 all the samples from Opetjie plot near the cotectic line in the Qz-Ab-Or ternary diagram. The samples from Borodino and Piksteel deviate away from the cotectic line into the area of primary quartz. In the An-Ab-Or ternary diagram most of the samples plot onto a trend which leads away from the cotectic line into the area of primary quartz and plagioclase. In summary it can be said that the analysed samples have possibly been generated from cotectic melts. The general trend leading away from the Or end member of both ternary diagrams may either represent an original melt which was relatively undersaturated in K_2O or indicate post-genetic alteration processes of the country rock (e.g. sericitisation of K-feldspar) which were not isochemical.

The ternary Rb-Ba-Sr diagram of El Bouseily *et al.* (1975) supports the assumption that the analysed specimens were partly affected by post-genetic alteration processes 'which may have disturbed the original element distribution patterns (Fig. 8.3). All the data points either plot into the field for anomalous granites which was selected by EI Bouseily *et al.* (1975) "to cover types that suffered from metasomatism" but which also could be occupied by gra-

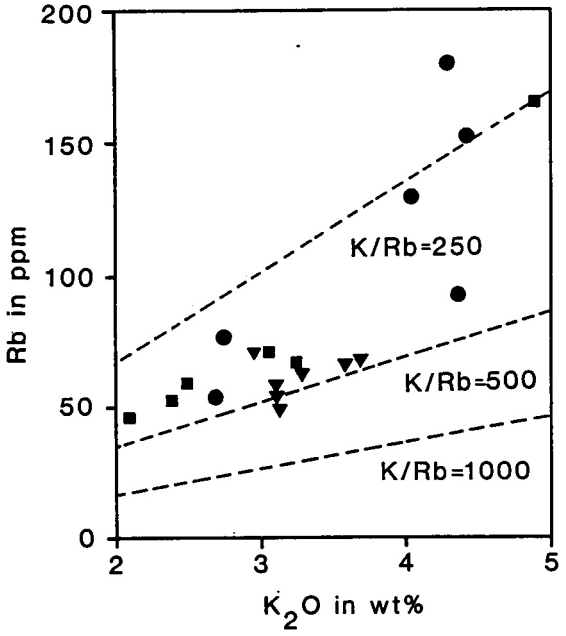

Figure 8.4: K_2O versus Rb diagram for the analysed granitoids of the Piksteel Intrusive Suite. (Same symbols as in Figure 8.2)

nitic samples which underwent metamorphism, or they plot into the field for granodiorites and quartz diorites.

The data scatter in the K_2O versus Rb diagram (Fig. 8.4) neither confirms nor contradicts a post-genetic alteration of the K_2O and Rb systems of the analysed specimens. It does show that the Opetjie samples, because of their higher Rb and K_2O contents, seem to be somewhat more differentiated than the rest of the samples if the present position of the samples is not due to a higher degree of alteration.

The Rb versus Sr diagram (Fig. 8.5) clearly shows a negative correlation of Sr and Rb contents of the samples of the Opetjie and Borodino plutons while the data points of the Piksteel pluton do not plot on a linear array. The fact that such a correlation is still visible between mobile elements such as Rb and Sr for most of the Opetjie and Borodino samples indicates that alteration processes probably did not affect the Rb and Sr ratios and concentrations of these samples significantly. In addition it can again be seen that the Opetjie samples tend to be Rb-enriched in comparison with the samples from the other plutons, thus indicating a possibly higher degree of differentiation of the Opetjie pluton.

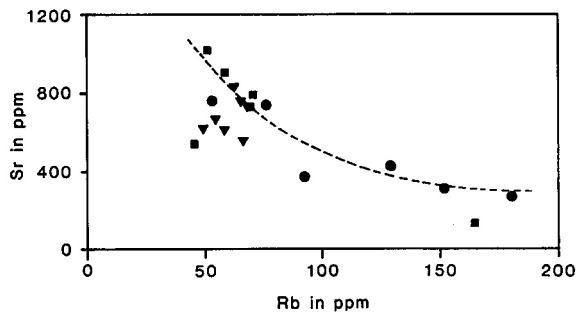

Figure 8.5: Rb versus Sr diagram for the analysed granitoids of the Piksteel Intrusive Suite. (Same symbols as in Figure 8.2)

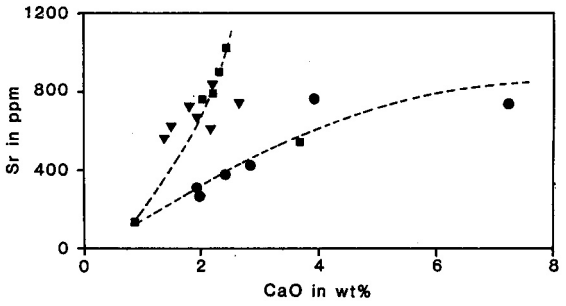

Figure 8.6: CaO versus Sr diagram for the analysed granitoids of the Piksteel Intrusive Suite. (Same symbols as in Figure 8.2)

A high positive correlation of CaO and Sr among the majority of the Opetjie and Borodino samples can be observed in the CaO versus Sr diagram (Fig. 8.6) while the data points representing the samples from the Piksteel pluton again scatter. This indicates that the concentrations of the alkaline earths of the Opetjie and Borodino plutons probably did not change significantly during post-genetic alteration while the Sr and CaO contents of the Piksteel samples may have been affected to a greater degree by post-genetic alteration if the observed data scatter is not attributable to improper mapping of the area.

Based on the geochemical observations it can be said that the plutons of the Piksteel Intrusive Suite found on Borodino and Piksteel either represent I-type magmas with a certain deficiency of alkaline earths, or they might represent anatectic S-type magmas generated under cotectic conditions from upper crustal parent material which has been slightly depleted in K_2O. The Opetjie granitoids could also have been generated from both S- or I-type magmas but their degree of differentiation was certainly higher than that of the Piksteel and Borodino granitoids.

8.3.2 K-Ar analyses

The results of the K-Ar analyses of the biotite separates from granitic and granodioritic (KAW3030) intrusions on Borodino, Opetjie and Piksteel are listed in Table 16 (see Appendix).

The individual ages of the Borodino biotites are 606.7 Ma ± 6.8 Ma and 954 Ma ± 8.5 Ma. The biotite separate from an Opetjie granite yielded an age of 619.4 Ma ± 8.0 Ma. The individual ages of the Piksteel biotites are 646.6 Ma ± 6.5 Ma, 864.0 Ma ± 8.7 Ma and 902.0 Ma ± 9.9 Ma. The percentage of radiogenic ^{40}Ar in the analysed biotite separates always ranges between 98.68% $^{40}Ar_{rad}$ and 99.28% $^{40}Ar_{rad}$.

The current lowest whole-rock Rb-Sr age published for the Gamsberg Granite Suite is at 1079 Ma ± 25 Ma (Reid *et al.*, 1988), much higher than the obtained K-Ar ages and yet the Gamsberg Granite Suite is supposedly younger than

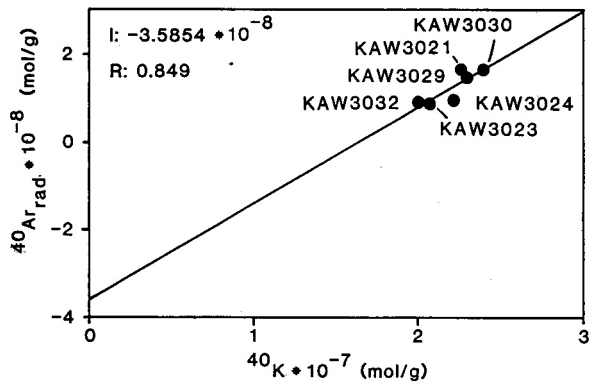

Figure 8.7: ^{40}K versus $^{40}Ar_{rad}$ diagram for the analysed biotite separates from some of the analysed granitoids of the Piksteel Intrusive Suite

the Piksteel Intrusive Suite (SACS, 1980). Therefore it is evident that these ages are too low to represent the formation ages of the analysed biotites.

The low ^{36}Ar contents of less than $0.54*10^{-12}$ mol/g, resulting in a high percentage of radiogenic argon, indicate that no significant admixture of atmospheric argon with the sample argon has occurred. A comparison of the K content of the analysed samples, ranging between $20.06*10^{-8}$ mol K/g and $24.03*10^{-8}$ mol K/g, with that of average biotites from literature (e.g. Deer *et al.*, 1962), ranging between $26*10^{-8}$ mol K/g and $30*10^{-8}$ mol K/g clearly shows that the analysed biotites must have been partly altered (e.g. chloritised). A partial chloritisation of biotite leads to a loss of K and to a loss of argon. In optimal conditions, i.e. if a complete loss of argon has occurred during the alteration of the analysed biotites, it is thus only possible to date the alteration event with the K-Ar method on biotites. The large scatter of ages obtained (606.7 Ma - 954.7 Ma) points more towards a partial loss of argon during an alteration event younger than 606.7 Ma than towards a complete loss of argon at individual stages for each sample analysed.

The aforementioned assumptions are supported by the ^{40}K versus $^{40}Ar_{rad}$ diagram (Fig. 8.7) where a barely correlated regression line (R = 0.849) drawn through the scattered data points yields a negative intercept at $^{40}Ar_{rad} = -3.585*10^{-8}$ mol/g and thus shows that argon must have been lost in excess of the loss of K from the samples. A plot of the $1/^{36}Ar$ ratios of the analysed biotites versus their $^{40}Ar/^{36}Ar$ ratios (Fig. 8.8) shows that the assumptions discussed above are not based upon mixing phenomena as the data points clearly show an uncorrelated scatter.

In summary it can be said that the individual biotite ages obtained for several intrusions of the Piksteel Intrusive Suite represent post-formation rejuvenation processes. These rejuvenating alteration processes must have occurred between the intrusion of the Gamsberg Granite Suite at about 1100 Ma and the present time and might possibly be related to the Damara orogeny. Furthermore it can be said that Damaran-related metamorphism did not reach the K-Ar blocking temperature of 300°C further south than 23°35'S and it can thus be confirmed that the K-Ar ages of the Naukluft Nappe Complex of 478 Ma to 547Ma of Ahrendt *et al.* (1977) do not represent *in situ* ages but rather transported ages.

8.3.3 Rb-Sr analyses

The results of the 21 whole-rock Rb-Sr analyses of granitoids from Piksteel, Borodino and Opetjie are listed in Table 17 (see Appendix).

The graphic presentation of the eight analysed samples from Piksteel in the 87Rb/86Sr versus 87 Sr/86Sr isochron diagram (Fig. 8.9) shows a certain scatter of data points. Upon closer examination it is possible to subdivide the data points and to calculate two well-correlated reference lines through the two resulting data groups. The granodioritic sample KAW3030 was disregarded for all calculations as it plots far off the two proposed reference lines. The younger reference line A, which was calculated through KAW3031, KAW3032, KAW3174 and KAW3176 yields an age of

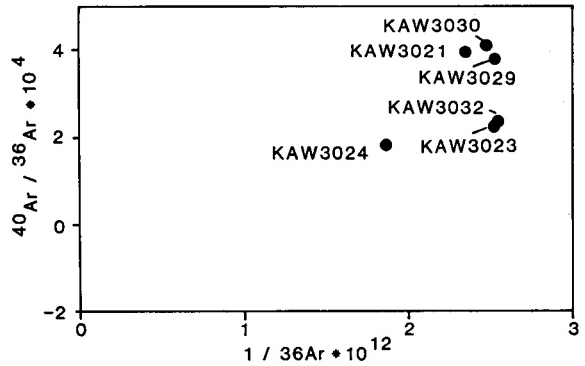

Figure 8.8: $1/^{36}Ar$ versus $^{40}Ar/^{36}Ar$ diagram for the analysed biotite separates

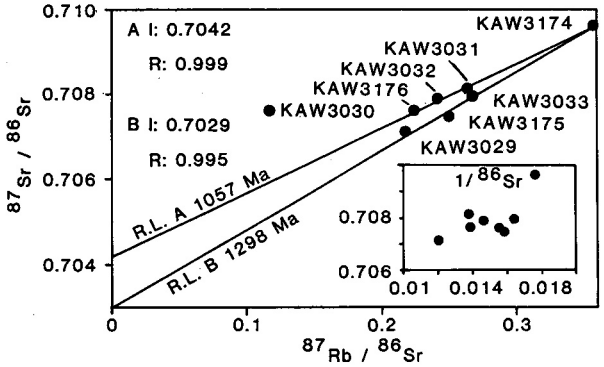

Figure 8.9: $^{87}Rb/^{86}Sr$ versus $^{87}Sr/^{86}Sr$ isochron diagram for the whole-rock analyses of the granitoids of the Piksteel pluton (inset=$1/^{86}Sr$ versus $^{98}Sr/^{86}Sr$ diagram for the same samples)

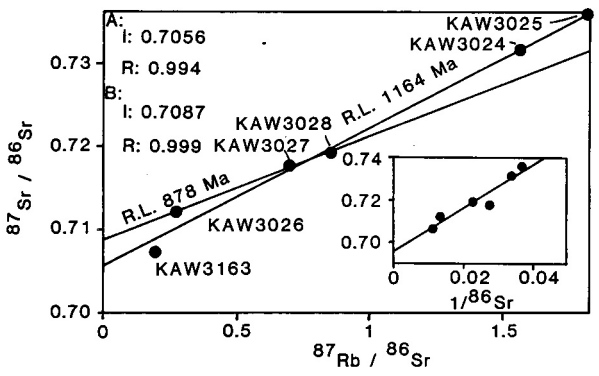

Figure 8.10: $^{87}Rb/^{86}Sr$ versus $^{87}Sr/^{86}Sr$ isochron diagram for the whole-rock analyses of the granitoids of the Opetjie pluton (inset = $1/^{86}Sr$ versus $^{87}Sr/^{86}Sr$ diagram for the same samples)

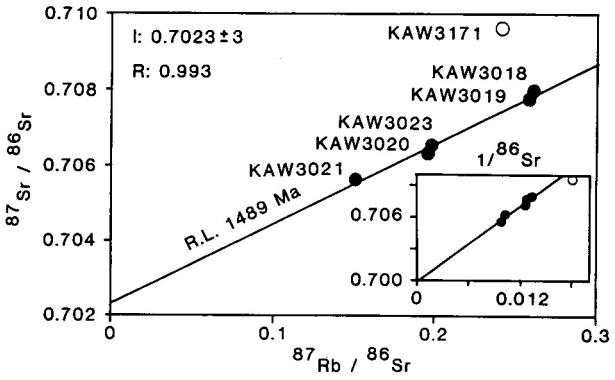

Figure 8.11: $^{87}Rb/^{86}Sr$ versus $^{87}Sr/^{86}Sr$ isochron diagram for the whole-rock analyses of the granitoids of the Borodino pluton (inset = $1/^{86}Sr$ versus $^{87}Sr/^{86}Sr$ diagram for the same samples). Sample KAW3022 plots outside the range of the diagram

1057 Ma ± 35 Ma with an intercept at $^{87}Sr/^{86}Sr$ = 0.7042 ± I and a high correlation coefficient of 0.999. An age of 1298 Ma ± 92 Ma was obtained for reference line B which was calculated through KAW3029, KAW3033, KAW3175 and again KAW3174. The correlation coefficient of line B is somewhat lower with a value of 0.995. The calculated initial $^{87}Sr/^{86}Sr$ ratio for the samples representing line B is quite low with a value of 0.7029 ± 4. Both reference ages are within a range that would be expected for granites of the Gamsberg Suite but they are much lower than would be expected for granites of the Piksteel Intrusive Suite according to the literature (e.g. SACS, 1980). Therefore the suspicion arises that the obtained reference lines might represent much older material which has undergone homogenising and/or mixing processes in the course of its history. The suspicion of an admixture of common Sr is not tenable when considering that a diagram of the $1/^{86}Sr$ ratios of the samples versus their $^{87}Sr/^{86}Sr$ ratios (see inset in Fig. 8.9) does not show a significant correlation of the data points, and when considering the low initial $^{87}Sr/^{86}Sr$ ratios of 0.7042 and 0.7029 for the calculated reference lines. Based on the Rb-Sr data it can be concluded that the two obtained reference lines probably represent homogenisation and rejuvenation phases of the Rb-Sr system between 1050 Ma and 1300 Ma which probably took place isochemically, as the obtained initial $^{87}Sr/^{86}Sr$ ratios and the $1/^{86}Sr$ versus $^{87}Sr/^{86}Sr$ diagram do not indicate significant admixture of foreign material with the analysed samples.

Two well-correlated reference lines may be calculated through the data points, of the Opetjie pluton in the $^{87}Rb/^{86}Sr$ versus $^{87}Sr/^{86}Sr$ isochron diagram (Fig. 8.10). Reference line A, calculated through all the data points, yields an age of 1163.6 Ma ± 61.4 Ma with a correlation coefficient R of 0.994 and an intercept I at $^{87}Sr/^{86}Sr$ = 0.7056 ± 0.00097, while reference line B, calculated through three of the Opetjie data sets, yields an age of 878 Ma with a correlation coefficient R of 0.999 and an intercept I at $^{87}Sr/^{86}Sr$ = 0.7087 ± 0.0004. The initial $^{87}Sr/^{86}Sr$ ratio of 0.7056 ± 0.00097 of reference line A is somewhat higher than the initial ratios obtained for the granitoids from Piksteel, while the reference age A of 1164 Ma is lower than the age which would be expected for a member of the Piksteel Intrusive Suite. As the reference age A is within the known age range for members of the Gamsberg Granite Suite (see above), it possibly represents a reset age induced by the intrusion of Gamsberg magmas in the area. Reference line B with its "post-Gamsberg age" and its high initial of 0.7087 ± 0.0004 shows that alteration processes affected the Opetjie pluton after the end of the Gamsberg-related magmatism in the area, resulting in a partial rejuvenation of the Rb-Sr systems of several samples combined with an increase of the initial $^{87}Sr/^{86}Sr$ ratios of the same samples. The age of reference line B of 878 Ma possibly represents a partial rejuvenation occurring in connection with the Damara orogeny. A plot of all the $1/^{86}Sr$ ratios of the analysed Opetjie samples versus their $^{87}Sr/^{86}Sr$ ratios (see inset in Fig. 8.10) shows, because of the fairly linear array of the data points, that mixing phenomena may have occurred in the Opetjie intrusives, which is not surprising regarding the considerations mentioned above. It thus seems highly probable that the obtained reference ages represent multiple rejuvenation processes of locally variable intensity which occurred in relation with the intrusion of members of the Gamsberg Granite Suite and due to Damaran-related processes. This would also explain the slightly increased $^{87}Sr/^{86}Sr$ initial ratios of the Opetjie granitoids.

With the exception of KAW3022 and KAW3171, which plot far off the calculated reference line (see discussion below), all the Borodino samples plot on a well-correlated reference line (R= 0.993) of 1489 Ma ± 101 Ma in the $^{87}Rb/^{86}Sr$ versus $^{87}Sr/^{86}Sr$ isochron diagram (Fig. 8.11). The intercept of the line is at a low value of $^{87}Sr/^{86}Sr$ = 0.7023 ± 0.0003. Because of its reference age of 1489 Ma, which is distinctly higher than the known ages of the Gamsberg Granite Suite, the Borodino reference line would support the theory of post-formation disturbances of the Rb-Sr systems of the other analysed members of the Piksteel Intrusive Suite. This would, however, only be the case if the obtained reference line does not represent a mixing line. The $1/^{86}Sr$ versus $^{87}Sr/^{86}Sr$ diagram (see inset in Fig. 8.11) where, with

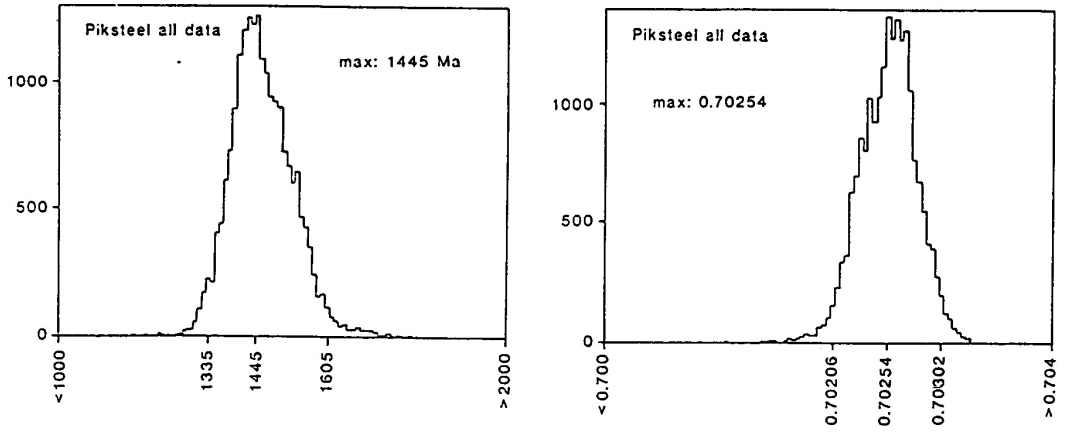

Figure 8.12 (above and overleaf): Histograms showing the frequency distribution of 20 000 ages and intercepts obtained by the bootstrap method of Diaconis and Efron (1983) and Kalsbeek and Hansen (1989). The diagrams on the left show the age versus frequency distribution while diagrams on the right show the initial $^{87}Sr/^{86}Sr$ versus frequency distribution. Indicated are 100 classes with marked upper and lower limits. Furthermore the 2.5 percentile, the 50 percentile and the 97.5 percentile are labelled. **A**: Bootstrap analyses of all the Rb/Sr data obtained for the Piksteel , Opetjie and Borodino plutons (except KAW3022, KAW3030 and KAW3171)

the exception of KAW3171, all the samples form a linear array, can unfortunately not exclude the possibility of the obtained reference line representing a mixing line. Furthermore, the very low initial $^{87}Sr/^{86}Sr$ ratio of 0.7023, which almost represents a Sr composition of mantle material, might indicate that the obtained reference line represents an isochron which was steepened by alteration processes with participating fluids of low $^{87}Sr/^{86}Sr$ ratios. A two-point isochron calculated through KAW3022 and KAW3171 yields a "Gamsberg age" of 1105 Ma with an initial $^{87}Sr/^{86}Sr$ ratio of 0.7058, thus complicating the interpretation of the Borodino data even more. The obtained Gamsberg age might indicate either that parts of the Borodino pluton as it is represented on the 1:1 000 000 map of Namibia have been incorrectly assigned to the Piksteel Intrusive Suite and in reality represent magmas of the Gamsberg Granite Suite, or it again confirms the occurrence of local post-formation alteration processes of locally variable magnitude, which would locally have reset some Rb-Sr systems of the Piksteel Intrusive Suite as late as about 1105 Ma ago. The calculated initial $^{87}Sr/^{86}Sr$ ratio of 0.7058, which is much higher than that obtained for the rest of the samples, implies either that the first possibility of a wrong classification of certain outcrops is correct, or that not all of the pluton was affected in the same way by fluids with extremely low $^{87}Sr/^{86}Sr$ ratios.

Up to this point it is not clear whether the Rb-Sr reference ages obtained for the granitoids of the Piksteel Suite represent magmatic or post-genetic processes or an interference of both kinds of processes. For this reason all the obtained Rb-Sr data were examined by the bootstrap method of Diaconis and Efron (1983) using a modified computer programme of Kalsbeek and Hansen (1989) which is based on the interpolation of random data points, in order to get more statistical information on the nature of the Rb-Sr system of the Piksteel Intrusive Suite. Graphic displays of the obtained statistical results are given in Figures 8.12A and 8.12B. The bootstrap frequency distribution of 20 000 calculated ages and initials of all the granitoids of the Piksteel Intrusive Suite (except KAW3022, KAW3030 and KAW3171, which had to be disregarded for the calculation of the reference lines discussed above), shows distinct maxima at 1445 Ma and $^{87}Sr/^{86}Sr$ = 0.70254 respectively, in a distribution pattern whose significant spectrum ranges from 2.5 percentile values of 1335 Ma and $^{87}Sr/^{86}Sr$ = 0.70206 respectively, to 97.5 percentile values of 1605 Ma and $^{87}Sr/^{86}Sr$ = 0.70302 respectively (Fig. 8.12A). This result suggests that the analysed plutons formed before the intrusion of the Gamsberg Granite Suite from magmas containing Sr of primitive (mantle) composition (low $^{87}Sr/^{86}Sr$ values). This would, however, only be tenable if the Rb-Sr systems of all the analysed samples had not been severely affected by post-formation alteration processes. This is certainly not the case, according to the above discussion of the obtained reference lines. Furthermore, the maxima obtained for the bootstrap frequency distributions of the ages and initials of the single plutons differ from the calculated reference lines of the individual set of samples from the same plutons. The bootstrap age and initial frequency distribution of 20 000 samples calculated for the Piksteel pluton (Fig. 8.12B) shows maxima at 1258 Ma and 0.70315 respectively, which plot between the ages of 1057 Ma and 1298 Ma, and the intercepts of $^{87}Sr/^{86}Sr$ = 0.7043 and 0.7029 obtained for the two reference lines, which can be calculated through the same data set based on graphic analyses of the results. Some difference can also be seen for the Opetjie pluton where the maxima of the bootstrap calculations are at 898 Ma and 1363 Ma with corresponding $^{87}Sr/^{86}Sr$ initials of 0.70873 and 0.70333 (Fig. 8.12B) respectively, while the calculated reference lines show ages of 878 Ma and 1164 Ma with initial $^{87}Sr/^{86}Sr$ values of 0.7087 and 0.7056 respectively. The comparison of the results obtained for the Borodino pluton is 'in good agreement with the results obtained by the two methods yielding ages of 1465 Ma and 1489 Ma respectively, and an identical $^{87}Sr/^{86}Sr$ initial of 0.7023.

The comparison of the results of the bootstrap analyses with the results of the "ordinary" way of calculating iso-

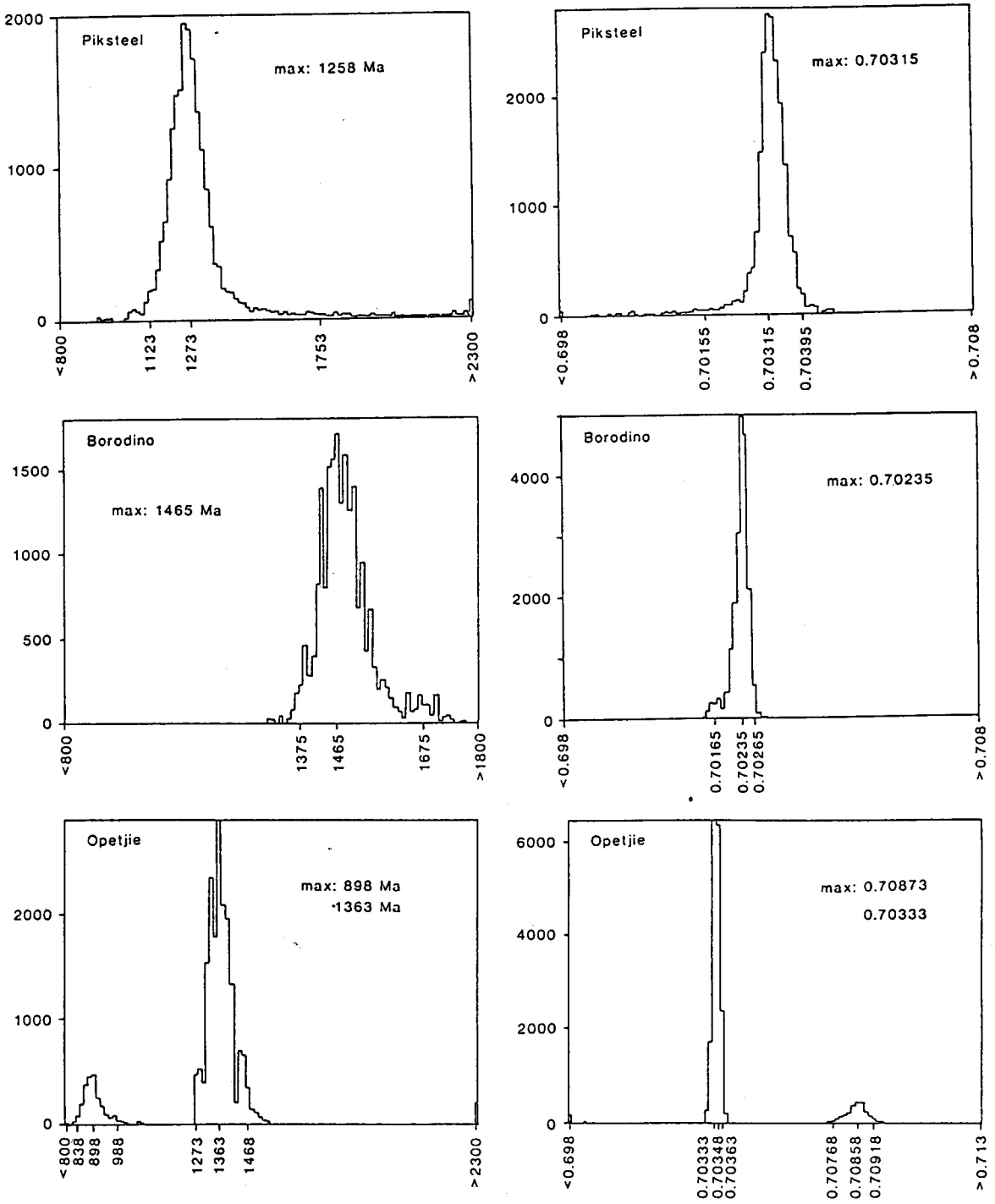

Figure 8.12 (continued): B: Bootstrap results obtained for the individual plutons

chrons shows that other sample collections from the same localities in the Piksteel, Opetjie and Borodino plutons might well have yielded the similar ages and intercept'> of the respective maxima of the distribution patterns, which deviate slightly from the calculated reference lines and which also could be readily interpreted as geologically significant. As the obtained frequency distribution patterns are quite symmetrical around the 50 percentile, and because their maxima within certain limits correspond to the ages obtained by the calculation of reference lines, the bootstrap method cannot solve the problem of whether the obtained older reference ages of the three analysed plutons represent formation or reset ages.

8.3.4 U-Pb analyses

More information about the formation age of the analysed plutons is given by the results of the U-Pb analyses which are listed in Table 18 (see Appendix).

The analysed three zircon separates of the samples KAW3029, KAW3174 and KAW3176 from the farm Piksteel, yielded apparent $^{207}Pb/^{206}Pb$ ages between 1299 Ma

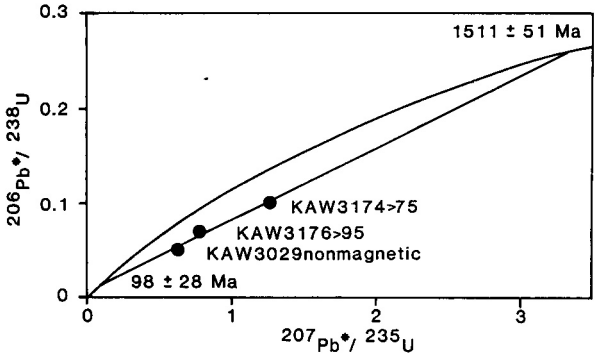

Figure 8.13: Concordia diagram of Wetherill (1956) for the analysed zircon separates of granitoids of the Piksteel pluton

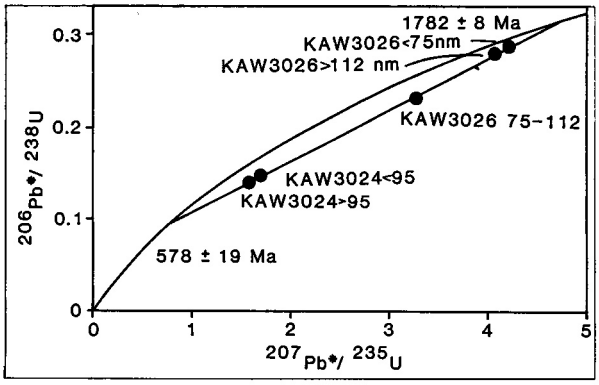

Figure 8.15: Concordia diagram of Wetherill (1956) for the analysed zircon separates from a diorite (KAW3026) and a granite (KAW3024) of the Opetjie pluton

and 1421 Ma, while the apparent $^{206}Pb/^{238}U$ and $^{207}Pb/^{235}U$ ages are much lower with scattering values ranging between 338 Ma and 826 Ma, with the $^{206}Pb/^{238}U$ ages always significantly lower than the $^{207}Pb/^{235}U$ ages. This strong discordancy is confirmed by the Concordia diagram of Wetherill (1956) (Fig. 8.13) where the obtained results plot on a Discordia intercepting the Concordia at 1511 Ma ± 51 Ma and 98 Ma ± 28 Ma. The data points on the lower third of the Discordia clearly indicate that more than 50% of radiogenic lead must have been lost from the analysed zircons. This observation is not surprising considering that many of the individual zircons of the first enrichments, which were later purified, often have inclusions of opaque minerals and frequently show signs of alteration such as the occurrence of porous white rims. A situation similar to that of the Wetherill diagram is encountered when examining the Concordia diagram of Tera and Wasserburg (1972), where the analysed zircons plot on a Discordia whose upper and lower intercepts conform to ages of approximately 1505 Ma ± 69 Ma and 95 Ma ± 34 Ma respectively (Fig. 8.14). Although the upper intercepts of the Discordias in both diagrams of 1511 Ma and 1505 Ma respectively, are subject to a large uncertainty due to strong extrapolation of the data and the low $^{206}Pb/^{204}Pb$ ratios of the analysed separates leading to large common corrections, they are believed to represent minimum ages for the formation of the analysed zircons. These minimum ages exceed the apparent $^{207}Pb/^{206}Pb$ ages by at least 84 Ma and they exceed all the

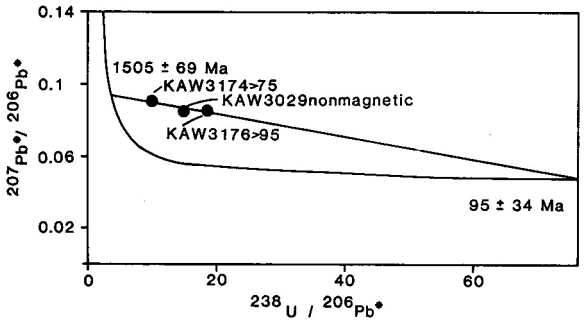

Figure 8.14: Concordia diagram of Tera and Wasserburg (1972) for the analysed zircon separates of granitoids of the Piksteel pluton

known Rb-Sr ages obtained for the pluton of the type locality of the Piksteel Intrusive Suite (this report, Reid *et al.*, 1988) by at least 200 Ma. Considering the observed massive loss of radiogenic lead and the uncertainties of the extrapolation of Discordias in the given order it has to be assumed that the analysed members of the Piksteel Intrusive Suite on the farm Piksteel are much older than the $^{207}Pb/^{206}Pb$ minimum age of 1421 Ma obtained for KAW3174 and are probably even older than the obtained Discordia ages of 1505 Ma and 1511 Ma. This indicates that the Rb-Sr systems of the analysed specimens must have been reset after the formation of the Piksteel Intrusives. It is probable that the strong phase of alteration, which led to the observed strong saussuritisation of the analysed Piksteel samples and was capable of at least partly resetting their whole-rock Rb-Sr system, might also have been partly responsible for the observed severe loss of lead from the analysed zircons. Nonetheless it has to be borne in mind that the lower intercept ages of 98 Ma ± 28 Ma in the Wetherill diagram (1956) and 95 Ma ± 34 Ma in the diagram of Tera and Wasserburg (1972) are much lower than the ages of intrusion of the Gamsberg Granite Suite and the Damara orogeny, probably both responsible for the observed rejuve-nation processes of the Rb-Sr systems of the analysed samples between 1050 Ma and 1300 Ma and between 420 Ma and 850 Ma. As there is no known major tectonic event from the Rehoboth Basement Inlier which could have reset the U-Pb systems of the analysed zircons at about 100 Ma, it can be assumed that the obtained lower intercepts are the result of recent and/or diffusive loss of lead.

The three fractions of optically clear and euhedral zircons of the dioritic KAW3026 yielded apparent $^{207}Pb/^{206}Pb$ ages ranging between 1667 Ma and 1739 Ma, with quite high $^{206}Pb/^{204}Pb$ ratios ranging between 800 and 2800 thus resulting in relatively low corrections for common lead. The respective $^{206}Pb/^{238}U$ and $^{207}Pb/^{235}U$ ages range between 1344 Ma and 1675 Ma. The two fractions of partly metamict zircons from the granitic KAW3024 are more discordant with their apparent $^{207}Pb/^{206}Pb$ ages of 1258 Ma and 1290 Ma respectively, as well as their corresponding $^{206}Pb/^{238}U$ and $^{207}Pb/^{235}U$ ages which range between 841 Ma and 1009 Ma. The graphic display of the obtained results for the Opetjie pluton in the Wetherill diagram (1956) yields a Discordia with an

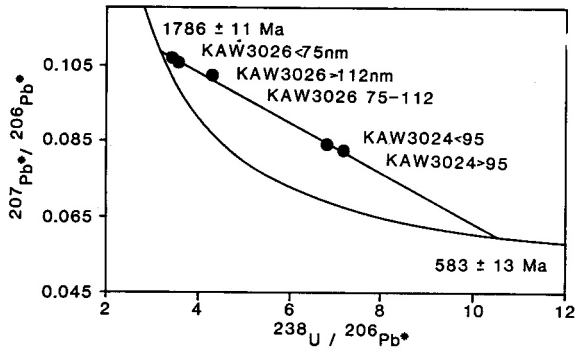

Figure 8.16: Concordia diagram of Tera and Wasserburg (1972) for the analysed zircon separates from a diorite and a granite of the Opetjie pluton

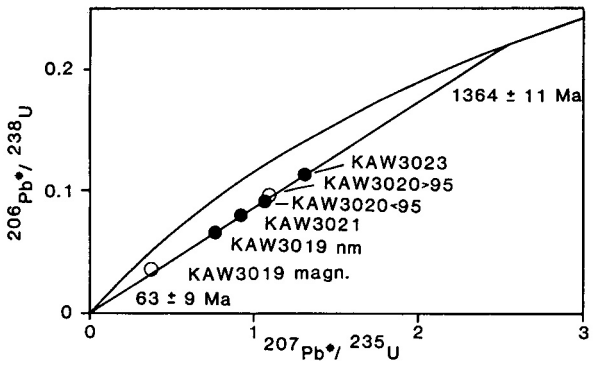

Figure 8.17: Concordia diagram of Wetherill (1956) for the analysed zircon separates from several granitoids of the Borodino pluton

upper intercept of 1782 Ma ± 8 Ma and a lower intercept of 578 Ma ± 19 Ma (Fig. 8.15). According to their position on the Discordia, the zircons from sample KAW3026 must have lost between 15% and 40% of their radiogenic lead, while the zircons from KAW3024 must have lost between 80% and 90% of their radiogenic lead. The results of the Wetherill diagram are confirmed by the Concordia diagram of Tera and Wasserburg (1972) where the data points plot on a Discordia with an upper intercept of 1786 Ma ± 11 Ma and a lower intercept of 583 Ma ± 13 Ma (Fig. 8.16). The following conclusions can be drawn for the Opetjie pluton under the assumption that a direct genetic relation between the dioritic sample KAW3026 and the granitic sample KAW3024 exists, which must be assumed according to field work and the 1:1 000 000 geological map of Namibia (1980):

- The analysed zircons define an upper intercept age of 1782 Ma, which can thus be interpreted as minimum formation age for this member of the Piksteel Intrusive Suite. This is supported by the apparent $^{207}Pb/^{206}Pb$ minimum ages which are, in the case of KAW3026, not below 1667 Ma.
- As the lower intercept of the Opetjie Discordia indicates an age of 578 Ma, which is within the age range of the Damara orogeny according to Miller (1983), it might readily be interpreted as the age of episodic loss of radiogenic lead from the analysed zircons during the Damara orogeny. Such a suggestion would only be tenable if the obtained zircon data represent a two-stage model, which is clearly not the case if the Rb-Sr and K-Ar results which were obtained for the same samples are taken into consideration. The lower intercept age of the Opetjie Discordia may therefore not be interpreted by a two-stage model and is thus geologically insignificant.

If, however, the analysed samples KAW3026 and KAW3024 are not genetically directly related, it has to be concluded that the Opetjie pluton of the Piksteel Intrusive Suite is, in reality, a complex body consisting of old dioritic material with a formation age of 1782 Ma and younger granitic material with a minimum age of 1258 Ma to 1290 Ma.

No solution to this problem is given by the Rb-Sr analyses which have been discussed above, where the Opetjie samples plot on reference lines corresponding to ages of 1164 Ma and 878 Ma and show bootstrap ages of 1363 Ma and 898 Ma respectively. Nontheless it can be deduced from the Rb-Sr data that the analysed samples must have undergone alteration processes which disturbed the analysed isotopic systems between 1363 Ma and maximally, 878 Ma. These alteration processes certainly could have affected the analysed zircons but were obviously not strong enough to reset the U-Pb clock.

Four out of six analysed zircon fractions from the samples KAW3019, KAW3020, KAW3021 and KAW3023 of the Borodino pluton of the Piksteel Intrusive Suite, plot on a Discordia in the Wetherill Concordia diagram (1956) of Figure 8.17. The upper intercept age of is 1364 Ma ± 11 Ma while the lower intercept age is 63 Ma ± 9 Ma. The resulting Discordia of the same samples in the Concordia diagram of Tera and Wasserburg (1972) yields an upper intercept of 1 369 Ma ± 8 Ma and a lower intercept of 65 Ma ± 4 Ma (Fig. 8.18). The apparent $^{207}Pb/^{206}Pb$ ages of the four samples which plot onto the Oiscordias of both diagrams range between 1288 Ma and 1317 Ma while those of the two fractions which have been rejected due to their low $^{206}Pb/^{204}Pb$ ratios are 1133 Ma and 1265 Ma. The apparent $^{206}Pb/^{238}U$ and $^{207}Pb/^{235}U$ ages of the four samples which plot on the Discordia, range between 410 Ma and 847 Ma, while those of the remaining two fractions range between 227 Ma and 752 Ma. The positions of all the data points in Figure 8.17 clearly indicate that the analysed zircon separates lost at least 45% of their radiogenic lead content. The obtained

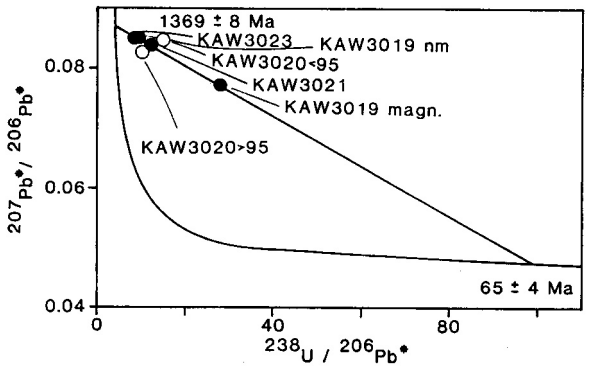

Figure 8.18: Concordia diagram of Tera and Wasserburg (1972) for the analysed zircon separates from several granitoids of the Borodino pluton

$^{207}Pb/^{206}Pb$ and Discordia ages give minimum ages for the formation of the analysed zircons which clearly indicate that they must have formed prior to the intrusion of the magmas of the Gamsberg Granite Suite, and that the Borodino pluton of the Piksteel Intrusive Suite probably has a minimum upper (Discordia) age of 1364 Ma. This age of 1364 Ma, however, is in conflict with the same samples' much older whole-rock Rb-Sr reference and bootstrap ages of 1489 Ma ± 10 1.1 Ma and 1465 Ma respectively (see above). In order to explain this difference it should be assumed that post-formation alteration processes must have affected the U-Pb systems of the analysed zircons and the whole-rock Rb-Sr systems in such an extraordinary away that the rejuvenation of the U-Pb zircon systems was stronger than that of the whole-rock Rb-Sr systems. A possible explanation for the present situation is that sometime after 1364 Ma the Borodino pluton was affected by hydrothermal alteration processes which caused lead loss from the analysed zircons and altered the whole-rock Rb-Sr system in such a way that the present isochrons are somewhat steepened and now indicate a higher age. This interpretation is supported by the very low initial $^{87}Sr/^{86}Sr$ ratio of the Borodino reference line of 0.7023, which might also indicate a steepening of this reference line.

8.4 CONCLUSIONS

The present study on the geochemical and isotopic properties of three plutons assigned to the Piksteel Intrusive Suite has shown primarily that the analysed systems have been severely affected by post-formation alteration processes. These processes can be followed from thin-section investigation, where most of the analysed samples show strong signs of saussuritisation, to geochemical analyses, where elements such as K_2O seem to have been mobilised on a scale exceeding the size of the samples, to the analyses of various isotopic systems, which all show signs of disturbance. Nevertheless, it is possible to describe some of the characteristic properties of the Piksteel Intrusive Suite "ad to evaluate some of the stations in the course of the history of the analysed plutons.

All the analysed samples are peraluminous calc-alkaline granitoids of granitic to dioritic composition. With the exception of one sample, all the specimens showed small amounts of normative corundum and A/CNK values scattering around 1.1, the value which separates I-type from S-type granites, according to Chappell and White (1974). The study of the normative mineral contents has shown that the analysed granitoids possibly derive from cotectic melts which have either been partly undersaturated in K_2O or have been affected by non-isochemical post-genetic alteration processes. Furthermore, it is of interest that the Opetjie pluton shows a higher degree of differentiation in comparison with the Borodino and Piksteel plutons. Further evaluation of the K_2O, CaO, Rb, Ba, and Sr relationships in the analysed samples could neither confirm nor reject the occurrence of the aforementioned post-genetic alteration processes, but could show that such processes could not significantly have changed the content of K_2O, CaO, Rb and Sr in the majority of the samples from the Borodino and Opetjie plutons. The sum of the geochemical observations gives as many arguments for an I-type origin of the analysed granitoids as it does for an S-type origin, while the observed initial $^{87}Sr/^{86}Sr$ values of the analysed plutons of between 0.702 and 0.706, if not the result of secondary alteration processes, rather indicate I -type magmatism for the magmas of the Piksteel Intrusive Suite.

Besides establishing several minimum ages, the U-Pb method of dating could, due to the lack of concordant data, indicate that all the analysed zircons from the three analysed plutons must have suffered from severe loss of lead. The obtained Discordia minimum ages of 1505 Ma ± 69 Ma for the Piksteel pluton, 1786 Ma ± 11 Ma for the Opetjie pluton and 1369 Ma ± 8 Ma for the Borodino pluton, clearly show that the members of the Piksteel Intrusive Suite formed a long time before the intrusion of the Gamsberg Granite Suite with its maximum Rb-Sr age of about 1250 Ma (Burger and Coertze, 1973). The U-Pb minimum age of the Opetjie pluton of 1786 ± II Ma clearly gives a minimum age for the formations of the Rehoboth Sequence, which is intruded by this pluton. This minimum age, which is for the most part defined by the dioritic sample KAW3026, is somewhat older than the whole-rock Rb-Sr age of the Naub diorite of 1725 Ma ± 74 Ma of Reid *et al.* (1988) which up to now defined the minimum age of the Rehoboth Sequence.

The Rb-Sr method of dating shows, in combination with the U-Pb method, that all the analysed plutons were affected by post-formation alteration and homogenisation processes. The obtained reference ages of 1057 Ma ± 35 Ma and 1298 Ma ± 92 Ma of the Piksteel pluton are in agreement with a bootstrap age of 1258 Ma, while the reference ages of 1164 Ma and 878 Ma and the bootstrap ages of 1363 Ma and 898 Ma obtained for the Opetjie pluton are only partially conformable. The Rb-Sr ages of the Piksteel pluton are below its respective U-Pb minimum ages, thus indicating the Rb-Sr system of the Piksteel pluton being reset by hydrothermal processes contemporaneous with the formation of the Gamsberg Granite Suite, which is possibly also the major reason for the loss of lead from the analysed zircons. It has to be assumed that the intrusion and cooling of Gamsberg magmas created hydrothermal fluid circulation, which caused the observed disturbance of the analysed isotopic systems of the Piksteel pluton. The Opetjie pluton was probably affected by a multitude of alteration processes, some of which might have occurred as early as 1363 Ma while the last alteration phase probably did not occur before 878 Ma. The reference age of 1489 Ma ± 101 Ma of the Borodino pluton is in agreement with a bootstrap age of the same samples of 1465 Ma but is in conflict with U-Pb ages of 1369 Ma ± 11 Ma. These diverging ages probably document the existence of hydrothermal fluids with $^{87}Sr/^{86}Sr$ ratios as low as 0.702, which caused a steepening of the calculated reference line and a simultaneous lowering of the relative initial $^{87}Sr/^{86}Sr$ ratios. Several samples which do not plot near the respective reference lines and which partly indicate a "Gamsberg age" might indicate that parts of the analysed plutons have been improperly mapped. The results of the analyses of several biotite separates from the three analysed plutons by the K-Ar method, range between 646.6 Ma ± 6.5 Ma and 954.7 Ma ± 8.5 Ma. This indicates that alteration processes which,

however, have not been strong enough to completely reset the analysed K-Ar systems, must have occurred in the analysed plutons after the closure of the Rb-Sr systems of the same samples. Such processes may best be related to the Damara orogeny whose convergent phase ended about 420 Ma ago (Miller, 1983). In this context it is worth noting that the Damaran-related metamorphism of the Rehoboth Basement Inlier was not capable of completely resetting the K-Ar systems of biotites further south than 23°35'S, which means that temperatures of 300°C were not reached in the southern part of the Inlier during the Damara orogeny. This again confirms that the Damaran K-Ar ages obtained for the Naukluft Nappe Complex by Ahrendt *et al.* (1977), which range between 478 Ma and 547 Ma, do not represent ages which formed *in situ* but rather transported ages.

9. NUECKOPF FORMATION AND OTHER ACID VOLCANICS

9.1 INTRODUCTION

The aim of this chapter is to compare the geochemical properties of acid volcanic dykes crosscutting the Marienhof Formation, the Weener and Piksteel Intrusive Suites and the Gamsberg Granite Suite with those of the Nueckopf Formation, which represents the largest mass of acid volcanic rocks occurring in the Rehoboth Basement area. The obtained results are also compared with the geochemical data of the intrusive rocks of the respective formations.

Prior to SACS (1980) the Nueckopf volcanics were assigned to various other formations. De Kock (1934) described them as "Quartz-Porphyries" on his map of the western Rehoboth area, while Handley (1965) and Martin (1965) included them in the Skumok Formation. De Waal (1966) subdivided the "Quartz-Porphyries" of De Kock (1934) and included them in his Sinclair Formation. Schalk (1970) assigned them to his Grauwater Formation of which they formed the lower part and which he described as "Nueckopf Porphyry of the Grauwater Formation".

The generally weakly metamorphosed volcanics of the Nueckopf Formation overlie the intensely tectonised and metamorphosed succession of rocks of the Gaub Valley, Billstein, Marienhof, Elim and Neuhof Formations and the Mooirivier Complex. They are partly intruded by members of the Gamsberg Granite Suite which are believed to be genetically associated with the acid Nueckopf volcanics, according to SACS (1980).

Radiometric age determinations of Burger and Coertze (1973,1973-74,1975-76) and Burger and Walraven (1975¬76) by the U-Pb method, yielded ages for the Nueckopf volcanics ranging between 932 ± 50 Ma and 1232 ± 30 Ma. An extremely high U-Pb age of 1770 ± 35 Ma, which is untenable considering the field relationships of the area (the Nueckopf volcanics overlie members of the Gamsberg Granite Suite with known ages which do not exceed 1246 Ma), was determined by Burger *et al.* (1975-76) on a "Porphyry of the Nueckopf Member of the Grauwater Formation". Some acid dykes on the farm Nauzerus yielded a Rb-Sr isochron age of 1030 Ma with a very high initial $^{87}Sr/^{86}Sr$ ratio of 0.732 (Reid *et al.*, 1988). According to U-Pb, Rb-Sr and K-Ar age determinations by Reid *et al.* (1988), Seifert (1986), Burger and Coertze (1973,1973-74,1975-76) and the authors, the age of the Gamsberg Granite Suite ranges between 1079 ± 25 Ma and 1246 Ma while the age of the Piksteel intrusives ranges between 1057 Ma and 1786 ± II Ma. The initial $^{87}Sr/^{86}Sr$ values of the Gamsberg Granite Suite range between 0.700 and 0.708 while those of the Piksteel intrusives range between 0.702 and 0.710 according to Seifert (1986), Reid *et al.* (1988) and this study. Rb-Sr dating of the Weener Intrusive Suite by Seifert (1986) and Reid *et al.* (1988) yielded ages between 1206 ± 102 Ma and 1871 ± 143 Ma with initial $^{87}Sr/^{86}Sr$ ratios ranging between 0.700 and 0.705.

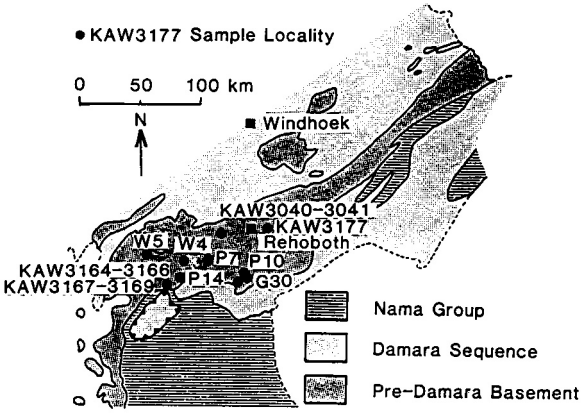

Figure 9.1: Map of sample localities of the analysed rhyolites

9.2 SAMPLE COLLECTION AND DESCRIPTION

All the whole-rock samples of Nueckopf volcanics were collected in areas assigned to the Nueckopf Formation on Schalk's unpublished 1:50 000 map of the Rehoboth area. Six of the samples were collected on the farms Auchas 347 (KAW3164-KAW3166) and Stoffbakkies 346 (KAW3167-KAW3169) while one sample comes from an outcrop of Nueckopf volcanics just south of Rehoboth Stasie (KAW3177). The two whole-rock samples of rhyolites from the Marienhof Formation were collected on the farm Marienhof 577 (KAW3040 and KAW3041). One sample of a "Gamsberg" rhyolite was collected on the farm Groendraai 367 (G30) while the "Piksteel" rhyolites were collected on the farms Karikomasis 364 (P10), Dymoeb 517 (P7) and Groendraai 367 (P14). The "Weener" volcanics come from the farms Namibgrens 154 (W5) and Naies 338 (W4). The sample localities are shown on Figure 9.1 and the exact coordinates of all sample localities are listed in Table 19 (see Appendix). The Rb-Sr whole-rock samples each weighed 30 to 40 kg while the geochemistry whole-rock samples weighed 3 to 5 kg.

The Nueckopf rhyolites are generally fine- to very fine-grained, partly recrystallised rocks. Porphyritic potassic feldspar, plagioclase and quartz up to 2 mm in diameter are embedded in a fine-grained quartz-feldspar-sericite matrix. Most of the samples show a narrow parallel texture. The frequently occurring fissures are mostly filled with quartz and calcite.

The volcanics from dykes crosscutting the Marienhof formation are fine- to very fine-grained metarhyolites with some relict porphyritic potassic feldspar up to 3 mm in diameter and rare porphyritic plagioclase up to I mm in diameter. The completely recrystallised matrix, which shows a narrow parallel texture, consists of quartz, feldspar, sericite, biotite/chlorite, epidote minerals and accessory magnetite/

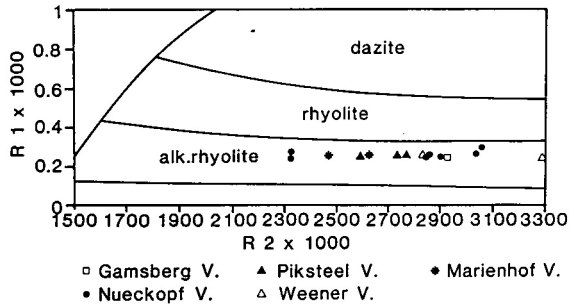

Figure 9.2: Classification diagram of De La Roche *et al.* (1980) for the analysed rhyolites (R1 = 6Ca+2Mg+Al; R2 = 4Si-11(Na+K)-2(Fe+Ti))

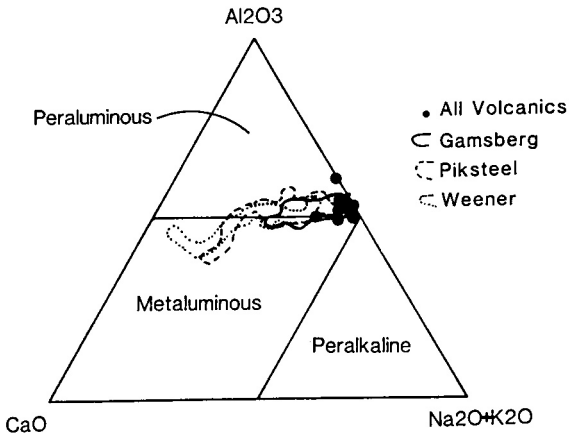

Figure 9.3: Wt% Al_2O_3-CaO-(Na_2O+K_2O) ternary diagram after Shand (1927 and 1951) for the analysed rhyolites in comparison with the fields for Gamsberg-, Piksteel- and Weener-type magmas as determined in Chapter 3

hematite and zircon. The zircons from both samples are heterogeneous in size, shape and colour. They often show small inclusions of opaque minerals and are commonly surrounded by white alteration rims. A K-Ar analysis of biotites from sample KAW3041 yielded an age of 516.6 ± 5.3 Ma (see Chapter 7) and is therefore representative of the Damaran metamorphism which affected the Marienhof samples.

The analysed "Gamsberg" and "Piksteel" volcanics have a completely different appearance. They resemble De Kock's (1934) Quartz-Porphyry dykes, which he found crosscutting several granites in his "southern belt of eruptive rocks" and which he classified as potash-rhyolites. With the exception of a slight cataclasis they are practically undeformed and show only minor signs of alteration. Porphyritic potassic feldspar up to one centimetre in diameter, plagioclase, and quartz are embedded in a fine- to very fine-grained matrix consisting of quartz, feldspar, sphene, ± biotite, ± sericite.

The two "Weener" volcanics are most similar in appearance to the volcanics from the areas mapped as Piksteel and Gamsberg Intrusives. They show a slightly higher mica content and stronger signs of alteration.

9.3 DISCUSSION OF THE ANALYTICAL RESULTS

9.3.1 Geochemistry

The results of all the geochemical analyses are listed in Table 19 (see Appendix).

All the analysed specimens plot in the field for alkali rhyolites in Streckeisen's (1981) modified version of the R1 versus R2 classification diagram for volcanic rocks of De La Roche *et al.* (1980), where R1 = 4Si-2(Fe+ Ti)-11 (Na+K) and R2 = Al+2Mg+6Ca (Fig. 9.2). This result confirms the work of De Kock (1934), who classified the "Quartz-Porphyries of the southern eruptive belt", the majority of which are included in today's Nueckopf Formation as potash-rhyolites. With a K_2O content 4.3% by weight, all the analysed specimens would also be classified as high-K rhyolites according to the classification scheme of Ewart (1979).

In the CaO-Al_2O_3-(Na_2O+K_2O) ternary diagram (Fig. 9.3), all the analysed samples plot in the field for peraluminous rocks, as their Al_2O_3 content exceeds that of (Na_2O+K_2O+CaO). They also plot well within the fields representing the Gamsberg, Piksteel and Weener granitoids according to the reconnaissance survey of this study (see Chapter 3). It is noteworthy that all the rhyolites plot towards the low-CaO end of the ternary diagram, thus indicating their enrichment in Na_2O+K_2O in comparison with the Rehoboth granitoids. With the exception of the rhyolites from dykes crosscutting the Marienhof Formation, the analysed rhyolites also plot in the same areas as the Piksteel, Gamsberg and Weener Intrusives in the tectonic discriminant Nb+Y versus Rb diagram of Pearce *et al.* (1984, Fig. 9.4). This indicates the close relationship of the analysed rhyolites with the Piksteel, Gamsberg and Weener magmas. The AFM ternary diagram (Fig. 9.5) gives a slightly different picture. The analysed volcanics more or less

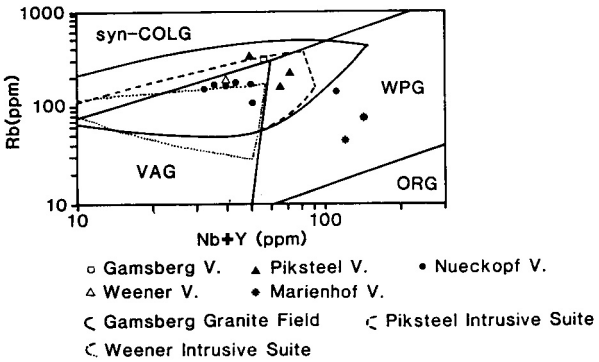

Figure 9.4: Nb+Y versus Rb diagram after Pearce *et al.* (1984) for the analysed rhyolites in comparison with the Gamsberg, Piksteel and Weener magmas as determined in Chapter 3. (syn-COLG = syn-Collision Granites; WPG = Within Plate Granites; VAG = Volcanic Arc Granites; ORG = Ocean Ridge granites)

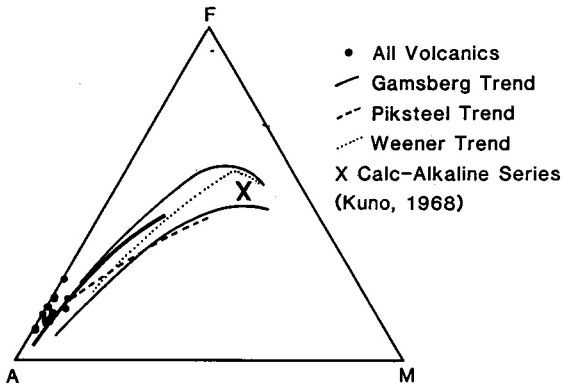

Figure 9.5: AFM ternary diagram after Kuno (1968) for the analysed rhyolites in comparison with the magmatic evolution trends of the Gamsberg-, Piksteel- and Weener-type magmas as described in Chapter 3

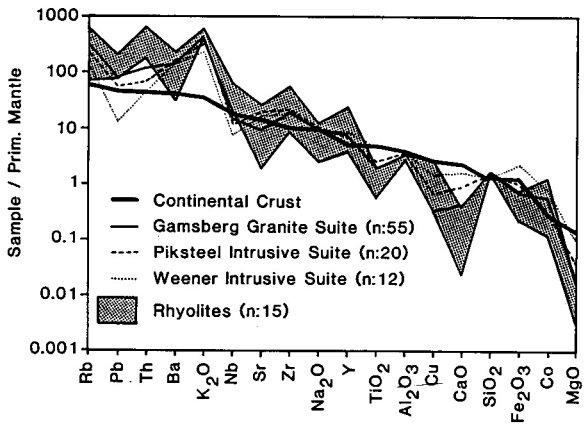

Figure 9.7: Mantle normalised element concentration patterns of the rhyolites from the Rehoboth Basement Inlier in comparison with average crust and the average of Gamsberg-, Piksteel- and Weener-type magmas after Chapter 5 (see text for explanation)

form a continuation of the evolution trends of the Piksteel, Gamsberg and Weener granitoid suites according to Chapter 3. This higher degree of differentiation is also confirmed by the mol.% (Na_2O+K_2O+CaO) versus mol.% Al_2O_3 diagram (Fig. 9.6), where it is shown that the analysed rhyolites are generally enriched in (Na_2O+K_2O+CaO) in comparison with the plutonic rocks of the Rehoboth Basement Inlier. The A/CNK ratio in Figure 9.6 is generally below 1.1, thus indicating I-type magmatic origins for the analysed rhyolites after Chapell and White (1974). In Figure 9.7 the normalised element concentration patterns of the analysed specimens and the average of the Gamsberg, Piksteel and Weener Intrusives are plotted in order of increasing compatibility after Taylor and McLennan (1985). The element concentrations are normalised with their respective concentrations in the primitive mantle, after data from Jochum *et al.* (1988). With the exception of Ba and Sr, which

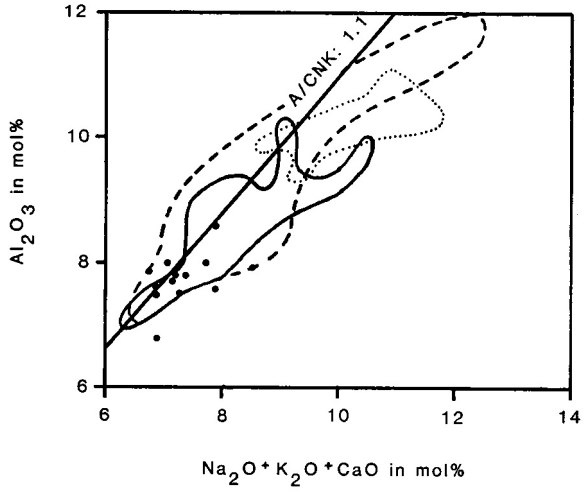

Figure 9.6: Mol.% Al_2O_3 versus mol.% (Na_2O+K_2O+CaO) diagram showing A/CNK saturation values (mol.% $K_2O+Na_2O+K_2O$) after Chappell and White (1974) for the analysed rhyolites in comparison with the fields of Gamsberg-, Piksteel- and Weener-type magmas as described in Chapter 3. (Same symbols used as in Figure 10.2)

are slightly depleted, most of the elements of the analysed rhyolites reflect a slightly more advanced stage of magmatic evolution as is shown by an enrichment of Rb, Pb, Th, K_2O and Nb and a depletion of Na_2O, TiO_2, CaO, Fe_2O_3, Co and MgO in comparison with the average values of the Gamsberg, Piksteel and Weener magmas. The high K_2O/Na_2O ratios, the slightly negative correlation of K_2O and Na_2O, and the constant K_2O+Na_2O contents with increasing SiO_2 of the samples might indicate post-genetic K-metasomatic processes affecting the investigated rhyolites which were similar to metasomatic processes described by Buletti (1985) for the Southern Alps. This is supported by the work of Behr *et al.* (1983) who described metasomatic alteration processes in the Duruchaus Formation and related them to pre-Damaran volcanics of the Rehoboth Basement Inlier.

From the present data it may be deduced that the analysed rhyolites represent highly evolved magmas which developed and extruded in relation to the generation of the large granitic bodies found throughout the Rehoboth Basement Inlier, and that post-genetic metasomatic processes may have affected the analysed rhyolites.

9.3.2 Rb-Sr analyses

The results of the Rb-Sr analyses of 7 Nueckopf rhyolites are listed in Table 20 (see Appendix). With the exception of KAW3166, which deviates towards higher $^{87}Sr/^{86}Sr$ ratios, probably because of strong penetration by small calcite-filled clefts, samples all plot on a reference line of 948.0 ± 24.7 Ma in the $^{87}Rb/^{86}Sr$ versus $^{87}Sr/^{86}Sr$ isochron diagram (Fig. 9.8). The reference line calculated after York (1969), with equally weighted samples and no correlation of errors, has an intercept I at $^{87}Sr/^{86}Srr = 0.7079 \pm 0.0051$ and a correlation coefficient R of 0.998. The age of 948 Ma broadly coincides with U-Pb age determinations for the Nueckopf Formation of Burger and Coertze (1973, 1973¬74, 1975-76) and Burger and Walraven (1975-76), who obtained ages between 93 ± 50 Ma and 1232 ± 30 Ma for various occurrences of Nueckopf volcanics in the Rehoboth Base-

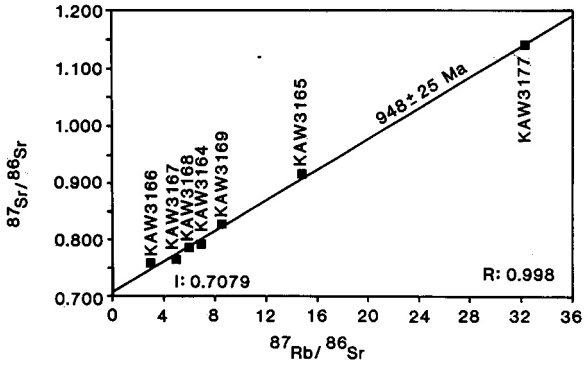

Figure 9.8: $^{87}Rb/^{86}Sr$ versus $^{87}Sr/^{86}Sr$ isochron diagram for the analysed rhyolites from the Nueckopf Formation

ment Inlier. The obtained initial $^{87}Sr/^{86}Sr$ ratio of 0.7079 is within the range of values (0.700 - 0.710) found for Piksteel and Gamsberg Intrusives (Seifert, 1986; Reid *et al.*, 1988; this study), and is slightly higher than the initial values of 0.700 - 0.705 observed in the Weener Intrusive Suite (Seifert, 1986; Reid *et al.*, 1988), but falls well below the initial value of 0.732 of the acid dykes of Nauzerus according to Reid *et al.* (1988). As shown in Chapter 9.3.1, metasomatic processes may have affected the analysed rhyolites. It is thus possible that the Rb-Sr systems of the rhyolitic rocks of the Rehoboth Basement Inlier have been affected by such processes which would also partly have changed the properties of the observed isochrons. Evidence for the existence of such processes is given by the high initial $^{87}Sr/^{86}Sr$ ratio of 0.732 obtained by Reid *et al.* (1988) for acid dykes from the farm Nauzerus. .

A two-point isochron can be calculated with the Rb-Sr results obtained for the rhyolites from the farm Marienhof 577 (Table 20, see Appendix). It yields an age of 813 Ma and an intercept of $^{87}Sr/^{86}Sr$ = 0.71705 and is therefore in conflict with the results of the U-Pb analyses which are discussed below. The relatively high initial $^{87}Sr/^{86}Sr$ ratio of 0.71705 and the low age may again be related to post-genetic metasomatic processes affecting the Rb-Sr system of the analysed specimens.

9.3.3 U-Pb analyses

The results of the analysed zircon fractions of KAW3040 and KAW3041 are listed in Table 21 (see Appendix). The obtained apparent $^{206}Pb/^{238}U$, $^{207}Pb/^{235}U$ and $^{207}Pb/^{206}Pb$ ages are discordant and range between 746 Ma and 1107 Ma. In the Concordia diagram of Wetherill (1956), the analysed zircon fractions plot on a Discordia intercepting the Concordia at 1210 ± 8 Ma and 349 ± 13 Ma (Fig. 9.9). The sample points are located about halfway between the upper and lower intercept of the Discordia with the Concordia and therefore reflect about 40-60% loss of radiogenic lead from the analysed zircons. The Concordia diagram of Tera and Wasserburg (1972) confirms the results of the Wetherilll diagram, as the Discordia defined by the analysed zircons intercepts the Concordia at 1210 ± 7 Ma and 350 ± 12 Ma (Fig. 9.10). The upper intercept age of 1210 ± 7 Ma, representing a minimum age for the formation of the analysed zircons, is much higher than that of the two-point Rb-Sr isochron discussed above. The lower intercept age of 350 ± 12 Ma is probably geologically meaningless, as a continuous diffusive loss of lead must be assumed for the analysed zircons. As indicated by biotites from sample KAW3041 (see Chapter 7) yielding a K-Ar age of 516.6 ± 5.3 Ma, the sample locality has been affected by Damaran metamorphism. This event probably also affected the Rb-Sr systems of the samples KAW3040 and KAW3041, resulting in the relatively low Rb-Sr age of 813 Ma. The U-Pb system of the analysed zircons, although having suffered from lead loss, still reflects the probable age of intrusion of the studied rhyolitic dykes into the Marienhof Formation. The U-Pb age of 1210 ± 7 Ma therefore gives a reliable minimum age for the Marienhof Formation itself.

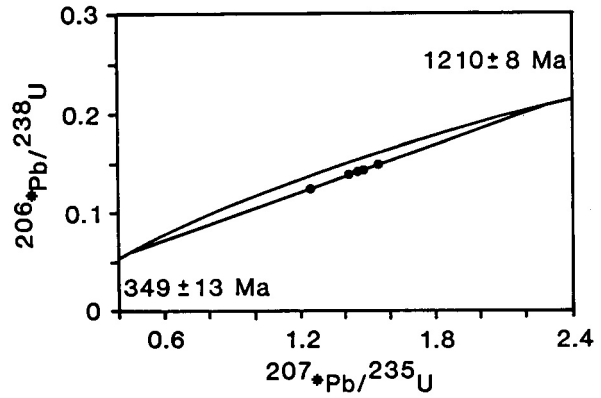

Figure 9.9: Concordia diagram of Wetherill (1956) for the analysed zircons from rhyolitic dykes crosscutting the Marienhof Formation (see text for explanation)

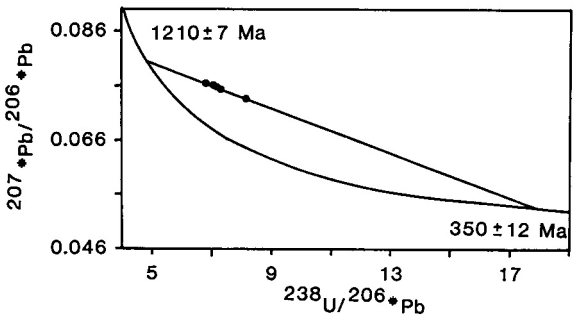

Figure 9.10: Concordia diagram of Tera and Wasserburg (1972) for the analysed zircons from rhyolitic dykes crosscutting the Marienhof Formation (see text for explanation)

9.4 CONCLUSIONS

All the analysed volcanic rocks from the Rehoboth Basement Inlier are peraluminous high-K rhyolites. Although they were sampled from different localities, formations and tectonic settings, they all show similar geochemical properties. A close relationship to Gamsberg-, Weener- and especially Piksteel-type magmas may be deduced from their element distribution patterns, although it seems that the analysed rhyolites represent more evolved magmas of the Gamsberg, Piksteel and Weener type, rather than magmas of these types themselves. Post-genetic K-metasomatic processes have to be considered for the analysed rhyolites based on their high K_2O/Na_2O ratios. The Rb-Sr isochron age of 948.0 ± 24.7 Ma obtained for Nueckopf rhyolites and the U-Pb age of 1210 ± 7 Ma of zircons from rhyolitic dykes crosscutting the Marienhof Formation, indicate that the analysed volcanics formed in connection with the intrusion of plutons assigned to the Gamsberg, Piksteel and Weener Suites, whose ages range between 1057 and 1871 ± 143 Ma, according to various authors. As, according to SACS (1980), Seifert (1986) and this study, an age exceeding a careful estimate of 1500 Ma must be assumed for the Weener and Piksteel magmatism, it must be suggested that the analysed dykes crosscutting the Marienhof Formation formed in connection with the Gamsberg magmatism. The same goes for the Nueckopf volcanics, whose relatively high initial $^{87}Sr/^{86}Sr$ ratio of 0.7079, if not the result of metasomatic processes, at least clearly excludes a relation of these volcanics with the Weener Intrusive Suite, whose initial $^{87}Sr/^{86}Sr$ ratios of 0.700 to 0.705 are significantly lower.

Furthermore, a minimum age of 1210 ± 7 Ma for the Marienhof Formation is also provided by the U-Pb results obtained for the zircons from dykes crosscutting the Marienhof Formation.

10. BASIC DYKES CROSSCUTTING THE REHOBOTH BASEMENT INLIER

10.1 INTRODUCTION

Basic igneous dykes crosscutting the Mokolian sequence occur throughout the Rehoboth Basement Inlier. They are generally weathered dark brown to black and are elongate intrusive bodies up to several metres thick and a few metres to several kilometres long. The contacts be-tween the dykes and the country rock are mostly sharp and do not show signs of strong alteration inferred by the intrusion of the basic magmas. The dykes themselves, although altered, seem to be virtually unaffected by any kind of regional metamorphism. Two varieties of dykes may be recognised throughout the area. One type comprises a very fine-grained, homogeneous and massive rock with almost no readily recognisable phenocrysts, while the other, also comprised of fine-grained and massive rock, is speckled with large, white, porphyritic inclusions of up to several centimetres. As at first glance the dykes often are more resistant to weathering and show fewer signs of alteration than their host rocks, they seem to be much younger than the surrounding country rock. The majority of the basic dykes strike in a northeast-southwest direction, which more or less parallels the strike of the Areb shear zone of the Rehoboth Basement Inlier. The orientation of strike changes to a more north-northeast-south-southwest direction towards the southwest of the area (i.e. in the area of the farms Piksteel 209 and Solitaire 412).

Previous work on the basic dykes is scarce. It is important to note that the basic dykes of this report should not be confused with occurrences of other intrusive basic rocks in the Rehoboth area which are related to the much older Alberta Complex according to Schalk (pers. comm., 1987), and much younger Cretaceous to Tertiary intrusive alkali rocks of the area between Windhoek and Rehoboth. This is supported by radiometric age determinations on some of the aforementioned basic intrusives which have shown that the age of the Alberta Complex is approximately 1442 Ma ± 32 Ma (Reid *et al.*, 1988), while an age of 32 Ma should be assumed for the alkali rocks of the area between Windhoek and Rehoboth based upon $^{40}Ar/^{39}Ar$ dating of the Aris phonolite by FM Consultants, London (Schalk, pers. comm., 1987). Rb-Sr dating of some mafic dykes from the farm Nauzerus II by Reid *et al.* (1988) which these authors consider to be the youngest intrusives of the Nauzerus area, yielded a whole-rock isochron age of 1030 Ma ± 185 Ma with an intercept at $^{87}Sr/^{86}Sr = 0.7064$.

10.2 SAMPLE COLLECTION AND DESCRIPTION

Five whole-rock samples weighing 30 kg each were collected from basic dykes in the western part of the Rehoboth Basement Inlier (Fig. 10.1). The exact coordinates of the sample localities are listed in Table 22 (see Appendix). All of the sampled dykes were found to intrude either granitic host rocks assigned to the Piksteel Intrusive Suite and to the Gamsberg Granite Suite or, in one case (KAW3162), amphibolites of the Elim Formation. Although all the samples show some signs of alteration none of the analysed dykes shows signs of foliation.

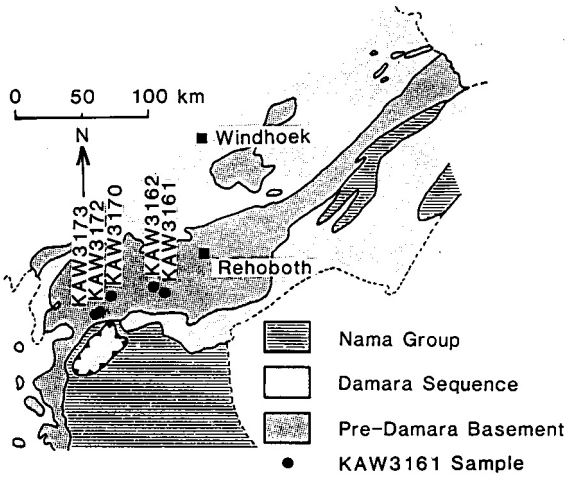

Figure 10.1: Sample localities for the analysed basic dykes (see Table 22 in the Appendix for coordinates)

Sample KAW3161 is a fine-grained and massive aphyric dyke which is composed of 40% plagioclase (labradorite), 37% pyroxene, 20% chlorite/white mica, 3% opaque minerals and accessory albite and epidote minerals. Plagioclase and pyroxene form an inequigranular, holocrystalline texture with interstitial growth of the minerals. Chlorite, white mica, albite and epidote minerals formed at the expense of plagioclase and pyroxene. KAW3162 is a porphyritic basic dyke with greenish-white, completely saussuritised plagioclase up to 5 mm in diameter which is embedded in a very fine-grained matrix. The matrix is composed of strongly altered amphiboles, completely saussuritised plagioclase and small amounts of opaque minerals and sphene. No primary plagioclase is readily visible in both matrix and porphyrites as these minerals have been completely transformed into a very tine-grained texture consisting of epidote minerals, chlorite, sericite and some albite. KAW3170 is a fine-grained dyke with hypidiomorphic to idiomorphic plagioclase phenocrysts up to 5 mm in diameter embedded in an interstitial matrix consisting of 40% plagioclase, 50% pyroxene, 5% chlorite/sericite, 2% epidote minerals and 3% opaque minerals. Epidote minerals, chlorite, sericite and albite occur as alteration products of plagioclase and pyroxene. KAW3172 is another fine-grained, aphyric dyke with an interstitial texture. It is composed of 55% labradoritic, partly saussuritised plagioclase, 25% pyroxene, 5% opaque minerals and 15% alteration products such as chlorite, sericite, albite, epidote minerals and calcite. Finally. KAW3173 is a fine- to medium-grained basic dyke with subophitic texture. The rock is composed of 35% labradoritic to bytownitic plagioclase which is partly strongly saussuritised, 2% opaque minerals and 13% alteration products, such as epidote minerals, chlorite, albite and sericite.

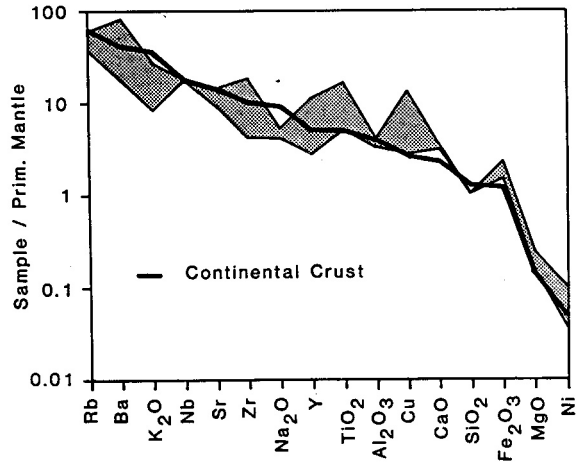

Figure 10.2: Mantle-normalised element concentration patterns of the basic dykes from the Rehoboth Basement Inlier in comparison with average crust (see text for explanation)

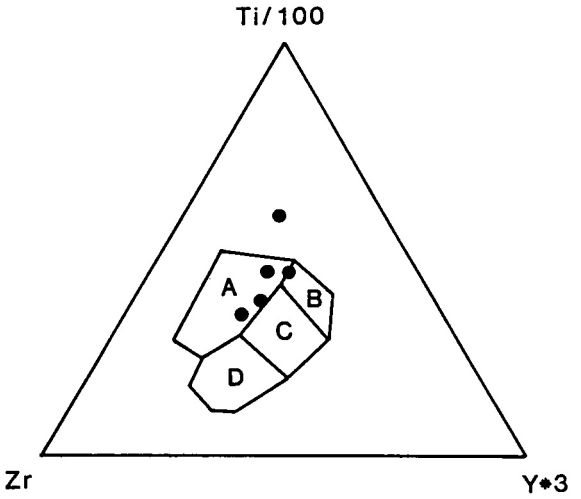

Figure 10.3: Ti/100-Zr-Y*3 ternary diagram of Pearce and Cann (1973) for the analysed basic dykes. (Field A = Within Plate Basalts; B = Island Arc Tholeiites; C = Mid Ocean Ridge Basalts; D = Calc-Alkaline Basalts)

Because of the strong alteration of the amphiboles of KAW3162 and the lack of other primary minerals which could be dated by the Rb-Sr and K-Ar methods in all the basic dykes, it was decided that only whole-rock analyses of the collected sample material should be carried out.

10.3 DISCUSSION OF THE ANALYTICAL RESULTS

10.3.1 Geochemistry

The results of the geochemical analyses are listed in Table 22 and the results of the CIPW-normative calculations are given in Table 22A (see Appendix).

All the analysed basic dykes fit into the "basalt sieve" of Manson (1967) and all of them are of tholeiitic nature when considering their FeO/MgO, Na_2O, K_2O and SiO_2 contents. The tholeiitic chemistry of the analysed dykes is confirmed by the calculation of CIPW-normative minerals (Table 22A, Appendix) which shows that all the specimens have little or no free quartz and have no or little normative olivine, respectively. According to their normative mineral content the analysed dykes would therefore plot in the vicinity of the quartz saturation plane of the Di-Ne-Fo-Q basalt tetrahedron (after the normative classification of basalts of Yoder and Tilley, 1962). In Figure 10.2 the mantle-normalised element concentration patterns of the analysed specimens have been plotted in order of increasing incompatibility of the elements (after Taylor and McLennan, 1985). The values for the primitive mantle used to normalise the analytical results of the basic dykes were taken from Jochum *et al.* (1988). A comparison of the data of the basic dykes with average continental crust, for which the data were taken from Taylor and McLennan (1985), shows that the basic dykes are somewhat depleted in Rb, Ba, K_2O, Sr and Na_2O while they are enriched in TiO_2, Cu, CaO and Fe_2O_3. The normalised contents of Nb, Zr, Y, Al_2O_3, SiO_2, MgO and Ni scatter around the average crustal composition. Bearing the limitations of tectonic discriminant variation diagrams in mind (e.g as discussed by Wilcox, 1979), we nonetheless tried to plot the obtained data onto the tectonic discriminant ternary Ti/100-Zr-3*Y diagram of Pearce and Cann (1973) (Fig. 10.3). With the exception of KAW3161, all the basic dykes plot into the field for Within Plate Basalts, which is not surprising, as all the analysed specimens stem from a definitely continental environment.

Based on the discussion above it can be said that the analysed post-Gamsberg basic dykes of the Rehoboth Basement Inlier represent tholeiitic magmatism generated and intrusive in a continental tectonic environment under the influence of dilatational processes parallel to the Areb shear zone.

10.3.2 K-Ar results

The results of the whole-rock K-Ar analyses are listed in Table 23 (see Appendix). The apparent individual ages of the samples range between 540.8 Ma ± 6.7 Ma and 1934.5 Ma ± 14.0 Ma. The content of $^{40}Ar_{rad}$ of all the samples ranges between 81.88% and 94.77% of the total argon content of the samples. This indicates that a certain amount of non-radiogenic argon is present in the analysed K-Ar systems. The low contents of ^{36}Ar in the samples (see Table 23, Appendix) show, however, that the low percentage of radiogenic ^{40}Ar of the samples is due to the low K contents of the samples which, in combination with minor amounts of inherited or admixed argon of atmospheric composition, lead to such low $^{40}Ar_{rad}$ percentages. A calculation of the correlation coefficients of the $^{40}Ar_{rad}$ and ^{40}K contents and the $^{40}Ar/^{36}Ar$ and $^{40}K/^{36}Ar$ ratios of the analysed samples yields very low values which thus indicate that the analysed samples do not represent a common K-Ar system.

The two basic dykes represented by the samples KAW3161 and KAW3170 yield K-Ar ages of 1290.3 Ma ± 10 Ma and 1934Ma ± 14.0 Ma, respectively. They intrude the Kanaus and Borodino granite bodies whose U-Pb ages of 1064 Ma ± 20 Ma and 1369 Ma ± 8 Ma respectively,

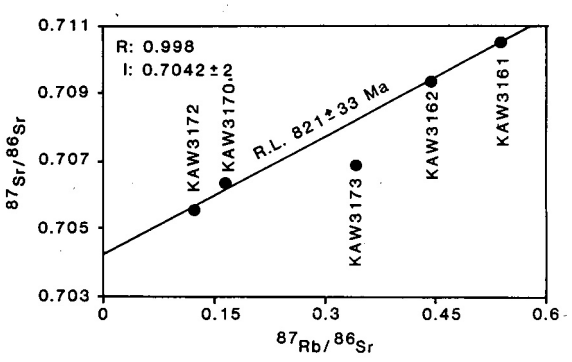

Figure 10.4: $^{87}Rb/^{86}Sr$ versus $^{87}Sr/^{86}Sr$ diagram for the analysed basic dykes

(Burger and Coertze, 1973-74; this study) are below the K-Ar ages obtained for the intrusive dykes. It has thus to be assumed that the whole-rock K-Ar ages of these two dykes do not represent their formation ages. It is consequently also evident that these samples have inherited a certain argon over pressure which might have formed by contact metamorphic reactions of K -feldspar and other K-bearing phases of the wall rock during the intrusion of the basaltic magmas into the granitic host material.

The ages of KAW3172 and KAW3173 of 789.1 Ma ± 8.8 Ma and 747.1 Ma ± 7.1 Ma respectively, are somewhat below the age of 821 Ma obtained for a Rb-Sr reference line calculated through four of the analysed basic dykes, which unfortunately do not include KAW3173 (see next paragraph). The obtained K-Ar ages might thus indicate a partial loss of argon from KAW3172 and KAW3173 relative to the Rb-Sr reference age due to post-formation alteration processes. They also indicate that Damaran-related metamorphism, which is known to have affected the northern part of the Rehoboth Basement Inlier until at least 490 Ma before today (see e.g. Chapter 7), was not capable of resetting the whole-rock K-Ar systems of these two basic dykes which were sampled south of 23°46'S.

The age of 588.9 Ma ± 7.7 Ma of sample KAW3162, which was collected at 23°33'S, was also not completely reset by the Damara orogeny. If this sample did not inherit argon over pressure, a possibility which has to be taken into consideration as was shown for KAW3161 and KAW3170, the age of 589 Ma might represent a minimum age for the intrusion of the basic dykes.

10.3.3 Rb-Sr analyses

The results of the Rb-Sr analyses are listed in Table 24 (see Appendix). Dating of the basic dykes of the Rehoboth area proved to be more successful with the Rb-Sr method than with the K-Ar method. With the exception of KAW3173, which plots far off the other four data points without obvious explanation, all the analysed samples plot onto a well-correlated (R = 0.998) reference line representing an age of 821 : ± 33 Ma (Fig. 10.4). The intercept of this line is at $^{87}Sr/^{86}Sr = 0.7042 \pm 0.0002$. As a strong overprint of the analysed dykes by Damaran-related metamorphism is quite unlikely, based on the K-Ar data discussed above and because other strong post-Mokolian alteration phases are not known from the area, it should be assumed that the obtained reference line gives a significant age for the intrusion of the analysed basic dykes.

10.4 CONCLUSIONS

This chapter shows that the basic dykes of the Rehoboth Basement Inlier represent a basaltic magmatism with tholeiitic chemical properties, which was generated in a continental tectonic environment under a dilatational regime. The total-rock K-Ar systems of the analysed specimens could not give sufficient information on the formation age of the basic dykes as all of them show either argon over pressure or loss of argon. Nonetheless, it can be shown, based on the K-Ar data, that Damaran-related metamorphism was not capable of resetting the K-Ar systems of the analysed samples, all of which were collected south of 23°33'S. The well-correlated Rb-Sr reference line of 821 Ma ± 33 Ma gives a reasonable age for the intrusion of the analysed basic dykes, although it seems to be too young in comparison with the age of the Nauzerus mafic dykes of 1030 Ma ± 185 Ma (Reid *et al.*, 1988). A comparison of the $^{87}Sr/^{86}Sr$ intercept of this report with the intercept of the isochron of Reid *et al.* (1988) shows that the Nauzerus intercept of $^{87}Sr/^{86}Sr = 0.7064$ is considerably higher than the intercept of $^{87}Sr/^{86}Sr = 0.7042$ of this study's reference line. It is thus possible that the Nauzerus mafic dykes do not represent the same kind of magmatism which has been dated in this paper.

The Rb-Sr age of 821 Ma ± 33 Ma obtained in this study might give a useful age indication for the occurrence of initial dilatational processes which led to the formation of the Damara geosyncline. Such an assumption is supported by the occurrence of basic dykes subparallel to the Areb shear zone throughout the Rehoboth Basement Inlier, which could only have fanned due to late- to post-Mokolian dilatational processes.

11. SM-ND DATING OF THE REHOBOTH BASMENT INLIER AND ITS IMPLICATIONS FOR THE REGIONAL GEOLOGY

11.1 INTRODUCTION

Nd-isotope studies carried out in South Africa and Zimbabwe on both crustal and mantle rocks and on xenoliths in kimberlites by various authors (e.g. Hawkesworth *et al.*, 1984; De Paolo and Wasserburg, 1976; Hamilton *et al.*, 1977 and 1979; Bor-ming Jahn *et al.*, 1982), yielded a broad spectrum of Sm-Nd isochron and model ages ranging between 2.5 and 3.6 Ga. The oldest Sm-Nd ages have been determined in the Onverwacht greenstone belt, while Sm-Nd ages between 2.5 Ga and 2.7 Ga were found in Zimbabwe for the Great Dyke and up to 3 Ga old for the members of various greenstone belts which intrude basement rocks. These old formations are interpreted as Archaean Transvaal and Zimbabwe nucleii surrounded by mobile belts composed of new and reworked crustal material (Hawkesworth, 1984) which consequently yield younger Sm-Nd ages. The Transvaal and Zimbabwe nucleii are connected by the old Limpopo Mobile Belt, whose maxi-mum U-Pb age is about 3.85 Ga for the Sand River Gneiss (Barton *et al.*, 1977 and 1978). During its evolution the Limpopo Belt was affected by various events, among which the Eburnian event at approximately 2 Ga is one of the most important and best known (Clifford *et al.*, 1970; SACS, 1980). The rocks of the Namaqua-Natal belt neighbouring the Archaean nucleii to the west and south, yielded ages of 1.0 Ga - 1.4 Ga (Barton *et al.*, 1981; Hawkesworth *et al.*, 1984).

The aim of these first Sm-Nd analyses in this area of the Kalahari Craton, which were carried out in addition to K-Ar, Rb-Sr, U-Pb and REE studies on the same samples which have been discussed in the previous chapters, was to provide crustal ages which were expected to give a maximum age for the formation of the continental crust of the northwestern rim of the Kalahari Craton (Fig. 11.1), and thus narrow the time span during which the volcano sedimentary sequences and igneous complexes of the Rehoboth Basement were initially formed. Moreover, it was expected that the Sm- Nd isotope geochemistry would give information on the evolutionary trends of the magmatic rocks of the area, and would elucidate some of the genetic relationships between the Damara Orogen and the Rehoboth Basement Inlier.

A total of 35 samples was selected from various formations and localities of the Basement Inlier in order to achieve these goals. Five amphibolitic samples come from the northernmost outcrop of the Neuhof Formation, while a set of seven amphibolite samples was chosen from two localities of the Elim Formation. These samples from volcano sedimentary formations were selected in order to provide estimates of the crustal residence time of the material which forms these formations. Another 19 samples were taken from the Borodino, Piksteel and Opetjie plutons of the Piksteel Intrusive Suite, which intrudes the Rehoboth Sequence and has provided minimum ages for the Rehoboth Sequence and its underlying formations by other dating techniques. Four samples of the abundant basic dykes, which are found crosscutting all the Mokolian series of the Rehoboth Basement Inlier, were included in this study as they represent the last pre-Karoo magmatic activities within the Rehoboth Inlier. The precise coordinates of the sample localities are listed in Table 25 (see Appendix).

11.2 SM-ND ISOTOPE SYSTEMATICS

The results of the Sm-Nd analyses are listed in Table 25 (see Appendix). A graphic presentation of all the Sm-Nd results is shown in Figure 11.2 where the $^{147}Sm/^{144}Nd$ ratios of all the samples from various formations are plotted against their $^{143}Nd/^{144}Nd$ ratios. It is evident that 20 of the 35 data points form a linear array while the remaining 15 data sets plot above this linear trend. A reference line calculated through the linear array of 20 data sets yields an age of

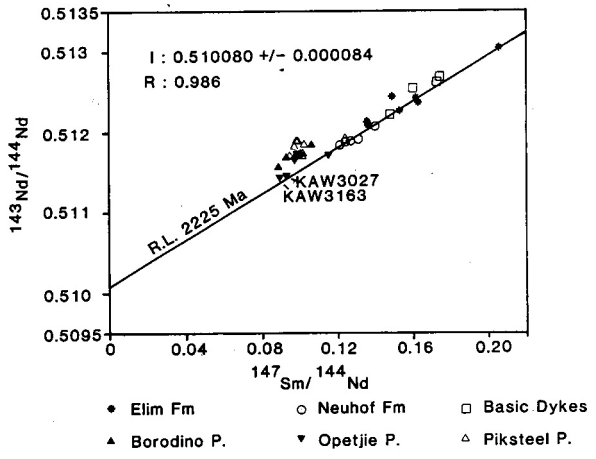

Figure 11.2: $^{147}Sm/^{144}Nd$ versus $^{143}Nd/^{144}Nd$ isochron diagram for all the analysed specimens from the Rehoboth Basement Inlier

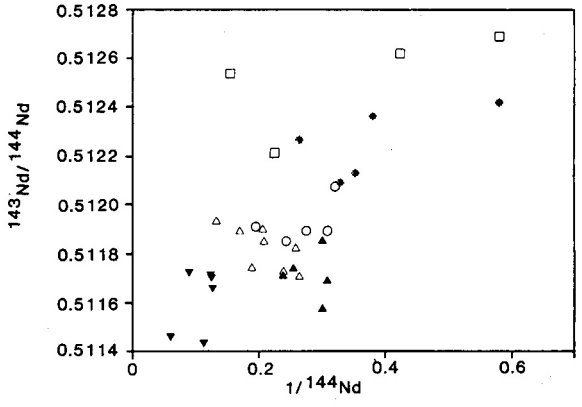

Figure 11.4: $1/^{144}Nd$ versus $^{143}Nd/^{144}Nd$ diagram for all the analysed specimens. (KAW3011 and KAW 3012 are outside the range of the diagram)

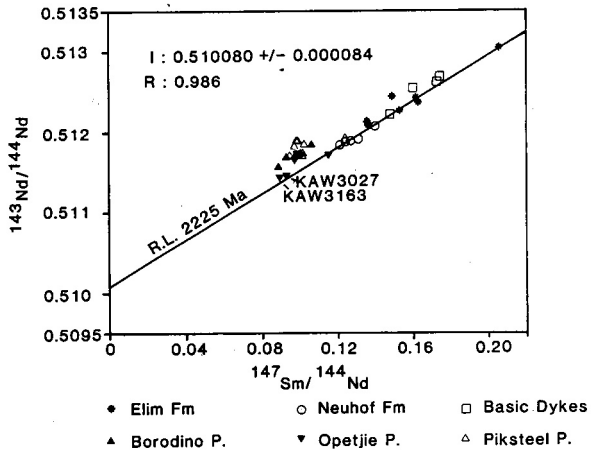

Figure 11.2: $^{147}Sm/^{144}Nd$ versus $^{143}Nd/^{144}Nd$ isochron diagram for all the analysed specimens from the Rehoboth Basement Inlier

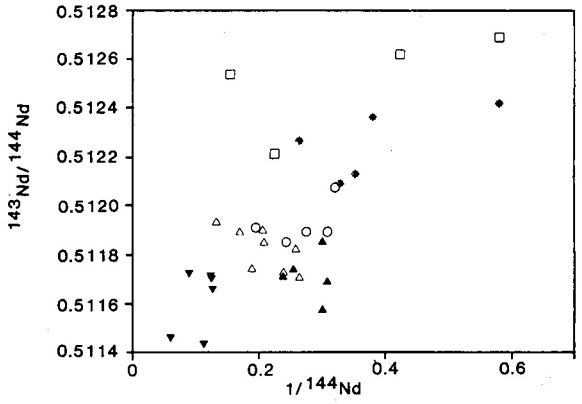

Figure 11.4: $1/^{144}Nd$ versus $^{143}Nd/^{144}Nd$ diagram for all the analysed specimens. (KAW3011 and KAW 3012 are outside the range of the diagram)

2225 ± 88 Ma with a correlation coefficient R of 0.986 and an intercept I at $^{143}Nd/^{144}Nd = 0.510080 \pm 0.000084$. If the samples KAW3027 and KAW3163 are disregarded, the best-fit regression line calculated through the remaining 18 data sets yields an age of 2287 ± 117 Ma with a correlation coefficient R of 0.979 and an intercept I at $^{143}Nd/^{144}Nd = 0.51002 \pm 0.00012$, which is within the error limits most similar to the result obtained for the calculation of the 20 data sets. The frequency distributions of 30 000 ages and intercepts of Figure 11.3A and 11.3A obtained by the bootstrap method for the 20 linear data sets show slightly skew distribution patterns with distinct maxima at 2175 Ma and $^{143}Nd/^{144}Nd = 0.510125$ respectively. A comparison of both calculation techniques shows that the results of the two methods are in good agreement and thus might indicate a certain significance of the obtained array of 20 data sets from various formations. The skewness of the bootstrap frequency distribution indicates that the analysed sample population is not normally distributed. It cannot be decided on the base of the present data whether this should be attributed to abnormally distributed sample collection or whether this skewness has a definite geological significance. The $1/^{144}Nd$ versus $^{143}Nd/^{144}Nd$ diagram (Fig. 11.4) on which no linear patterns between the 35 samples could be found, nonetheless indicates that the calculated regressions do not represent geologically meaningless two-component mixture lines.

Figure 11.3 (below): A: Frequency distribution patterns of 30 000 ages calculated by the bootstrap method of Diaconis and Efron (1983) for the 20 samples which plot on the reference line in Figure 11.2
B: Frequency distribution of 30 000 intercepts calculated for the same 20 samples

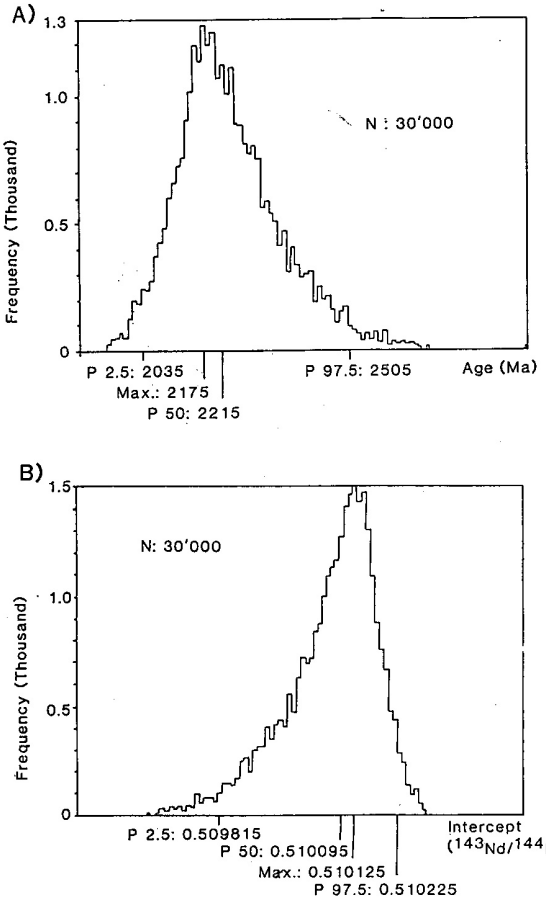

It is of interest that the remaining 15 data sets which plot above the calculated reference line of 2225 Ma do not form a linear array, which could indicate another phase of crustal generation in the Rehoboth Basement Inlier. The set of 15 data points is composed of all the samples from the Borodino pluton, 3 out of 6 samples from the Opetjie pluton and 7 out of 8 samples from the Piksteel pluton. This indicates either that the majority of the whole-rock Sm-Nd systems of the Piksteel Intrusive Suite were disturbed after the formation of the continental crust of the Rehoboth Inlier (e.g. by crustal reworking and mixing) or, if the measured isotopic properties represent the original properties of these samples, that they derive from various sources different from those of the 20 samples forming a linear array.

A closer look at the individual results of the analysed formations and intrusions shows several individual reference lines which are helpful in interpreting the Sm-Nd characteristics of the Rehoboth Basement Inlier. A reference line calculated through the data points of the Neuhof Formation (Fig. 11.5A) yields a reference age of 1821 Ma ± 305 Ma with a

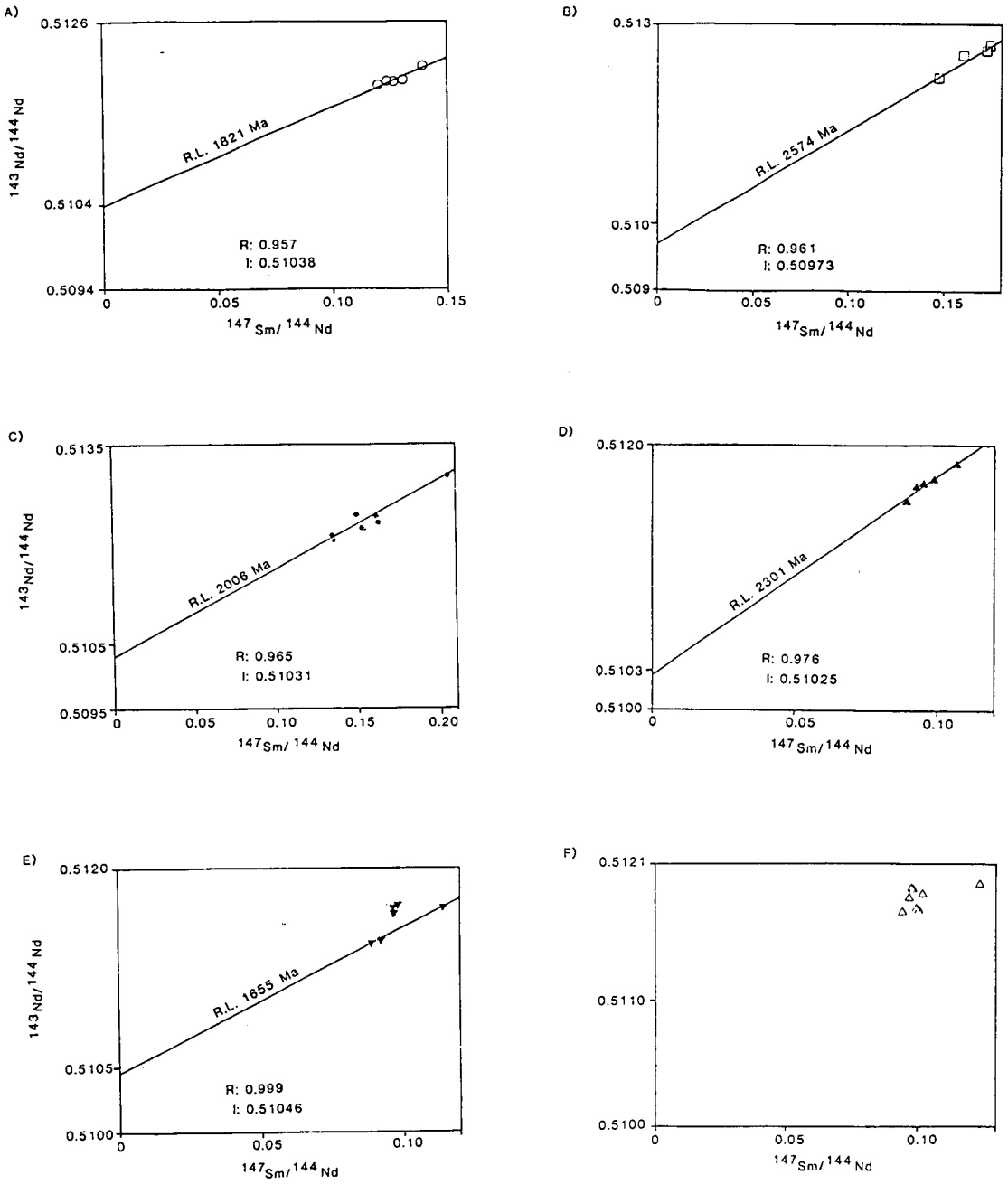

Figure 11.5: A : $^{147}Sm/^{144}Nd$ isochron diagram for the analysed amphibolites of the Neuhof Formation.
B: Isochron diagram for the analysed basic dykes.
C: Isochron diagram for the analysed amphibolites of the Elim Formation.
D: Isochron diagram for the analysed granitoids of the Borodino pluton of the Piksteel Intrusive Suite.
E: $^{147}Sm/^{144}Nd$ versus $^{143}Nd/^{144}Nd$ diagram for the analysed samples from the Opetjie pluton of the Piksteel Intrusive Suite.
F: Isochron diagram for the analysed samples from the Piksteel pluton of the Piksteel Intrusive Suite

low correlation coefficient R of 0.957 and an intercept I at $^{143}Nd/^{144}Nd = 0.51038 \pm 0.00026$. The reference line calculated for the basic dykes (Fig. 11.58) yields an age of 2574 Ma ± 504 Ma with a low correlation coefficient R of 0.961 and an intercept I at $^{143}Nd/^{144}Nd$ at 0.50973 ± 0.00055. The amphibolites of the Elim Formation plot on a reference line of 2006 Ma ± 237 Ma with a correlation coefficient R of 0.965 and an intercept I at $^{143}Nd/^{144}Nd = 0.51031 \pm 0.00025$ (Fig. 11.5C). A regression line calculated through the five data points of the Borodino pluton, which plot above the overall reference line of the 20 data sets discussed above, yields an age of 230 I Ma ± 289 Ma with a correlation coefficient R of 0.976 and an intercept I at $^{143}Nd/^{144}Nd = 0.51025 \pm 0.00018$ (Fig. 11.5D). No reference line with a correlation coefficient 0.7 can be fitted through the scattered data of the Opetjie pluton (Fig. 11.5E). A reference line calculated through the samples KAW3026. KAW3027 and KAW3163, which also plot on the overall regression

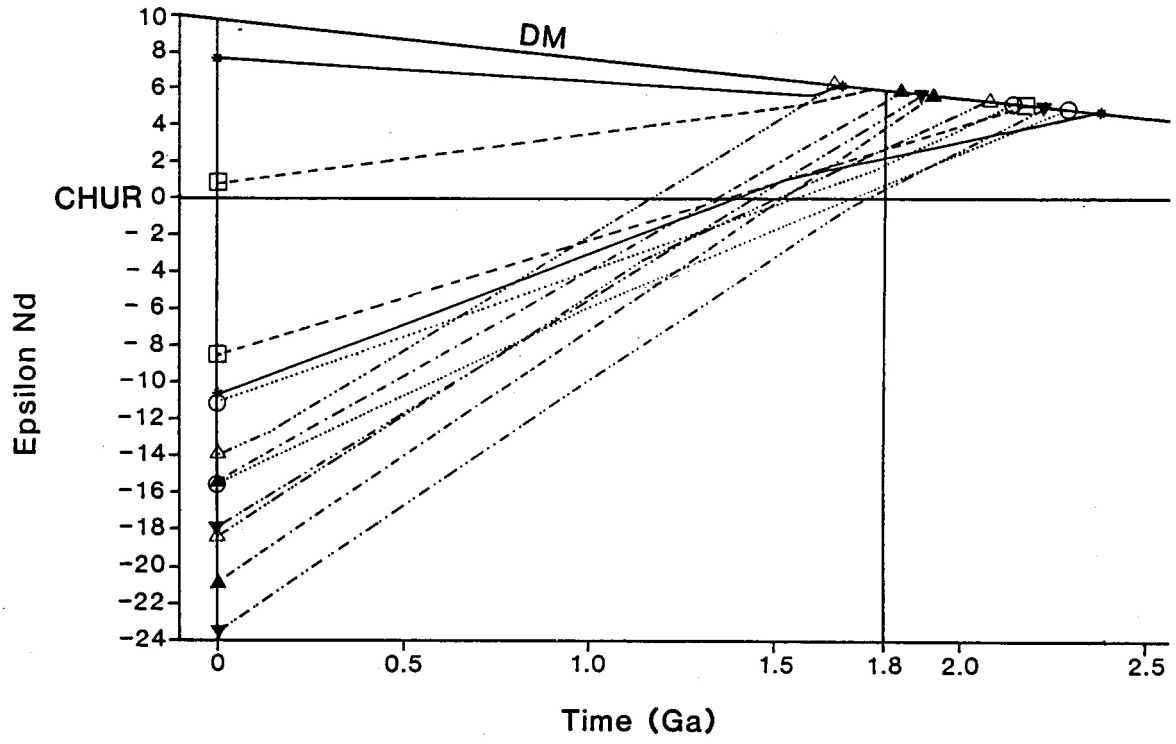

Figure 11.6: Model age versus Epsilon Nd diagram for all the analysed specimens from the Rehoboth Basement Inlier (same symbols as in Figure 11.2)

line of the 20 data sets, yields a surprisingly low age of 1655 ± 76 Ma with a correlation coefficient R of 0.999 and an intercept I at $^{143}Nd/^{144}Nd = 0.51046 \pm 0.00005$. The scattering data of the Piksteel pluton also do not fit on a well-correlated regression line (Fig. 11.5F) and it does not seem to be possible to fit a reasonable small scale reference line through any combination of the Piksteel data points.

11.3 RB-SR, U-PB AND K-AR ISOTOPE SYSTEMATICS

The results of the Rb-Sr, U-Pb and K-Ar analyses of all the samples dealt with in this text have been discussed in great detail in the previous chapters. Tabular compilations of the results which are relevant for the interpretation of the Sm-Nd data, and for the discussion of the evolution models of the Rehoboth Basement Inlier, are reproduced in Table 26 and Table 27 (see Appendix). The investigated U-Pb, Rb-Sr and K-Ar systems all showed disturbances such as the loss of argon from the analysed biotites, the loss of lead from the analysed zircons and partial to complete resetting of the whole-rock Rb-Sr systems by various post-formation alteration processes. The ages in Table 26 determined by these methods could thus not provide more than minimum ages of limited significance for the analysed formations. In Chapter 8 it was nonetheless possible to show that the Piksteel Intrusive Suite has a minimum age of approximately 1800 Ma, which thus also gives a minimum age for the formation of the Rehoboth Sequence and its underlying formations. A major phase of alteration must have affected the Rb-Sr systems of the Piksteel Intrusive Suite in connection with the intrusion of the Gamsberg Granite Suite with a known maximum age range of 1079 Ma - 1222 Ma (Reid *et al.*, 1988; Seifert, 1986 and Burger *et al.*, 1973-74), as is indicated by the Rb-Sr isochrons obtained for the members of the Piksteel Intrusive Suite, which yielded ages ranging between 1057 Ma and 1489 Ma (Chapter 8). In spite of the strong disturbance of the Rb-Sr systems of the area, Reid *et al.* (1988) give a doubtful estimate of approximately 2 Ga for the maximum age of formation of the crustal protoliths in the area, based on their Rb-Sr data. A later phase of alteration related to the Damara orogeny was the reason for partial to complete rejuvenation of the K-Ar systems of the formations of the Rehoboth Basement Inlier, depending on their location in relation to the Damara Orogen (see previous chapters).

11.4 DISCUSSION

11.4.1 The Sm-Nd ages

The obtained isochron age of 2225 Ma ± 88 Ma for a reference line calculated through 20 out of 35 data sets from different formations could represent a reasonable age for the formation of this part of the continental crust of southern Africa, which today forms the northwestern rim of the Kalahari Craton. This is supported by the bootstrap analysis of the same data sets which yields a similar age of 2175 Ma + 330 Ma - 140 Ma. The reference lines which have been calculated through the data sets representing one single forma-

tion are in conflict with the overall isochron of 20 samples. The reference ages of the Neuhof and Elim Formations are, at 1821 Ma ± 305 Ma and 2006 Ma ± 237 Ma respectively, too low in comparison with the overall reference age, while the reference age of the basic dykes at 2574 Ma ± 504 Ma is higher than the age of the overall isochron. Nonetheless, it is worthy of note that all these individual reference ages are within the uncertainty range of the overall reference line, and the suggested formation age of approximately 2.2 Ga of this part of the Kalahari Craton thus still seems tenable.

The reference age of 2301 Ma ± 289 Ma calculated for the five samples of the Borodino pluton confirms the aforementioned formation age of the continental crust of the Rehoboth area, but the fact that these samples all plot above the "overall reference line" discussed above indicates a more radiogenic Nd composition than was observed for the samples plotting on the" overall reference line". This, in turn, indicates the possibility that not all the analysed formations derive from the same magma source, or that some of the analysed Sm-Nd systems suffered from alteration processes, occurring after separation from a mantle source. The existence of alternative magma sources in the upper mantle or later alteration processes is supported by the different initial $^{143}Nd/^{144}Nd$ ratios of the overall and the Borodino reference lines of 0.510080 ± 0.000084 and 0.51025 ± 0.00018, respectively. If, however, the analysed Borodino specimens had been affected by alteration processes severe enough to change the REE-patterns of this pluton (during the intrusion of magmas of the Gamsberg Granite Suite, for example), it follows that the Sm-Nd age pattern of this pluton would also have been altered. As this is not the case for the isochron age of the Borodino pluton, nor for the individual model ages (see below) which plot in a range between 1.8 Ga and 2.5 Ga, it may be concluded that any occurrence of alteration processes, must have taken place in the age range between 1.8 Ga and 2.5 Ga. As the $T_{(DM)}$ model ages of the Borodino samples range between 1.85 Ga and 1.93 Ga (see below) it may be concluded that the present situation of the Nd composition of the Borodino samples, being more radiogenic than the samples plotting on the "overall reference line" mentioned above, is due to primary magmatic properties (i.e. different magma sources) rather than to hydrothermal fluid reaction processes.

The remaining 10 samples plot above the "overall reference line" of Figure 11.2 leading to more problems. With the exception of KAW3026, KAW3027 and KAW3163 which plot on a reference line of low 1655 ± 76 Ma, which is in conflict with the U-Pb data obtained for KAW3026 of 1786 Ma ± 11 Ma (see Chapter 8), no linear array is evident within these 10 data sets. There may be several reasons for this. For instance, on the basis of thin section and geochemical investigations of the analysed specimens, the possibility cannot be ruled out that due to incorrect mapping of the area not all the analysed specimens derive from the same pluton. However, if all the samples come from the same pluton, it would have to be assumed that the Sm-Nd systems of these samples have been disturbed by syn- or post-magmatic processes in a such a way that their crustal formation is no longer recorded.

11.4.2 The model ages

Under the assumption that crustal lithologies either derive from an unfractionated chondritic uniform reservoir (CHUR) or from a light REE-depleted mantle (DM) by fractional crystallisation, Nd model ages have been calculated in two different ways (see e.g. De Paolo, 1988). These model ages indicate the intercept of the $^{143}Nd/^{144}Nd$ ratio of the analysed sample with the $^{143}Nd/^{144}Nd$ evolution curve of CHUR and DM, respectively, depending on the Sm-Nd fractionation factor of the sample (see Appendix for calculation formulas). These model ages should indicate approximately the age of separation of the crustal protolith from its mantle source. This, however, is only valid if the Sm/Nd ratio of the analysed specimen has not been changed in the interim. Unfortunately this condition is not entirely fulfilled for all the analysed samples of the Rehoboth Basement Inlier, as can be deduced from the discussion of the Sm-Nd data of the Rehoboth granitoids and from the data obtained for the Rb-Sr systems of the same samples, which show severe signs of alteration (see previous chapters).

The results of both kinds of calculation, $T_{(CHUR)}$ and $T_{(DM)}$, are listed in Table 28 (see Appendix). As discussed in many recent papers (e.g. De Paolo, 1988; Smith *et al.*, 1989; Jacobsen, 1988), the upper mantle as source region of the crustal rocks does not have the composition of CHUR but, through the formation of continental lithosphere, has been depleted in various elements such as the light REEs. The $T_{(CHUR)}$ model ages calculated for the analysed specimens, ranging between 171 Ma and 1733 Ma, seem to confirm this assumption, as they are lower than the U-Pb minimum age of 1786 ± 11 Ma (see Chapter 10) which must be accepted for all the analysed formations with the exception of the basic dykes, which intruded after the formation of the Gamsberg Granite Suite (see Chapter 10). If the Sm-Nd systems have not been severely disturbed by post-genetic alteration processes, an unfeasible assumption for most of the analysed samples based on the considerations of the previous chapters and on REE patterns described for some Rehoboth granitoids (see Chapter 3), these results mean that all the analysed specimens derive from a depleted source region in the upper mantle. The calculation of $T_{(DM)}$ yields model ages ranging between 1663 and 2373 Ma. The fact that three granitoid samples and one amphibolitic sample fall below the U-Pb minimum age of 1786 Ma might indicate the occurrence of post-genetic alteration processes affecting the Sm-Nd systems of some of the analysed samples. The $T_{(DM)}$ model ages of the basic dykes, ranging between 1769 Ma and 2184 Ma, indicate that the material of these dykes separated from the mantle contemporaneously with the material of the Rehoboth Basement Inlier, long before their intrusion and crystallisation as basic dykes.

The relationships of the various model ages are best seen in Figure 11.6, in which the model ages of the samples have been plotted against their ε_{Nd} values at certain times during their evolution. The $\varepsilon_{Nd(0)}$ values of the granitoid samples are between -13.89 and -23.49, while those of the amphibolitic samples and the basic dykes cover a wide range between -15.49 and 7.67. At t=1800 the $\varepsilon_{Nd(1800)}$ value of the depleted

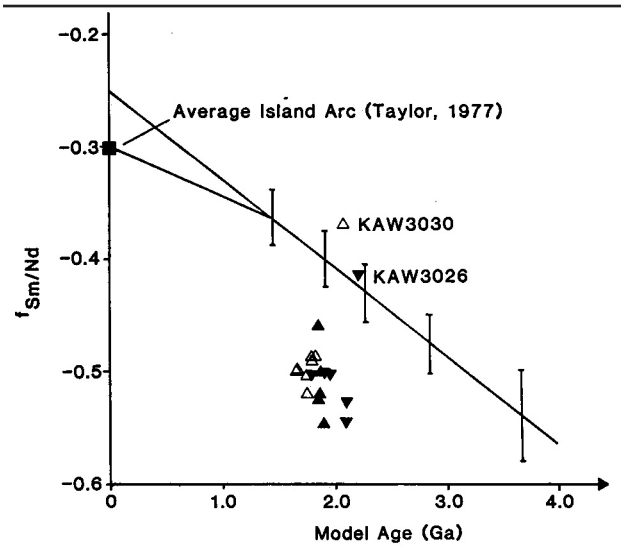

Figure 11.7: Plot of the age dependence of the Sm/Nd fractionation factor for crustal rocks as published by De Paolo (1988) in comparison with the model age versus $\varepsilon_{Sm/Nd}$ relationships observed in the Rehoboth Basement Inlier (same symbols as used in Figure 11.2)

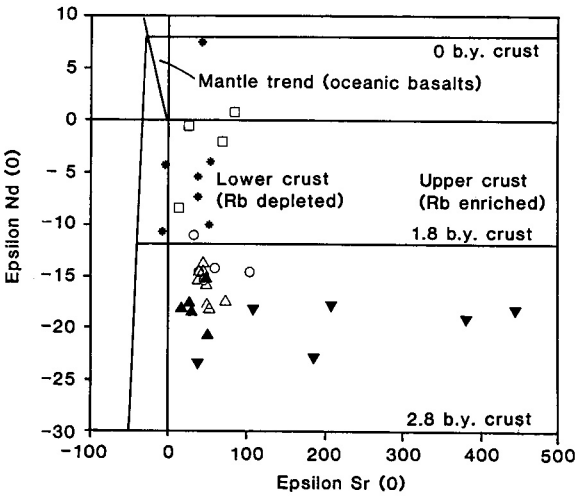

Figure 11.8: Epsilon $Sr_{(0)}$ versus Epsilon $Nd_{(0)}$ diagram for the analysed specimens of the Rehoboth Basement Inlier (see text for explanation; same symbols as in Figure 11.2)

mantle was approximately 6.2. Six of the 35 analysed samples have $\varepsilon_{Nd(1800)}$ values greater than 6.2, while the rest of the samples plot in a narrow range between 0.70 and 5.62. The bulk of the analysed samples thus indicates that their material probably separated from a depleted mantle source sometime between 1800 Ma and 2400 Ma, which is in agreement with the results obtained for various Sm-Nd reference lines calculated through the same data sets (see above). This implies that the rocks of the Rehoboth Basement Inlier for the most part represent barely evolved primitive crust which could not have undergone multiple cycles of reworking between its separation from DM and crystallisation in the analysed formations. Four of the six samples with $\varepsilon_{Nd(1800)} > 6.2$ are members of the Piksteel pluton, while the other two are members of the basic dykes and the Elim Formation, respectively. It is of interest that the four granitoids of the Piksteel pluton not only have excessively high $\varepsilon_{Nd(1800)}$ values but they also do not fit on any Sm-Nd isochron. It has thus to be assumed that these four granitoids of the Piksteel pluton, and possibly the Elim amphibolite and the basic dyke, which also show increased $Nd_{(1800)}$ values, either represent material which separated from a depleted mantle source region after the bulk of the analysed samples, or their Sm-Nd system did not preserve their initial properties due to syn- or post-genetic alteration processes such as wall rock assimilation, mantle crust interaction or metasomatic processes.

De Paolo (1988) argued that the slope of the evolution curves in the age versus ε_{Nd} diagrams for continental crust appears to be age-dependent. The preserved remnants of Archaean crust should, accordingly, have lower Sm/Nd ratios than crust of Proterozoic age and the crustal Sm/Nd ratio should increase systematically with decreasing age. The model ages of the analysed Rehoboth granitoids have been plotted versus their $\varepsilon_{Sm/Nd}$ values in Figure 11.7 in order to compare the Sm-Nd evolution of the Rehoboth granitoids with the results of De Paolo (1988). With the exception of KAW3026 and KAW3030, the Rehoboth granitoids do not confirm De Paolo's assumption of increasing Sm/Nd ratios with decreasing age, but scatter far off the evolution line proposed by De Paolo (1988). Moreover, the slope of a hypothetical regression line calculated through the Rehoboth data would be much steeper than the slope of De Paolo's evolution curve. The conclusion which can be drawn from these observations is that the magmatic sources of the Rehoboth samples had different $\varepsilon_{Sm/Nd}$ values than the areas described by De Paolo (1988), which in turn would mean if t = approximately 2 Ga, the $\varepsilon_{Sm/Nd}$ value of derivates of crustal composition from the depleted mantle was variable on a global scale between different areas of the depleted upper mantle. This again would have to be explained by regional differences of the chemical properties of the depleted mantle respective to Sm and Nd which, in turn, would question the commonly used global linear evolution curve of the depleted mantle. The only other plausible explanation for the observed deviations of the $\varepsilon_{Sm/Nd}$ values from the trend of De Paolo (1988), is that the $\varepsilon_{Sm/Nd}$ values of the analysed Rehoboth granitoids were changed from their original depleted mantle value by processes such as wallrock interaction and fractional crystallisation, shortly after the material separated from its mantle source.

11.4.3 ε_{Nd} - ε_{Sr} studies

In search of traces of the early history of the Rehoboth Basement Inlier the commonly used ε_{Nd} - ε_{Sr} analyses have been affected despite the different formation ages of the analysed formations, and expected post-formation alteration of the Sr-systems of the analysed samples (see above). The ε_{Nd} and ε_{Sr} values calculated for t = 0 and t = 1800 Ma and the assumed minimum formation age of the analysed formations according to Chapter 11.3 (except for the basic dykes), are listed in Table 28 (see Appendix). In Figure 11.8 the $\varepsilon_{Sr(0)}$ values of the analysed samples have been plotted versus their $\varepsilon_{Nd(0)}$ values. All the granitoid samples fall in the area de-

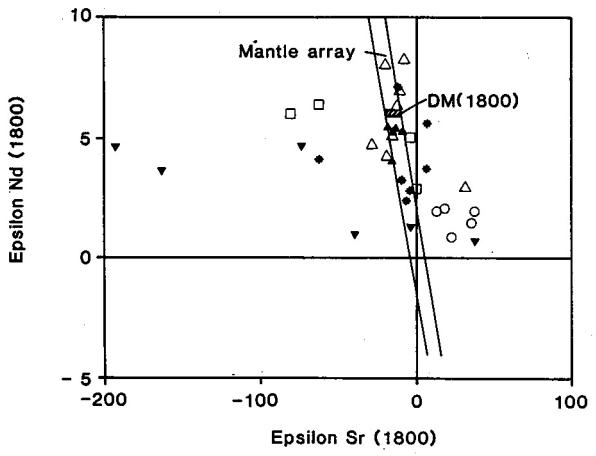

Figure 11.9: Epsilon $Sr_{(1800)}$ versus Epsilon $Nd_{(1800)}$ diagram for the analysed specimens of the Rehoboth Basement Inlier (see text for explanation; same symbols as in Figure11.2)

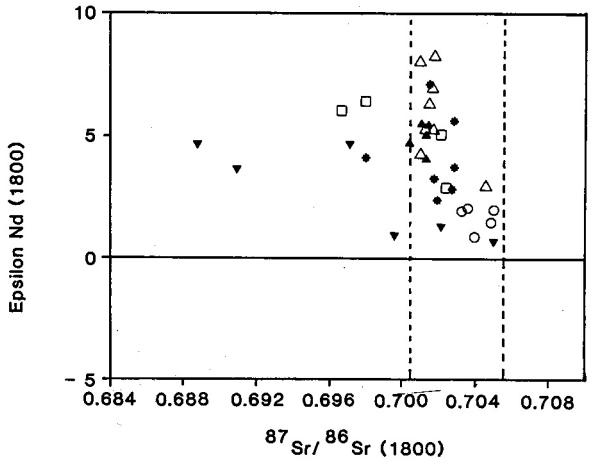

Figure 11.10: $^{87}Sr/^{86}Sr_{(1800)}$ versus Epsilon $Nd_{(1800)}$ plot for the analysed specimens of the Rehoboth Basement Inlier. The dashed lines represent the possible range of $^{87}Sr/^{86}Sr$ ratios in the upper mantle at t = 1800 Ma according to Faure (1986). (See text for explanation; same symbols as in Figure 11.2)

noted by De Paolo (1988), where continental crust of an age between 1.8 Ga and 2.8 Ga would be expected to plot. With the exception of KAW3024, KAW3025, KAW3027 and KAW3028 from the Opetjie pluton, which plot in the area typical for Rb-rich upper crustal rocks, all the analysed granitoids plot in the area for Rb-depleted lower crust. Due to their higher $\varepsilon_{Sm/Nd}$ the analysed basic rocks plot in the area of 0-Ga- to 1.8-Ga-old crust in the prolongation of the oceanic basalt trend. The reason for plotting the analyses of the basic rocks into this diagram together with the data obtained for crustal rocks is to show that the degree of Rb-Sr fractionation of both rock types must have been similar. This confirms the assumption of the previous chapter that most of the analysed specimens from the Rehoboth Basement Inlier represent primitive crust deriving directly from a depleted mantle source.

In Figure 11.9 the $\varepsilon_{Sr(1800)}$ values of all the analysed specimens have been plotted versus their $\varepsilon_{Nd(1800)}$ values. The hypothetical age of 1.8 Ga was chosen because it at least represents a minimum formation age for the analysed specimens (except for the basic dykes) according to Chapter 10.3. The analysis of this diagram shows that all the analysed specimens have $\varepsilon_{Nd(1800)}$ values in the range observed for the mantle (De Paolo and Johnson, 1979), but that six of the samples have $\varepsilon_{Nd(1800)}$ higher than 6.2, the ε_{Nd} value of DM at t = 1800 Ma(see Chapter 10.4.2 for discussion). The majority of the $\varepsilon_{Sr(1800)}$ values plot closely in and around the mantle array once more indicating that these samples might represent primitive crust derived directly from a source in the upper mantle. The samples deviating towards the right of the mantle array in Figure 11.9 (KAW3008, KAW3011, KAW3026, KAW3030, KAW3050-KAW3054), i.e. towards $\varepsilon_{Sr(1800)}$ values between 5 and 40, indicate that these samples either have a higher crystal¬lisation age than 1800 Ma or their Sr isotopic system was disturbed by the admixture of Sr with higher $^{87}Sr/^{86}Sr$ ratios. The $\varepsilon_{Sr(1800)}$ values of five granitoid samples from the Opetjie and Piksteel plutons (KAW3024, KAW3025, KAW3027, KAW3028, KAW3174), one amphibolite of the Elim Formation (KAW3005) and two basic dykes (KAW3161 and KAW3162) are below -20 and thus clearly deviate from the mantle array. This can be explained by considering that either the crystallisation age of these samples is younger than 1800 Ma, which is true for the basic dykes, or their Sr system was disturbed by the admixture of Sr with extremely low $^{87}Sr/^{86}Sr$ ratios. The former explanation for the observed deviation towards low $\varepsilon_{Sr(1800)}$ values of some samples seems, with the exception of the basic dykes, quite unlikely as is discussed above. It can thus be assumed that these samples suffered from the admixture of Sr of a primitive composition, which means that the Rb-Sr ages obtained for these formations do not represent the formation age of these Rb-Sr systems. Furthermore, the Sm-Nd systems of all the analysed basic dykes still have preserved their original properties (indicating their T(DM) age), while the Sr systems of at least two of them must have been disturbed during the course of their evolution.

Some of the questions arising with the above discussion are clarified by plotting the $^{87}Sr/^{86}Sr_{(1800)}$ ratios versus the

$\varepsilon_{Nd(1800)}$ values of the samples (Fig. 11.10). Assuming that the Sr composition of most of the samples was not severely altered, (unlikely for most of the samples according to Chapter 10.3), Figure 1 1.10 shows that at t =1800 the bulk of the samples had $^{87}Sr/^{86}Sr$ values ranging between 0.700 and 0.705. These values are, according to Faure (1986), within the range of possible $^{87}Sr/^{86}Sr$ ratios calculated for the upper mantle at t = 1800 (see dashed lines), and thus would indicate a primitive source in the upper mantle for the analysed specimens. The maximum ratio of 0.705 also restricts to an absolute minimum the post-crystallisation admixture of Sr with high $^{87}Sr/^{86}Sr$ ratios to some of the samples by alteration processes discussed above. Conversely this diagram shows that those samples which had partly primordial $^{87}Sr/^{86}Sr_{(1800)}$ ratios 0.700 in addition to $\varepsilon_{Sr(1800)}$ values below -20, cannot represent the product of magmatic processes occurring 1800 Ma ago. The Sr system of these samples must either have been disturbed by post-formation admixture of Sr with relatively low $^{87}Sr/^{86}Sr$ ratios of around 0.700 to 0.704, which in a calculation of $^{87}Sr/^{86}Sr_{(1800)}$ would result in primordial $^{87}Sr/^{86}Sr_{(1800)}$ values, or the samples would have to be significantly younger than 1800 Ma, a possibility which has already been ruled out for all the samples save the basic dykes, which are known to have intruded at t = 821 Ma.

11.4.4 Regional interpretation of the obtained results

The obtained isochron and model ages of the Rehoboth Basement Inlier of 1.8 - 2.5 Ga are all below the ages obtained for the formation of the Archaean nucleii of southern Africa, indicating that the crust of the Rehoboth Basement Inlier is of post-Archaean origin, the obtained ages are significantly older than the Namaqua-Natal belt to the south and west of the Archaean craton area of South Africa and Zimbabwe, but their ages plot well within the range expected for rocks formed during the Eburnian orogeny. This indicates that after the formation of the Archaean nucleii, crustal accretion continued in a belt between the two nucleii of today's Kalahari craton into the areas of the Irumide Belt of Drysdall *et al.* (1972) and the Limpopo Belt of Clifford *et al.* (1970), whose Eburnian event also includes the Rehoboth Basement Inlier. Only much after this major episode did crustal accretion continue in the area of the Namaqualand-Natal belt. McDermott (1986) and Hawkesworth *et al.* (1983) obtained $T_{(DM)}$ model ages for various granites of the Damara Orogen ranging between 1.1 Ga and 2.9 Ga, and $T_{(CHUR)}$ model ages of 1.0 Ga to 2.1 Ga for Damaran metasediments. This wide range of ages indicates that the Damaran belt is composed of new crustal material and of remobilised pre-existing crust which probably originally formed contemporaneously with the crust of the Rehoboth Basement Inlier. The four $T_{(DM)}$ model ages 2.5 Ga: obtained by McDermott (1986) for some granitoids and one orthogneiss of the Damara Orogen, indicate, however, that the Damara orogeny, to some extent possibly also reworked crustal material which is significantly older than the $T_{(DM)}$ model ages obtained for the Rehoboth Basement Inlier. This would mean that in the central area of Namibia, Archaean cratonic nucleii might have existed prior to the formation of to day's Rehoboth crust.

11.5 CONCLUSIONS

The present study of the Sm-Nd isotopic systems of the Rehoboth Basement Inlier under consideration of Rb-Sr and U-Pb data of the same area elucidates parts of the early history of the Rehoboth Basement Inlier which could not be unravelled until now by other radiometric dating techniques. The agreement between a reference line representing an age of 2225 Ma which can be fitted through 20 out of 35 data sets, and a "bootstrap" age of 2175 Ma of the same data sets, indicates that most of the Rehoboth crust formed about 2.2 Ga ago. This also accounts for the analysed basic dykes with a known intrusive age of 821 Ma which thus represent reworked crustal or subcrustal material of the Rehoboth Basement Inlier itself. Barring mapping errors, if the remaining 15 data sets deviate to positions above the calculated reference line, they either represent a source of material different from that of the isochron samples due to mantle in homogeneity or they indicate alteration processes (e.g. mixing processes due to crustal reworking) affecting the Sm- Nd systems after the separation of a common source in the upper mantle. Such irregularities of the Sm-Nd systems are also supported by the slightly higher intercept of a reference line calculated through the samples of the Borodino pluton (1: $^{143}Nd/^{144}Nd = 0.51025$) which all plot above the overall reference line compared to the intercept of the overall reference line (I: $^{143}Nd/^{144}Nd = 0.510080$).

The model $T_{(DM)}$ ages of 1663 Ma to 2373 Ma largely confirm the conclusions drawn from the isochron observations mentioned above, having shown that with few exceptions, the analysed sample material separated from a depleted mantle source between an assumed minimum age of 1786 Ma (as given by the U-Pb age determinations of Chapter 8) and 2373 Ma. The few younger model ages either indicate inhomogeneities in the mantle source or post-separation alteration processes of the Sm-Nd systems of some of the samples.

The ε_{Nd} - ε_{Sr} studies show that the Rehoboth Basement Inlier is composed of primitive crust which consolidated shortly after the separation of its material from a depleted mantle source, and that its Sr isotopic systems have been severely disturbed by post-consolidation alteration processes.

The regional comparison of the obtained results shows that the Rehoboth Basement Inlier forms part of a mobile belt which adjoined the pre-existing Transvaal and Zimbabwe nucleii of the Kalahari Craton at about 2.25 Ga, which would mean that the Rehoboth Basement Inlier represents a continuation of the Eburnian event of the Limpopo Belt. Furthermore, it can be said that the Damara Orogen, for the most part, consists of reworked material equivalent in age to the Rehoboth Basement Inlier.

12. SYNTHESIS

Thin-section analyses of the samples 'collected throughout the Rehoboth Basement Inlier have shown that most of them were affected by post-formation alteration processes. This may be deduced from the saussuritisation of plagioclase, the partial chloritisation of biotite, the formation of chlorite and epidote minerals from original amphiboles, the widespread strong fracturing and partial mylonitisation of many rocks, and the subsequent formation of veinlets consisting to a large degree of quartz, calcite and epidote minerals. Great care had to be taken in interpreting the obtained results of the geochemical and isotopic analyses due to the occurrence of alteration phenomena.

12.1 GEOCHEMISTRY

12.1.1 Granitoids

Major and trace element whole-rock geochemistry has permitted classification of the analysed granitoids of the Weener and Piksteel Intrusive Suites, the Gamsberg Granite Suite, the Neuhof Formation and the Mooirivier Complex according to the classification scheme of De La Roche (1980) and Streckeisen (1981), in which a wide compositional range from alkaline granites through granites, diorites, quartz monzonites, tonalites and granodiorites to gabbros can be observed. This large scatter indicates a certain mobility of the alkalis during the widespread post-formation alteration of the granitoids as is best seen according to the analyses of the Neuhof granitoids, where two samples plot in the fields for syenites and' alkali syenites. According to the index of Shand (1927), the analysed granitoids can be classified as peraluminous intrusives. Generally the A/CNK values of the analysed granitoids range between 0.9 and 1.4 with most of the samples plotting between 1.0 and 1.2. The Weener granitoids show a strong tendency towards higher values, while many of the Gamsberg and Piksteel samples plot at the lower end of the observed range. As most of the data from the analysed plutons scatter around 1.1, which, according to Chappell and White (1974), separates S-type granites (> 1.1) from I-type granites « 1.1), it is not clear-cut whether granitic crust of the Rehoboth Basement Inlier has been generated from either S- or I-type magmatism. Nonetheless, it can be stated that the overall degree of alumina saturation is high, and thus would indicate upper crustal origins for most of the analysed plutons. All the analysed granitoids plot on a calc-alkaline trend on the AFM ternary diagram after Kuno (1968). As calc-alkaline magmas are predominantly produced in continental-collision and continental- and island-arc tectonic settings, as well as during post-orogenic magmatism, this indicates the formation of the Rehoboth granitoids during various stages of the development of tectonic settings along active plate margins. This is confirmed by the frequently dubious (according to the considerations of Wilcox, 1979) tectonic discriminant Nb+Y versus Rb diagrams of Pearce *et al.* (1984), where the majority of the analyses plot in the field for volcanic-arc granites and where only a few exceptions plot in the fields for syn-collision granites and within-plate granites. Most of the few data points plotting in the fields for within-plate granites are samples assigned to the Gamsberg Granite Suite, the youngest large-scale magmatic event in the Rehoboth Basement Inlier. Consequently, they might indicate a change of the plate tectonic style of the area during Gamsberg magmatism from a collisional to a more extensional tectonic regime.

Some doubts about an upper crustal and possible S-type origin of several of the analysed granitoids may arise with the study of the Rb-Sr and Sm-Nd isotope systematics of the Rehoboth granitoids by various authors (Reid *et al.*, 1988; Seifert, 1986; this study). The initial $^{87}Sr/^{86}Sr$ ratios of the Weener intrusives range between 0.700 and 0.705 (Seifert, 1986; Reid *et al.*, 1988), while those of the granitoids of the Mooirivier Complex and the Neuhof Formation are approximately 0.704. The intrusives of the Gamsberg Granite Suite and the Piksteel Intrusive Suite cover a wide range of initial $^{87}Sr/^{86}Sr$ ratios from 0.700 to 0.708 and 0.702 to 0.709, respectively (Seifert, 1986; Reid *et al.*, 1988; this study). These generally low to very low initial ratios are below the $^{87}Sr/^{86}Sr$ ratio of today's Uniform Reservoir of 0.7045 (De Paolo, 1988). They indicate that in spite of post-formation alteration and at least partial resetting of the Rb-Sr systems of many of the analysed plutons, most of the material forming the Rehoboth granitoids originally derives from a primitive source in the upper mantle or in the lower crust. If the analysed granitoids today do, in fact, represent S-type material deriving from upper crustal origins, it can be said that their source material consisted of material with primitive Sr composition (low $^{87}Sr/^{86}Sr$ ratios), low Rb-Sr ratios, and that no significant amount of material with $^{87}Sr/^{86}Sr$ and high Rb-Sr ratios was admixed to this source material during later processes of crustal reworking and alteration. This view is conditionally supported by the ε_{Sr} and ε_{Nd} characteristics of some granitoids of the Piksteel Intrusive Suite, which clearly confirm a Rb-depleted source in the upper mantle for these granitoids. The analyses of the Rare Earth Element (REE) composition of several Piksteel and Gamsberg granitoids have shown quite flat chondrite-normalised patterns in a range which is typical for granitoid rocks. The patterns decrease from chondrite-normalised La values of approximately 100, to chondrite-normalised Yb values of about 10. Several samples showed slightly concave-up REE patterns similar to those described for Namaqualand by McCarthy and Kable (1978).

12.1.2 Amphibolites

The analyses of amphibolites from the metavolcano-sedimentary Neuhof and Elim Formations and the Mooirivier Complex have shown that most of the specimens are of orthogenic origin and most of the samples reflect tholeiitic magmatism. No general plate tectonic environment could be assigned to the analysed amphibolites according to the classification schemes of Pearce *et al.* (1973), as they were

found to plot in all the fields assigned to various plate tectonic settings. It is not clear whether this variation indicates the occurrence of diverse plate tectonic settings in one single formation, or whether it represents the effects of post-formation alteration of the analysed specimens. The initial $^{87}Sr/^{86}Sr$ ratios of all the analysed sets of amphibolitic samples range between 0.702 and 0.706. These low values and the corresponding low Rb-Sr fractionation factors confirm the magmatic origin of the analysed samples, and also show that post-formation alteration of the Rb-Sr systems through metamorphism did not admix large amounts of highly radiogenic common Sr. The ε_{Sm} and ε_{Nd} studies of some amphibolites of the Elim and Neuhof Formations also suggest that these specimens derive from magmatic sources which probably lie in the depleted upper mantle.

12.1.3 Acid volcanics

The comparison of acid volcanic dykes crosscutting the Marienhof Formation, the Weener and Piksteel Intrusive Suites and the Gamsberg Granite Suite with those of the post-Gamsberg Nueckopf Formation, representing the largest mass of volcanic rocks occurring in the Rehoboth Basement Inlier, has shown that all the analysed acid volcanics are peraluminous high-K rhyolites. The analysed volcanics may be regarded as more evolved Gamsberg-, Piksteel- and Weener-type magmas according to their element distribution patterns and their position in the AFM ternary diagram. Except for one sample, all the A/CNK ratios are below 1.1, thus indicating I -type sources for the analysed volcanics. The observed initial $^{87}Sr/^{86}Sr$ ratio of 0.708 lies at the upper end of the range observed for magmas of the Gamsberg Granite Suite and for the Piksteel Intrusive Suite and thus might also corroborate a continuation of the trends observed for these suites. In the tectonic discriminant Nb+ Y versus Rb diagram of Pearce *et al*. (1984) most of the volcanics plot into those areas of the fields for volcanic-arc granites and for within-plate granites, which are also covered by the Gamsberg and Piksteel Intrusive Suites.

12.1.4 Basic dykes

The five analysed post-Gamsberg basic dykes crosscutting the Rehoboth Basement Inlier are all of basaltic tholeiitic origin. According to the classification of Pearce *et al*. (1973) they probably derive from a continental plate-tectonic environment. Their low initial $^{87}Sr/^{86}Sr$ ratios and their ε_{Nd} values suggest an origin in the lower crust or in the upper mantle where their melts were generated from much older source material (see below) due to post-Mokolian dilatational processes in the Rehoboth inlier.

12.1.5 Metasediments

The analyses of the partly garnetiferous biotite schists of the Mooirivier Complex have shown a slight enrichment of incompatible elements such as Rb, Ba, K, La, Ce, Nd and Zr, while compatible elements such as Al, Ca, Sc, Fe, Mg and Ni are slightly depleted. The initial $^{87}Sr/^{86}Sr$ ratios of a fan of isochrons calculated through the Rb-Sr results of the Mooirivier schists yielded crustal upper and lower limits of 0.711 and 0.707 respectively, while a small-scale isochron indicates the addition of Sr with an initial ratio exceeding 0.766.

The analysed mica schists and marbles of the Elim Formation were found by geochemical means to be typical representatives of their species. The initial $^{87}Sr/^{86}Sr$ ratios of two Elim marbles are 0.707 and 0.714 respectively, clearly indicating the admixture of highly radiogenic Sr to the analysed samples by metamorphic fluids, as according to Faure (1986), the composition of Sr in sea water before 1000 Ma ago never exceeded a value of 0.707.

12.2 AGE DETERMINATIONS

12.2.1 Sm-Nd dating

The analyses of 35 whole-rock samples of the Piksteel Intrusive Suite, the Elim and Neuhof Formations and basic dykes by the Sm-Nd method have provided a sound insight into the age of the crust of the Rehoboth Basement Inlier. The $T_{(DM)}$ model ages of all the samples range between 1.6 Ga and 2.4 Ga. A reference line fitted through 20 of the 35 data points yielded an age of 2.23 Ga, while reference lines calculated through the individual sets of samples from different localities yielded ages between 1655 Ma and 2574 Ma. The fact that only 20 out of 35 analysed specimens plot on a reference line, while the rest plot above this line, indicates the occurrence of either post -separation alteration processes (such as the reworking of crustal material), and/or primary inhomogeneities of the source regions in the upper mantle. The $T_{(DM)}$ model ages of the basic dykes which did not intrude before 850 Ma (see Rb-Sr data below) and thus are much younger than the minimum age of the other analysed specimens of approximately 1.8 Ga (see U-Pb data below), range between 1.77 Ga and 2.10 Ga, while a reference line calculated through their data points shows an age of approximately 2.6 Ga. Four out of eight samples from the Piksteel pluton of the Piksteel Intrusive Suite, an amphibolite of the Elim Formation and a basic dyke, have shown $T_{(DM)}$ model ages between 1.66 Ga and 1.79 Ga; in the case of the Piksteel and Elim samples, these $T_{(DM)}$ model ages are below the assumed minimum formation age of these formations of 1.8 Ga and thus indicate the occurrence post-formation (hydrothermal?) alteration processes disturbing some of the analysed Sm-Nd systems.

In spite of a diversity of alteration features it can be proposed that the Rehoboth crust formed during the early Proterozoic between 1.8 Ga and 2.6 Ga by the separation of material from a source in the depleted mantle and by subsequent reworking of this material with the possible addition of new source material. Therefore it must be assumed that the Rehoboth Basement Inlier is part of an accretionary belt coeval with the younger events of the Limpopo Province connecting the Archaean nucleii of the Kalahari craton of South Africa and Zimbabwe. The comparison of the results of this study with Sm-Nd data for the Damara Orogen of other workers (McDermott, 1986; Hawkesworth *et al*., 1983) strongly suggests that the Damara Orogen is primarily composed of crustal material derived from sources which formed contemporaneously with the Rehoboth Basement Inlier, but it also shows that crustal material

older than the material of the Rehoboth Basement Inlier possibly existed in the area of the Damara Orogen.

12.2.2 U-Pb dating

A total of 19 zircon fractions from II samples of the Piksteel, Borodino and Opetjie plutons of the Piksteel Intrusive Suite and two rhyolite dykes crosscutting the Marienhof Formation, were analysed by the U-Pb method during the course of this study. All the analysed zircon fractions are characterised by loss of between 10% and more than 60% radiogenic lead. This indicates the occurrence of post-formation processes capable of affecting the analysed zircons. The zircon fractions of the rhyolite dykes showed a discordant age of 110 Ma ± 7 Ma which probably represents the age of intrusion of the analysed dykes crosscutting the Marienhof Formation, and which thus indicates that these dykes probably belong to the Gamsberg-related magmatism of the Rehoboth area.

The Discordias which were calculated through the zircon data of the analysed plutons of the Piksteel Intrusive Suite yielded minimum ages of 1786 Ma ± 11 Ma for the Opetjie pluton, 1506 Ma ± 69 Ma for the Piksteel pluton and 1369 Ma ± 8 Ma for the Borodino pluton. The minimum age of the Opetjie pluton which intrudes the Elim Formation thus gives a good minimum age for the Elim and older Formations of the Rehoboth Basement Inlier. Moreover, such a minimum can also be assumed for the members of the Rehoboth Sequence, which is intruded by several members of the Piksteel Intrusive Suite. This Opetjie minimum age of approximately 1800 Ma also served as a lower limit for the considerations based on Sm-Nd dating (see above). The highly discordant minimum ages of the Piksteel and Borodino plutons of 1506 Ma and 1369 Ma respectively, in our view, do not represent more than minimum ages reflecting a severe loss of lead from the analysed zircons. Nonetheless these ages clearly separate the members of the Piksteel Intrusive Suite from the members of the Gamsberg Granite Suite which intruded the Rehoboth area between 1.0 Ga and 1.2 Ga ago.

12.2.3 Rb-Sr dating

Whole-rock Rb-Sr analyses were carried out on five biotite schists, four amphibolites and two granitoids of the Mooirivier Complex, six amphibolites and four granitoids of the Neuhof Formation, 21 amphibolites and two marbles of the Elim Formation, 21 granitoids of the Piksteel Intrusive Suite, seven Nueckopf volcanics, two acid rhyolitic dykes and five basic dykes.

It has been shown that the southern part of the Mooirivier Complex was intruded by late Mokolian granites with a "Gamsberg" age of 1100 Ma, which were able to reset and homogenise the whole-rock Rb-Sr systems of the analysed specimens. The Rb-Sr systems of the analysed specimens from the Spreetshoogte Pass area in the northern outcrop area of the Mooirivier Complex were affected even after the intrusion of late Mokolian Gamsberg-type granites by processes probably related to the Damara orogeny. This can be shown by a small-scale reference line yielding an age of 634 Ma.

The analyses of the Neuhof samples showed an age pattern which is similar to that of the Mooirivier Complex. The southern outcrops of the Neuhof Formation were also intruded by Mokolian Gamsberg-type granitoids which were capable of resetting the whole-rock Rb-Sr systems of the analysed amphibolites and granitoids to an age of about 1167 Ma ± 9 Ma. The samples from the northern outcrops of the Neuhof Formation yielded a scatter of data corresponding to reference lines of 1122 Ma and 2569 Ma. The younger reference line might be related to the intrusion of late Mokolian Gamsberg-type granitoids in the area, while the older line, whose age exceeds the Sm-Nd crustal age of the Neuhof Formation (see above), certainly represents alteration processes affecting the analysed Rb-Sr systems.

None of the analysed sets of amphibolitic and greenschist samples from various localities of the Elim Formation showed satisfying results in terms of Rb-Sr isochrons. The obtained ages for reference lines calculated through various sections of the analysed sets of samples range between 396 Ma and 1174 Ma and thus indicate the occurrence of post-Gamsberg, and at least partly, post-Damaran alteration processes affecting the Rb-Sr systems of the analysed specimens. The samples from the farm Naub plot well on a reference line corresponding to an age of 1788 Ma with an intercept at $^{87}Sr/^{86}Sr = 0.7022$ calculated through the data of the Naub diorite intruding the Elim Formation on the same farm (with a Rb-Sr age of 1725 Ma ± 74 Ma; Reid *et al.*, 1988), and through the samples collected during this study. This confirms to the minimum age of the Elim Formation at approximately 1780 Ma as deduced from the U-Pb analyses of the Opetjie pluton, and it also shows that homogenisation between rocks of the Elim Formation and the intruding Naub diorite has conceivably taken place.

Rb-Sr dating of several plutons of the Piksteel Intrusive Suite has shown reference ages of 1298 Ma and 1057 Ma for the Piksteel-type locality, 11M Ma and 878 Ma for the Opetjie pluton and 1489 Ma for the Borodino pluton. All these reference ages are well below the assumed minimum age for the members of the Piksteel Intrusive Suite of about 1.8 Ga, and thus clearly indicate the occurrence of rejuvenation processes affecting these granitoids. The obtained reference ages might be explained by the occurrence of Gamsberg-related alteration and homogenisation processes while those of the Opetjie pluton also indicate a later phase of alteration which could possibly be related to the Damara orogeny. The reference age of the Borodino pluton of 1489 Ma, higher than the U-Pb zircon age of 1369 Ma of the same samples, probably reflects a partial reset of the analysed Rb-Sr system of this pluton, in combination with a steepening of its isochron due to alteration processes taking place after 1369 Ma.

The analyses of seven Nueckopf rhyolites yielded a reference age of 948 Ma ± 25 Ma, which might very well represent the formation age of these volcanics which partly overlie members of the Gamsberg Granite Suite and thus could not be affected by Gamsberg-related alteration. A two-point isochron calculated through the data of two rhyolitic dykes crosscutting the Marienhof Formation yielded an age of

813 Ma with an intercept at a high $^{87}Sr/^{86}Sr$ ratio of 0.717. This age, which is in conflict with the U-Pb age of the samples of 1210 Ma and the comparatively high initial ratio, indicates that the Rb-Sr system of these two samples must have been disturbed after their formation.

The analyses of 5 basic dykes crosscutting the whole sequence of the Rehoboth Basement Inlier yielded a reference age of 821 Ma ± 33 Ma for four of the five specimens. This age probably represents late-to post-Mokolian dilatational tectonic processes related to the early rifting stages of the Damara system.

12.2.4 K-Ar dating

K-Ar age determinations were carried out on five biotite separates from samples of the Mooirivier Complex collected in the Spreetshoogte Pass area, two biotite separates and nine muscovite/sericite separates from various outcrops of the Elim Formation, one biotite and 11 white mica/phyllite concentrates and seven phyllite whole-rock aliquots from samples collected within outcrops of the Marienhof Formation, five white mica separates from the Billstein Formation, six biotite concentrates of members of the Piksteel Intrusive Suite and five whole-rock aliquots of basic dykes crosscutting the Rehoboth Basement Inlier.

The obtained results have shown that formation ages are no longer recorded by the analysed K-Ar systems and that some radiogenic argon was lost from most of the separates due, to alteration processes occurring after the closure of the K-Ar systems. Nonetheless, this method has proved to be very successful in analysing the younger history of the Rehoboth Basement Inlier.

The analyses of the Marienhof and Billstein samples, which were collected in the northern central part of the Rehoboth Basement Inlier and along the central section of the Areb shear zone, all yielded individual apparent ages between 490 Ma and 529 Ma, thus indicating that the K-Ar systems of biotites and white micas of the northern part of the Rehoboth Basement Inlier were reset by the Damara orogeny. The biotite separates of the Mooirivier samples, which were collected in the vicinity of the western branch of the Areb shear zone in the Spreetshoogte Pass area, yielded ages ranging between 404 Ma and 545 Ma, thus indicating Damaran as well as post-Damaran alteration processes affected the analysed biotites. Samples collected further towards the east yielded higher ages compared to those collected further west. This might indicate alteration processes influenced by the opening of the South Atlantic. The apparent individual ages of biotites and white micas of Elim samples collected on the farm Areb, in the central part of the Areb shear zone, yielded individual apparent ages between 315 Ma and 397 Ma, while individual ages between 728 Ma and 782 Ma were observed for white mica concentrates collected a few hundred metres away from the shear zone. This indicates that the Areb shear zone must have been active after the Damara orogeny until at least 315 Ma ago, and that these activities were restricted to the vicinity of the shear zone, as the ages of the white micas collected further away were not completely reset by the Damara orogeny. A decrease of the influence of the Damara orogeny could also be shown with the analyses of biotite separates from Piksteel granitoids which yielded ages between 647 Ma and 955 Ma, thus showing that post-Gamsberg rejuvenation processes must have occurred, probably in connection with the Damara orogeny, and at the same time indicating that the Damaran-related metamorphism did not reach the biotite K-Ar reset temperature of 300°C further south than 23°55'S. This in turn indicates that Damaran K-Ar ages of 478 Ma to 547 Ma, which are reported for the Namib Naukluf Nappe Complex to the south of the Rehoboth Basement Inlier by Ahrendt *et al.* (1977) must represent transported ages. The whole-rock K-Ar dating of the basic dykes did not show results which are consistent with the know ledge of the geology of the area, due to the occurrence of argon exchange processes such as loss and/or inheritance of argon of the analysed K-Ar systems.

12.3 DISCUSSION OF THE SIGNIFICANCE AND LIMITATIONS OF THE APPLIED ISOTOPIC DATING TECHNIQUES

With the exception of Seifert (1986), who was working in a limited area, all the earlier workers who carried out radiometric age determinations in the Rehoboth area, such as Clifford (1967), Burger *et al*. (1973, 1973-74, 1975-76 a and b, 1977-78 and 1980), Ahrendt *et al*. (1977) and Reid *et al*. (1988), used only one method of dating for their respective studies on relatively isolated areas within the Rehoboth Basement Inlier. This prevented the recognition of the continuity of the multitude of tectonic stages affecting the Rehoboth area, but nonetheless led to the construction of a general framework for the geological history of the Rehoboth Inlier. During this study, more age determinations were carried out than had previously been done. The application of various methods of dating and geochemical investigations on the same rock samples now enables us to provide a better insight into the history of the Rehoboth Basement Inlier.

The combination of Sm- Nd and REE studies on various granitoids and amphibolites has shown that the respective systems have been relatively unaffected by the observed hydrothermal and up to low-grade metamorphic alteration of the analysed specimens. The Sm-Nd method of dating was thus capable of providing the oldest ages obtained during this study. These first Sm- Nd ages of the Rehoboth area are considered to represent formation ages for the Rehoboth crust. The use of the U-Pb method of dating on zircon populations of members of the Piksteel Intrusive Suite has shown that the late-Mokolian intrusion of the Gamsberg Granite Suite and the Damara orogeny led to a severe loss of lead from the analysed zircons. As the zircon populations of rhyolitic dykes assigned to the Gamsberg Granite Suite and crosscutting the Marienhof Formation have preserved a "Gamsberg age" of 1210 Ma, it can be assumed that the alteration processes leading to the observed lead loss from the zircons of samples of the Piksteel Intrusive Suite occurred in relation to the intrusion of the Gamsberg Granite Suite, which also led to the occurrence of a major hydrothermal alteration phase in the Rehoboth Basement Inlier. The existence of such a

hydrothermal alteration phase in relation to the intrusion of the Gamsberg Granite Suite can be deduced from thin-section investigations showing, for example, saussuritisation of plagioclase and partial chloritisation of biotite of pre-Gamsberg lithologies throughout the Rehoboth Basement Inlier, as is also shown by the Rb-Sr results of this study. None of the pre-Gamsberg formations was datable by the Rb-Sr method. Almost all the attempts at dating pre-Gamsberg amphibolitic to granitoid lithologies by the Rb-Sr method resulted either in "Gamsberg ages" ranging between 1000 and 1250 Ma, or in ages ranging between the age of the Gamsberg intrusive cycle and the assumed age of the Piksteel Intrusive Suite. The fact that the Gamsberg plutons themselves and the younger basic dykes are datable by the Rb-Sr method (Seifert, 1986; Reid, 1988; this study) shows that the Rb-Sr whole-rock systems of the rocks of Rehoboth Basement Inlier were virtually unaffected in post-Gamsberg times, although further alteration processes must have affected the entire area as is shown by the K-Ar data of this study. The K-Ar method of dating was a good tool to investigate the influence of the Damara orogeny on the Rehoboth Basement Inlier as it showed a complete resetting of the K-Ar systems of biotite and white micas in the northern part of the inlier, while in the southern part of the inlier only a rejuvenation of the K-Ar systems was detectable, thus indicating a decreasing influence of the pan-African Damara orogeny towards the south. A rejuvenation of the K-Ar ages of biotites and white mica/sericite to values below 400 Ma could be observed along zones of major tectonic lineaments, thus indicating tectonic activity in the area after the end of the Damara orogeny. It can be concluded that the K-Ar systems of biotites and white micas were much more sensitive to the alteration processes occur-ring in the Rehoboth Basement Inlier compared to whole-rock Rb-Sr systems and to U-Pb zircon systems, which were affected by post-formation alteration processes in relation to the Gamsberg magmatism but which have not, in any of the investigated areas, been reset by the Damara orogeny. The whole-rock Sm-Nd systems of the analysed specimens therefore represent the only isotopic systems which remained virtually closed to the multitude of alteration processes occurring in the Rehoboth area.

12.4 SHORT SUMMARY OF THE GEOLOGICAL HISTORY OF THE REHOBOTH BASEMENT INLIER

(BASED ON THE RESULTS OF THIS STUDY)

A combination of the results of the Sm-Nd and U-Pb analyses has shown that the major part of the Rehoboth crust must have formed during the early Proterozoic between 2.6 and 1.8 Ga as an accretionary belt extending the Archaean nucleii of the Kalahari craton in a northwesterly direction, as an equivalent of the younger parts of the South African and Zimbabwean Limpopo Province. During the early stages of this crustal evolution, the freshly formed crust must also have been readily reworked by various stages of erosional, metamorphic and anatectic processes, in order to be present today as a metamorphosed volcano sedimentary sequence, including the lithologies from the Mooirivier Complex at its base to the Billstein Formation at its top. This theory of an early reworking of the originally formed crust is supported by the occurrence of granitic pebbles and boulders in various formations of the Rehoboth Sequence. The majority of the formations from the Mooirivier Complex to the Billstein Formation originally had similar lithological compositions, thus casting doubt on the present stratigraphic classification according to SACS (1980), which is primarily based on tectonic and metamorphic considerations. During the Eburnian orogeny, between about 2.0 Ga and 1.8 Ga, the Rehoboth area was intruded by the calc-alkaline members of the Weener and Piksteel Intrusive Suites, most likely generated in a collisional tectonic environment. At about 1.4 Ga, the Alberta Mafic Complex and related intrusives were emplaced in the northern parts of the Rehoboth Basement Inlier. This was followed, between 1.25 and 1.0 Ga, by the intrusion of the members of the Gamsberg Granite Suite and related rhyolitic dykes, whose related hydrothermal activities led to the strong alteration of most of the intruded rock sequence. At about 950 Ma the final stages of the Gamsberg magmatism led to the extrusion of the high potassium rhyolites of the Nueckopf Formation. About 130 Ma later, at approximately 820 Ma, the whole area of the Rehoboth Basement Inlier was then intruded by swarms of basic dykes in a diverging tectonic regime parallelling the direction of the Areb shear zone.

The compressional phase of the Damara orogeny to the north of the Rehoboth Basement Inlier led to metamorphic conditions (300°C) in the northern part of the inlier capable of resetting the K-Ar systems of biotites and white micas, while south of 23°55/S they were not strong enough to completely reset the K-Ar systems of biotites. The Rehoboth Basement Inlier must therefore have been overridden by nappes of the Damara Orogen as may be deduced from the Damaran ages of micas from the Namib Naukluft Nappe Complex. After the Damara orogeny the Rehoboth Inlier was affected by the break-up of Gondwana, resulting in the opening of the South Atlantic and the reactivation of the Areb shear zone, as evidenced by the partial rejuvenation of biotite and white mica separates from samples of the Mooirivier Complex and the Elim Formation collected along the Areb shear zone, which currently yield apparent ages of 315 Ma to 427 Ma.

REFERENCES

Ahrendt, H., Hunziker, J.C. and Weber, K. 1977. Age and degree of metamorphism and time of nappe emplacement along the southern margin of the Damara Orogen/Namibia (SW-Africa). *Geol. Rdsch.*, **67**, 719-742.

Almeida, F.F.M. de, Hasui, Y. and De Brito Neves, B.B. 1976. The upper Precambrian of South America. *Inst. Geosci. Univ. Sao Paulo Boletim*, **7**, 45-80.

Barton, E.S., Harmer, R.E. and Burger, A.J. 1981. Isotopic studies in the Namaqua-Natal mobile belt. *Abs. Geol.Soc. S. Afr. Geocongress, 1981*.

Barton, J.M., jr., and Ryan, B. 1977. A review of the geochronologic framework of the Limpopo Mobile Belt. *Bull. Geol. Surv. Botswana*, **12**, 183-200.

Barton, J.M., jr., Ryan, B. and Fripp, R.E.P. 1978. The relationship between Rb-Sr and U-Th-Pb whole-rock and zircon systems in the 3 790 m.y. old Sand River Gneisses, Limpopo Mobile Belt, Southern Africa. Short papers of the Fourth International Conference on Geochronology, Cosmochronology, Isotope Geology 1978. *U.S. Geol. Surv. Open-file Rep*., **78-701**, 27-28.

Behr, H.J., Ahrendt, H., Porada, H., Roehrs, J. and Weber, K. 1983. Upper Proterozoic Playa and Sabkha Deposits in the Damara Orogen, Namibia. *Spec. Publ. Geol. Soc. S. Afr.*, **11**, 1-20.

Blaine, J.L. 1977. Tectonic evolution of the Waldau Ridge structure and the Okahandja Lineament in part of the Central Damara Orogen, west of Okahandja, South West Africa. *Bull. Precambrian Res. Unit, Univ. Cape Town*, **21**, 99 pp.

Bor-ming Jahn, Gruau, G. and Glikson, A.Y. 1982. Komatiites of the Onverwacht Group, S. Africa: REE geochemistry, Sm-Nd age and mantle evolution. *Contrib. Mineral.Petrol.*, **80**, 25-40.

Bewitz, H.W. 1974. Montangeologische Erkundung und Genese der metamorphen, exhaiative-sedimentaeren Zn-Cu-Lagerstaette Kobos im Altkristallin des Nauchas Hochlandes,SW-Afrika. *Clausthaler geol.Arb*., **18**, 128 pp.

Buletti, M. 1985. *Petrographisch-Geochemische Untersuchungen im Luganer porphyrgebiet*. Unpubl. Ph.D. thesis, Univ. Berne, Switzerland.

Burger, A.J. and Coertze, F.J. 1973. Radiometric age measurements on rocks from Southern Africa to the end of 1971. *Bull. Geol. Surv. S. Afr.*, **58**, 46 pp.

Burger, A.J. and Coertze, F.J. 1973-74. Age determinations - April 1972 to March 1974. *Ann. Geol. Surv. S. Afr*., **10**, 135-141.

Burger, A.J. and Coertze, F.J. 1975-76a. Summary of age determinations carried out during the period April 1974 to March 1975. *Ann. Geol. Surv. S. Afr*., **11**, 317-321.

Burger, A.J. and Walraven, F. 1975-76b. Summary of age determinations carried out during the period April 1975 to March 1976. *Ann. Geol. Surv. S. Afr*., **11**, 323-329.

Burger, A.J. and Walraven F. 1977-78. Summary of age determinations carried out during the period April 1976 to March 1977 and also: Summary of age determinations carried out during the period April 1977 to March 1978. *Ann. Geol. Surv. S. Afr*., **12**, 199-218.

Burger, A.J. and Walraven, F. 1980. Summary of age determinations carried out during the period April 1978 to March 1979. *Ann. Geol. Surv. S. Afr*., **14/2**, 109-118.

Chappell, B.W. and White, A.J.R. 1974. Two contrasting granite types. *Pacific Geology*, **8**, 173-174.

Clifford, T.N. 1967. The Damaran episode in the upper Proterozoic-lower Paleozoic structural history of southern Africa. *Spec. Paper Geol. Soc. Am*., **92**, 100 pp.

Clifford, T.N. 1970. The structural framework of Africa. *In*: Clifford, T.N. and Gass, I.G., Ed. *African magmatism and tectonics*. Oliver & Boyd, Edinburgh, 461 pp.

Corner, B. 1983. An interpretation of the aeromagnetic data covering the western portion of the Damara Orogen in South West Africa/Namibia. *Geol. Soc. S. Afr Spec. Publn*, **11**, 339-354.

Cullers, R.L. and Graf, J.L. 1984. Rare earth elements in igneous rocks of the continental crust: intermediate and silicic rocks - ore petrogenesis. *In*: Henderson, P. Ed. *Rare Earth Element Geochemistry*. Elsevier, Amsterdam. 275-316.

Dalrymple, G.B. and Lanphere, M.A. 1969. *Potassium-Argon dating*. W.H. Freeman, San Francisco, 258 pp.

Deer, F.RS., Howie, F.G.S. and Zussman, M.A. 1962. *Rock forming minerals. Vol. 3. Sheet silicates*. Longman, Hongkong. 270 pp.

De Kock, G. in prep. Die geologie van ‘n gebied suidoos van Karibib, SWA. *Rep. Geol. Surv. S.W.Afr/Namibia*.

De Kock, W.P. 1934. The geology of the western Rehoboth. *Mem. Dep. Mines S.W.A.*, **1**, 149 pp.

De la Roche, Leterrier, J., Grandclaude, P. and Marchal, M. 1980. A classification of volcanic and plutonic rocks using R1-R2 diagram and major element analyses. Its relationships with current nomenclature. *Chem. Geol.*, **29**, 183-210.

De Paolo, D.J. 1988. *Neodymium Isotope Geochemistry. An Introduction*. Springer, Berlin, 187 pp.

De Paolo, D.J. and Johnson, R.W. 1979. Magma genesis in the New Britain island arc: constraints from Nd and Sr isotopes and trace element patterns. *Contrib. Mineral. Petrol*., **70**, 367-379.

De Paolo, D.J. and Wasserburg, G.J. 1976. Nd isotopic variations and petrogenetic models. *Geophys. Res. Lett.*, **3**, 5, 249-252.

De Waal, S.A. 1966. *The Alberta Complex, a metamorphosed layered intrusion, north of Nauchas, South West Africa, the surrounding granites and related folding in the younger Damara system*. Unpubl. PhD thesis Univ. Pretoria, 207 pp.

Diaconis, P. and Efron, B. 1983. Computer-intensive methods in statistics. *Sci. Am*., **248** (May issue): 96-108.

Drysdall, A.R., Johnson, R.L., Moore, T.A. and Thieme, J.G. 1972. Outline of the geology of Zambia. *Geologie en Mijnbouw*, **51**, 265-276.

El Bouseily, A.M. and El Sokkary, A.A. 1975. The relation between Rb, Ba and Sr in granitic rocks. *Chem. Geol.*, **16**, 207-219.

Ewart, A. 1979. A review of the mineralogy and chemistry of Tertiary-Recent dacitic, latitic, rhyolitic, and related sialic volcanic rocks. *In*: Barker, F., Ed. *Trondhjemites, Dacites, and Related Rocks*. Elsevier, Amsterdam, 13-121.

Faure, G. 1986. *Principles of Isotope Geology*. 2nd edition. Wiley, New York, 589 pp.

Flisch, M. 1982. Potassium Argon analysis. *In*: Odin, G.S. Ed. *Numerical Dating in Stratigraphy*, John Wiley, Chichester, 151-158.

Flisch, M. 1986. K-Ar Dating of Quaternary Samples. *In*: Hurford, A.J., Jaeger, E, and Ten Cate, J.A.M. Ed. *Dating Young Sediments*. CCOP Technical Secretariat, Bangkok, Thailand, 393 pp.

Froehlich, F. 1960. Ein Beitrag zur Geochemie des Chroms. *Geoch. Cosmoch. Acta*, **20**, 215-240.

Geological Map of South West Africa, 1963. 1:1 000 000. Govt. Printer, Pretoria.

Geological map of South West Africa/Namibia (1980 Edition), 1:1 000 000. Govt. Printer, Pretoria.

Green, R.W.E. 1983. Seismic refraction observations in the Damara Orogen and flanking craton and their bearing ondeated processes in the orogen. *Geol. Soc. S. Afr. Spec. Publn*, **11**, 355-367.

Guj, P. 1970. The Damara mobile belt in the south-western Kaokoveld, South West Africa. *Bull. Precambr. Res. Unit. Univ. Cape Town*, **18**, 168pp.

Gurich, G. 1891-92. Deutsch-Suedwestafrika. *Mitt. d. Geographischen Ges. zu Hamburg*.

Haelbich, I.W. 1970. *The geology of the western Windhoek and Rehoboth Districts: a stratigraphic-structural analysis of the Damara System*. Unpubl. D.Sc. thesis, Univ. Stellenbosch. 199 pp.

Hamilton, P.J., O'Nions, R.K. and Evensen, N.M. 1977. Sm-Nd dating of Archaean basic and ultrabasic volcanics. *Earth Planet. Sc. Lett.*, **36**, 263-268.

Hamilton, P.J., Evensen, N.M., O'Nions, R.K., Smith, H.S. and Erlank, A.J. 1979. Sm-Nd dating of Onverwacht Group Volcanics, southern Africa. *Nature*, **279**, 298-300.

Handley, J.F. 1965. General geological succession on the farm Klein Aub 350, and environs, Rehoboth District, South West Africa. *Trans. Geol. Soc. S. Afr*., **68**, 211-224.

Harper, C.T. 1970. Graphical solutions to the problem of radiogenic ^{40}Ar loss from metamorphic minerals. *Eclogae Geologicae Helveticae*, **63**, 119-140.

Hartmann, O., Hoffer, E. and Haack, U. 1983. Regional metamorphism in the Damara Orogen: Interaction of crustal motion and heat transfer. *Geol. Soc. S. Afr. Spec. Publn*, **11**, 233-241.

Hawkesworth, C.J., Marsh, J.S., Duncan, A.R., Erlank, A.J. and Norry, M.J. 1984. The role of continental lithosphere in the generation of the Karoo volcanic rocks: evidence from combined Nd- and Sr- isotope studies. *Geol. Soc. S. Afr. Spec. Publn*, **13**, 341-354.

Hawkesworth, C.J. and Marlow, A.G. 1983. Isotope evolution of the Damara belt. *Geol. Soc. S. Afr. Spec. Publn*, **11**, 397-407.

Henderson, P. 1984. General Geochemical Properties and Abundances of Rare Earth Elements. *In*: Henderson, P. Ed. *Rare Earth Element Geochemistry*. Elsevier, Amsterdam, 1-32.

Hoffer, E. 1977. *Petrologische Untersuchungen zur Regionalmetamorphose Al-reicher Metapelite im suedlichen Damara Orogen (Süd West Afrika)*. Habilitationsschrift, Univ. Goettingen, 150 pp.

Hofmann, A.W. 1988. Chemical differentiation of the earth: the relationship between mantle, continental crust and oceanic crust. *Earth Planet. Sc. Lett.*, **90**, 297-314.

Hoffmann, K.H. 1983. Lithostratigraphy and facies of the Swakop Group of the southern Damara belt, Namibia. *Geol. Soc. S. Afr., Spec. Publn*, **11**, 43-63.

Hugo, P.J. and Schalk, K.E.L. 1971-72.The isotopic ages of certain granites and acid lavas in the Rehoboth and Maltahoehe Districts, South West Africa. *Ann. Geol. Surv. S. Afr.*, **9**, 103-105.

Jacobsen, S.B. 1988. Isotopic and chemical constraints on mantle-crust evolution. *Geoch. Cosmoch. Acta*, **52**, 1341-1350.

Jaeger, E. 1979. The Rb-Sr method. *In*: Jaeger, E. and Hunziker, J.C. Ed. *Lectures in isotope geology*. Springer, Berlin. 13-25.

Jochum, K.P., Hofmann, A.W., Seufert, M. and White, W.M. 1988. *The mid-ocean ridge basalts*. Max Planck Institute, Mainz. Manuscript in preparation.

Kalsbeek, F. and Hansen, M. 1989. Statistical analyses of Rb-Sr isotope data by the "bootstrap" method. *Chem. Geol. (Isotope Geoscience Section)*, **73**, 289-297.

Kasch, K.W. 1979. A continental collision model for the tectonothermal evolution of the (southern) Damara belt. *Precambrian Res. Unit Univ. Cape Town Ann. Rept*., **16**, 101-107.

Kasch, K.W. 1983. Regional P-T variations in the Damara Orogen with particular reference to early high-pressure metamorphism along the southern margin. *Spec. Publ. Geol. Soc. S. Afr.*, **11**, 43-63.

Kasch, K.W. 1983a. Tectonothermal evolution of the southern Damara Orogen. *Geol. Soc. S. Afr. Spec. Publn*, **11**, 255-265.

Kasch, K.W. 1983b. Continental Collision, Suture Progradation and Thermal Relaxation: A Plate Tectonic Model for the Damara Orogen in central Namibia. *Spec. Publ. Geol. Soc. S. Afr.*, **11**, 423-429.

Kirsten, T. 1966. Determination of radiogenic Argon. *In*: Schaeffer, O.A, and Zaehringer, J. Ed. *Potassium Argon Dating*. Springer, Heidelberg, 7-39.

Klein, J .A. 1980. *Geological report on area 2115A*. Unpubl. geol. Surv. S. W. Afr./Namibia.

Kroener, A. 1975. Geochronology. *13th A. Rep. Precambrian Res. Unit*. Univ. Cape Town, 139-143.

Krogh, T. 1973. A low-contamination method for hydrothermal decomposition of zircon and extraction of U and Pb for isotopic age determinations. *Geochim. Cosmochim. Acta*, **37**, 485-494.

Kukley, L.N. 1975. Origin of amphibolites of the Precambrian Ol'khonsk series (northwestern Barykal region). *Trans.from Geokhimiya*, **1**, 26-35.

Kuno, H. 1968. Differentiation of basaltic magma. *In*: Hess, H.H., and Poldervaart, A. Ed. *Basalts*. Interscience Publ., N. York, 623-688.

Leake, B.E. 1964. The chemical distinction between ortho- and para-amphibolites. *J. Petr.*, **5**, 238-254.

Malling, S. 1978. Some aspects of the lithostratigraphy and tectonometamorphic evolution in the Nauchas-Rehoboth area, S.W.A. (Namibia). *14th and 15th A. Rep., Chamber of Mines Precambr. Res. Unit, Univ. Cape Town*, 183-193.

Malling, S. in prep. *Metamorphism. geochronology and other aspects of the crustal evolution at the southern margin of the Damara Orogenic Belt, South West Africa, Namibia*. Ph.D. thesis, Univ. Cape Town.

Manson, V. 1967. Geochemistry of basaltic rocks: major elements. *In*: Hess, H.H. and Poldervaart, A. Ed. *Basalts*, Vol. **1**, 215-270.

Martin, H. 1965. The Precambrian geology of South West Africa and Namaqualand. *Precambrain Res. Unit, Univ. Cape Town*, **15**, 153-165.

Martin, H. and Porada, H. 1977. The intracratonic branch of the Damara Orogen in South West Africa. II. Discussion of relationships with th Pan-African mobile belt system. *Precambrian Research*, **5**, 339-357.

Martin, H. 1983. alternative geodynamic models for the Damaran orogeny. A critical discussion. *In*: Martin, H. and Eder, F.W., Ed. *Intracontinental fold belts*. Springer Verlag Berlin.

Masuda, A., Nakamura, N. and Tanaka, T. 1973. Fine structures of mutually normalized rare earth patterns of chondrites. *Geochim. Cosmochim. Acta*, **37**, 239-248.

McCarthy, T.S. and Kable, E.J.D. 1978. On the behaviour of rare earth elements during partial melting of granitic rocks. *Chem. Geol*., **22**, 21-29.

McDermott, F. 1986. *Granite petrogenesis and crustal evolution studies in the Damaran pan-African orogenic belt, Namibia*. Unpubl. PhD thesis, Open University (UK), Department of Earth Sciences, 303 pp.

Miller, R. McG. 1973. *Geological map 2013 - Cape Cross*, scale 1:250 000. Geol. Surv. S.W.Afr./Namibia (unpubl.)

Miller, R. McG, Sawyer, E.W., Hill, R.S. and Engelbrecht, L.N.J. 1975. *Geological map of the Conception Bay - Meob Bay area - 2414*. Geol. Surv. S.W. Afr./Namibia (unpubl.).

Miller, R. McG. 1979. The Okahandja Lineament, a fundamental tectonic boundary in the Damara Orogen of South West Africa/Namibia. *Trans. Geol. Soc. S. Afr*., **82**, 349-361.

Miller, R. McG. 1980. Geology of a portion of central Damaraland, South West Africa/Namibia. *Mem. Geol. Surv. S. Afr., S. W. Afr. Ser.*, **6**, 78 pp.

Miller, R. McG. 1983. The Pan-African Damara Orogen of South West Africa/Namibia. *Geol. Soc. S. Afr. Spec. Puhln*, **11**, 431-515.

Miller, R. McG. 1983a. Tectonic implications of the contrasting geochemistry of Damaran mafic rocks, South West Africa/Namibia. *Geol. Soc. S. Afr. Spec. Puhln*, **11**, 115-138.

Miller, R. McG. 1983b. Economic implications of plate tectonic models of the Damara Orogen. *Spec. Puhl. Geol. Soc. S. Afr.*, **11**, 385-395.

Pearce, A.J. and Cann, J.R. 1973. Tectonic setting of basic volcanic rocks determined using trace element analyses. *Earth Planet. Sc. Lett*., **19**, 290-300.

Pearce, A.J., Harris, N.B.W. and Tindle, A.G. 1984. Trace element discrimination diagrams for the tectonic interpretation of igneous rocks. *J. Petrol*., **25**, 956-983.

Porada, H. 1979. The Damara-Ribeiro Orogen of the Pan-African-Brasiliano cycle in Namibia (South West Africa) and Brazil as interpreted in terms of continental collision. *Tectonophysics*, **57**, 237-265.

Porada, H. 1983. Geodynamic model for the geosynclinal development of the Damara orogen. *In*: Martin, H. and Eder, F.W., Ed. *Intracontinental fold belts.* Springer Verlag Berlin.

Porada, H. and Wittig, R. 1983. Turbidites in the Damara Orogen, South West Africa/Namibia. *Spec. Puhl. Geol. Soc. S. Afr.*, **11**, 21-36.

Reeves, C.V. 1978. Interpretation of the reconnaissance aeromagnetic survey of Botswana. *Rep. Geol. Surv. Botswana*, 199 pp.

Reid, D.L., Mailing, S. and Allsopp, H.L. 1988. Rb-Sr ages of granitoids in the Rehoboth-Nauchas area, South West Africa/ Namibia. *Communs Geol. Surv. S.W. Africa/ Namibia*, **4**, 19-27.

Reid, D.L., Welke, H.J., Erlank, A.J. and Moyes, A. 1987. The Orange River Group: a major Proterozoic calcalkaline volcanic belt in the western Namaqua Province, southern Africa. *In*: Geochemistry and Mineralization of Proterozoic Volcanic Suites. Pharaoh, T.C., Beckinsale, R.D. and Rickard, D. Ed. *Geol. Soc. Spec. Publ*., **33**, 327-346.

Rimann, E. 1915. *Geol. Untersuchungen des Bastardlandes in Deutsch-Süd-West-Afrika*. Dietr. Reimer, Berlin.

Rogers, N.W. and Hawksworth, C.J. 1982. Proterozoic age and cumulate origin for granulite xenoliths, Lesotho. *Nature*, **299**, 409-413.

Sawyer, E.W. 1981. Damaran structural and metamorphic geology of an area south-east of Walvis Bay, Namibia. *Mem. Geol. Surv. S. W. Afr./Namibia*, **7**, 94pp.

Schalk, K.E.L. 1961. *The geology of the country around Dordabis*. Unpubl. Rep. Geol. Surv. S. Afr.

Schalk, K.E.L. 1967. *The geology of the country between Tsumis and Klein Aub. Expl. Sheets 2316D (Klein Aub) and 2317C (Tsumis)*. Unpubl. Rep. Geol. Surv. S. Afr.

Schalk, K.E.L. 1970. Some late Precambrian formations in central South West Africa. *Ann. Geol. Surv. S. Afr.*, **8/2**, 29-47.

Schalk, K.E.L. 1973. *Explanatory notes to sheet 2317A (Rehoboth)*: Geol. Surv. S. Afr. (unpubl.).

Schalk, K.E.L. 1975. *Expl. sheet 2316 (Rehohoth)*. Unpubl. Rep. Geol. Surv. S. Afr.

Schalk, K.E.L. and Germs, G. 1975. *Geological map of Area 2416 (Mariental)*. Explanatory Remarks. Geol. Survey S. Afr., Pretoria, 7 pp.

Schalk, K.E.L. and Haelbich, I.W. 1965. *The geology of the country around Windhoek. Rehohoth and Dordabis: Expl. sheets 22I7C (Windhoek). 22I7D (Dordabis). 2317A (Rehohoth) and 2317B (Klein Nauas)*. Unpubl. Rep. Geol. Surv. S. Afr.

Schulze-Hulbe, A. 1979. *The Areh shear zone*. Unpubl. Rep. Geol. Surv. Windhoek.

Schumacher. E. 1975. Herstellung von 99.9997 % ^{38}Ar fuer die ^{40}K/^{40}Ar Geochronologie. *Chimia*, **29**, 441-442.

Seifert, N.L. 1986. Geochronologie am Suedrand des Damara Orogens. Namibia: Hydrothermale Beeinflussungen von Isotopensystemen und Abkuehlalter in praekambrischen Basementgesteinen. *Schweiz. Min. Petro Mitt.*, **66**, 413-451.

Seifert, N.L. 1986a. *Geochronologische Ontersuchunf(en an Basement Gesteinen am Suedrand des Damara Orogens. S.W.A./Namibia*. Diss. Uni. Bern. unpubl. 126 pp.

Shand, S.J. 1927 and 1951. *Eruptive Rocks*. J. Wiley. N. York, 488 pp.

Smith, A.D. and Ludden, J.N. 1989. Nd isotopic evolution of the Precambrian mantle. *Earth Planet. Sc. Lett*., **93**, 14-22.

Soehnge, P.C. 1974. Sedimentary ore deposits: A review of research trends. *Trans. Geol. Soc. S. Afr*., **77**, 159-168.

South African Committee for Stratigraphy (SACS) 1980. *Stratigraphy of South Africa. Part I (comp. L.E. Kent). Lithostratig raphy of the Republic of South Africa, Bophuthatswana, Transkei and Venda*: Handb. Geol. Surv. S. Afr., **8**, 690 pp.

Stacey, J.S. and Kramers, J.D. 1975. Approximation of terrestrial lead isotope evolution by a two stage model. *Earth Planet. Sc. Lett*., **26**, 207-221.

Stapff, F.M. 1887. *Karte des unteren Khuisebtales*. Pet. Mitt., 33, 202. Also: *Das untere Khuisebtal und sein Strandgebiet.* Verh. d. Ges. f. Erdkunde, Berlin. I.

Steiger, R.H. and Jaeger, E. 1977. Subcommission on geochronology: convention on the use of decay constants in geo- and cosmochronologgy. *Earth Planet. Sc. Lett*., **36**, 358-362.

Streckeisen, A. 1981. Provisional remarks on chemical classifications. IUGS Subc. *Igneous Rocks. circ. no*. **34**, contr. no. 90.

Stromer von Reichenbach, E. 1896. *Die Geologie der deutschen Schutzgebiete in Afrika*. Muenchen und Leipzig.

Tankard, A.J., Jackson, M.P.A., Eriksson, K.A., Hobday, O.K., Hunter, D.R. and Minter, W.E.L. 1982. *Crustal Evolution of Southern Africa. 3.8 Billion Years of Earth History*. Springer, New York, 523 pp.

Taylor, S.R. 1977. Island arc models and the composition of the continental crust. *In*: Talwani, M. Pitman, W.C. Ed. *Island arcs. deep sea trenches and hack arc basins*. American Geophysical Union, Washington. 325-336.

Taylor, S.R. and McLennan, S.M. 1985. *The continental Crust: Its Composition and Evolution*. Blackwell. Oxford. 312 pp.

Taylor, S.R. and Gorton, M.P. 1977. Geochemical application of spark source mass spectrography - III. Element sensitivity, prccision and accuracy. *Geochim. Cosmochim. Acta*, **41**, 1375-1380.

Tera, F. and Wasserburg, G.J. 1972. U-Th-Pb asystematics in three Apollo 14 basalts and the problem of initial Pb in Lunar rocks. *Earth Planet. Sc. Lett.*, **14**, 281-304.

The geology of South West Africa Namibia, 1982. Compiled by the Geological Survey of Namibia.

Voit, F.W. and Stollreither, G. 1904. *Beitrag zur Geolofie der Kupererzgehiete in D.S.W. Afrika*. Abhandl. d. Kgl. Preuss. Geol. Landesanstalt. Berlin.

Walker, K.R., Joplin, G.A., Lovering, J.F. and Green, R. 1960. Metamorphic and metasomatic convergence of basic igneous rocks and lime-magnesia sediments of the Precambrian of north-western Queensland. *J. Geol. Soc. Australia*, **6**, 149-177.

Wasserburg, G.J., Jacobsen, S.B., De Paolo, D.J., McCulloch, M.T. and Wen, T. 1981. Precise determination of Sm-Nd ratios, Sm and Nd isotopic abundances in standard solutions. *Geoch. Cosmoch. Acta*, **45**, 2311-2323.

Watters, B.R. 1974. Stratigraphy, igneous petrology and evolution of the Sinclair Group in southern South West Africa: *Bull. Precambrian Res. Unit, Univ. Cape Town*, **16**, 235 pp.

Watters, B.R. 1978. Petrogenesis of the felsic rock units of the late-Precambrian Sinclair Group, South West Africa. *Geol. Rdsch.*, **67**, Heft 2, 743-773.

Weber, K., Ahrendt, H. and Hunziker, J.C 1983. Geodynamic aspects of structural and radiometric investigations on the northern and southern margins of the Damara Orogen, South West Africa/Namibia. *Geol. Soc. S. Afr. Spec. Publn*, **11**, 307-319.

Wedepohl, K.H. 1969. *Handbook of geochemistry*, Vol. **11/5**. Elements La(57) to U(92). Springer, Berlin.

Wetherill, G.W. 1956. Discordant Uranium Lead Ages I. T*rans. Am. Geophys*., **37**, 320 pp.

Wilcox, R.E. 1979. The liquid line of descent and variation diagrams. *In*: Yoder, H.S., jr., Ed. *The evolution of the igneous rocks. Fiftieth anniversary perspectives*. Princeton Press, Princeton, New Jersey, 205-232.

Winchester, J.A. 1976. Different Moinian amphibolite suites in northern Ross-shire. *Scott. J. Geol*., **12**, 87-204.

Winkler, H.G.F. 1979. *Petrogenesis of metamorphic rocks*. Springer, New York, 348 pp.

Yoder, H.S. and Tilley, C.E. 1962. Origin of basaltic magmas: an experimental study of natural and synthetic rock systems. *J. Petrol*., **3**, 342-532.

York, D. 1969. Least squares fitting of a straight line with correlated errors. *Earth Planet. Sc. Lett.*, **5**, 320-324.

APPENDIX

ANALYTICAL TECHNIQUES

1. SAMPLE PREPARATION

Crushing of all the samples was carried out in Windhoek by means of a jaw crusher. Grinding, sieving, splitting, separation by Wilfley table and separation by heavy liquids was done at the laboratory of the Geological Survey in Windhoek as well as at the University of Berne. Thin sections of all the whole-rock samples collected for age determinations were produced by technicians of the Geological Survey, while the thin sections of the geochemistry samples were produced by Mr Huber at the University of Berne. Final mineral separation using sieves, a dry shaking table, Atterberg cylinders, a buoyancy tube, a Frantz magnetic separator, various other magnetic separators and heavy liquids, was carried out in Berne. All the whole-rock aliquots were ground in Berne for at least 18 hours under alcohol in a Retsch agate mill after they were ground for several seconds in a tungsten carbide mill. Powder and glass pills of all the geochemistry samples were produced in Berne for the analyses of trace and major elements by X-ray fluorescence spectrometry from an aliquot of the samples which was ground for several minutes in a tungsten carbide mill. An aliquot of the geochemistry split of every whole-rock sample was also used for the characterisation of the modal composition of the specimens by X-ray diffractometry on various Philips X-ray diffractometers.

2. WHOLE-ROCK ANALYSES

Ten major and 21 trace elements in whole-rock aliquots were determined on Philips PW1400 and PW1450 X-ray fluorescence spectrometers at the University of Fribourg and at the Eidgenoessische Landwirtschaftliche Forschungsanstalt Liebefeld in Berne, Switzerland, respectively. Loss on ignition was determined by heating of an aliquot of each sample for two hours at 1150°C.

An estimate of the analytical error (which depends on the element species) on the X-ray fluorescence data is as follows: 50 ± 0.5 wt%, 10 ± 0.2 wt%, 1 ± 0.05 wt%, 1000 ppm ± 5 %, 100 ppm ± 20% and 10 ppm ± 50%.

Detection limits in ppm for the analysed trace elements are: Nb 11, Zr 23, Y 5, Sr 16, Rb 14, Th 13, Pb 16, Ga 5, Zn 18, Cu 9, Ni 12, Co 3, Cr 26, V 26, Ce 46, Nd 26, Ba 40, La 44, Sc 7, U 31, S 216. (*Editor:* High detection limits attributed to statistical methods of Reusser, 1987).

For the analysis of the Rare Earth Element (La, Ce, Nd, Sm, Eu, Tb, Yb and Ta) and Hf concentrations of various selected samples a pulverised aliquot of each sample was irradiated with thermal neutrons in the SAPHIR research reactor of the Paul Scherrer Institute in Wuerenlingen, Switzerland, for 5 to 15 hours. The REE concentrations were then subsequently determined by the measurement of the gamma-ray emission of the activated elements in question by the use of Ge (Li) semiconductor diodes by Dr U. Kraehenbuehl of the Laboratory for Radiochemistry of the Institute for Anorganic, Analytic and Physicalic Chemistry of the University of Berne, Switzerland.

2.1 K-AR METHOD

An aliquot of each sample was dissolved in a mixture of hydrofluoric and perchloric acid before it was diluted in 0.1 n hydrochloric acid for the determination of its potassium content, subsequently determined twice on an Ingold flame-photometer with a reproducibility of ± 1%. In the case of the whole-rock analyses of five basic dykes (see Chapter 8), the K contents were determined on an "Ion Instruments" solid source thermanisation mass spectrometer by the isotope dilution method (according to Jaeger, 1979) using a ^{40}K spike. The argon of all the K-Ar samples was extracted and purified from another (undissolved) aliquot of each sample in a Pyrex line constructed by M. Flisch (1982, 1986) before it was analysed by the isotope dilution method according to Kirsten (1966) and Dalrymple and Lanphere (1969) on a VG MM1200 vacuum mass spectrometer operated in static mode. Highly enriched ^{38}Ar (Schumacher, 1975) served as spike for the calibration of the measurements. Mass discrimination, air correction and blank correction were calculated on a PDP11 system programmed by R. Siegenthaler. The following constants were used for the calculation of the K-Ar results:

Potassium: $\lambda^{40}K = 5.543 * 10^{-10}a^{-1}$ (total ^{40}K decay constant)
$\lambda^{40}K^{e} = 0.581 * 10^{-10}a^{-1}$ ($^{40}K \rightarrow {}^{40}Ca$ decay constant)
(Steiger and Jaeger, 1977)

Isotopic ratios: $^{39}K/^{41}K = 13.8567$
$^{40}K/^{41}K = 0.001734$

Argon: $^{40}Ar/^{36}Ar_{atmosphere} = 295.5$
$^{38}Ar/^{36}Ar_{atmosphere} = 0.1869$
(Steiger and Jaeger, 1977)

2.2 RB-SR METHOD

The analyses of Rb and Sr followed the method of Jaeger (1979). Aliquots of about 0.4 grams of all the whole-rock samples were dissolved in a mixture of hydrofluoric and perchloric acid before they were diluted in 2.5 n hydrochloric acid. Highly pure ^{84}Sr and ^{87}Rb spike was then added to a portion of these dissolved whole-rock aliquots. Sr was subsequently separated from the other elements by the use of cation exchange columns. The obtained elemental Sr was then loaded on single Ta-filaments with nitric acid before it was measured on a VG-Sector thermal ionisation mass spectrometer. Fractionation corrections and concentrations of Sr were calculated on line with an IBM XT personal computer.

After loading with sulphuric acid on triple Ta-Re-Ta-filaments Rb was measured directly on an Ion Instruments AVCO solid source mass spectrometer controlled by a PDP11 computer.

Only the two sigma errors of the individual measurements on the determinations of the $^{87}Sr/^{86}Sr$ ratios are listed in the tabular listing of the results and a total error of ± 0.01% of the obtained values must be assumed for these ratios. The obtained $^{87}Rb/^{86}Sr$ ratios have an estimated total error of ± 1%.

The following constants were used for data reduction and the calculation of ages:

Rubidium: $\lambda^{87}Rb = 1.42 * 10^{-11}a^{-1}$ (Steiger and Jaeger, 1977)
$^{85}Rb/^{87}Rb = 2.59265$

Strontium: $^{86}Sr/^{88}Sr = 0.1194$
$^{84}Sr/^{86}Sr = 0.056584$

Uniform Reservoir (UR): $^{87}Sr/^{86}Sr_{(0)} = 0.7045$
$^{87}Rb/^{86}Sr_{(0)} = 0.0827$
(De Paolo, 1988)

$^{87}Sr/^{86}Sr_{x(T)} = {}^{87}Sr/^{86}Sr_{x(0)} - {}^{87}Rb/^{86}Sr_{x(0)} * (\varepsilon^{\lambda SmT} - 1)$
(x denotes sample, CHUR or DM; T denotes any time in the past - see also Sm-Nd method).

2.3 U-PB METHOD

Dr U. Schaltegger kindly introduced us to the U-Pb technique of dating.

Approximately 1 to 5 mg of hand-picked zircons were washed in nitric and hydrochloric acid before they were directly spiked with a highly pure $^{205}Pb/^{235}U$ mixed spike. They were then dissolved in PTFE-bombs according to the method of Krogh at a temperature of approximately 215 °C. Element separation was carried out following the procedure of Krogh (1973) using several ion exchange columns. In a second batch of samples, lead was purified using a technique based on HBr-chemistry. Elemental Pb was loaded with phosphoric acid and silica gel on single Re filaments while elemental U was loaded with HNO_3 (2%) and silica gel on triple Re-filaments. Both U and Pb were then measured on a VG Sector thermal ionisation mass spectrometer. The obtained data were then processed by the use of a computer programme written in collaboration with Dr Schaltegger during this study.

The following constants and common-Pb ratios after the two-stage model of Stacey and Kramers (1975) were used for the U-Pb calculations:

Uranium: $\lambda^{238}U = 0.155125 * 10^{-9}a^{-1}$
$\lambda^{235}U = 0.98485 * 10^{-9}a^{-1}$
(Steiger and Jaeger, 1977)
$^{235}U/^{238}U = 1/137.88$

Lead: Common Pb ratios after Stacey and Kramers (1975)
for t = 1210 Ma (acid volcanics)
$^{206}Pb/^{204}Pb = 16.692$

$^{207}Pb/^{206}Pb = 15.466$
$^{208}Pb/^{204}Pb = 36.358$
for t = 1370 Ma (Borodino pluton)
$^{206}Pb/^{204}Pb = 16.396$
$^{207}Pb/^{206}Pb = 15.427$
$^{208}Pb/^{204}Pb = 36.047$
for t = 1510 Ma (Piksteel pluton)
$^{206}Pb/^{204}Pb = 16.132$
$^{207}Pb/^{206}Pb = 15.386$
$^{208}Pb/^{204}Pb = 35.773$
for t = 1780 Ma (Opetjie pluton)
$^{206}Pb/^{204}Pb = 15.605$
$^{207}Pb/^{206}Pb = 15.291$
$^{208}Pb/^{204}Pb = 35.239$

Six Pb-analyses of the NBS 983 isotopic standard yielded the following isotope ratios and one sigma analytical errors:

$^{206}Pb/^{204}Pb$: 2710.5 ± 28.6
$^{207}Pb/^{204}Pb$: 192.99 ±1.92
$^{208}Pb/^{204}Pb$: 32.05 ± 0.22
$^{207}Pb/^{206}Pb$: 0.07121 ± 0.00007

Four U-analyses of the U900 isotopic standard yielded a $^{235}U/^{238}U$ ratio of 10.384 ± 0.008.
The double determination of the Nam-1 zircon showed a reproducibility of 0.6% for the $^{206}Pb/^{238}U$ ratios and 0.3% for the $^{207}Pb/^{235}U$ ratios of 0.3%.

2.4 SM-ND METHOD

The adaptation and set-up of the Sm-Nd method at the KAW Laboratory in Berne in collaboration with Dr M. Flisch and O. Krebs formed an important part of this study. The method used in Berne follows the classical "alpha-HIBA" technique. It is presently undergoing refinement and improvement at our laboratory.

Whole-rock aliquots of a weight of 0.4 to 3 grams ground to a very fine grain size, were dissolved in open crucibles in a 20:1 mixture of hydrofluoric and perchloric acid before being diluted in 2.5 n hydrochloric acid. A mixed spike composed of ^{150}Sm and ^{145}Nd was then added to an aliquot of the resulting solution for the determination of the Sm and Nd concentrations, while another aliquot remained unspiked for the precise determination of the Nd isotopic ratios. The REEs were subsequently separated from both aliquots by cation exchange columns operated with 2.5 normal and 6 normal hydrochloric acid. Sm and Nd were isolated by a second cation exchange column operated with alpha-hydroxiisobutyric acid (alpha-HIBA). Elementary Sm and Nd were loaded on single and triple Re filaments respectively, before they were measured on a VG-Sector thermal ionisation mass spectrometer. The concentrations of Sm and Nd were determined using five static collectors while the isotopic composition of Nd was determined by dynamic measurements of the various masses on five collectors. The $^{143}Nd/^{144}Nd$ ratios were corrected for fractionation to $^{146}Nd/^{144}Nd = 0.72190$ before they were renormalised to $^{142}Nd/^{144}Nd = 1.141827$.

The mean $^{143}Nd/^{144}Nd$ ratio of eight measurements of the international La Jolla Nd isotopic standard normalised to $^{146}Nd/^{144}Nd = 0.72190$ was 0.511839. Several of the samples were determined twice in order to test reproducibility. In such cases the better of the two results was included in the text. The results discussed in Chapter 12 represent all the analysed specimens, i.e. none of the obtained sample points was omitted.

All the results obtained were calculated using a computer programme written during this study by U. Ziegler. The following constants and formulae were used for all calculations:

Samarium:

$\lambda^{147}Sm$: $6.54 * 10^{-12} a^{-1}$
$^{149}Sm/^{147}Sm = 0.92160$
$^{150}Sm/^{147}Sm = 0.49213$
(Wasserburg *et al.*, 1981)

Neodymium:

$^{142}Nd/^{144}Nd = 1.141827$
$^{145}Nd/^{144}Nd = 0.348417$
$^{146}Nd/^{144}Nd = 0.721900$
(Wasserburg *et al.*, 1981)

Chondritic mantle (CHUR):

$^{147}Sm/^{144}Nd_{(0)} = 0.1967$
$^{143}Nd/^{144}Nd_{(0)} = 0.51264$
(De Paolo, 1988)

Depleted mantle (DM):

$^{147}Sm/^{144}Nd_{(0)} = 0.2136$
$^{143}Nd/1^{44}Nd_{(0)} = 0.51315$
(De Paolo, 1988)

$$T_{CHUR} = \frac{1}{\lambda} Sm * \ln (1 + \frac{(^{143}Nd \backslash ^{144}Nd_{sample(0)} - ^{143}Nd \backslash ^{144}Nd_{CHUR(0)})}{(^{147}Sm \backslash ^{144}Nd_{sample(0)} - ^{147}Sm \backslash ^{144}Nd_{CHUR(0)})})$$

$$T_{DM} = \frac{1}{\lambda} Sm * \ln (1 + \frac{(^{143}Nd \backslash ^{144}Nd_{sample(0)} - ^{143}Nd \backslash ^{144}Nd_{DM(0)})}{(^{147}Sm \backslash ^{144}Nd_{sample(0)} - ^{m147}Sm \backslash ^{144}Nd_{DM(0)})})$$

$$E_{Sm \backslash Nd} = \frac{(^{147}Sm \backslash ^{144}Nd_{sample(0)} - ^{147}Sm \backslash ^{144}Nd_{CHUR(0)})}{(^{147}Sm \backslash ^{144}Nd_{CHUR(0)})}$$

$$(^{143}Nd \backslash ^{144}Nd_{X(T)}) = (^{143}Nd \backslash ^{144}Nd_{X(0)} - ^{147}Sm \backslash ^{144}Nd_{X(0)} * (\varepsilon^{\lambda SmT} - 1)$$

(X denotes sample, CHUR or DM; T = any time T in the past: T = (0) = today)

Epsilon Nd and Epsilon Sr are derivations in parts per 10^4 from chondritic Nd and Sr, respectively, at the time T (Epsilon $Nd_{(0)}$ = Epsilon Nd today).

3. DATA PROCESSING

The VG MM1200 vacuum mass spectrometer and the Ion Instruments solid source mass spectrometer are controlled by a PDP11 computer programmed by R. Siegenthaler while the measurements on the VG Sector mass spectrometer are controlled by an IBM XT personal computer using a software package of VG Isotopes UK Ltd. All data evaluation programmes used during this study, either written or adapted by the authors, perform on an Olivetti M24 SP personal computer. Linear regressions were calculated according to York (1969) with no correlation of errors, and equal weighing of all data points. In order to determine the precision of the obtained slope and intercept values of the best-fit lines according to the method of York (1969), some of the Rb-Sr and Sm-Nd datasets were tested by the bootstrap method of Diaconis and Efron (1983) using a computer programme of Kalsbeek and Hansen (1986) which was modified by the authors. The term "reference line" used in this text refers to a line fitted through the obtained data sets by the statistical methods discussed above with the consequence that error estimates are attributed to the resulting reference ages and intercepts. Constants used are those of Steiger and Jaeger (1977) and of Wasserburg *et al.* (1981) (see above). The Lotus Symphony and Microsoft Word programmes were utilised for data management and word processing, respectively.

APPENDIX : TABLES

Sample	G01	G02	G03	G04	G05	G06	G07	G08	G09	G10
Farm	Rehoboth DG	Swartmodder	Swartmodder	Rehoboth DG	Neuras	Kanasis	Awasab	Koichas	Koichas	Diergaards
Coord.	23°10'02"S 17°06'38"E	23°23'13"S 17°04'42"E	23°23'13"S 17°04'42"E	23°25'41"S 17°06'51"E	23°29'58"S 17°00'37"E	23°31'08"S 16°59'22"E	23°31'32"S 17°06'34"E	23°31'15"S 17°05'32"E	23°31'15"S 17°05'32"E	23°41'34"S 17°03'04"E
Major elements in wt%										
SIO2	75.82	74.33	68.43	72.06	72.80	72.94	72.72	72.49	72.93	71.04
TIO2	0.07	0.19	0.80	0.42	0.45	0.50	0.48	0.35	0.31	0.32
AL203	12.55	13.06	13.54	12.53	13.04	12.64	12.63	13.16	13.22	13.55
FE203	0.71	1.17	4.95	2.47	2.49	2.46	2.56	1.88	1.83	2.17
MNO	0.07	0.03	0.11	0.04	0.06	0.05	0.06	0.03	0.03	0.06
MGO	0.28	0.38	1.27	0.52	0.69	0.69	0.74	0.51	0.53	1.11
CAO	0.60	0.65	2.41	1.45	1.27	0.84	1.54	0.62	0.68	1.41
NA2O	4.08	2.48	2.66	2.52	2.96	2.61	2.79	2.45	2.54	3.09
K2O	4.22	5.79	3.80	5.31	5.27	5.32	4.90	5.81	5.72	4.47
P2O5	0.08	0.06	0.21	0.07	0.11	0.14	0.09	0.06	0.07	0.09
LOI	0.40	0.56	1.26	0.65	0.44	0.90	0.56	0.87	1.14	1.39
SUM	98.88	98.70	99.44	98.04	99.58	99.09	99.07	98.23	99.00	98.70
Trace elements in ppm										
NB	18			10		14	11			
ZR	57	111	263	248		239	286	259	225	153
Y	8	18	36	55		24	42	30	25	22
SR	107	192	294	56		138	146	86	108	251
U										
RB	197	132	140	282		184	166	205	212	207
TH			13	25			13	13		15
PB	54	23		22		21	17		18	20
GA	20	14	18	16		17	17	18	15	18
ZN	25		45	37		41	40	41	26	43
CU		48								9
NI										
CO	22	16	24	18		15	106	160	12	14
CR										
V						53		32		52
CE		78	125	117		135	108	85	81	62
ND			62	37		59	45			
BA	146	1801	1004	709		1112	1156	1003	1100	1001
LA		61	88	64		105	97	56	51	74
SC			9	9		10	8			
S										
SUM	654	2494	2101	1705		2167	2258	1988	1873	1941

	G12	G13	G14	G15	G16	G17	G18	G19	G20	G21	G22
	Diergaards	Diergaards	Kobos	Kanaus Suid	Kobos	Dymoeb	Dymoeb	Samkubis	Samkubis	Samkubis	Naies
	23°41'50"S 17°02'25"E	23°42'15"S 17°02'39"E	23°35'31"S 16°39'14"E	23°35'54"S 16°37'50"E	23°35'54"S 16°39'25"E	23°40'26"S 16°41'24"E	23°43'06"S 16°39'26"E	23°42'30"S 16°38'46"E	23°41'15"S 16°35'26"E	23°41'23"S 16°35'28"E	23°40'44"S 16°34'13"E
	72.24	71.39	71.45	74.27	69.19	68.25	77.67	67.66	69.48	73.08	70.22
	0.21	0.19	0.57	0.18	0.45	0.59	0.12	0.68	0.54	0.16	0.31
	13.89	13.53	13.02	12.27	13.62	13.48	11.09	13.53	15.59	13.72	14.17
	1.54	1.13	3.64	1.33	3.10	3.87	1.02	4.40	3.00	1.28	2.70
	0.04	0.05	0.07	0.06	0.07	0.08	0.01	0.08	0.08	0.04	0.05
	0.64	0.61	0.82	0.26	0.56	1.07	0.38	1.07	0.97	0.61	1.37
	0.97	1.08	1.74	0.59	1.87	2.44	0.02	2.61	0.88	0.92	2.03
	3.44	3.31	2.76	2.98	3.20	3.14	2.18	2.95	3.73	3.37	3.02
	5.07	5.06	4.07	5.03	4.83	4.62	5.63	4.37	5.57	4.79	3.74
	0.07	0.07	0.22	0.06	0.12	0.18	0.07	0.19	0.14	0.07	0.13
	0.76	0.75	0.85	0.66	0.80	0.84	0.60	0.93	0.93	0.87	1.63
	98.87	97.17	99.21	97.70	97.82	98.57	98.80	98.48	100.92	98.93	99.38
			22				23				
	115	99	101	213	211	228	94	245	455	135	256
	20	13	25	31	38	40	40	34	32	14	17
	185	171	237	106	131	217	21	232	165	265	223
	237	221	285	160	199	165	355	165	111	131	112
	14		38	16	16		14				
	31	18	57							27	
	18	16	22	12	18	17	17	18	19	17	18
	29	27	32	41	41	51	18	52	60	31	48
			24					9	11		
	89	85		26	110	103	94	90	101	10	143
	22			151	39	56		59	31		40
	46			138	96	143		144	256	52	134
				42	29			50	106		44
	782	726	739	516	698	1052	142	1015	2117	1461	1602
	46	45		69	61	91		66	182		98
				11	7	10		11	12		
											596
	1634	1421	1582	1532	1694	2173	818	2190	3658	2143	3331

Table 1 (pages 87, 88 and 89): Major and trace element analyses of the **Gamsberg Granite Suite.** (No data recorded where concentration of trace element is below detection limit)

Detection limits:
Nb 11 Zr 23 Y 5 S r16 U 31 Rb 14 Th 13 Pb 16 Ga 5 Zn 18 Cu 9 Ni 12 Co 3 Cr 26 V 26 Ce 46 Nd 26 Ba 40 La 44 Sc 7 S 216

Table 1 (continued)

G23	G24	G25	G26	G27	G28	G29	G31	G32	G33	G34
Grauwater	Aukukams	Aukukams	Aukukams	Aukukams	Aukukams	Brakkom	Nauchas	Damas	Morgenroth	Morgenroth
23°44'08"S 16°35'07"E	23°40'45"S 16°47'32"E	23°41'41"S 16°48'23"E	23°42'46"S 16°49'38"E	23°39'24"S 16°49'56"E	23°39'21"S 16°52'19"E	23°44'29"S 16°54'12"E	23°37'04"S 16°22'00"E	23°38'30"S 16°22'16"E	23°39'16"S 16°26'50"E	23°39'22"S 16°27'21"E
68.03	74.28	71.19	73.76	76.90	70.57	76.67	76.76	73.29	70.70	73.58
0.46	0.16	0.29	0.20	0.07	0.44	0.30	0.13	0.18	0.29	0.43
13.87	12.94	12.72	12.99	12.56	13.45	10.14	11.90	13.75	12.99	13.28
2.57	1.21	1.85	1.35	0.82	2.92	1.46	0.89	0.83	1.84	2.07
0.06	0.05	0.05	0.05	0.03	0.07	0.08	0.03	0.03	0.05	0.07
1.09	0.33	1.03	0.49	0.23	0.81	0.55	0.20	0.36	1.19	0.54
1.58	0.79	1.59	1.15	1.02	1.61	7.71	0.06	1.09	0.91	0.67
3.18	3.11	3.23	3.55	2.58	2.75	0.19	3.28	4.33	2.76	3.28
5.41	5.22	4.30	4.60	5.61	5.17	1.09	4.85	4.00	5.57	4.94
0.14	0.04	0.07	0.05	0.02	0.13	0.08	0.03	0.08	0.09	0.08
0.75	0.53	0.67	0.48	0.44	0.93	1.17	0.50	0.62	0.73	0.70
97.15	98.67	97.00	98.70	100.29	98.87	99.46	98.64	98.59	97.13	99.65
	14					11	16			14
226	118	141	117	105	251	276	123	99	200	321
31	25	21	15		36	46	11	7	15	23
219	109	171	154	251	175	597	24	261	154	185
148	244	180	221	154	251	66	284	90	153	155
	13				23	22	13			
	33		20	24	23	69	18	38		
16	18	15	18	15	19	16	20	17	17	19
45	19	30	26		50	96			26	46
		12			33			313		
17	11	83	107	13	112	123	9	93	126	13
32					60				27	44
95		47			147	150			112	135
33					51	57			27	39
1254	521	566	705	1059	915	250	100	594	1135	1377
66					115	75	58		85	86
7					7		7			10
2189	1125	1266	1383	1621	2268	1854	683	1512	2077	2467

G35	G37	G39	G40	G42	G43	G44	G45	G46	G47	G48
Morgenroth	Guisis	Guisis	Guisis	Alberta	Namibgrens	Namibgrens	Nauchas	Goellschau	Goellschau	Rohenheim
23°39'47"S 16°26'39"E	23°46'13"S 16°17'35"E	23°46'49"S 16°16'00"E	23°47'05"S 16°15'25"E	23°37'46"S 16°16'37"E	23°36'41"S 16°14'40"E	23°37'00"S 16°14'25"E	23°37'02"S 16°21'25"E	23°18'15"S 16°30'44"E	23°18'55"S 16°28'30"E	23°18'21"S 16°24'19"E
65.05	67.41	72.50	70.74	73.35	72.38	72.80	75.63	75.04	68.67	70.47
0.83	0.34	0.28	0.60	0.24	0.39	0.33	0.14	0.06	0.64	0.47
14.78	14.62	12.35	14.59	13.47	12.76	12.38	12.00	12.04	13.82	13.24
4.60	2.94	1.52	3.23	1.65	1.96	1.77	0.94	1.23	4.16	3.11
0.10	0.08	0.05	0.08	0.05	0.05	0.04	0.07	0.03	0.09	0.07
1.74	1.82	0.77	0.86	0.72	0.74	0.76	0.26	0.28	1.10	0.77
3.03	2.51	0.68	1.72	0.87	1.25	0.94	0.54	0.54	2.36	1.92
3.51	4.54	3.14	3.37	3.51	3.07	3.39	3.35	3.26	2.99	2.99
3.67	3.21	4.96	4.61	4.66	4.97	4.65	4.91	5.03	4.60	4.99
0.25	0.14	0.06	0.22	0.06	0.12	0.09	0.02	0.01	0.17	0.10
1.07	1.90	0.68	1.04	0.63	0.49	0.52	0.33	0.49	0.79	0.72
98.64	99.52	97.00	101.08	99.22	98.19	97.68	98.22	98.02	99.42	98.87
12			18				15	36	13	
364	144	190	316	172	220	194	102	81	247	200
63	7	22	23	23	23	8	16	107	41	39
468	446	115	310	152	186	144	22		168	133
95	102	153	111	174	141	149	304	415	152	186
							25			15
							30	17	17	23
19	16	15	18	20	15	15	17	23	18	16
70	52	25	51	26	28	20		39	59	36
23	86	94	16	168	110	156	14	144	23	14
92	42		94		30				78	37
197		87	134	73	129	59	92		132	189
92			48		41				69	85
2195	1278	917	1402	1117	1024	780	117	77	1304	924
111			105		66		75		106	125
10			11				7		15	9
3811	2173	1618	2657	1925	2013	1525	836	939	2412	2031

Table 1
(continued)

G49	G50	G51	G52	G53	G54	G55	G56	G57	G58	G59	G60
Hohenheim		Weener	Gamsberg	Gamsberg	Isabis	Isabis	Doornboom	Marienhof	Marienhof	Sandpuetz	Rehoboth DG
23°18'08"S 16°22'25"E		23°23'15"S 16°17'12"E	23°22'06"S 16°18'00"E	23°19'46"S 16°20'45"E	23°21'10"S 16°31'12"E	23°22'06"S 16°30'12"E	23°26'29"S 16°33'25"E	23°23'34"S 16°48'53"E	23°24'02"S 16°49'28"E	23°20'51"S 16°58'18"E	23°20'08"S 17°00'08"E
75.21	71.02	73.60	72.36	65.55	67.77	69.82	76.62	70.97	76.57	75.90	75.12
0.08	0.46	0.40	0.50	0.89	0.83	0.62	0.11	0.41	0.25	0.09	0.50
12.77	12.98	12.69	12.87	13.59	14.19	12.34	11.77	13.17	12.00	12.00	13.25
1.06	2.70	2.47	3.02	6.02	5.27	3.80	0.86	2.18	1.25	0.49	2.34
0.04	0.06	0.06	0.07	0.11	0.11	0.08	0.02	0.05	0.03	0.01	
0.15	0.66	0.71	0.81	1.66	1.30	1.00	0.19	0.69	0.31	0.23	0.21
0.36	1.55	1.22	1.31	3.54	2.70	1.78	0.13	1.28	0.37	0.58	0.37
3.36	2.78	2.72	2.59	3.88	3.10	2.79	2.90	3.58	2.85	2.22	7.74
5.04	4.74	4.86	4.86	1.81	3.85	4.30	5.18	4.80	5.40	6.33	0.10
0.01	0.09	0.08	0.10	0.21	0.27	0.17	0.06	0.22	0.04	0.03	0.17
0.59	0.64	0.65	0.82	0.76	0.94	0.67	0.56	0.68	0.39	0.40	0.15
98.68	97.69	99.49	99.34	98.03	100.36	97.38	98.41	98.05	99.48	98.30	99.98
25			15		13		20				
102	243	203	246	187	239	199	93	172	164	48	
93	41	36	39	37	40	36	93	17	48		
	108	116	111	218	196	130	17	165	72	208	
294	171	165	181	76	115	158	283	149	132	116	
14							20	34			
28		17					18				
20	15	16	16	16	19	9	14	13	12	10	
41	36	34	38	84	68	75		29			
				15		14					
				14							
87	79	19	19	24	28	45	103	10	48	23	
	33	51	81	136	78	48		52			
	119	132	138	117	163	93		181	94		
	40	58	56	41	78	49		33			
84	1032	1087	957	997	1282	1256	63	730	514	1090	
	69	93	108	46	127	68		118	81		
	10	11	14	14	15	10	7				
788	1996	2038	2019	2022	2461	2190	731	1703	1165	1495	

Table 2 (pages 90 and 91): Major and trace element analyses of the **Piksteel Intrusive Suite.**

(No data recorded where concentration of trace element is below detection limit)

Detection limits:

Nb 11 Zr 23 Y 5 Sr 16 U 31 Rb 14 Th 13 Pb 16 Ga5 Zn 18 Cu 9 Ni 12 Co 3 Cr 26 V 26 Ce 46 Nd 26 Ba 40 La 44 Sc 7 S 216

Sample	P01	P02	P03	P04	P05	P06	P08	P09	P11	P12
Farm	Rehoboth DG	Rehoboth DG	Rehoboth DG	Rehoboth DG	Neuras	Oudam	Klein Aub	Dymoeb	Karikomasis	Kankoes
Coord.	23°23'13"S 17°03'17"E	23°23'27"S 17°03'05"E	23°23'43"S 17°06'09"E	23°26'10"S 17°05'44"E	23°26'55"S 17°03'00"E	23°38'15"S 16°41'46"E	23°46'00"S 16°36'14"E	23°45'43"S 16°38'32"E	23°40'22"S 16°56'52"E	23°37'03"S 16°56'40"E
Major elements in wt%										
SIO2	71.00	67.05	67.81	68.97	72.29	74.95	59.06	63.85	77.16	75.63
TIO2	0.47	0.60	0.85	0.41	0.41	0.12	0.70	0.63	0.22	0.21
AL203	13.26	13.70	13.30	14.92	13.61	12.35	17.20	15.78	11.31	11.83
FE203	3.05	3.96	5.47	2.69	2.41	1.10	4.75	4.23	1.72	1.98
MNO	0.06	0.08	0.07	0.05	0.07	0.04	0.09	0.07	0.03	0.06
MGO	0.81	0.95	1.02	0.99	0.61	0.09	2.50	1.69	0.15	0.23
CAO	3.16	2.44	2.78	2.58	1.22	0.69	3.71	3.65	0.09	0.36
NA20	2.22	3.03	2.29	3.38	3.58	3.24	3.48	3.75	3.22	3.09
K20	4.24	4.02	4.08	3.73	3.93	4.92	4.89	3.03	4.39	5.40
P205	0.10	0.16	0.21	0.12	0.10	0.01	0.26	0.19	0.04	0.03
LOI	0.88	1.75	1.29	0.96	0.83	0.56	2.25	1.71	0.40	0.31
SUM	99.27	97.75	99.20	98.82	99.07	98.08	98.92	98.59	98.75	99.15
Trace elements in ppm										
NB			12			16			13	11
ZR	189	272	386	171	243	104	149	202	217	254
Y	31	41	45	11	11	65	20	21	72	31
SR	470	256	206	630	233	26	525	694	47	37
U										
RB	92	120	170	94	88	379	149	77	187	149
TH						37				18
PB	26					30			17	19
GA	18	20	20	18	16	18	18	21	15	15
ZN	21	44	52	38	41	20	60	53		21
CU			72				30	16		
NI							16	14		
CO	15	17	26	17	14	65	23	88	12	17
CR			27				42			
V			95	56	50		117	61		
CE		70	119	78	137		75	94	98	273
ND			64	26	48		40	39	78	71
BA	1176	1047	1103	1187	1351	89	1700	1614	591	330
LA			89	65	65		78	55	150	179
SC		8	17		8		12	8	7	8
S										
SUM	2038	1895	2503	2391	2305	849	3054	3057	1504	1433

	P13	P15	P16	P17	P18	P20	P21	P22	P23	P24	KAM3018
	Kankoes	Groendraai	Kabiras	Kabiras	Kabiras	Nauzerus	Nauzerus	Stofbakkies	Stofbakkies	Nauchas	Borodino
	23°37'44"S 16°56'21"E	23°42'32"S 16°58'49"E	23°44'36"S 16°23'34"E	23°44'36"S 16°23'04"E	23°44'36"S 16°22'44"E	23°49'19"S 16°20'30"E	23°48'50"S 16°20'04"E	23°48'29"S 16°20'13"E	23°48'05"S 16°20'00"E	23°38'57"S 16°17'39"E	23°40'08"S 16°16'05"E
	73.06	67.91	52.14	76.30	58.77	68.40	72.33	72.51	54.19	70.21	72.37
	0.27	0.52	0.15	0.18	0.81	0.32	0.30	0.32	0.91	0.64	0.09
	13.03	14.27	20.97	12.47	16.78	15.59	13.79	14.11	15.76	15.78	14.82
	2.32	4.07	1.47	1.57	6.82	2.87	2.46	2.35	8.33	3.12	0.82
	0.05	0.10	0.08	0.04	0.16	0.06	0.03	0.03	0.14	0.10	0.03
	0.28	1.35	0.93	0.58	3.20	1.31	1.03	1.06	6.16	1.09	0.24
	0.49	2.32	12.12	0.87	5.66	2.20	1.84	1.95	7.32	2.65	2.01
	3.42	4.03	6.42	3.95	2.83	5.18	2.47	2.54	3.43	4.09	4.05
	5.66	2.11	0.25	1.97	2.20	2.59	3.25	3.29	2.29	2.37	3.25
	0.04	0.18	0.03	0.05	0.31	0.15	0.09	0.09	0.37	0.19	0.03
	0.47	1.66	3.96	1.23	2.61	0.69	1.40	1.29	1.80	1.14	0.71
	99.11	98.54	98.62	99.23	100.18	99.39	99.01	99.56	100.74	101.39	98.43
	12					17				12	
	341	227	90	91	199	274	136	86	86	404	65
	41	17			22	29	7		20	29	
	52	402	309	240	570	177	518	384	774	351	758
	146	77		58	87	137	64	98	74	63	65
	14					14					
						37					
	17	17	17	16	19	18	19	13	18	20	15
	41	57	28	28	131	26	48	21	89	39	
		73		17	53			17	69	23	
					28				65		
	66	15	9	103	27	10	18	11	63	14	14
					34				144		
		56			109		54	34	191		
	304		65		79	94	83		204	104	
	33		39		39	33	33		106	47	
	510	995		740	899	1323	898	1765	1112	1438	2474
	104	46			56	64	63	32	53	47	
	11	11			10				24	8	
	1692	1993	557	1293	2362	2253	1941	2461	3092	2599	3391

Table 2
(continued)

KAM3019	KAM3021	KAM3022	KAM3023	KAM3024	KAM3025	KAM3026	KAM3027	KAM3028	KAM3029	KAM3030	KAM3031	KAM3032	KAM3033
Borodino	Borodino	Borodino	Borodino	Opetjie	Opetjie	Opetjie	Opetjie	Opetjie	Piksteel	Piksteel	Piksteel	Piksteel	Piksteel
23°40'41"S 16°17'05"E	23°40'55"S 16°16'43"E	23°41'03"S 16°16'38"E	23°41'44"S 16°16'23"E	23°40'16"S 16°44'54"E	23°40'28"S 16°44'51"E	23°41'00"S 16°44'27"E	23°42'10"S 16°44'38"E	23°39'58"S 16°44'46"E	23°47'05"S 16°07'46"E	23°47'08"S 16°07'53"E	23°47'02"S 16°08'13"E	23°47'15"S 16°08'23"E	23°47'08"S 16°08'29"E
70.64	70.86	74.68	71.81	70.03	70.15	53.40	65.17	67.49	69.41	69.14	73.17	71.39	70.29
0.18	0.16	0.16	0.17	0.34	0.33	0.68	0.82	0.47	0.21	0.37	0.15	0.19	0.31
15.38	15.03	12.66	15.27	14.30	13.94	18.67	14.65	14.79	14.80	14.76	14.39	15.00	15.16
1.69	1.50	0.97	1.42	2.41	2.36	6.64	5.29	3.41	1.92	2.69	1.46	1.69	2.53
0.05	0.05	0.03	0.04	0.06	0.06	0.12	0.10	0.06	0.04	0.07	0.04	0.05	0.06
0.56	0.48	0.11	0.38	1.04	0.83	4.23	1.45	1.21	0.58	0.86	0.32	0.50	0.74
2.19	2.42	0.86	2.29	1.91	1.96	7.22	2.40	2.83	2.18	2.64	1.79	1.92	2.15
4.15	4.37	2.86	4.71	3.40	3.27	3.25	3.29	3.22	4.13	4.09	3.74	4.41	3.99
3.04	2.39	4.89	2.47	4.43	4.30	2.73	4.36	4.04	3.28	2.96	3.70	3.11	3.10
0.10	0.07	0.03	0.12	0.11	0.11	0.15	0.27	0.15	0.08	0.12	0.04	0.08	0.12
1.46	0.61	0.64	0.76	1.06	0.94	2.26	1.37	1.15	0.70	0.50	0.54	0.73	1.00
99.46	97.95	97.90	99.45	99.11	98.26	99.37	99.19	98.83	97.34	98.21	99.35	99.08	99.46
		22					12						
105	105	109	100	157	152	76	322	207	112	128	104	105	156
		25		18	25	21	37	23		18			
789	1018	128	904	305	264	737	369	421	832	738	723	666	611
70	51	165	58	152	180	76	92	129	62	70	68	54	58
		16											
21	19	28	19		18		21				20		
22	20	18	20	17	18	24	23	19	20	23	18	20	22
26	40		32	34	34	81	91	48	37	58	35	42	63
18				10		84	15	17	12				14
						55		12					
78	71	64	64	111	62	55	49	74	51	68	59	82	76
						45							
27				42	38	128	60	54	34	32			37
		62			85	130	156	139		47			54
				37	27	68	69	47					
2071	1870	453	1717	942	823	1069	2035	1490	1680	904	1876	1693	1381
				73	62		119	71					
						19	13						
3227	3194	1090	2914	1898	1788	2668	3483	2751	2840	2086	2903	2662	2472

Sample	W01	W02	W03	W06	W07	W08	W09	W10	W11	W12	W13	W14
Farm	Morgenroth	Morgenroth	Morgenroth	Namibgrens	Corona	Corona	Corona	Corona	Corona	Weener	Weener	Weener
Coord.	23°39'23"S 16°26'34"E	23°39'34"S 16°26'45"E	23°39'49"S 16°26'32"E	23°37'27"S 16°15'18"E	23°23'34"S 16°09'53"E	23°23'26"S 16°10'11"E	23°23'42"S 16°10'56"E	23°23'42"S 16°11'11"E	23°23'32"S 16°12'56"E	23°23'32"S 16°13'05"E	23°23'26"S 16°13'32"E	23°23'17"S 16°13'51"E
Major elements in wt%												
SIO2	66.82	68.89	63.68	68.38	61.05	58.53	64.56	64.86	60.33	50.49	51.31	48.43
TIO2	0.39	0.32	0.49	0.54	0.88	0.86	0.84	0.84	0.83	1.53	1.51	0.89
AL203	14.86	14.71	14.84	13.84	16.42	15.39	15.30	15.55	15.97	14.38	14.95	18.33
FE203	3.29	2.57	4.18	3.20	7.39	8.74	6.48	6.12	6.78	14.50	13.97	11.62
MNO	0.07	0.08	0.08	0.06	0.12	0.15	0.09	0.10	0.11	0.24	0.25	0.18
MGO	2.05	1.37	2.76	0.94	3.04	3.87	3.44	2.29	3.22	5.58	6.09	7.35
CAO	3.00	1.46	3.92	2.06	4.78	5.82	3.32	3.86	5.26	8.88	7.97	10.58
NA2O	3.60	3.17	2.87	3.22	3.38	2.92	3.64	2.93	3.45	2.99	3.47	1.72
K2O	3.64	4.72	3.83	4.63	1.96	1.79	2.40	2.87	1.75	0.82	1.02	0.34
P2O5	0.18	0.14	0.21	0.15	0.19	0.14	0.20	0.15	0.18	0.33	0.29	0.07
LOI	1.10	1.16	1.88	0.69	1.13	1.61	0.81	1.22	0.86	0.75	0.70	2.25
SUM	99.02	98.62	98.76	97.72	100.36	99.84	101.10	100.81	98.78	100.55	101.59	101.80
Trace elements in ppm												
NB				13								
ZR		130	152	258	173	155	175	188	167	238	225	55
Y		8	11	42	52	49	31	33	25	51	52	14
SR		290	605	267	313	277	246	274	369	187	217	230
U												
RB		144	100	140	65	61	97	85	54	33	36	
TH												
PB		25										
GA		19	19	18	20	19	18	20	20	22	24	20
ZN		140	35	41	76	75	59	68	72	125	124	102
CU		48	9	13	51	66	11	54	46	48	70	43
NI		17	45		50	61	54	31	63	51	69	103
CO		93	83	61	84	70	69	88	50	79	96	91
CR			51		50	72	63	39	91	177	193	167
V		46	68	37	121	159	110	114	141	192	200	201
CE		50	93	126	97	140	97	103	102	217	186	164
ND			37	49	65	79	46	54	53	118	107	98
BA		1674	1732	1315	741	353	723	1429	1067	214	305	85
LA		58		80				44	63	56	54	
SC			7	7	19	23	15	13	12	50	55	32
S										902		455
SUM		2742	3047	2467	1977	1659	1814	2637	2395	2760	2013	1860

Table 3: Major and trace element analyses of the **Weener Intrusive Suite**. (No data recorded where concentration of trace element is below detection limit)

Detection Limits:
Nb 11 Zr 23 Y 5 Sr 16 U 31 Rb 14 Th 13 Pb 16 Ga 5 Zn 18 Cu 9 Ni 12 Co 3 Cr 26 V 26 Ce 46 Nd 26 Ba 40 La 44 Sc 7 S 216

Sample	KAM3029	KAM3033	P15	P11	KAM3021	KAM3022	P18	P17	KAM3026	P06	G53	G49
Farm	Piksteel	Piksteel	Groendraai	Karikomasis	Borodino	Borodino	Kabiras	Kabiras	Opetjie	Oudam	Gamsberg	Hohenheim
Coord.	23°47'05"S 16°07'46"E	23°47'08"S 16°08'29"E	23°42'32"S 16°58'49"E	23°40'22"S 16°56'52"E	23°40'55"S 16°16'43"E	23°41'03"S 16°16'38"E	23°44'36"S 16°22'44"E	23°44'36"S 16°23'04"E	23°41'00"S 16°44'27"E	23°38'15"S 16°41'46"E	23°19'46"S 16°20'45"E	23°18'08"S 16°22'25"E
REE in ppm												
La	28	24	39	127	27	26	34	12	29	52	51	30
Ce	48	67	81	122	43	57	73	16	64	93	95	62
Nd	23	20	41	79	23	28	37	2	38	44	45	31
Sm	3.9	3.2	7.2	17	3	4.5	6	0.97	7.4	7.9	8.5	7.6
Eu	0.88	0.81	1.7	1.85	0.96	0.47	1.7	0.47	1.5	0.34	1.3	0.23
Tb	0.34	0.31	0.98	3.15	0.26	0.6	1.3	0.05	0.99	1.8	0.34	1.9
Yb	1.15	1.25	2.7	11	1.4	3.8	2.3	1	2.9	10.8	3.5	20.9
Sum REE	105.27	116.57	173.58	361	98.62	120.37	155.3	32.49	143.79	209.84	204.64	153.63
Ta and Hf in ppm												
Ta	1.4	1.2	0.46	2	0.73	3	0.74	2.7	0.75	5.5	1.15	11.9
Hf	4	5.4	6.7	9.2	3.9	2.7	5.6	3.2	3.1	6.2	6	7.7
Chondrite normalised Ree-ratios												
Eu/Sm	0.60	0.67	0.63	0.29	0.85	0.28	0.75	1.29	0.54	0.11	0.41	0.08
La/Yb	16.08	12.68	9.54	7.62	12.73	4.52	9.76	7.92	6.60	3.18	9.62	0.95
La/Sm	4.38	4.57	3.30	4.55	5.49	3.52	3.45	7.54	2.39	4.01	3.66	2.41
Eu/Eu*	0.77	0.85	0.74	0.32	1.09	0.33	0.79	1.76	0.64	0.12	0.57	0.08
Tb/Yb	1.26	1.05	1.54	1.22	0.79	0.67	2.40	0.21	1.45	0.71	0.41	0.39

Table 4: Analytical results of 12 REE analyses (including Ta and Hf) of selected Rehoboth granitoids.

Sum = sum of the analysed REE, ratios are chondrite-normalised (see text for explanation)

Sample	KAW3060	KAW3061	KAW3062	KAW3063	KAW3064	KAW3082	KAW3083	KAW3084	KAW3085	KAW3086	KAW3087
Lithology	Schist	Schist	Schist	Schist	Schist	Amphibolite	Amphibolite	Amphibolite	Amphibolite	Granitic	Granitic
Farm	Ubib	Ubib	Ubib	Ubib	Ubib	Mooiriver	Mooiriver	Mooiriver	Mooiriver	Mooiriver	Mooiriver
Coord.	23°39'33"S 16°09'43"E	23°39'31"S 16°09'46"E	23°39'29"S 16°09'44"E	23°39'37"S 16°10'00"E	23°39'40"S 16°10'04"E	24°42'19"S 16°10'32"E	24°42'28"S 16°10'30"E	24°42'25"S 16°10'23"E	24°42'29"S 16°10'16"E	24°42'30"S 16°10'16"E	24°42'37"S 16°10'05"E
Major elements in wt%											
SIO2	69.93	67.55	69.32	70.81	68.23	51.81	47.72	47.02	48.61	68.51	70.73
TIO2	0.37	0.44	0.39	0.51	0.65	3.52	1.61	3.15	1.62	0.45	0.28
AL2O3	14.33	14.30	14.56	15.10	14.89	13.57	15.85	13.45	17.46	15.58	13.76
FE2O3	4.68	4.44	4.69	3.42	4.42	16.12	12.64	16.22	11.65	2.85	2.24
MNO	0.23	0.10	0.21	0.06	0.07	0.28	0.20	0.25	17	0.04	0.04
MGO	1.38	1.74	1.36	1.21	1.23	3.84	7.19	6.10	5. 1	1.21	0.64
CAO	0.59	0.80	0.73	2.70	2.27	7.68	10.33	10.34	10.09	2.33	1.39
NA2O	2.11	1.56	2.03	3.57	3.44	2.68	1.24	2.58	2.87	4.85	3.20
K2O	4.79	4.30	4.38	2.40	2.89	1.03	1.76	0.93	0.93	2.88	4.92
P2O5	0.07	0.06	0.08	0.09	0.09	0.46	0.14	0.29	0.17	0.14	0.08
LOI	1.24	1.74	1.45	1.05	1.12	0.60	1.80	0.62	0.93	1.17	1.06
SUM	99.72	97.03	99.20	100.92	99.30	101.59	100.48	100.95	99.71	100.01	98.34
Trace elements in ppm											
NB											
ZR	250	209	267	258	249	302	101	164	129	208	209
Y	34	31	39	32	31	66	29	42	29	7	13
SR	79	51	92	366	330	216	198	254	320	419	198
U											
RB	134	120	133	71	88	41	110	44	37	112	155
TH		13									
PB											
GA	19	19	21	19	20	27	22	24	22	25	20
ZN	52	46	52	50	61	158	102	129	98	68	48
CU						19	85	148	82	18	
NI				13	15		93	65	53		
CO	96	98	53	68	68	88	82	72	59	56	90
CR				36	45	49	281	154	165		
V	41	59	55	54	72	222	334	411	226	46	27
CE	68	83	77	98	89	257	204	250	178		121
ND				35	35	158	121	144	106		46
BA	1186	1355	1543	1232	1269	294	173	159	113	1289	1361
LA		44		53	47	130	48	81			69
SC	12	11	12	9	11	61	55	62	40		
S								246	278		
SUM	1971	2139	2344	2394	2430	2088	2038	2449	1935	2248	2357

Table 5: Major and trace element analyses of the analysed whole-rock samples from the Mooirivier Complex. (No data recorded where concentration of trace element is below detection limit)

Detection Limits:
Nb 11 Zr 23 Y 5
Sr 16 U 31 Rb 14
Th 13 Pb 16 Ga 5
Zn 18 Cu 9 Ni 12
Co 3 Cr 26 V 26
Ce 46 Nd 26 Ba 40
La 44 Sc 7 S 216

Sample KAW	^{40}K $*10^{-8}$mol/g	$^{40}Ar_{rad}$ $*10^{-8}$mol/g	$^{40}Ar_{rad}$ %	^{36}Ar $*10^{-12}$mol/g	Age Ma	Error Ma	Age corr. Ma
3060 Biotite >100 Mesh	21.1324	0.5561	94.72	1.0495	404.1	4.6	1729.5
3061 Biotite	20.8638	0.4394	91.14	1.4509	330.0	5.0	1705.7
3062 Biotite >100 Mesh	22.0577	0.6176	96.00	0.8727	427.1	5.1	1701.0
3063 Biotite >100 Microns	23.3710	0.8641	99.32	0.2022	545.1	5.5	1709.6
3064 Biotite < 60 Mesh	22.4457	0.8158	99.02	0.2735	537.0	5.3	1740.7

Table 6: tabulation of the K-Ar results obtained for the analysed Mooirivier biotites from the Spreetshoogte Pass area. (Age corr. = Individual ages corrected for the loss of $^{40}Ar_{rad}$ determined on the basis of the Harper diagram of Figure 5.7)

Sample KAW	Rb ppm	Sr ppm	$^{87}Sr/^{86}Sr$	+/- 2 Sigma	$^{87}Rb/^{86}Sr$	+/- 2 Sigma	Rb/Sr
3060	143.25	90.34	0.80814	1	4.654	47	1.568
3061	126.87	57.75	0.82447	1	6.429	64	2.197
3062	141.24	99.59	0.80391	1	4.142	41	1.418
3063	73.61	369.49	0.72061	2	0.577	6	0.199
3064	92.10	336.57	0.72469	1	0.759	8	0.274
3082	35.36	206.32	0.71138	2	0.496	5	0.171
3083	110.19	208.16	0.72700	1	1.534	15	0.529
3084	41.83	246.64	0.71142	1	0.491	5	0.170
3085	34.43	318.31	0.71119	3	0.313	3	0.108
3086	118.37	442.28	0.71662	2	0.775	8	0.268
3087	162.33	210.88	0.74046	2	2.234	2	0.770

Table 7: Tabular listing of the Rb-Sr results obtained for the analysed whole-rock samples from the Mooirivier Complex

Sample	KAM3050	KAM3051	KAM3052	KAM3053	KAM3054	KAM3076	KAM3077	KAM3078	KAM3079	KAM3080	KAM3081
Lithology	Amphibolite	Amphibolite	Amphibolite	Amphibolite	Amphibolite	Granitoid	Granitoid	Granitoid	Granitoid	Amphibolite	Amphibolite
Farm	Koichas	Koichas	Swartskaap	Koichas	Koichas	Neuhof	Neuhof	Neuhof	Neuhof	Neuhof	Neuhof
Coord.	23°29'39"S 17°05'51"E	23°29'39"S 17°05'51"E	23°29'32"S 17°06'02"E	23°29'47"S 17°05'34"E	23°29'47"S 17°05'34"E	24°48'42"S 16°09'09"E	24°48'38"S 16°09'18"E	24°48'41"S 16°09'22"E	24°48'36"S 16°09'24"E	24°48'44"S 16°09'13"E	24°48'32"S 16°09'18"E
Major elements in wt%											
SIO2	52.08	49.99	49.77	49.65	50.44	59.69	75.65	62.89	74.62	54.70	49.47
TIO2	0.68	0.66	0.70	0.63	0.86	0.32	0.09	0.38	0.26	0.96	1.35
AL203	16.27	15.66	13.32	15.96	15.68	17.86	12.67	17.98	12.23	11.02	11.17
FE203	10.73	10.58	10.08	9.73	10.98	3.33	1.03	4.36	2.39	9.07	13.31
MNO	0.19	0.20	0.21	0.21	0.22	0.05	0.01	0.02	0.02	0.16	0.16
MGO	7.02	7.07	9.79	7.65	7.23	0.29	0.13	0.09	0.15	8.34	7.65
CAO	10.85	10.12	11.90	10.55	11.21	2.60	0.16	0.09	0.30	9.39	8.92
NA2O	2.71	2.90	2.30	2.68	2.69	4.70	3.07	2.77	3.41	4.10	2.44
K2O	1.04	1.13	0.80	1.42	1.24	7.34	5.68	11.27	5.78	0.78	3.02
P2O5	0.16	0.15	0.14	0.14	0.20	0.04	0.01	0.08	0.04	0.57	1.17
LOI	1.62	1.69	1.31	2.09	1.55	0.78	0.29	0.54	0.36	1.00	1.09
SUM	103.35	100.15	100.32	100.71	102.30	97.00	98.79	100.47	99.56	100.09	99.75
Trace elements in ppm											
NB						25		35			
ZR	93	68	50	53	74	403	41	463	284	180	137
Y	16	12	15	12	22	153	36	406	108	51	33
SR	495	464	445	360	458	465		26	30	341	343
U											
RB	27	29	12	34	32	302	254	474	202	41	149
TH								26			
PB											
GA	18	17	16	12	14	34	24	29	22	18	17
ZN	80	81	83	111	101	28	20	40	44	90	81
CU	49	70	12	23	54						285
NI	40	48	107	68	39			21		89	49
CO	64	60	83	58	59	74	116	55	170	61	67
CR	201	179	271	264	101			30		416	175
V	314	305	319	260	322	43		73		171	310
CE	234	187	194	92	134	232		337	83	170	232
ND	129	101	113	49	75	122		172	40	98	133
BA	670	610	414	736	587	788		1260	581	748	2056
LA						103		162	51	24	67
SC	62	59	69	47	53			12		54	49
S		260			836	296		329		888	
SUM	2492	2550	2203	2179	2961	3068	491	3950	1615	3440	4183

Table 8: Tabular listing of the results of the major and trace element analyses of amphibolitic and granitoid rocks from the Neuhof Formation. (No data recorded where concentration of trace element is below detection limit)

Detection Limits:

Nb 11 Zr 23 Y 5 Sr 16 U 31 Rb 14 Th 13 Pb 16 Ga 5 Zn 18 Cu 9 Ni 12 Co 3 Cr 26 V 26 Ce 46 Nd 26 Ba 40 La 44 Sc 7 S 216

Sample KAW	Rb ppm	Sr ppm	$^{87}Sr/^{86}Sr$	+/- 2 Sigma	$^{87}Rb/^{86}Sr$	+/- 2 Sigma	Rb/Sr
3050	23.75	482.73	0.70728	2	0.142	1	0.049
3051	28.55	487.44	0.70765	14	0.169	2	0.059
3052	10.67	436.66	0.70680	4	0.071	1	0.024
3053	33.92	360.33	0.71189	1	0.272	3	0.094
3054	28.33	449.69	0.70869	1	0.182	2	0.063
3076	311.07	485.14	0.73649	2	1.860	18	0.641
3077	258.68	16.36	1.53210	2	49.44	49	15.81
3078	463.22	28.90	1.23922	2	48.79	49	16.03
3079	223.85	47.93	0.92614	5	13.80	14	4.670
3080	40.11	331.92	0.71182	2	0.350	3	0.121
3081	141.78	345.72	0.72657	2	1.189	12	0.410

Table 9: Tabular listing of the Rb-Sr results obtained for the Neuhof Formation

Sample	KAW3001	KAW3002	KAW3003	KAW3004	KAW3005	KAW3006	KAW3008	KAW3009	KAW3010	KAW3011
Lithology	Mica schist	Itabirite	Amphibolite	Amphibolite	Amphibolite	Amphibolite	Greenschist	Amphibolite	Amphibolite	Amphibolite
Farm	Samkubis	Samkubis	Samkubis	Samkubis	Samkubis	Samkubis	Kobos	Kobos	Kobos	Kobos
Coord.	23°43'22"S 16°38'23"E	23°43'24"S 16°38'14"E	23°42'10"S 16°37'32"E	23°43'16"S 16°37'34"E	23°43'13"S 16°37'35"E	23°43'07"S 16°38'27"E	23°32'36"S 16°38'14"E	23°32'35"S 16°38'19"E	23°32'34"S 16°38'22"E	23°32'34"S 16°38'27"E
Major elements in wt%										
SIO2	48.73	47.36	48.67	51.44	51.67	56.87	53.43	55.15	48.72	49.02
TIO2	1.02	0.04	1.16	0.88	0.89	1.05	0.81	0.95	0.19	0.28
AL2O3	17.38	0.69	14.95	14.98	14.95	13.78	14.57	11.71	15.41	14.48
FE2O3	13.87	43.51	12.49	10.00	9.94	11.57	11.24	10.98	9.16	11.03
MNO	0.31	1.44	0.28	0.19	0.18	0.19	0.19	0.20	0.18	0.20
MGO	4.02	2.51	7.02	7.07	7.04	4.49	6.67	8.08	9.41	8.46
CAO	7.01	2.41	11.51	9.57	10.21	7.84	7.16	8.55	12.13	12.30
NA2O	2.32	0.00	2.42	2.74	2.41	2.87	3.42	1.92	1.61	1.54
K2O	2.35	0.01	0.76	1.63	1.26	0.84	0.26	0.50	0.82	0.27
P2O5	0.35	0.48	0.13	0.16	0.16	0.17	0.24	0.23	0.03	0.03
LOI	2.59	0.58	1.09	1.50	1.53	0.89	2.43	1.90	2.31	2.16
SUM	99.95	99.03	100.48	100.16	100.24	100.56	100.42	100.17	99.97	99.77
Trace elements in ppm										
NB										
ZR	385		92	93	90	123	55	102		
Y	34	16	23	13	11	28	13	15	8	11
SR	255	43	209	224	225	264	172	256	109	81
U										
RB	75		17	53	35	22			19	
TH		20		0						
PB										
GA	16	6	16	12	14	18	11	16	9	10
ZN	102	41	144	99	90	72	86	89	62	78
CU	427			47	61	84	151	95	33	61
NI	21	14	146	69	72	21	33	108	116	103
CO	57	31	71	56	67	64	65	71	71	68
CR	34		529	219	225	95	91	471	478	444
V	148		341	221	233	248	236	255	190	250
CE	184	109	180	116	141	128	78	129	136	153
ND	69	33	68	33	76	74	48	77	75	80
BA	500	54	177	678	563	335	99	353	260	99
LA	70									
SC	28		60	44	47	41	43	31	60	62
S	1180									
SUM	3585	367	2073	1977	1950	1617	1181	2068	1626	1500

Table 10 (pages 95 and 96): Tabular listing of the results of the major and trace element analyses of the Elim samples. (No data recorded where concentration of trace element is below detection limit)

Detection Limits:
Nb 11 Zr 23 Y 5 Sr 16 U 31 Rb 14 Th 13 Pb 16 Ga 5 Zn 18 Cu 9 Ni 12 Co 3 Cr 26 V 26 Ce 46 Nd 26 Ba 40 La 44 Sc 7 S 216

Sample KAW	Rb ppm	Sr ppm	$^{87}Sr/^{86}Sr$	+/- 2 Sigma	$^{87}Rb/^{86}Sr$	+/- 2 Sigma	Rb/Sr
3050	23.75	482.73	0.70728	2	0.142	1	0.049
3051	28.55	487.44	0.70765	14	0.169	2	0.059
3052	10.67	436.66	0.70680	4	0.071	1	0.024
3053	33.92	360.33	0.71189	1	0.272	3	0.094
3054	28.33	449.69	0.70869	1	0.182	2	0.063
3076	311.07	485.14	0.73649	2	1.860	18	0.641
3077	258.68	16.36	1.53210	2	49.44	49	15.81
3078	463.22	28.90	1.23922	2	48.79	49	16.03
3079	223.85	47.93	0.92614	5	13.80	14	4.670
3080	40.11	331.92	0.71182	2	0.350	3	0.121
3081	141.78	345.72	0.72657	2	1.189	12	0.410

Table 9: Tabular listing of the Rb-Sr results obtained for the Neuhof Formation

Sample	KAW3001	KAW3002	KAW3003	KAW3004	KAW3005	KAW3006	KAW3008	KAW3009	KAW3010	KAW3011
Lithology	Mica schist	Itabirite	Amphibolite	Amphibolite	Amphibolite	Amphibolite	Greenschist	Amphibolite	Amphibolite	Amphibolite
Farm	Saakubis	Saakubis	Saakubis	Saakubis	Saakubis	Saakubis	Kobos	Kobos	Kobos	Kobos
Coord.	23°43'22"S 16°38'23"E	23°43'24"S 16°38'14"E	23°42'10"S 16°37'32"E	23°43'16"S 16°37'34"E	23°43'13"S 16°37'35"E	23°43'07"S 16°38'27"E	23°32'36"S 16°38'14"E	23°32'35"S 16°38'19"E	23°32'34"S 16°38'22"E	23°32'34"S 16°38'27"E
Major elements in wt%										
SIO2	48.73	47.36	48.67	51.44	51.67	56.87	53.43	55.15	48.72	49.02
TIO2	1.02	0.04	1.16	0.88	0.89	1.05	0.81	0.95	0.19	0.28
AL2O3	17.38	0.69	14.95	14.98	14.95	13.78	14.57	11.71	15.41	14.48
FE2O3	13.87	43.51	12.49	10.00	9.94	11.57	11.24	10.98	9.16	11.03
MNO	0.31	1.44	0.28	0.19	0.18	0.19	0.19	0.20	0.18	0.20
MGO	4.02	2.51	7.02	7.07	7.04	4.49	6.67	8.08	9.41	8.46
CAO	7.01	2.41	11.51	9.57	10.21	7.84	7.16	8.55	12.13	12.30
NA2O	2.32	0.00	2.42	2.74	2.41	2.87	3.42	1.92	1.61	1.54
K2O	2.35	0.01	0.76	1.63	1.26	0.84	0.26	0.50	0.82	0.27
P2O5	0.35	0.48	0.13	0.16	0.16	0.17	0.24	0.23	0.03	0.03
LOI	2.59	0.58	1.09	1.50	1.53	0.89	2.43	1.90	2.31	2.16
SUM	99.95	99.03	100.48	100.16	100.24	100.56	100.42	100.17	99.97	99.77
Trace elements in ppm										
NB										
ZR	385		92	93	90	123	55	102		
Y	34	16	23	13	11	28	13	15	8	11
SR	255	43	209	224	225	264	172	256	109	81
U										
RB	75		17	53	35	22			19	
TH		20		0						
PB										
GA	16	6	16	12	14	18	11	16	9	10
ZN	102	41	144	99	90	72	86	89	62	78
CU	427			47	61	84	151	95	33	61
NI	21	14	146	69	72	21	33	108	116	103
CO	57	31	71	56	67	64	65	71	71	68
CR	34		529	219	225	95	91	471	478	444
V	148		341	221	233	248	236	255	190	250
CE	184	109	180	116	141	128	78	129	136	153
ND	69	33	68	33	76	74	48	77	75	80
BA	500	54	177	678	563	335	99	353	260	99
LA	70									
SC	28		60	44	47	41	43	31	60	62
S	1180									
SUM	3585	367	2073	1977	1950	1617	1181	2068	1626	1500

Table 10 (pages 95 and 96): Tabular listing of the results of the major and trace element analyses of the Elim samples. (No data recorded where concentration of trace element is below detection limit)

Detection Limits:

Nb 11 Zr 23 Y 5 Sr 16 U 31 Rb 14 Th 13 Pb 16 Ga 5 Zn 18 Cu 9 Ni 12 Co 3 Cr 26 V 26 Ce 46 Nd 26 Ba 40 La 44 Sc 7 S 216

Sample	KAW3001	KAW3002	KAW3003	KAW3004	KAW3005	KAW3006	KAW3008	KAW3009	KAW3010	KAW3011	KAW3012
al	26.82	1.00	19.99	21.53	21.48	22.94	22.42	17.82	20.08	19.19	19.29
fm	43.70	92.64	45.61	44.45	44.19	43.96	48.46	52.89	46.59	47.42	47.39
c	19.67	6.34	27.98	25.01	26.67	23.73	20.03	23.66	28.73	29.64	29.15
alk	9.81	0.02	6.42	9.01	7.66	9.37	9.09	5.63	4.61	3.75	4.17
si	127.60	116.38	110.44	125.47	125.99	160.67	139.52	142.45	107.72	110.27	109.39
k	0.40	1.00	0.17	0.28	0.26	0.16	0.05	0.15	0.25	0.10	0.17
mg	0.36	0.10	0.52	0.58	0.58	0.43	0.54	0.59	0.67	0.60	0.60

Sample	KAW3013	KAW3014	KAW3015	KAW3016	KAW3017	KAW3045	KAW3046	KAW3047	KAW3048	KAW3049	KAW3068
al	45.84	41.51	45.21	47.07	46.19	19.57	24.23	32.59	25.10	18.21	18.90
fm	26.89	32.98	31.11	24.44	28.81	48.33	64.45	34.96	43.02	48.71	43.23
c	4.12	6.68	4.67	3.45	4.37	26.01	5.24	22.05	25.92	31.45	34.76
alk	23.16	18.83	19.00	25.05	20.63	6.09	6.09	10.40	5.96	1.62	3.12
si	355.46	311.42	273.53	382.15	355.60	109.21	135.01	207.99	131.54	134.23	101.77
k	0.62	0.45	0.61	0.51	0.77	0.20	0.06	0.18	0.03	0.15	0.08
mg	0.42	0.32	0.29	0.35	0.37	0.41	0.49	0.45	0.63	0.55	0.46

Sample	KAW3070	KAW3071	KAW3072	KAW3066	KAW3067	KAW3073	KAW3074	KAW3075	KAW3007	KAW3065
al	19.14	22.02	19.60	43.04	42.29	42.76	45.00	39.74	0.48	0.40
fm	50.49	47.99	48.24	19.75	18.29	41.04	38.78	38.67	40.51	49.52
c	25.54	22.27	27.46	10.61	11.38	4.82	2.21	12.52	59.01	50.01
alk	4.83	7.73	4.70	26.61	28.05	11.37	14.02	9.08	0.00	0.07
si	111.04	150.63	114.82	376.19	346.48	292.78	385.77	311.74	3.56	1.73
k	0.16	0.12	0.12	0.35	0.30	0.94	0.95	0.97		0.80
mg	0.43	0.34	0.43	0.37	0.36	0.63	0.75	0.62	0.97	0.99

Table 10A: Niggli values of the analysed specimens from the Elim Formation

Sample KAW	^{40}K $*10^{-8}$mol/g	$^{40}Ar_{rad}$ $*10^{-8}$mol/g	$^{40}Ar_{rad}$ %	^{36}Ar $*10^{-12}$mol/g	Age Ma	Error Ma
3014 Muscovite 60-135 mesh	23.4307	1.969	99.73	0.1825	1062.3	10.6
3015 Muscovite 60-270 mesh	25.9678	2.159	99.77	0.1705	1053.8	10.5
3016 Muscovite	25.9678	2.405	99.60	0.3316	1142.3	11.4
3017 Muscovite 60-325 mesh	25.8484	2.647	99.65	0.3175	1229.5	12.3
3047 Biotite > 100 mesh	21.4906	1.405	99.56	0.2099	874.4	8.7
3066 Sericite	20.6250	0.4120	99.64	0.05132	314.7	3.3
3067 Biotite 60-90 mesh	20.6250	0.5313	94.38	1.0728	396.5	4.3
3073 Muscovite 100-180 mesh	22.5054	1.279	99.85	0.06631	781.7	7.8
3074 Muscovite 100-180 mesh	19.6400	1.085	99.68	0.1217	763.5	7.9
3075a Muscovite 100-270 mesh	23.5800	1.228	99.45	0.2329	727.9	7.5
3075b Muscovite 100-270 mesh	23.5800	1.234	99.81	0.0808	730.4	8.2

Table 11: Tabulation of the K-Ar results obtained for the analysed mineral separates of the Elim Formation

Sample KAW	Rb ppm	Sr ppm	$^{87}Sr/^{86}Sr$	+/- 2 Sigma	$^{87}Rb/^{86}Sr$	+/- 2 Sigma
3001	71.48	253.15	0.71967	1	0.818	8
3002	0.26	30.62	0.70589	3	0.025	1
3003	14.44	205.94	0.70717	4	0.203	2
3004	48.80	230.71	0.71277	1	0.612	6
3005	31.55	229.28	0.70829	7	0.399	4
3006	17.68	259.97	0.70717	1	0.198	2
3008	3.52	173.95	0.70434	3	0.059	1
3009	7.88	255.59	0.70404	2	0.089	1
3010	17.26	111.58	0.71012	2	0.448	4
3011	5.42	86.94	0.70751	8	0.181	2
3012	9.95	109.52	0.70834	1	0.263	3
3045	19.21	482.86	0.70522	1	0.115	1
3046	3.53	287.12	0.70405	7	0.036	1
3047	34.24	219.82	0.71431	10	0.451	5
3048	1.57	178.21	0.70421	2	0.026	1
3049	1.25	300.15	0.70459	9	0.012	1
3068	2.08	267.77	0.70542	1	0.022	1
3069	1.61	319.66	0.70647	5	0.015	1
3070	15.50	152.92	0.70864	2	0.293	3
3071	10.42	95.24	0.70970	5	0.316	3
3072	6.65	134.97	0.70804	5	0.143	1
3007	0.33	80.68	0.70729	2	0.012	1
3065	2.79	59.27	0.71436	1	0.136	1

Table 12: tabulation of the Rb-Sr whole-rock results of the analysed amphibolites, greenschists and marbles of the Elim Formation

Table 13 (below): Tabulation of the K-Ar results obtained for the Marienhof Formation. (Age corr. = Individual ages corrected for the loss of $^{40}Ar_{rad}$ on the basis of the $^{40}Ar/^{36}Ar$ corr. ratios which were determined on the basis of the Harper diagram of Figure 3.1)

Sample KAW	^{40}K $*10^{-8}$mol/g	$^{40}Ar_{rad}$ $*10^{-8}$mol/g	$^{40}Ar_{rad}$corr. $*10^{-8}$mol/g	$^{40}Ar_{rad}$ %	^{36}Ar $*10^{-12}$mol/g	Age Ma	Error Ma	Age corr. Ma
3034 Phyllite								
Whole Rock	14.386736	0.470192	0.503682	99.64	5.79936	489.6	5.0	519.9
30-80 Microns	12.477646	0.417787	0.451277	99.73	3.96154	500.1	5.2	534.8
2-30 Microns	19.908616	0.667370	0.700860	98.74	0.291027	500.6	6.1	522.4
3035 Phyllite								
Whole Rock	11.551176	0.384992	0.418402	97.54	0.331056	490.1	6.4	535.6
30-80 Microns	17.281992	0.603080	0.637370	98.69	0.275133	519.1	7.3	543.9
2-30 Microns	19.460896	0.646181	0.679671	99.41	0.131116	496.5	5.3	518.8
3036 Phyllite								
Whole Rock	14.207648	0.476011	0.509501	99.37	0.103566	500.4	5.5	530.9
2-30 Microns	21.520408	0.740134	0.701624	99.16	0.217156	516.7	5.4	536.7
3037 Phyllite								
Whole Rock	12.476464	0.422025	0.455515	99.11	0.129652	504.6	5.0	539.2
30-80 Microns	13.998712	0.486824	0.520314	99.59	7.02684	516.9	6.1	547.6
2-30 Microns	21.401016	0.755639	0.789129	99.02	0.257163	523.8	7.2	543.8
3038 Phyllite								
Whole Rock	12.267528	0.407079	0.440569	99.54	6.60600	496.2	5.3	531.5
2-30 Fractions	16.207464	0.538054	0.572344	98.95	0.196647	497.0	5.4	523.0
3039 Quartzite								
White Mica	21.848736	0.756672		99.46	0.141178	515.0	5.4	
3041 Rhyolite								
Biotite	9.805068	0.340769		99.12	0.103921	516.6	5.3	
3042 Quartzite								
White Mica	20.177248	0.720083		99.66	0.42901	520.6	5.5	
3043 Quartzite								
White Mica	21.192080	0.719813		99.74	6.37674	506.4	5.1	

Sample KAW	^{40}K $*10^{-8}$mol/g	$^{40}Ar_{rad}$ $*10^{-8}$mol/g	$^{40}Ar_{rad}$ %	^{36}Ar $*10^{-12}$mol/g	$^{40}Ar/^{36}Ar$	Age Ma	Error Ma
3055 White Micas	22.475544	0.785338	99.73	0.074076	106314	519.0	5.5
3056 White Micas	22.296456	0.760772	98.33	0.444947	17573	513.1	5.7
3057 White Micas	21.460712	0.744687	99.75	0.064587	115596	515.9	5.3
3058 White Micas	21.430864	0.725340	99.27	0.100044	40404	504.8	5.2
3059 White Micas	24.982776	0.849760	99.76	0.071202	119507	507.0	5.1

Table 14: Tabulation of K-Ar results obtained for the Billstein Formation

Sample	KAM3018	KAM3019	KAM3021	KAM3022	KAM3023	KAM3024	KAM3025	KAM3026	KAM3027	KAM3028
Lithology	Granite	Granite	Granite	Granite	Granite	Granite	Granite	Diorite	Granite	G.Diorite
Farm	Borodino	Borodino	Borodino	Borodino	Borodino	Opetjie	Opetjie	Opetjie	Opetjie	Opetjie
Coord.	23°40'08"S 16°16'05"E	23°40'41"S 16°17'05"E	23°40'55"S 16°16'43"E	23°41'03"S 16°16'38"E	23°41'44"S 16°16'23"E	23°40'16"S 16°44'54"E	23°40'28"S 16°44'51"E	23°41'00"S 16°44'27"E	23°42'10"S 16°44'38"E	23°39'58"S 16°44'46"E
Major elements in wt%										
SIO2	72.37	70.64	70.86	74.68	71.81	70.03	70.15	53.40	65.17	67.49
TIO2	0.09	0.18	0.16	0.16	0.17	0.34	0.33	0.68	0.82	0.47
AL203	14.82	15.38	15.03	12.66	15.27	14.30	13.94	18.67	14.65	14.79
FE203	0.82	1.69	1.50	0.97	1.42	2.41	2.36	6.64	5.29	3.41
MNO	0.03	0.05	0.05	0.03	0.04	0.06	0.06	0.12	0.10	0.06
MGO	0.24	0.56	0.48	0.11	0.38	1.04	0.83	4.23	1.45	1.21
CAO	2.01	2.19	2.42	0.86	2.29	1.91	1.96	7.22	2.40	2.83
NA2O	4.05	4.15	4.37	2.86	4.71	3.40	3.27	3.25	3.29	3.22
K2O	3.25	3.04	2.39	4.89	2.47	4.43	4.30	2.73	4.36	4.04
P2O5	0.03	0.10	0.07	0.03	0.12	0.11	0.11	0.15	0.27	0.15
LOI	0.71	1.46	0.61	0.64	0.76	1.06	0.94	2.26	1.37	1.15
SUM	98.42	99.44	97.94	97.89	99.44	99.09	98.25	99.35	99.17	98.82
Trace elements in ppm										
NB				22					12	
ZR	65	105	105	109	100	157	152	76	322	207
Y				25		18	25	21	37	23
SR	758	789	1018	128	904	305	264	737	369	421
U										
RB	65	70	51	165	58	152	180	76	92	129
TH				16						
PB		21	19	28	19	13	18		21	
GA	15	22	20	18	20	17	18	24	23	19
ZN		26	40		32	34	34	81	91	48
CU		18				10		84	15	17
NI								55		12
CO	14	78	71	64	64	111	62	55	49	74
CR								45		
V		27				42	38	128	60	54
CE				62			85	130	156	139
ND						37	27	68	69	47
BA	2436	2045	1844	435	1689	919	807	1054	2057	1492
LA						73	62		119	71
SC								19	13	
SUM	3353	3201	3168	1072	2886	1888	1772	2653	3505	2753

Table 15 (pages 99 and 100): Tabular listing of the major and trace element concentrations of the analysed granitoids of the Piksteel Intrusive Suite. (No data recorded where concentration of trace element is below detection limit)

Detection Limits:
Nb 11 Zr 23 Y 5 Sr 16 U 31 Rb 14 Th 13 Pb 16 Ga 5 Zn 18 Cu 9 Co 3 Cr 26 V 26 Ce 46 Nd 26 Ba 40 La 44 Sc 7 S 216

	KAM3029	KAM3030	KAM3031	KAM3032	KAM3033	KAM3163	KAM3171	KAM3174	KAM3175
	Granite	G.Diorite	Granite	Granite	Granite	G.Diorite	G.Diorite	Granite	Granite
	Piksteel	Piksteel	Piksteel	Piksteel	Piksteel	Opetjie	Borodino	Piksteel	Piksteel
	23°47'05"S 16°07'46"E	23°47'08"S 16°07'53"E	23°47'02"S 16°08'13"E	23°47'15"S 16°08'23"E	23°47'08"S 16°08'29"E	23°36'08"S 16°42'30"E	23°41'12"S 16°16'32"E	23°46'42"S 16°09'19"E	23°47'00"S 16°09'00"E
	69.41	69.14	73.17	71.39	70.29	63.86	68.25	74.47	74.63
	0.21	0.37	0.15	0.19	0.31	0.60	0.46	0.11	0.16
	14.80	14.76	14.39	15.00	15.16	17.35	16.30	14.69	15.08
	1.92	2.69	1.46	1.69	2.53	4.43	3.90	1.36	1.61
	0.04	0.07	0.04	0.05	0.06	0.08	0.07	0.04	0.05
	0.58	0.86	0.32	0.50	0.74	1.83	1.26	0.28	0.43
	2.18	2.64	1.79	1.92	2.15	3.91	3.67	1.37	1.48
	4.13	4.09	3.74	4.41	3.99	4.14	3.59	4.14	4.13
	3.28	2.96	3.70	3.11	3.10	2.67	2.08	3.59	3.13
	0.08	0.12	0.04	0.08	0.12	0.24	0.18	0.03	0.08
	0.70	0.50	0.54	0.73	1.00	1.49	1.23	0.52	0.79
	97.33	98.20	99.34	99.07	99.45	100.60	100.99	100.60	101.57
	112	128	104	105	156	173	122	98	96
		18				14		9	9
	832	738	723	666	611	762	540	556	621
	62	70	68	54	58	53	45	66	49
							18		12
			20					19	19
	20	23	18	20	22	17	150	15	17
	37	58	35	42	63	60	51	26	32
	12				14	20	14	11	12
						18	14		
	51	68	59	82	76				
	34	32			37	68	71		
		47			54				
	1644	878	1847	1664	1357	1582	2021	1633	1750
	2804	2060	2874	2633	2448	2767	3046	2633	2617

Table 15 continued

Sample	KAM3018	KAM3019	KAM3021	KAM3022	KAM3023	KAM3024	KAM3025	KAM3026	KAM3027	KAM3028	KAM3029	KAM3030	KAM3031	KAM3032	KAM3033	KAM3163	KAM3171	KAM3174	KAM3175
Si02	74.13	72.22	72.92	76.87	72.87	71.61	72.26	55.38	67	69.34	71.97	70.96	74.16	72.71	71.58	64.72	68.68	74.51	74.17
Ti02	0.09	0.18	0.16	0.16	0.17	0.35	0.34	0.71	0.84	0.48	0.22	0.38	0.15	0.19	0.32	0.61	0.46	0.11	0.16
Al203	15.18	15.72	15.47	13.03	15.5	14.62	14.36	19.36	15.06	15.2	15.35	15.15	14.59	15.28	15.44	17.58	16.4	14.7	14.99
Fe203	0.33	0.66	0.58	0.4	0.56	0.98	0.96	2.27	2.11	1.34	0.78	1.05	0.59	0.68	0.99	1.64	1.35	0.55	0.63
FeO	0.43	0.89	0.81	0.49	0.74	1.24	1.24	3.93	2.79	1.82	1.02	1.44	0.75	0.88	1.33	2.4	2.18	0.68	0.81
MnO	0.03	0.05	0.05	0.03	0.04	0.06	0.06	0.12	0.1	0.06	0.04	0.07	0.04	0.05	0.06	0.08	0.07	0.04	0.05
MgO	0.25	0.57	0.49	0.11	0.39	1.06	0.85	4.39	1.49	1.24	0.6	0.88	0.32	0.51	0.75	1.85	1.27	0.28	0.43
CaO	2.06	2.24	2.49	0.89	2.32	1.95	2.02	7.49	2.47	2.91	2.26	2.71	1.81	1.96	2.19	3.96	3.69	1.37	1.47
Na20	4.15	4.24	4.5	2.94	4.78	3.48	3.37	3.37	3.38	3.31	4.28	4.2	3.79	4.49	4.06	4.2	3.61	4.14	4.1
K20	3.33	3.11	2.46	5.03	2.51	4.53	4.43	2.83	4.48	4.15	3.4	3.04	3.75	3.17	3.16	2.71	2.09	3.59	3.11
P205	0.03	0.1	0.07	0.03	0.12	0.11	0.11	0.16	0.28	0.15	0.08	0.12	0.04	0.08	0.12	0.24	0.18	0.03	0.08
Sum	100.01	99.98	100.00	99.98	100.00	99.99	100.00	100.01	100.00	100.00	100.00	100.00	99.99	100.00	100.00	99.99	99.98	100.00	100.00
Q	32.37	29.89	31.1	38.34	29.95	28.14	29.97	2.25	22.46	25.86	28.11	27.56	33.18	29.37	29.84	18.39	29.33	33.09	34.46
or	19.67	18.37	14.53	29.74	14.81	26.77	26.17	16.73	26.49	24.53	20.1	17.95	22.16	18.72	18.65	15.99	12.37	21.22	18.38
ab	35.1	35.9	38.05	24.91	40.45	29.42	28.5	28.52	28.62	27.99	36.24	35.52	32.08	38.01	34.38	35.5	30.57	35.05	34.73
an	10.01	10.44	11.88	4.19	10.73	8.95	9.28	29.34	10.43	13.42	10.67	12.64	8.74	9.17	10.06	18.07	17.14	6.6	6.78
C	1.08	1.55	1.05	1.2	0.99	0.72	0.62		0.82	0.34	0.71	0.32	1.09	1.1	1.65	1.13	1.91	1.58	2.38
di								4.04											
hedn								1.42											
en	0.61	1.43	1.23	0.28	0.96	2.65	2.13	9.05	3.71	3.1	1.5	2.2	0.81	1.27	1.88	4.62	3.16	0.7	1.06
fs	0.42	0.88	0.84	0.36	0.69	1	1.03	3.65	2.17	1.55	0.94	1.28	0.72	0.82	1.23	2.2	2.26	0.69	0.81
mt	0.48	0.96	0.84	0.58	0.81	1.42	1.39	3.29	3.06	1.94	1.13	1.52	0.85	0.99	1.43	2.38	1.96	0.8	0.91
il	0.18	0.35	0.31	0.31	0.33	0.66	0.65	1.34	1.6	0.92	0.41	0.72	0.29	0.37	0.6	1.15	0.88	0.21	0.3
ap	0.07	0.24	0.17	0.07	0.29	0.27	0.27	0.37	0.66	0.37	0.2	0.29	0.1	0.19	0.29	0.58	0.43	0.07	0.19
Sum	99.99	100.01	100.00	99.98	100.01	100.00	100.01	100.00	100.02	100.02	100.01	100.00	100.02	100.01	100.01	100.01	100.01	100.01	100.00
C.I.	1.69	3.61	3.22	1.54	2.79	5.73	5.2	22.8	10.54	7.5	3.98	5.72	2.66	3.45	5.13	10.36	8.25	2.39	3.08
Norm.Plag	22.53	22.53	23.8	14.4	20.97	23.33	24.55	50.71	26.7	32.4	22.75	26.24	21.4	19.44	22.64	33.73	35.92	15.85	16.33
Q'	33.32	31.60	32.54	39.45	31.22	30.17	31.91	2.93	25.52	28.17	29.55	29.42	34.50	30.83	32.11	20.91	32.80	34.48	36.52
ANOR	33.73	36.24	44.98	12.35	42.01	25.06	26.18	63.69	28.25	35.36	34.68	41.32	28.28	32.88	35.04	53.05	58.08	23.72	26.95

Table 15A: CIPW-normative mineral contents of the analysed Piksteel granitoids. CIPW-Norm (recalculation of oxides to 100% volatile-free. Fe_2O_3/FeO according to Le Maitre (1976))

Sample	^{40}K	$^{40}Ar_{rad}$	$^{40}Ar_{rad}$	^{36}Ar	Age	Error
KAW	$*10^{-8}$mol/g	$*10^{-8}$mol/g	%	$*10^{-12}$mol/g	Ma	Ma
Borodino						
3021 Biotite > 100 mesh	22.6546	1.656	99.25	0.4239	954.7	8.5
3023 Biotite > 270 mesh	20.7444	0.8691	89.68	0.3959	606.7	6.8
Opetjie						
3024 Biotite > 100 mesh	22.1706	0.9523	98.37	0.5363	619.4	8.0
Piksteel						
3029 Biotite > 180 mesh	22.9830	0.1480	99.22	0.3951	864.0	8.7
3030 Biotite > 100 mesh	24.0276	1.634	99.28	0.4026	902.0	9.9
3032 Biotite 100-180 mesh	20.0579	0.9062	98.75	0.3902	646.6	6.5

Table 16: Results of the K-Ar analyses of the Piksteel biotite separates

Sample	Rb	Sr	$^{87}Sr/^{86}Sr$	+/-	$^{87}Rb/^{86}Sr$	+/-	Rb/Sr
KAW	ppm	ppm		2 Sigma		2 Sigma	
Borodino							
3018	69.94	776.22	0.70799	1	0.261	3	0.090
3019	72.44	812.28	0.70774	2	0.258	3	0.089
3020	68.24	1009.07	0.70632	1	0.196	2	0.068
3021	54.86	1051.98	0.70562	2	0.151	2	0.052
3022	166.42	133.84	0.76305	1	3.617	36	1.243
3023	62.29	909.10	0.70655	2	0.198	2	0.069
3171	47.65	573.07	0.70965	1	0.241	2	0.083
Opetjie							
3024	164.69	304.14	0.73155	1	1.570	16	0.541
3025	175.56	279.58	0.73594	1	1.822	18	0.628
3026	71.80	756.65	0.71208	30	0.275	3	0.095
3027	90.16	373.21	0.71766	1	0.700	7	0.242
3028	131.30	445.79	0.71923	3	0.853	9	0.295
3163	55.36	819.64	0.70717	1	0.195	2	0.068
Piksteel							
3029	64.61	854.61	0.70712	2	0.219	2	0.076
3030	70.55	743.14	0.70764	14	0.120	1	0.095
3031	68.29	746.89	0.70813	5	0.265	3	0.091
3032	58.71	702.82	0.70788	2	0.242	2	0.084
3033	58.33	628.90	0.70796	1	0.268	3	0.093
3174	72.28	584.24	0.70962	2	0.358	4	0.124
3175	56.47	651.77	0.70745	2	0.251	3	0.087
3176	51.59	663.75	0.70761	1	0.225	2	0.078

Table 17: Results of the Piksteel whole-rock Rb-Sr analyses

Sample	Fraction	U	Pb_{rad}	Pb_{nonrad}	$^{206}Pb/^{204}Pb$	$^{206}Pb/^{238}U$	$^{207}Pb/^{235}U$	$^{207}Pb/^{206}Pb$	$^{208}Pb/^{206}Pb$	$^{206}Pb/^{238}U$	$^{207}Pb/^{235}U$	$^{207}Pb/^{206}Pb$
KAW	Microns	ppm	ppm	ppm	measured	Atomic Ratios				Apparent ages		
Borodino												
3019	nonmagn	2243	161.2	129.0	84.418	0.0657	0.769	0.08486	0.1852	410	579	1312
3019	magn	3256	143.9	273.6	41.778	0.0384	0.383	0.07747	0.3543	227	329	1133
3020	> 95	1024	220.9	111.6	68.897	0.0962	1.098	0.08280	1.5136	592	752	1265
3020	< 95	952	109.3	85.2	77.234	0.0915	1.073	0.08506	0.0371	564	740	1317
3021		1555	239.9	46.6	175.311	0.0800	0.925	0.08381	1.1495	496	665	1288
3023		1308	148.7	49.5	191.284	0.1113	1.304	0.08499	0.1037	680	847	1315
Opetjie												
3024	> 95	437	92.1	111.7	47.254	0.1393	1.585	0.08253	0.6696	841	964	1258
3024	< 95	693	154.8	182.3	48.043	0.1470	1.700	0.08390	0.6776	884	1009	1290
3026	112 nm	251	74.4	1.5	2718.497	0.2793	4.070	0.10567	0.1273	1588	1648	1726
3026	75-112 nm	310	75.2	4.8	882.746	0.2318	3.272	0.10237	0.1136	1344	1474	1667
3026	< 75 nm	254	78.9	1.7	2554.709	0.2866	4.206	0.10645	0.1548	1624	1675	1739
Piksteel												
3029	nonmagn	1528	88.7	42.9	129.375	0.0539	0.626	0.08429	0.1672	338	494	1299
3174	> 75	958	108.7	65.8	103.329	0.1015	1.256	0.08980	0.2081	623	826	1421
3176	> 95	946	69.7	92.8	56.376	0.0669	0.778	0.08439	0.1955	417	585	1302

Table 18: Tabular listing of the results of the U-Pb analyses of the Piksteel zircon separates

Sample	G30	P07	P10	P14	KAM3040	KAM3041	KAM3164	KAM3165	KAM3166	KAM3167	KAM3168	KAM3169	KAM3177	W04	W05
Lithology	Rhyolite	Rhyolite	Rhyolite	Rhyolite	Rhyolite	Rhyolite	Rhyolite	Rhyolite	Rhyolite	Rhyolite	Rhyolite	Rhyolite	Rhyolite	Rhyolite	Rhyolite
Farm	Groendraai	Dymoeb	Karikomasis	Groendraai	Marienhof	Marienhof	Auchas	Auchas	Auchas	Stofbakkies	Stofbakkies	Stofbakkies	Rehoboth DG	337	Namibgrens
Coord.	23°41'20"S 16°58'00"E	23°40'00"S 16°42'14"E	23°40'34"S 16°56'50"E	23°42'33"S 16°59'55"E	23°24'05"S 16°47'39"E	23°23'31"S 16°46'37"E	23°47'55"S 16°28'19"E	23°47'15"S 16°27'35"E	23°47'13"S 16°25'42"E	23°48'14"S 16°18'46"E	23°48'26"S 16°20'09"E	23°48'25"S 16°20'10"E	23°19'37"S 17°11'28"E	23°40'57"S 16°29'25"E	23°37'31"S 16°15'51"E
Major elements in wt%															
SIO2	77.08	76.39	75.75	77.49	75.46	75.05	74.38	78.86	75.27	75.88	77.80	78.53	79.28	77.05	76.57
TIO2	0.13	0.12	0.18	0.10	0.27	0.29	0.34	0.21	0.29	0.27	0.25	0.10	0.12	0.25	0.15
AL203	11.56	11.86	11.98	11.89	12.36	12.24	13.20	12.03	12.27	13.71	12.31	12.63	11.99	10.47	12.05
FE203	0.97	1.02	1.11	0.83	2.51	1.55	2.04	1.24	1.55	1.61	1.23	0.75	1.46	1.34	0.96
MNO	0.02	0.03	0.04	0.02	0.04	0.04	0.03	0.03	0.04	0.03	0.03	0.05	0.02	0.05	0.02
MGO	0.31	0.30	0.36	0.17	0.16	0.12	0.18	0.14	0.12	0.46	0.32	0.15	0.16	0.56	0.28
CAO	0.30	0.14	0.53	0.34	0.64	0.91	0.12	0.07	0.92	0.08	0.45	0.16	0.27	1.27	0.42
NA20	2.52	2.94	2.78	4.05	3.53	3.68	3.46	2.79	3.69	2.42	2.38	3.46	3.91	0.82	3.35
K20	5.50	5.48	5.37	4.74	4.61	5.04	5.75	5.68	5.06	4.67	5.41	4.80	4.32	6.46	4.50
P205	0.02	0.02	0.05	0.02	0.02	0.05	0.08	0.05	0.05	0.12	0.04	0.01	0.01	0.05	0.04
LOI	0.30	0.62	0.43	0.31	0.58	0.73	0.26	0.21	0.73	1.24	0.63	0.30	0.21	0.36	0.41
SUM	98.71	98.92	98.58	99.96	100.18	99.70	99.84	101.31	99.99	100.49	100.85	100.94	101.75	98.68	98.75
Trace elements in ppm															
NB	14	29	13	12	39	26	15	17	14	13	15	28	31	12	
ZR	105	125	131	82	442	538	217	178	275	188	175	104	239	172	
Y	42	42	36	41	95	82	20	32	36	19	24	15	78	27	
SR	55	43	62	64	63	243	59	33	116	92	83	81		464	
U															
RB	318	225	336	157	79	36	171	171	109	154	167	180	145	190	
TH	31	48	48	14		21	16	23	21	32	33	52	42	15	
PB						34	18	17			19			35	
GA	17	11	16	8	21	22	12	12	9	16	12	14	18	13	
ZN		23	19		73	48	21	20		36	26	26		26	
CU					22	75	14	12	9	9	9	9	10	17	
NI															
CO	131	17	90	12	47	37								119	
CR															
V	11	15	4				34	24	12	16	13	4	10	14	
CE			76		117	154								72	
ND			33		62	55									
BA	195	646	268	178	934	452	1202	707	1228	1325	1354	457		1277	
LA			58		93	58								71	
SC						7									
S															
SUM	919	1224	1190	568	2087	1888	1799	1246	1829	1900	1930	970	573	2524	

Table 19: Major and trace element concentration of the analysed rhyolitic samples from the Rehoboth Basement Inlier. (No data recorded where concentration of trace element is below detection limit)

Detection Limits: Nb 11 Zr 23 Sr 16 U 31 Rb 14 Th 13 Pb 16 Ga 5 Nn 18 Cu 9 Ni 12 Co 3 Cr 26 V 26 Ce 46 Nd 26 Ba 40 La 4 Sc 7 S 216

Sample KAW	Rb ppm	Sr ppm	$^{87}Sr/^{86}Sr$	+/- 2 Sigma	$^{87}Rb/^{86}Sr$	+/- 2 Sigma	Rb/Sr
3040	85.36	74.88	0.75554	2	3.134	33	1.140
3041	35.17	245.18	0.72188	1	0.416	4	0.143
3164	178.79	61.95	0.82721	22	8.448	84	2.886
3165	177.89	35.47	0.91631	8	14.808	148	5.015
3166	118.16	120.34	0.75757	1	2.855	29	0.982
3167	163.44	96.79	0.76430	1	4.913	49	1.689
3168	181.74	89.18	0.78548	1	5.941	59	2.038
3169	193.05	81.72	0.79303	1	6.892	69	2.362
3177	152.91	14.29	1.14280	42	32.273	323	10.700

Table 20: Tabulation of the Rb-Sr results obtained for the analysed volcanics from the Nueckopf Formation

Sample KAW	Fraction Microns	U ppm	Pb_{rad} ppm	Pb_{nonrad} ppm	$^{206}Pb/^{204}Pb$ Measured	$^{206}Pb/^{238}U$ Atomic ratios	$^{207}Pb/^{235}U$ Atomic ratios	$^{207}Pb/^{206}Pb$ Atomic ratios	$^{208}Pb/^{206}Pb$ Atomic ratios	$^{206}Pb/^{238}U$ Apparent ages	$^{207}Pb/^{235}U$ Apparent ages	$^{207}Pb/^{206}Pb$ Apparent ages
3040	>112	206	33.1	15.9	131.252	0.1470	1.550	0.07646	0.1972	884	950	1107
3040	>95 mag	264	35.1	9.6	219.455	0.1227	1.247	0.07373	0.1893	746	822	1034
3040	95-112 mag	257	39.2	6.8	331.991	0.1395	1.456	0.07571	0.1916	842	912	1087
3041	<75 unmag	334	52.4	4.0	730.483	0.1414	1.483	0.07607	0.2111	853	924	1097
3041	>75 unmag	273	40.9	5.7	409.692	0.1367	1.420	0.07534	0.1970	826	898	1078

Table 21: Tabulation of the U-Pb results obtained for zircons from rhyolitic dykes crosscutting the Marienhof Formation **(see overleaf for Table 22)**

Sample KAW	^{40}K $*10^{-8}mol/g$	$^{40}Ar_{rad}$ $*10^{-8}mol/g$	$^{40}Ar_{rad}$ %	^{36}Ar $*10^{-12}mol/g$	Age Ma	Error Ma
3161	1.6201	0.1774	87.40	0.8660	1290.3	10.0
3162	2.2810	0.08357	81.88	0.6264	540.8	6.7
3170	0.08683	0.1749	94.77	0.3273	1934.5	14.0
3172	1.1324	0.06513	83.38	0.4401	789.1	8.8
3173	1.8852	0.1014	87.20	0.5041	747.1	7.1

Table 23: Tabular listing of the results of the whole-rock K-Ar analyses of the basic dykes

Sample KAW	Rb ppm	Sr ppm	$^{87}Sr/^{86}Sr$	+/- 2 Sigma	$^{87}Rb/^{86}Sr$	+/- 2 Sigma	Rb/Sr
3161	32.30	174.73	0.71052	2	0.535	5	0.185
3162	30.34	198.93	0.70937	2	0.441	4	0.153
3170	9.71	171.49	0.70634	2	0.163	2	0.057
3172	11.53	274.02	0.70552	1	0.122	1	0.042
3173	22.30	190.01	0.70689	1	0.340	3	0.117

Table 24: Tabular listing of the results of the Rb-Sr whole-rock analyses of the basic dykes

Sample	KAM3161	KAM3162	KAM3170	KAM3172	KAM3173
Formation	GGS	Elim	PIS	PIS	PIS
Farm	Kobos	Kobos	Borodino	Namakorabis	Namakorabis
Coord.	23°35'15"S 16°39'36"E	23°33'42"S 16°38'33"E	23°40'33"S 16°16'21"E	23°46'55"S 16°11'41"E	23°47'08"S 16°11'41"E
Major elements in wt%					
SIO2	46.58	46.51	48.77	48.91	48.70
TIO2	1.97	3.04	1.47	1.33	0.95
AL2O3	16.03	13.69	15.60	15.23	16.73
FE2O3	13.64	15.93	13.70	13.78	10.14
MNO	0.19	0.25	0.21	0.22	0.16
MGO	8.41	5.76	7.05	7.39	9.16
CAO	10.53	10.03	11.12	10.34	11.42
NA2O	1.64	1.75	1.75	1.75	1.39
K2O	0.54	0.83	0.26	0.35	0.53
P2O5	0.17	0.35	0.12	0.20	0.09
LOI	1.24	2.00	0.62	1.46	1.62
SUM	100.94	100.14	100.67	100.96	100.89
Trace elements in ppm					
NB		11			
ZR	45	180	55	99	41
Y	14	45	20	30	11
SR	165	183	166	267	179
U					
RB	32	30			20
TH					
PB					
GA	20	24	24	27	18
ZN	94	138	101	113	77
CU	111	375	134	78	83
NI	180	79	113	109	217
CO					
CR	195	184	149	250	320
V	261	448	256	284	202
CE					
ND					
BA	107	493	208	225	132
LA					
SC					
S					
SUM	1224	2190	1226	1482	1300

Detection limits:

Nb11 Zr23 Y5 Sr16 U31 Rb14 Th13 Pb16 Ga5 Zn18 Cu9
Ni12 Co3 Cr26 V26 Ce46 Nd26 Ba40 La44 Sc7 S216

Table 22: Tabular listing of the major and trace element contents of the analysed basic dykes

Sample	KAM3161	KAM3162	KAM3170	KAM3172	KAM3173
SiO2	47.2	47.95	49.28	49.7	49.44
TiO2	2	3.13	1.49	1.35	0.96
Al2O3	16.24	14.11	15.76	15.48	16.98
Fe2O3	3.52	4.68	3	2.88	2.49
FeO	9.27	10.57	9.75	10.01	7.02
MnO	0.19	0.26	0.21	0.22	0.16
MgO	8.52	5.94	7.12	7.51	9.3
CaO	10.67	10.34	11.24	10.51	11.59
Na2O	1.66	1.8	1.77	1.78	1.41
K2O	0.55	0.86	0.26	0.36	0.54
P2O5	0.17	0.36	0.12	0.2	0.09
Sum	99.99	100	100	100	99.98
Q	0	3.8	2	2.19	0.37
or	3.23	5.06	1.55	2.1	3.18
ab	14.06	15.27	14.96	15.05	11.94
an	35.25	27.89	34.3	33.2	38.42
ne	0	0	0	0	0
lc	0	0	0	0	0
C	0	0	0	0	0
wo	0	0	0	0	0
di	13.43	17.25	16.93	14.43	14.9
diwo	6.92	8.79	8.62	7.35	7.72
dien	4.27	4.88	4.74	4.03	5.08
difs	2.25	3.58	3.57	3.06	2.1
hy	21.67	17.18	22.81	25.82	25.54
hyen	14.19	9.91	13.01	14.68	18.08
hyfs	7.48	7.26	9.81	11.14	7.46
ol	3.07	0	0	0	0
olfo	1.94	0	0	0	0
olfa	1.13	0	0	0	0
mt	5.1	6.79	4.35	4.17	3.61
he	0	0	0	0	0
il	3.79	5.95	2.82	2.57	1.83
ap	0.41	0.85	0.29	0.48	0.22
Sum	100.01	100.04	100.01	100.01	100.01
C.I.	47.46	47.98	47.19	47.46	46.09
D.I.	17.3	14.12	18.51	19.35	15.49
Norm.Plag	71.48	64.62	69.63	68.81	76.29
Q	0.00	7.30	3.79	4.17	0.69
ANOR	91.61	84.64	95.68	94.05	92.36

Table 22A: CIPW-normative mineral content of the analysed basic dykes.

CIPW-norm (recalculation of oxides to 100% volatile-free. Fe_2O_3/FeO according to Irvine and Baragar (1971))

Sample KAW	Formation	Farm	Coordinates		Lithology	Sm ppm	Nd ppm	$^{147}Sm/^{144}Nd$	$^{143}Nd/^{144}Nd$	+/-	$f_{Sm/Nd}$
3003	Elim	Samkubis	23°42'10"S	16°37'32"E	Amphibolite	2.98	11.00	0.1626	0.512363	7	-0.1731
3005	Elim	Samkubis	23°43'13"S	16°37'35"E	Amphibolite	2.68	11.98	0.1354	0.512129	7	-0.3116
3006	Elim	Samkubis	23°43'07"S	16°38'27"E	Amphibolite	4.03	15.94	0.1528	0.512268	21	-0.2232
3008	Elim	Kobos	23°32'36"S	16°38'14"E	Amphibolite	1.94	7.25	0.1617	0.512420	5	-0.1779
3009	Elim	Kobos	23°32'35"S	16°38'19"E	Amphibolite	2.89	12.82	0.1361	0.512094	6	-0.3080
3011	Elim	Kobos	23°32'34"S	16°38'27"E	Amphibolite	0.54	1.58	0.2057	0.513037	100	0.0456
3012	Elim	Kobos	23°32'34"S	16°38'32"E	Amphibolite	0.50	2.04	0.1490	0.512443	115	-0.2427
3018	Piksteel	Borodino	23°40'08"S	16°16'05"E	Granite	2.07	14.08	0.0889	0.511576	5	-0.5480
3019	Piksteel	Borodino	23°40'41"S	16°17'05"E	Granite	2.47	14.06	0.1063	0.511853	7	-0.4596
3020	Piksteel	Borodino	23°40'43"S	16°16'58"E	Granite	2.71	16.60	0.0985	0.511740	4	-0.4991
3021	Piksteel	Borodino	23°40'55"S	16°16'43"E	Granite	2.80	17.78	0.0952	0.511710	4	-0.5162
3023	Piksteel	Borodino	23°41'44"S	16°16'23"E	Granite	2.11	13.75	0.0930	0.511692	9	-0.5275
3024	Piksteel	Opetjie	23°40'16"S	16°44'54"E	Granite	5.45	33.73	0.0978	0.511659	7	-0.5030
3025	Piksteel	Opetjie	23°40'28"S	16°44'51"E	Granite	5.49	34.10	0.0974	0.511705	7	-0.5050
3026	Piksteel	Opetjie	23°41'00"S	16°44'27"E	Diorite	6.52	34.25	0.1151	0.511713	4	-0.4150
3027	Piksteel	Opetjie	23°42'10"S	16°44'38"E	Granite	10.84	70.32	0.0931	0.511466	10	-0.5266
3028	Piksteel	Opetjie	23°39'58"S	16°44'46"E	Granodiorite	7.81	47.74	0.0989	0.511724	6	-0.4974
3029	Piksteel	Piksteel	23°47'05"S	16°07'46"E	Granite	3.45	20.34	0.1024	0.511850	5	-0.4795
3030	Piksteel	Piksteel	23°47'08"S	16°07'53"E	Granodiorite	6.56	32.02	0.1239	0.511932	7	-0.3701
3031	Piksteel	Piksteel	23°47'02"S	16°08'13"E	Granite	2.50	15.98	0.0947	0.511706	4	-0.5185
3032	Piksteel	Piksteel	23°47'15"S	16°08'28"E	Granite	2.63	16.31	0.0974	0.511823	5	-0.5049
3033	Piksteel	Piksteel	23°47'08"S	16°08'29"E	Granite	2.95	17.69	0.1009	0.511726	3	-0.4871
3050	Neuhof	Kolchas	23°39'43"S	16°05'51"E	Amphibolite	3.15	15.32	0.1243	0.511892	4	-0.3678
3051	Neuhof	Kolchas	23°39'46"S	17°05'55"E	Amphibolite	3.48	17.35	0.1213	0.511850	7	-0.3832
3052	Neuhof	Swartskaap	23°39'38"S	17°06'00"E	Amphibolite	3.05	13.15	0.1400	0.512074	4	-0.2881
3053	Neuhof	Kolchas	23°39'45"S	17°05'37"E	Amphibolite	2.87	13.68	0.1267	0.511891	5	-0.3556
3054	Neuhof	Kolchas	23°39'47"S	17°05'35"E	Amphibolite	4.71	21.75	0.1310	0.511911	12	-0.3339
3161	Basic Dykes	Kobos	23°35'15"S	16°39'36"E	Basic Dyke	2.09	7.26	0.1742	0.512686	7	-0.1144
3162	Basic Dykes	Kobos	23°33'42"S	16°38'33"E	Basic Dyke	7.25	27.37	0.1602	0.512538	4	-0.1857
3163	Piksteel	Opetjie	23°36'08"S	16°42'30"E	Granodiorite	5.55	37.49	0.0895	0.511440	3	-0.5452
3170	Basic Dykes	Borodino	23°40'33"S	16°16'21"E	Basic Dyke	2.84	9.94	0.1726	0.512617	45	-0.1224
3172	Basic Dykes	Namakorabis	23°46'55"S	16°11'41"E	Basic Dyke	4.60	18.82	0.1476	0.512211	23	-0.2494
3174	Piksteel	Piksteel	23°46'22"S	16°09'19"E	Granite	3.72	22.48	0.1001	0.511741	4	-0.4912
3175	Piksteel	Piksteel	23°47'00"S	16°09'00"E	Granite	4.07	24.88	0.0988	0.511893	4	-0.4979
3176	Piksteel	Piksteel	23°46'11"S	16°09'50"	Granite	3.33	20.49	0.0983	0.511899	4	-0.5003

Table 25: Tabular listing of the results of the Sm-Nd analyses

Sample KAW	$^{87}Rb/^{86}Sr$	$^{87}Sr/^{86}Sr$	+/-	$^{87}Sr/^{86}Sr_{(1800)}$
3003	0.203	0.707170	35	0.701917
3005	0.399	0.708292	65	0.697972
3006	0.197	0.707170	11	0.702077
3008	0.059	0.704339	32	0.702824
3009	0.089	0.704037	20	0.701729
3011	0.181	0.707507	76	0.702833
3012	0.263	0.708339	14	0.701531
3018	0.261	0.707993	13	0.701244
3019	0.258	0.707736	16	0.701056
3020	0.196	0.706322	11	0.701257
3021	0.151	0.705622	22	0.701717
3023	0.198	0.706549	15	0.701417
3024	1.570	0.731548	12	0.690893
3025	1.822	0.735938	9	0.688771
3026	0.275	0.712078	304	0.704967
3027	0.700	0.717656	9	0.699543
3028	0.853	0.719233	27	0.697146
3029	0.219	0.707121	17	0.701458
3030	0.120	0.707636	140	0.704541
3031	0.265	0.708130	53	0.701281
3032	0.242	0.707877	21	0.701620
3033	0.268	0.707957	14	0.701010
3050	0.142	0.707284	22	0.703598
3051	0.169	0.707647	143	0.703259
3052	0.071	0.706797	37	0.704967
3053	0.272	0.711889	11	0.704836
3054	0.182	0.708686	12	0.703966
3161	0.535	0.710521	20	0.696669
3162	0.441	0.709371	21	0.697945
3163	0.195	0.707168	10	0.702109
3170	0.164	0.706340	18	0.702101
3172	0.122	0.705521	10	0.702369
3174	0.358	0.709619	19	0.700351
3175	0.251	0.707447	17	0.700957
3176	0.225	0.707611	12	0.701789

Table 26 (left):
Tabular listing of the Rb-Sr data of the analysed samples.
($^{87}Sr/^{86}Sr_{(o)}$ = measured ratio today; $^{87}Sr/^{86}Sr_{(t\ =\ 1800)}$ = ratio at t = 1800 Ma)

Sample KAW	K/Ar Biotite	K/Ar Whole Rock	Rb/Sr Whole Rock Isochron	U/Pb 207/206 Pb	U/Pb Discordia Upper Intercept (Tera & Wasserburg)
	Ma	Ma	Ma	Ma	Ma
3003			396		
3005			396		
3006			396		
3008			1185		
3009			1185		
3011			685		
3012			685		
3018			1489		
3019			1489	1312 / 1133	1369 +/- 8
3020			1489	1265 / 1317	1369 +/- 8
3021	955		1489	1288	1369 +/- 8
3023	607		1489	1315	1369 +/- 8
3024	619		1164	1258 / 1290	1786 +/- 11
3025			1164		
3026			1164	1726 / 1667 / 1739	1786 +/- 11
3027			1164		
3028			1164		
3029	864		1298	1299	1505 +/- 69
3030	902				
3031			1057		
3032	647		1057		
3033			1298		
3050			1122 / 2569		
3051			1122 / 2569		
3052			1122		
3053			2569		
3054			1122 / 2569		
3161		1444	821		
3162		589	821		
3163			1164		
3170		2252	821		
3172		934	821		
3174			1057 / 1298	1421	1505 +/- 69
3175			1298		
3176			1057	1302	1505 +/- 69

Table 27 (above):
Radiometric ages obtained for the same samples by various other techniques

Sample KAW	T_{CHUR} Ma	T_{DM} Ma	$Nd_{(0)}$	$Nd_{(1800)}$	$Sr_{(0)}$	$Sr_{(1800)}$
3003	1254	2373	- 5.48	2.39	37.90	- 6.29
3005	1273	2002	-10.05	4.13	53.83	- 62.46
3006	1304	2226	- 7.33	2.82	37.90	- 4.02
3008	976	2165	- 4.37	3.73	- 2.29	6.62
3009	1382	2089	-10.73	3.28	- 6.57	- 8.96
3011	-	2351	7.67	5.62	42.68	6.75
3012	643	1686	- 3.92	7.14	54.49	- 11.79
3018	1508	1930	-20.83	4.08	49.58	- 15.88
3019	1332	1851	-15.43	5.48	45.93	- 18.55
3020	1401	1875	-17.63	5.07	25.86	- 15.69
3021	1400	1860	-18.22	5.26	15.93	- 9.14
3023	1397	1849	-18.57	5.42	29.08	- 13.40
3024	1515	1968	-19.21	3.66	383.93	-163.25
3025	1439	1902	-18.32	4.65	446.25	-193.46
3026	1734	2229	-18.16	0.70	107.57	37.13
3027	1729	2135	-22.98	0.95	186.74	- 40.10
3028	1431	1902	-17.95	4.67	209.13	- 74.22
3029	1282	1790	-15.49	6.33	37.20	- 12.82
3030	1488	2079	-13.89	2.94	44.51	31.07
3031	1400	1858	-18.30	5.28	51.53	- 15.34
3032	1259	1749	-16.02	6.96	47.93	- 10.52
3033	1458	1933	-17.91	4.24	49.07	- 19.21
3050	1581	2157	-14.67	2.05	39.51	- 17.64
3051	1602	2155	-15.49	1.93	44.67	12.82
3052	1530	2240	-11-12	1.98	32.60	37.13
3053	1637	2218	-14.69	1.48	104.88	35.26
3054	1697	2295	-14.30	0.88	59.42	22.89
3161	-	1828	0.82	6.04	85.46	81.01
3162	443	1769	- 2.07	6.40	69.14	- 62.85
3163	1707	2104	-23.49	1.29	37.87	- 3.55
3170	171	2012	- 0.53	5.06	26.12	- 3.67
3172	1344	2184	- 8.54	2.90	14.49	0.14
3174	1422	1899	-17.61	4.72	72.66	- 28.59
3175	1168	1677	-14.65	8.01	41.83	- 19.96
3176	1153	1663	-14.53	8.24	44.16	- 8.11

Table 28 (left):
Tabulation of Nd model ages and Epsilon Nd and Epsilon Sr values obtained for the analysed samples of the Rehoboth Basement Inlier